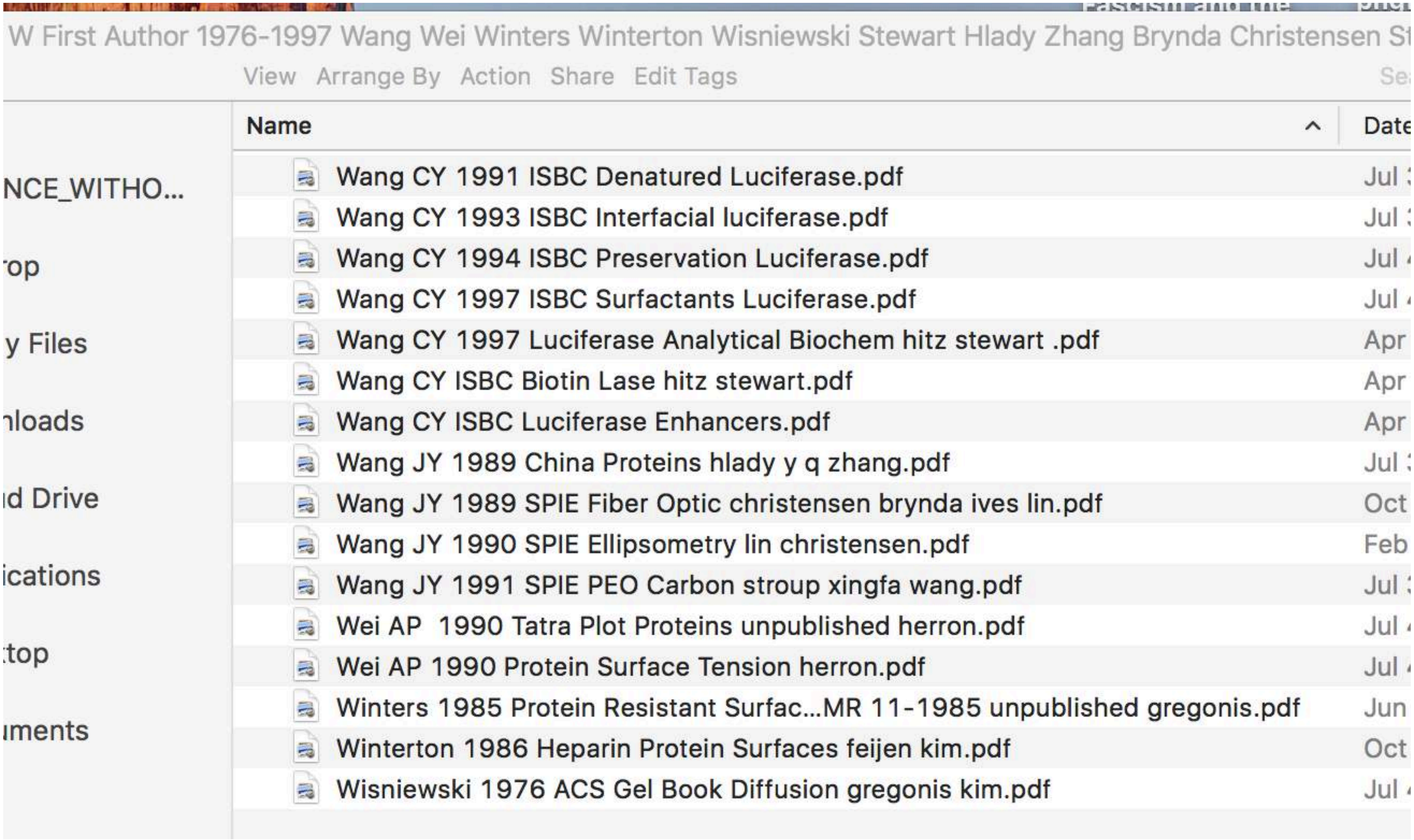

W First Author 1976-1997 Wang Wei Winters Winterton Wisniewski Stewart Hlady Zhang Brynda Christensen St

Name	Date
Wang CY 1991 ISBC Denatured Luciferase.pdf	Jul
Wang CY 1993 ISBC Interfacial luciferase.pdf	Jul
Wang CY 1994 ISBC Preservation Luciferase.pdf	Jul
Wang CY 1997 ISBC Surfactants Luciferase.pdf	Jul
Wang CY 1997 Luciferase Analytical Biochem hitz stewart .pdf	Apr
Wang CY ISBC Biotin Lase hitz stewart.pdf	Apr
Wang CY ISBC Luciferase Enhancers.pdf	Apr
Wang JY 1989 China Proteins hlady y q zhang.pdf	Jul
Wang JY 1989 SPIE Fiber Optic christensen brynda ives lin.pdf	Oct
Wang JY 1990 SPIE Ellipsometry lin christensen.pdf	Feb
Wang JY 1991 SPIE PEO Carbon stroup xingfa wang.pdf	Jul
Wei AP 1990 Tatra Plot Proteins unpublished herron.pdf	Jul
Wei AP 1990 Protein Surface Tension herron.pdf	Jul
Winters 1985 Protein Resistant Surfac...MR 11-1985 unpublished gregonis.pdf	Jun
Winterton 1986 Heparin Protein Surfaces feijen kim.pdf	Oct
Wisniewski 1976 ACS Gel Book Diffusion gregonis kim.pdf	Jul

DENATURATION OF FIREFLY LUCIFERASE

C.Y. Wang and J.D. Andrade

Department of Bioengineering, 2480 MEB University of Utah,
Salt Lake City, UT 84112, USA

INTRODUCTION

In order to improve the stability, duration and intensity of the light output of the firefly luciferase-luciferin system, we are studing the relationship between enzyme activity and conformation. Because the activity of recombinant luciferase is five times higher than natural purified luciferase, it is important to explore both firefly luciferases. Ultraviolt difference spectroscopy and fluoroescence are used to study the denaturation of luciferase. We have found that both luciferases denature at low urea concentration (50% denaturation), at about 1M, and at very low guanidinium chloride concentration (50% denaturation), about 0.5M. The light output of the luciferase-luciferin system at different urea concentrations was also measured to check luciferase activity. Scanning calorimetry also shows that luciferase is thermally labile. Denaturation temperature is about 40°C. The pH is also critical to the conformational stability of luciferase.

MATERIALS AND METHODS

Luciferase from Photinus pyralis was obtained from Sigma Chemical Company. The Sigma luciferase was chromatographically prepared, crystallized and lyophilized with 90% purity. The luciferase was dissolved in 0.5M, pH 7.7 Trizma succinate buffer, purchased from Sigma. The pH was measured by Corning pH meter 245 and pH indicator sticks (EM Laboratories Inc.). Recombinant firefly luciferase was prepared from a procaryotic recombinant host harboring the luc structural gene by Amgen Biologicals. It was purified by sequential chromatography to 95% purity. This recombinant luciferase is dissolved in 0.5M, pH 7.7 Trizma succinate buffer to obtain a homogeneous solution.

Urea and Guanidinium Chloride were purchased from Research Plus Inc. (absolute grade). The urea and GdnCl 8M stock solutions were prepared by weight (1) and then adjusted to pH 7.7. The stock solutions were then diluted to the desired concentration. Perkin Elmer UV spectrophotometer (model C688-0002) was used to measure the UV absorbance from 200nm to 350 nm. The concentration of protein used in the UV absorbance studies was 0.75mg/ml (A_{1cm}=0.75 mg/ml at 280 nm) (2). An ISS Grey 200 multifrequency phase fluorometer was used to measure tryptophan flourescence of the protein solution, excited at 280nm. The concentration of protein used in fluorescence detection was 0.3mg/ml. The temperature was controlled at 22°C in both experiments. The time required to reach equilibrium at the different denaturant concentrations was also measured. Further details on the assay and methods used for measuring the light emission of the luciferase-luciferin system are available (2). The pH of the solutions were adjusted to 7.2 and the experiments were repeated.

Bioluminescence and Chemiluminescence: Current Status P. E. Stanley and L. J. Kricka, eds., John Wiley & Sons (New York, 1991) pp. 427-432.

Thermal stability was determined by differential scanning calorimetry. The concentration of protein was 0.5mg/ml. The buffer used was 0.5M, pH 7.7 Glycylglycine. The scanning range was from 30°C to 70°C. UV absorbance was also used to determine the thermal denaturation curve.

RESULTS AND DISCUSSION

Both luciferases are not denatured by urea concentrations lower than 0.1M, at pH 7.7. They begin to denature at urea concentrations larger than 0.1M. When the urea concentration is larger than 3 M, both luciferases appear to be maximally "denatured" (Fig.1.a,b). There are no significant differences between the urea denaturation curves of these two luciferases. The activity (light output) measurements also support the above results (fig.2). Both luciferases begin to denature when the concentration of guanidinium chloride is greater than 0.1M, at pH 7.7, and are maximally denatured at 3M GdnCl (Fig. 3.a,b). When the pH is decreased to 7.2, the urea concentration for 50% denaturation decreases from 1.8M to 1M and GdnCl concentration for 50% denaturation decreases from 0.5M to 0.4M. The light intensity decreased 30% (2).

Scanning calorimetry curves show that the Sigma luciferase denatures at about 40°C and aggregates at 54°C. Thermal denaturation curves determined by UV absorbance at 280nm also show that both luciferases denature at about 40°C.

Firefly luciferase (photinus pyralis) is composed of 550 amino acids. The amino acid sequence was determined by the analysis of cDNA and genomic clones by Wood et al (3). Sixty percent of its amino acids are nonpolar (4), so it aggregates easily in aqueous solution. Urea and GdnCl can cause denaturation of both the Sigma and the recombinant luciferase. The conformational stability is poor, possibly because luciferase contains only six to seven sulfhydryl groups (5) which are important in protein structure and activity. Anions such as sulfate and chloride will inactivate the activity of luciferase (6). Both luciferases are thermally labile. They denature at low temperature, 40°C, probably due to their weak non-covalent interactions. At higher temperature they aggregate very quickly and lose their activity completely. This work is ongoing (7).

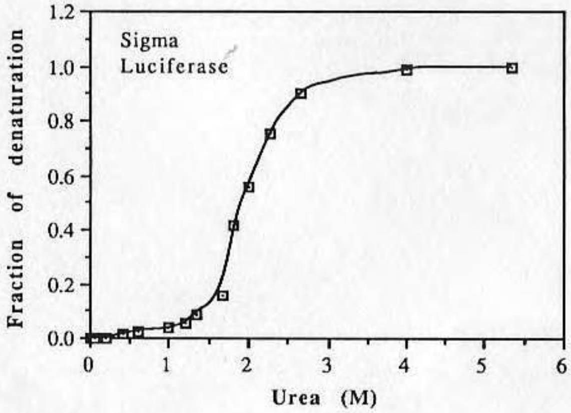

Fig.1.a Tryptophan fluorescence of Sigma luciferase (0.3mg/ml in 0.025M Glycylglycine) as a function of urea concentration (excitation wavelength 280nm, emission wavelength 340nm). Curve assumes a simple two-state denaturation model(2). The urea concentration for 50% "denaturation" is 1.8M.

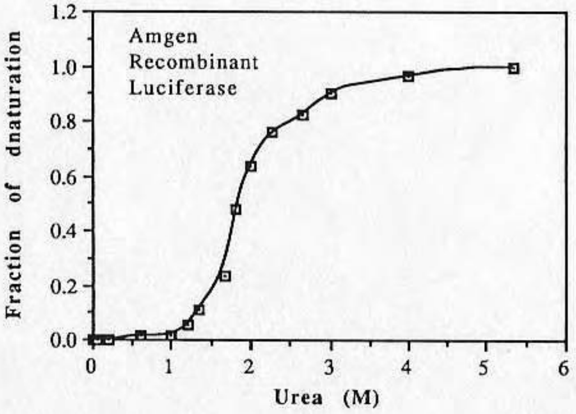

Fig.1.b Tryptophan fluorescence of recombinant luciferase (0.3mg/ml in 0.05M Trizma succinate) as a function of urea concentration (excitation wavelength 280nm, emission wavelength 340nm). Curve assumes a simple two-state denaturation model(2). The urea concentration for 50% "denaturation" is 1.8M.

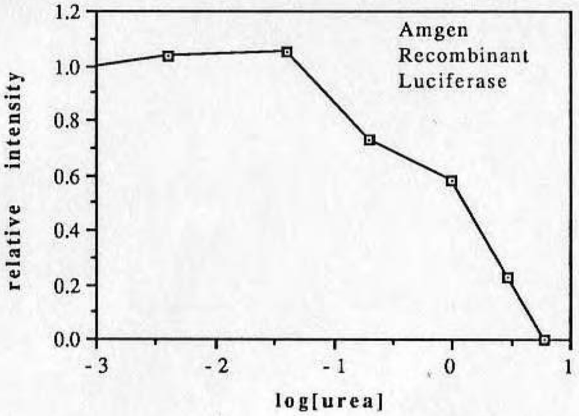

Fig.2 Relative intensity (based on solution without addition of urea) of the recombinant luciferase-luciferin system at different urea concentrations. Light output appears consistent with the fluorescence "denaturation" results, i.e. the enzyme is apparently inactivated at high urea concentration. The data for Sigma luciferase is very similar (not shown). The apparent small increase in light output at urea concentrations lower than 0.1M may be a real effect. This is being further studied.

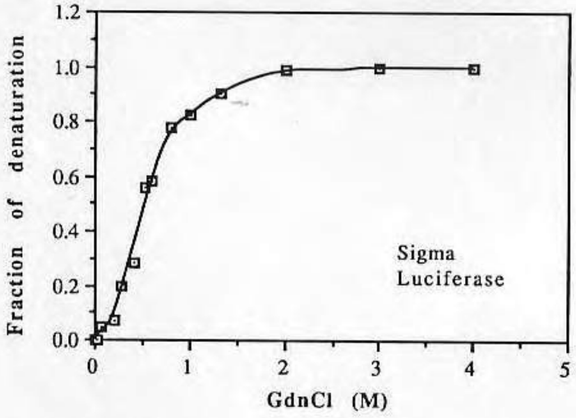

Fig.3.a Tryptophan fluorescence of Sigma luciferase (0.3mg/ml in 0.025M Glycylglycine) as a function of guanidinium chloride concentration (excitation wavelength 280nm, emission wavelength 340nm). Curve assumes a simple two-state denaturation model(2). The guanidinium chloride concentration for 50% "denaturation" is 0.5M.

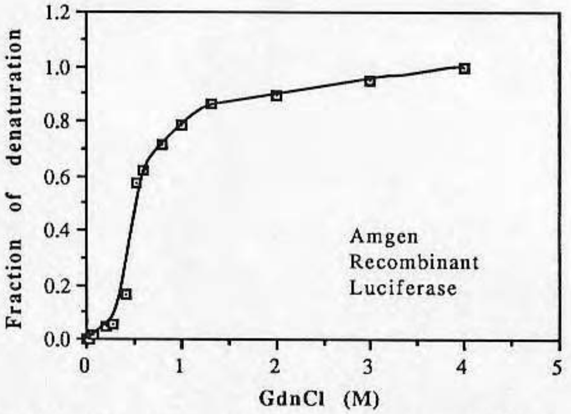

Fig.3.b Tryptophan fluorescence of recombinant luciferase (0.3mg/ml in 0.05M Trizma succinate) as a function of guanidinium chloride concentration (excitation wavelength 280nm, emission wavelength 340nm). Curve assumes a simple two-state denaturation model(2). The guanidinium chloride concentration for 50% "denaturation" is 0.5M

SUMMARY

Luciferase is hydrophobic and unstable in aqueous solution. Both the Sigma and recombinant luciferases are thermally labile ($T_d=40^oC$). Other hydrophobic proteins, such as lysozyme, can have much higher denaturation temperature.(8). The luciferases are also easily denatured by urea and guanidinium chloride. The anions easily inactivate luciferase possibly because they first denature the active sites of luciferase. It is important to find a stabilizer to protect luciferase from denaturing in aqueous solution. The stabilization of the enzyme by nonionic surfactants, such as PVP and PEG, has been studied (6). Other hydrophobic proteins may be helpful to enhance the stability of luciferase.

ACKNOWLEDGEMENTS

This work is supported by Protein Solutions Inc., Salt Lake City, Utah, USA.

REFERENCES

1. C. Nick Pace, B.A. Shirley and J.A. Thomson, Measuring the Conformational Stability of a Protein. In Protein Structure, T.E. Creighton(Eds), IRL Press, p.316(1989).
2. P.Y. Yeh, M.S, Thesis, Department of Materials Science and Engineering, University of Utah, Salt Lake City, Utah(1989).
3. J.R. DeWet, K.Y. Wood, M. Deluca, D.R. Helinski and S. Subramani, Firefly Luciferase Gene: Structure and Expression in Mammalian Cells, Mol. Cell. Biol. 7, p.725-737(1987).
4. C. R. Cantor and P. R. Schimmel, Biophysical Chemistry, 1, San Franciso, W.H. Freeman and Company, p.52(1980).
5. M. Deluca, G.W. Writz and W.D. McElory, Role of Sulfhydryl Groups in Firefly Luciferase. Biochem. 3, p.935-939(1960).
6. L.J. Kricka and M. De Luca, Effects of Solvents on Catalytic Activity of Firefly Luciferase. Archives of Biochemistry and Biophysics 217, p.674-681(1982)
7. C.Y. Wang, M.S. thesis, Department of Bioengineering, University of Utah, Salt Lake City, Utah, in preparation.
8. A.P. Wei, J.N. Herron and J.D. Andrade, The Role of Protein Structure in Surface Tension Kinetics. In From Clone to Clinic, D.J.A. Crommelin(Ed) in press(1990)

to smaller area at a specific surface pressure. There was a transition from liquid to solid state at π =8 mN/m (8), hence, less free space at lipid-water interfaces was available for luciferase and the $\Delta\pi$ was smaller for the DPPC monolayers. DOPC, with longer aliphatic chains and with a double bond on each chain, was more difficult to compress (less lateral compressibility). It remained in liquid state when π increasing to 25 mN/m. Two factors may contribute to the higher $\Delta\pi$: more free space at lipid-water interfaces is available for luciferase and longer aliphatic chains of DOPC may stabilize luciferase at lipid-water interfaces. DOPS had the same aliphatic chain as DOPC. The polar head of DOPS had a negative charge, the same as overall surface charge of luciferase (I.P.=6.5). The electrostatic interaction between DOPS and luciferase may contribute to the increase of $\Delta\pi$. The relationship between the surface concentration of luciferase and the surface pressure should be studied in the future work to further understand the behavior of luciferase at interfaces.

ACKNOWLEDGEMENTS

The authors would like to thank Dr. N. N. Ugarova, Dr. D. Grainger, and Dr. V. Hlady for their suggestions and guigance. This work was supported by Center for Biopolymers at Interfaces, University of Utah.

REFERENCES

1. Hlady, V., Yeh, P., and Andrade, J. D. Adsorption of Firefly Luciferase at Interfaces Studied by Total Internal Reflection Fluorescence Spectroscopy. J. Fluorescence 1991;1:47-55.
2. Ugarova, N. N.. Luciferase of Luciola mingrelica Fireflies. Kinetics and Regulation Mechanism. J. Biolum. Chemilum. 1989;4:406-418.
3. Dukhovich, A. F., Philippova N. Ju., Jefimov, A. I., and Ugarova, N. N.. Choline-containing Phospholipids as Specific Activators and Stabilizers of Firefly Luciferase. Dokl. Acad. Nauk SSSR 1988;298:1257-1260.
4. Goodin,D. L., Schmuck, M. N., Nowlan, M. P., and Gooding, K. M.. Optimization of Preparative Hydrophobic Interaction Chromatographic Purification Methods. J. Chromatography 1986;359:331-337.
5. Tripp, B. C.. Digital Image Pendent Drop Experimental Surface Tension Technique. In: Dynamic Surface Tension of Model Protein Solutions Measured Via Pendent Drop Tensiometry, Ph.D. thesis. University of Utah, 1992.
6. Trurnit, H. J.. A Theory and Method for the Spreading of Protein Monolayer. J. Colloid Sci 1960;15:1-13.
7. MacRitchie, F.,and Ter-Minassian-Saraga, L.. Stability of Highly Compressed Spread Monolayer of ^{125}I-labelled and Cold BSA. Prog. Colloid Polymer Sci 1983;68:14-19.
8. Ibdah, J. A., and Phillips, M. C.. Effects of Lipid Composition and Packing on the Adsorption of Apolipoprotein A-I to Lipid Monolayers. Biochemistry 1988;27:7155-7162.

INTERFACIAL BEHAVIOR OF FIREFLY LUCIFERASE

Chung-Yih Wang and Joseph D. Andrade
Department of Bioengineering, University of Utah, Salt Lake City, UT 84112, USA

INTRODUCTION

Firefly luciferase from Photinus pyralis is a hydrophobic protein. Sixty percent of its amino acid residues are hydrophobic. The adsorption of firefly luciferase onto hydrophobic quartz slide (modified by dimethyldichlorosilane), air-water interface, and hydrophilic quartz slide had been studied by V. Hlady et al.(1). They suggested that the interfacial behavior of luciferase was influenced by its hydrophobic nature. A phenylsuperose chromatography column is used to estimate the effective surface hydrophobicity. Bovine serum albumin, whose molecular weight (dimension 30x80x110 Å) is similar to luciferase, and lysozyme are used as model proteins. The results show that the hydrophobicity of firefly luciferase is moderate, suggesting that a portion of its hydrophobic residues are buried inside.

Dynamic surface tension of firefly luciferase is measured via pendant drop tensiometry. When luciferase concentration is high, the fast decrease of surface tension suggests that luciferase is very surface active. When luciferase concentration is low, a short induction time is observed. Luciferase adsorption at the air-water interface is studied via the Wilhelmy plate method.

N. N. Ugarova et al. reviewed the kinetics and regulation mechanism of firefly luciferase from Luciola mingrelica (2). They suggested that the choline-containing phospholipids were necessary for luciferase to maintain activity (3). To understand the role of lipids in enzyme activity, it is important to study the behavior of luciferase at lipid-water interfaces. Three different lipids, 1,2-dipalmitoyl-sn-glycerol-3-phosphocholine (DPPC), 1,2-dioleoyl-sn-glycerol-3-phosphocholine (DOPC) and 1,2-dioleoyl-sn-glycerol-3-[phospho-L-serine] [sodium salt] (DOPS), are used to study luciferase-lipid interactions. A lipid monolayer is spread and compressed to gas, liquid or solid phase. Luciferase is then injected from the subphase. The surface pressure change is measured with a Wilhelmy plate. The results suggest that luciferase interacts with phospholipid membrane and may even penetrate into lipid membranes.

MATERIALS AND METHODS

Bioluminescence and Chemiluminescence: Status Report A. A. Szalay, L. J. Kricka and P. E. Stanley, eds., John Wiley & Sons (New York, 1993) pp. 99-103.

Reagents

Firefly luciferase (Photinus pyralis), bovin serum albumin, lysozyme and glycyl-glycine were obtained from Sigma. Glycyl-glycine buffer was prepared in distilled water and the pH adjusted by 4 mol/l NaOH. The proteins were dissolved in 0.45 mol/l, pH=7.8 glycyl-glycine buffer respectively to make 1.2 mg/ml solution. No dithiothreitol was added in the luciferase solution. 1,2-dipalmitoyl-sn-glycerol-3-phosphocholine (DPPC), 1,2-dioleoyl-sn-glycerol-3-phosphocholine (DOPC) and 1,2-dioleoyl-sn-glycerol-3-[phospho-L-serine] [sodium salt] (DOPS) were purchased from Avanti Polar-Lipid, Inc.. All lipids were dissolved in chloroform to make a 36 μmol/ml solution.

Effective Surface Hydrophobicity

Protein interacts more strongly with phenyl groups than with most other nonpolar functional groups (4). A Phenyl Superose Fast Protein Liquid Chromatography (FPLC, from Pharmacia) was used to measure the retention time of the proteins. The column was washed and equilibrated with 0.025 mol/l glycylglycine buffer (pH 7.8). 100 μl of luciferase, albumin and lysozyme solutions were injected separately into the column. The UV absorbance at 280 nm was measured on a continuous basis. The retention time of protein was calculated and used to compare the effective surface hydrophobicity.

Dynamic Surface Tension

A pendant drop tensiometer was used to measure the dynamic surface tension of luciferase. Low concentration (0.01mg/ml) and high concentration (0.2 mg/ml) luciferase solutions were extruded into a needle tip separately. An image of the pendant drop was taken and analyzed via pendant drop shape analysis software (5).

Luciferase Monolayer and Luciferase-Lipid Interaction

A Lauda Langmuir film balance was used to study luciferase monolayer. 50 μl 0.6mg/ml luciferase was spread by Trurnit's method (6). The spreading rate was 0.1 ml/min. After 10-15 min for equilibrium, the barrier was moved at 10 cm^2/min. The π-A curve was obtained by recording the output of pressure transducer and surface area potentiometer.

A mini-trough (15x 97.2x 6.8 mm) made of Teflon was used to study protein adsorption to the air-water interface and protein-lipid interactions. The Wilhelmy plate, cut from Whatman No.1 filter paper, 1x1 cm, was used to measure the surface tension. The mini-trough was filled with 10 ml glycyl-glycine buffer (0.45 mol/l, pH=7.8). 50 μl of luciferase (1.2 mg/ml) was injected to the subphase. The change of surface tension was recorded by electrobalance. The surface pressure was calculated as : $\pi = \gamma_0 - \gamma$

A lipid monolayer was spread by a microsyringe and compressed to its gas, liquid, or solid phase. After equilibrium, 50 μl luciferase (1.2 mg/ml) solution was injected to the subphase. The change of surface tension causing by adsorption / penetration of luciferase was measured.

RESULTS AND DISSCUSSION

The retention time of three model proteins was shown in Table 1. Lysozyme with smaller molecular weight and percentage of nonpolar amino acids had a very long retention time. BSA and luciferase had shorter retention time. This suggests that only a portion of the hydrophobic patches of luciferase are exposed outside.

Table 1 Protein Retention Time on Phenyl Superose Column

Protein	Retention Time (min)	Molecular Weight	Hydrophobic residues (%)
Luciferase	8.5	62000	60
BSA	4	66000	37
Lysozyme	>30	14300	40

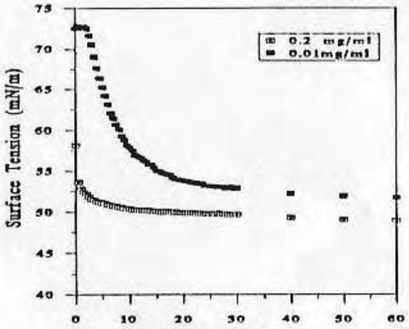

Fig.1 Dynamic surface tension of luciferase. The bulk concentration of luciferase was 0.01mg/ml and 0.2 mg/ml. The mesoequilibrium surface tension at 60 minutes was 51.6 mN/m and 48.9 mN/m, respectively. The induction time for 0.01mg/ml luciferase solution was 2.5 minutes.

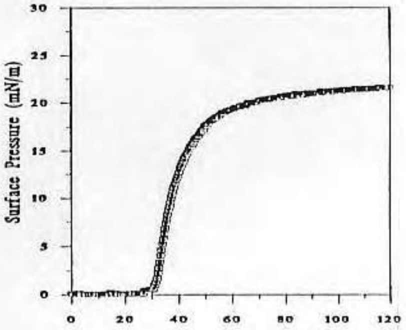

Fig.2 Adsorption of luciferase at air-water interfaces. 50 μl luciferase solution (1.2 mg/ml) was injected from the subphase.

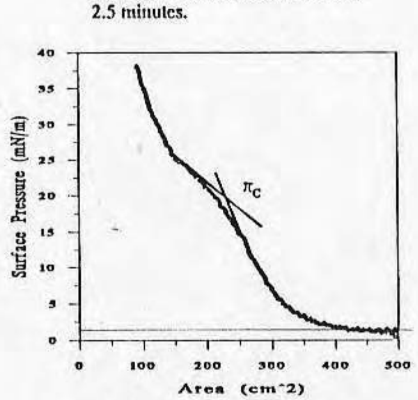

Fig.3 π-A curve of luciferase monolayer. 50 μl luciferase solution (0.6 mg/ml) was spread by Trurnit's method. The spreading rate was 0.1 ml/min and the compressing speed was 10 cm^2/min.

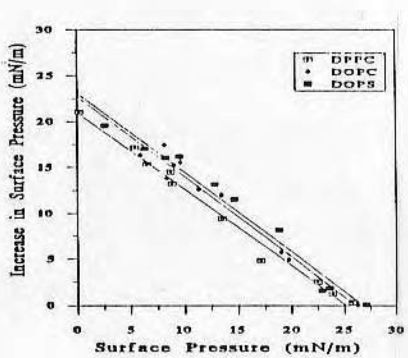

Fig.4 Change in surface pressure (Δπ) vs surface pressure of lipid monolayers. Lipids were dissolved in chloroform and spread by microsyringe. Lipid monolayers were compressed to desired pressure. After equilibrium, 50 μl luciferase solution (1.2 mg/ml) was injected to the subphase.

The results of the dynamic surface tension were given in Fig.1. A 2.5 min induction time was observed for luciferase with concentration 0.01 mg/ml. Lysozyme and BSA with the same concentration in PBS buffer showed 90 min and no induction period respectively (5). For luciferase with higher concentration, 0.2 mg/ml, the surface tension decreased immediately to 51.8 mN/m at 2.5 min. Lysozyme and BSA with higher concentration, 1 mg/ml, lowered the surface tension to 65.5 mN/m and 58.0 mN/m at 2.5 min respectively (5). The results show that luciferase is more surface active than lysozyme and BSA. Luciferase may adsorb to the air-water interface and unfold quickly to expose its hydrophobic residues at the air-water interface. Fig.2 shows the adsorption of luciferase at the air-water interface. The equilibrium surface pressure was 21.5 mN/m which was consistent with the surface pressure calculated from the dynamic surface tension of low luciferase concentration at 60 min. The study of protein behavior at the air-water interface suggests that there is a critical surface concentration for reducing the surface tension at the air-water interface. When bulk solution has high protein concentration (over the critical concentration), there is no induction period, and the surface tension drops rapidly. If the bulk solution has low protein concentration, an induction period is necessary to build-up a critical surface concentration. The effective surface hydrophobicity of native protein is not the only factor that determines the interfacial behavior of protein. The stability of protein at the air-water interface is also important because the unfolding of protein at the interface may change the effective surface hydrophobicity and adsorption behavior of protein.

Spreading of luciferase on the air-water interface caused a surface pressure increase. When luciferase monolayer was compressed, it showed a sigmoid π-A curve (fig.3). F. MacRitchie et al. defined the surface pressure of the first inflection point as the critical surface pressure, π_c (7). They found that the π_c of BSA was 16 mN/m. Our result showed that the of luciferase, 19.5 mN/m, was close to the mesoequilibrium pressure of the dynamic surface tension study. When the pressure was higher than critical pressure, hysteresis of the π-A curve became apparent and a gel-like structure at the air-water interface was formed. Both the desorption of luciferases from the air-water interface and the stronger intermolecular interactions, caused by highly unfolded state of luciferases and less available space between luciferases, may contribute to the hysteresis and the gel-like structure.

When different lipid monolayers were spread and compressed to the desired pressure, the luciferase injected from the subphase increased the surface pressure (Fig.4). The increase of surface pressure was higher at the gas-state lipid monolayer than the liquid-state lipid monolayer. There was no increase of surface pressure when the lipid monolayer was compressed to high surface pressure, π=30 mN/m. The adsorption of apolipoprotein A-I to lipid monolayers showed similar behavior (8). This suggests that luciferase can adsorb to air-water interfaces when the lipid monolayer is in the gas-state. When the lipid monolayer is closely packed, luciferase interacts with the polar head of the lipid monolayer and then partially penetrates into the lipid monolayer. At the same surface pressure, DPPC had the smallest Δπ, while DOPS had the largest Δπ. DPPC, with shorter aliphatic chains, could be compressed

PURIFICATION AND PRESERVATION OF FIREFLY LUCIFERASE

Chung-Yih Wang and Joseph D. Andrade
Department of Bioengineering , 2480 MEB, University of Utah, Salt Lake City, UT 84112, USA

Introduction

Most proteins in solution denature or deteriorate rapidly. Highly purified firefly luciferase was shown to be surface active (1) and denatured at low urea concentration (2). It is necessary to study the preservation of highly purified firefly luciferase as it is so important for diagnostic and sensor applications. A simple air drying protocol was studied using trehalose as protectant. Trehalose showed fair stabilization and cryoprotection of luciferase solutions. After drying in air, with or without trehalose, luciferase was stored at room temperature for one month. The activity of luciferase dried from solution containing 100 mg/ml trehalose was three fold higher than that without trehalose.

Immobilization of protein on different supports is important to the development of biosensors. There are three categories of immobilization techniques: chemical modification, physical adsorption and gel entrapment. However, modifying procedures such as covalent coupling usually produce some protein inactivation. The exposure of protein at air-water or air-solid interfaces may also lead to the denaturation of protein.

The gel entrapment technique has the advantages of better protein stability and ease of processing. Because firefly luciferase is very labile, a low gelling temperature(26 -30°C) agarose was used as a medium to entrap luciferase. Trehalose added to the gel can prevent the collapse of gel when drying and rehydrating (3). The thin bioluminescent film containing trehalose can be stored under less critical conditions and is ready to use for ATP analysis.

Recombinant firefly luciferase provides an excellent source for bioluminescence assay. The crude luciferase extracted from gene engineered *E. coli* (with *Psx(tac)Ppy*) was fractionated with ammonium sulfate, and further purified with a Pharmacia FPLC system. A purification factor of 68 fold for recombinant luciferase was achieved. Recombinant luciferase is less expensive and favorable for mass production of the thin bioluminescent films.

Materials and Methods

Luciferase from *Photinus pyralis* was obtained from Sigma Chemical Company and used in the preservation and gel entrapment study. Low melting temperature SeaPlaque agarose was purchased from FMC Bioproducts. All other reagents were obtained from Sigma.

Pharmacia FPLC system was used for chromatography. Pharmacia 16/60 Superdex prep grade gel filtration column and Mono Q HR 10/10 anion exchange column were used for protein purification. Luciferase activity was checked as before (2).

Luciferase solution (0.0375 mg/ml in 0.45 M Glycylglycine buffer, pH=7.8) was prepared with 10 mg/ml, 100 mg/ml trehalose or without trehalose. An aliquot of 20 µl luciferase solution was dried in air at room temperature for 2 hours. The dry luciferase was stored at different temperatures. The activity of rehydrated luciferase was checked and compared with luciferase solution stored in the same condition.

Luciferase was mixed and entrapped in a low gelling temperature agarose gels (4). The SeaPlaque agarose powder was mixed with 0.45 M Glycylglycine buffer (pH=7.8) to make 1.5% (w/w) solution. The gel solution was heated to 80 °C and then cooled to 37 °C.

Luciferase solution was added to gel solution with or without 100 mg/ml (final concentration) trehalose. The same air-drying protocol was used to dry the agarose gel. The dry gel with entrapped luciferase was rehydrated with 20 µl deionized water and the activity was checked.

E. coli was grown using the method modified from K. Wood (5). 4 mM isopropylthiogalactoside (IPTG) was added to the culture as the inducer of *tac* promotor. The *E. coli* pellet was collected and resuspended in extraction buffer (100 mM tricine with 1mM EDTA, 2mM DTT, and 2 % glycerol, pH=7.8). After two freez-thaw cycles, *E. coli* was disintegrated at 4 °C for 2 hours with 1mg/ml lysozyme. Then 2mg/ml protamine was added and the *E. coli* suspension was centrifuged at 13,000g, 4 °C for 25 min. to precipitate nucleic acids and cell debris. The supernatant was then fractionated with 40% and 65% ammonium sulfate. The precipitate from 65% fractionation was resuspended in 30 mM Tris buffer (pH=7.8). The suspension was filtered and applied to Pharmacia HiLoad 16/60 Superdex 200 column and Mono Q anion exchange column (with 0 to 0.5 M NaCl gradient in 30 mM Tris buffer). The eluate with luciferase activity was collected. Protein concentration was estimated by spectroscopic method (6). A sodiumm dedecyl sulfate-polyacrylamide gel electrophoresis (SDS-PAGE) was run with Pharmacia Phast system to check protein purity.

Results and Discussion

Solution of low luciferase concentration without addition of protectants, quickly lost 60% activity when stored at 4 °C for one week. Luciferase solution with 100 mg/ml trehalose retained up to 60% activity at the same storage conditions. However, after one month storage, all the luciferase solutions stored above 4 °C lost their activity. Frozen and stored without trehalose at -20 °C for one week resulted in about 70% loss in activity. Addition of trehalose provided some cryoprotection (figure 1-3). Samples air dried without trehalose lost about 40% activity, but the addition of trehalose kept 10% more activity. After one month storage at room temperature, the sample with trehalose retained about 50% activity, comparable to dry luciferase stored at -20 °C. The samples without trehalose retained only 15% activity. The reason dry luciferase lost 25% more activity after storage at -20 °C for one month may be caused by the content of residual water in the sample. Luciferase in dry state can be successfully stored at room temperature with the protection of 100 mg/ml trehalose. A lower concentration of trehalose (10 mg/ml) provids only minor protection.

Both gels, with or without trehalose, stored in wet form for one month resulted in loss of luciferase activity (figure 4-6). To improve the shelf life of entrapped luciferase, both agarose gels were dried in air at room temperature for two hours, stored at different temperatures and reconstituted with water before use. The activity of luciferase in both dry gels was retained after one month storage. Addition of trehalose prevented the collapse of agarose gel (4). Leakage of luciferases from agarose gel can be reduced by addition of trehalose to the gel (data not shown).

Bioluminescence and Chemiluminescence: Fundamentals and Applied Aspects
A. K. Campbell, L. J. Kricka and P. E. Stanley, eds., John Wiley & Sons
(New York, 1994) pp. 423-426.

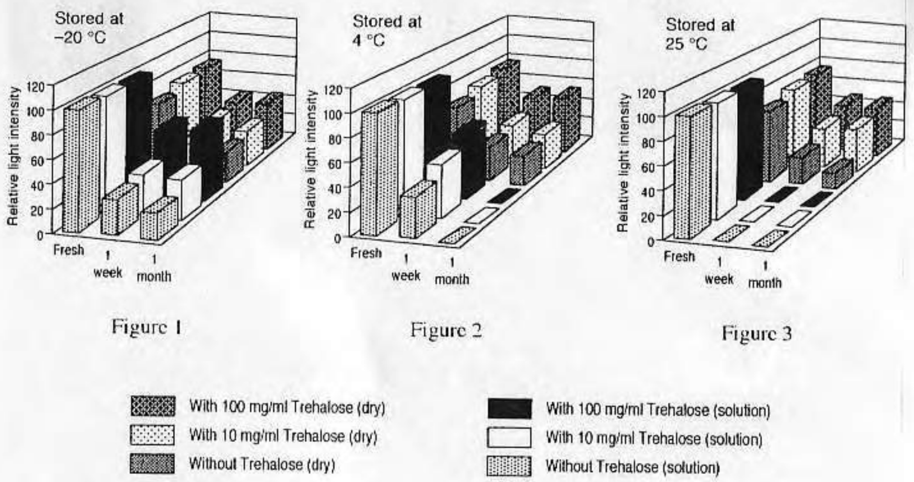

Figure 1 Figure 2 Figure 3

Figures 1–3. Activity of luciferase (0.0375 mg/ml in 0.45 M glycylglycine buffer, pH 7.8); stored with different storage time. The light intensity was measured at room temperature. Dry luciferase was reconstituted with water before test.

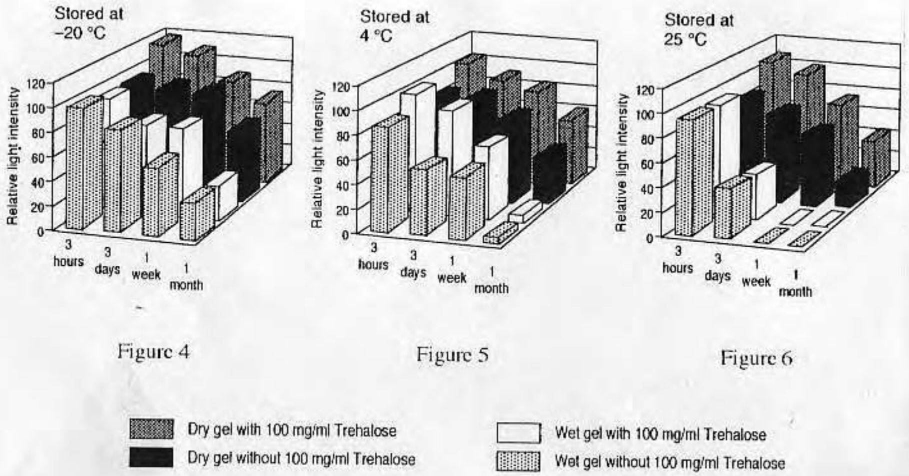

Figure 4 Figure 5 Figure 6

Figures 4–6. Activity of gel entrapped luciferase (0.0375 mg/ml luciferase, pH 7.8); stored with different storage time. The light intensity was measured at room temperature. Dry gel was reconstituted with water before test.

Table 1. Purification scheme for recombinant firefly luciferase.

Steps in Purification	Total Protein (mg)	Specific Activity (count/mg)	Purification Factor (fold)
Crude extract	354	665	1
Precipitate after saturation by 65% ammonium sulfate	50.1	2337	3.6
Eluate after chromatography on HiLoad column	8.1	10518	15.8
Eluate after chromatography on Mono Q column	1.6	45650	68.6
Sigma Luciferase	-	35539	-

Recombinant luciferase was purified from the lysate of *E. coli*. The lysate had an extremely high viscosity, caused by high content of nucleic acids. Protamine was added to precipitate those nucleic acids. The scheme of purification was shown in table 1. A purification factor of 68 fold was achieved after anion exchange chromatography. The result of SDS-PAGE showed a major band on 62 KD accompanied with very few low molecular weight impurity.

The use of trehalose in agarose gel permits the application of luciferase films which are not collapsed, are optically transparent, and maintain luciferase activity after one month storage. With less expensive recombinant luciferase, such films can be applied for broad biosensor applications.

Acknowledgements

We thank Dr. K. Wood for providing the gene engineered *E. coli* cell line with plasmid *Psx(tac)Ppy*.

References

1. Wang CY and Andrade JD, "Interfacial Behavior of Firefly Luciferase" in Bioluminescence and Chemiluminescence: Status Report, Szalay AA, Kricka LJ and Stanley PE, eds, Wiley, 1993; p.99-103.
2. Wang CY and Andrade JD, "Denaturation of Firefly Luciferase" in Bioluminescence and Chemiluminescence: Current Status, Stanley PE and Kricka LJ, eds, Wiley, 1991; p.427-432.
3. Roger BJ, United State Patent 4891319, 1990.
4. Wang CY and Andrade JD, Immobilization of Firefly Luciferase in Low-gelling Temperature Agarose, abstract, American Chemistry Society Meeting, Denver, 1993.
5. Wood KV, Luciferases of Luminous Beetles: Evolution, Color Variation, and Applications, Ph.D. dissertation, 1989.
6. Schleif RF and Wensick PC, Practical Methods in Molecular Biology, New York, Springer-Verlag, 1981.

SURFACTANTS AND COENZYME A AS COOPERATIVE ENHANCERS OF THE ACTIVITY OF FIREFLY LUCIFERASE

CY Wang and JD Andrade
Dept. of Bioengineering, University of Utah, SLC, UT 84112, USA

Introduction

Since protein folding depends on physical interactions with the solution, activators or inhibitors may modify protein structure via changes in the local solution environment, facilitating or inhibiting protein activity. Kricka and DeLuca found that nonionic surfactants, such as Triton X-100 and Tween 20, and some polymers, such as polyethylene glycol (PEG) and polyvinylpyrrolidone (PVP), stimulated luciferase activity (1). However, anionic and cationic surfactants failed to stimulate luciferase activity and behaved as inhibitors. They further titrated the active sites with dehydroluciferin and ATP-Mg^{2+} and showed the stimulation effect was not caused by recruitment of new active sites. Although the actual mechanism of stimulation is still unknown, they suggested that the binding of Triton X-100 or polymers to luciferase mat account for the stimulation effect. Other studies showed similar stimulation effects in some cases but not in others (2, 3). The inconsistent results may result from different preparations of firefly luciferases.

Coenzyme A (CoA) was found to reduce the decay rate of luciferase bioluminescence (4). Schroder found firefly luciferase (Photinus pyralis) was related to a plant enzyme, 4-coumarate CoA ligase, which utilized ATP and CoA (5). Since similarity between enzymes may suggest the conservation of specific functions, the existence of a CoA binding site is possible, although CoA is not a required substrate for firefly bioluminescence.

The enhancement effects of surfactants and polymers were determined with and without CoA. A significantly cooperative enhancement was observed in the presence of both surfactant/polymer and CoA. Triton X-100 was also found to be a protectant against the inhibition effect of 1,2-dioleoyl-sn-glycerol-3-[phospho-L-serine] (DOPS). Luciferase inactivated by DOPS recovered over 60% activity after incubation in Triton X-100.

Materials and Methods

Triton X-100 (avg. MW 650, density 1.059), Tween 20 (polyoxyethylene sorbitan monolaurate, MW 1228), PVP (MW 40,000) and PEG (MW 5,000) were purchased from Sigma. The stock solution for 10% (w/w%) Triton X-100 and Tween 20 and 10% (w/v%) PVP and PEG were prepared with glycylglycine buffer (0.45 mol/L, pH 7.8). The stock solutions were then diluted to 1%, and 0.1% with the same buffer.

Firefly luciferase (from Sigma, chromatographically prepared and lyophilized; showed a single band on SDS-PAGE) was used to prepare the enzyme-surfactant mixtures. 20 μL of luciferase solution (0.5 mg/mL) was mixed with 13.1 μL of glycylglycine buffer and 248.5 μL of surfactant or polymer solution. The final concentration of additives is 0.4800%, 0.0480%, and 0.0048%. In the control experiment, glycylglycine buffer was used to replace surfactant solution. 100 μL of luciferin stock solution (0.1 mmol/L luciferin and 10 mmol/L $MgSO_4$) was added to 20 μL of luciferase mixture and incubated for 3 minutes. 250 μL of ATP solution (10^{-4} mol/L or 10^{-6} mol/L) was then injected to initiate the bioluminescence reaction. The light intensity was recorded with a spectrofluorometer (I.S.S., Inc.).

The optimum concentration (the highest enhancement effect) of each individual additive was then mixed in combinations of two. The additivity of enhancements on luciferase activity was examined by assaying luciferase activity.

CoA (free acid, from Sigma) was added to ATP solution (10^{-4} mol/L and 10^{-6} mol/L) to make a 10^{-4} mol/L CoA solution. The ATP solution containing CoA was then added to the luciferase/surfactant mixtures and the enzyme activity determined as before.

For the protection experiment, 20 μL of luciferase (0.5 mg/mL) was first incubated with 248.5 μL Triton X-100 (10%) for 30 min. Preparation of 1,2-dioleoyl-sn-glycerol-3-phosphocholine (DOPC) and DOPS liposomes was described elsewhere (6). 13.1 μL of DOPS liposomes were added to the mixture and incubated for another 30 min. The final concentration of Triton X-100 was 0.48% and the molar ratio of DOPS to luciferase was 500:1. The activity of luciferase was then assayed. For the reactivation experiment, luciferase was first incubated with DOPS for 30 min. The Triton X-100 was then added and incubated for another 30 min. The activity of luciferase recoved was assayed. DOPC liposomes were used (in a molar ratio of 500 DOPC to 1 luciferase) to replace Triton X-100 and the experiments were repeated.

Results and Discussion

Some nonionic surfactants and polymers were effective in enhancing luciferase activity (1-3). In this study, all four additives were found to increase luciferase activity, which showed 28% to 118% higher initial velocity (maximum light intensity) at the 10^{-4} mol/L ATP concentration. PEG 5000 and Triton X-100 showed the most promiment enhancing effect at the peak intensity of bioluminescence. At the optimum concentration, Triton X-100 showed the slowest decay rate, which was maintained up to 326% of control at the plateau of bioluminescence, while PEG 5000 maintained the lowest bioluminescence (160%) in the same period (Table 1).

The optimum concentration for the four additives was further examined at 10^{-6} mol/L ATP. Higher stimulation effects at low ATP concentration was observed than at high ATP concentration (Table 1).

Table 1. Enhancement of additives at high and low ATP concentration. The bioluminescence intensity of pure luciferase solution is normalized as 100%.

Additives	Final concentration	Peak (%)	Plateau (%)	Peak (%)	Plateau (%)
		10^{-4} mol/L ATP		10^{-6} mol/L ATP	
Triton X-100	0.4800%	218	326	324	333
Tween 20	0.0048%	187	242	212	194
PEG 5000	0.4800%	198	160	267	140
PVP 40000	0.0480%	179	173	288	151

Bioluminescence and Chemiluminescence: Molecular Reporting with Photons
J.W. Hastings, L.J. Kricka, and P.E. Stanley, eds., John Wiley & Sons,
(New York, 1997) pp. 253 - 256.

The surfactants and polymers were mixed in pairs to examine the additivity of the enhancement effects. The results showed that Triton X-100 mixed with Tween 20 and PEG 5000 further enhanced the peak intensity 28 to 48%. There was no significantly further enhancement for the other combinations. The presence of other additives in the Triton X-100 solution further enhanced the light intensity at plateau. However, PVP and PEG hinder the enhancing effect of Tween 20 at plateau.

Coenzyme A was effective in preventing the decay of bioluminescence. The total light output increased 6 fold over a 30 sec period when using 10^{-4} mol/L ATP and 0.1 mol/L CoA as the substrates. CoA mixed with any one of the four surfactants/ polymers resulted in a significant cooperative enhancement (Table 2). The combination of Triton X-100 and CoA had the most significant enhancement, increasing the total light output up to 23 fold for the first 30 sec (Figure 1). The mechanisms of stimulation for these two chemicals was different and cooperative. A less prominent enhancement was also observed for 10^{-6} mol/L ATP.

Table 2. Cooperative enhancing effects of CoA (final concentration: 0.068 mmol/L) and surfactants/polymers (at concentration as Table 1). Light count was integrated for first 30 sec. The count of luciferase solution without additives and CoA was used as the reference. The enhancement was calculated by dividing each output result by the reference.

	Enhancement (fold)	
Components	ATP (10^{-4} mol/L)	ATP (10^{-6} mol/L)
Luciferase and CoA	7	1.1
Luciferase, CoA and Triton X-100	23	5.4
Luciferase, CoA and Tween 20	20	4.7
Luciferase, CoA and PEG 5000	12	1.9
Luciferase, CoA and PVP 40000	19	2.3

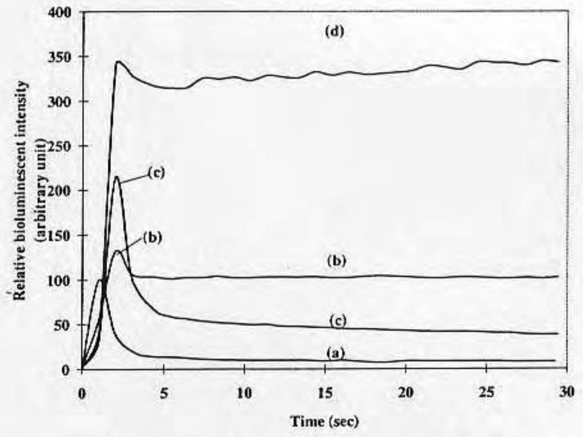

Figure 1. The Cooperative enhancement of Triton X-100 (0.4800%) and CoA on luciferase activity. (a) Luciferase; (b) luciferase with CoA; (c) luciferase with Triton X-100; (d) luciferase with CoA and Triton X-100.

Firefly luciferase was inactivated by negative charged lipids (6, 7). The presence of Triton X-100 (0.4800%) prevented inactivation by DOPS. Luciferase inactivated by DOPS can be partially reactivated by incubation with Triton X-100, the activity recovering from 17% to 64%. Although the mechanism is unknown, the recovered enzyme activity may be due to the replacement of DOPS by Triton X-100 at the same binding site; Triton X-100 may also enhance the activity of the remaining native enzyme. In the same experiment, DOPC was used to replace Triton X-100. There was no protection or reactivation effect for DOPC against DOPS.

The micelle environment was not required condition for the stimulation, since PEG and PVP do not form micelles. A large complex found by Kricka and DeLuca was proposed to be the enzyme-surfactant complex (1). The lack of an additivity effect between the combination of surfactants/polymers indicate a similarity to the enhancing mechanism. The binding of surfactants/polymers helps reactivate luciferase, which may have been inhibited by its substrates. Triton X-100 and Tween 20 may also help to modify the conformation and speed the release of oxyluciferin, enhancing enzyme turnover. Coenzyme A behaves differently with surfactants and polymers and probably binds to luciferase at a specific site. When added with Triton X-100, the bioluminescence intensity was enhanced further and maintained at a maximum level for at least 2 minutes. The high turnover rate was not inhibited by the accumulation of oxyluciferin. Other combinations with CoA produce less but still prominant total light output. The additivity effect enables a constant light output at high intensity. It is useful to develop direct reading biosensors which require those characteristics.

Acknowledgement

This work was partially supported by Protein Solutions, Inc., Salt Lake City, Utah via funding provided by an NSF STTR grant. We thank Drs. J. Herron and V. Hlady for access to equipment and facilities.

References

1. Kricka LJ, DeLuca M. Effect of solvents on the catalytic activity of firefly luciferase. Arch Biochem Biophys 1982;217:674-81.
2. Yeh PY. The properties of firefly luciferase in solution and at interfaces. Master thesis, University of Utah, 1989.
3. Simpson WJ, Hammond JRM. The effect of detergents on firefly luciferase reactions. J Biolumin Chemilumin 1991;6:97-106.
4. Airth RL, Rhodes WC, McElroy WD. The function of coenzyme A in luminescence. Biochim Biophys Acta 1958;27:519-32.
5. Schroder J, Protein sequence homology between plant 4-coumarate: CoA ligase and firefly luciferase. Nucleic Acids Res 1989;17:460-2.
6. Wang C-Y, Firefly Luciferase: Activity, Stability and Sensor Applications. Ph.D. Dissertation, University of Utah, Oct. 1996.
7. Dukhovich AF, Filippova NYu, Efimov AI, Ugarova NN, Berezin IB. Choline-containing phospholipids as specific activators and stabilizers of firefly luciferase. Dokl Akad Nauk SSSR, 1988;298:1257-60.

ANALYTICAL BIOCHEMISTRY **246**, 133–139 (1997)
ARTICLE NO. AB972006

\ WANG – 96

Specific Immobilization of Firefly Luciferase through a Biotin Carboxyl Carrier Protein Domain

Chung-Yih Wang, Sam Hitz, Joseph D. Andrade, and Russell J. Stewart
Department of Bioengineering, 2480 MEB, University of Utah, Salt Lake City, Utah 84112

Received October 28, 1996

Firefly luciferase (*Photinus pyralis*) was fused with a histidine tag and a biotin carboxyl carrier protein (BCCP) domain at its amino terminus. Highly purified recombinant luciferase was obtained by a one-step purification protocol, utilizing immobilized metal affinity chromatography. The novel BCCP–luciferase had properties, stability, and activity similar to those of native luciferase. The biotin molecule on the BCCP domain allowed specific immobilization of BCCP–luciferase on avidin-coated surfaces via the biotin–avidin interaction. © 1997 Academic Press

Firefly luciferase catalyzes bioluminescence in the presence of luciferin, adenosine 5′-triphosphate (ATP), magnesium ion, and oxygen with a quantum yield of 0.88 (1, 2). The firefly luciferase bioluminescent reaction can be used as an assay for ATP with detection limits of 10^{-13} M (3, 4). The sensitivity and convenience of the firefly luciferase assay have created considerable interest in firefly luciferase-based biosensors (5, 6).

Native luciferase, purified from firefly lantern, is relatively expensive. In addition, immobilization of native firefly luciferase by conventional methods has been inefficient, generally resulting in enzyme inactivation and low specific activities of immobilized firefly luciferase (7–11). Continued development of firefly luciferase-based biosensors would benefit from a source of inexpensive, easily purified, recombinant firefly luciferase that can be specifically immobilized with minimal enzyme inactivation. Therefore, we fused firefly luciferase with a six-histidine affinity tag and a biotin carboxyl carrier protein (BCCP)[1] domain. The histidine tag allows for one-step, affinity purification of firefly luciferase on an immobilized nickel column (12). The BCCP domain is a subunit of acetyl-CoA carboxylase that is posttranslationally modified with a biotin molecule covalently attached to a specific lysine residue (13). In this report, we demonstrate that the biotinylated firefly luciferase can be immobilized through the BCCP domain, with high specific activity, on avidin-coated solid supports.

MATERIALS AND METHODS

Construction of the pRSET-BCCP-luc plasmid. A *Bam*HI–*Stu*I fragment containing the firefly luciferase gene was isolated from the pGEM-luc plasmid (Promega Corp., Madison, WI). The *Bam*HI–*Stu*I luciferase fragment was ligated into the pRSET C expression vector (Invitrogen Corp., San Diego, CA) digested with *Bam*HI and *Pvu*II. The pRSET expression vectors utilized the T7 promoter and encoded six histidine residues on the amino side of the multiple cloning sites that can be used for immobilized metal affinity chromatography (IMAC). Colonies resulting from transforming the pRSET-luciferase ligation into *Escherichia coli* strain BL21 (DE3) were screened by sodium dodecyl sulfate–polyacrylamide gel electrophoresis (SDS–PAGE) for isopropyl β-D-thiogalactopyranoside (IPTG, from Sigma)-induced expression of firefly luciferase. A small-scale purification of the luciferase fusion protein on immobilized Ni^{2+} was carried out to test for luciferase activity (see below).

To fuse the BCCP with the luciferase, a BCCP DNA fragment was generated by PCR using the coding primer, GC TCT AGA ATG GAA GCG CCA GCA GC, and the noncoding primer, CCG CTT GTT GTT ATC GAA TCT AGA GC. Both primers encode a terminal *Xba*I site. The BCCP PCR product was digested with *Xba*I, gel purified, and ligated into pRSET-luc, which had been digested with *Nhe*I and treated with calf intestinal alkaline phosphatase. Following transformation into *E. coli* (BL21 (DE3)), clones with BCCP inserts

---

[1] Abbreviations used: BCCP, biotin carboxyl carrier protein; IMAC, immobilized metal affinity chromatography; IPTG, isopropyl β-D-thiogalactopyranoside; BSA, bovine serum albumin; DTT, dithiothreitol; PBS, phosphate-buffered saline.

0003-2697/97 $25.00
Copyright © 1997 by Academic Press
All rights of reproduction in any form reserved.

were identified by SDS–PAGE of cell lysates of IPTG-induced cultures. Insertion of the BCCP domain resulted in an increase of about 8 kDa in the molecular weight of the expressed proteins. Plasmids were purified from positive clones and restriction mapped to verify the correct insertion of the BCCP domain.

Purification of BCCP–luciferase. A 2-ml culture (LB plus 50 μg/ml ampicillin) was inoculated with a single colony from a freshly streaked plate. The culture was incubated at 37°C for 6–14 h and then used to inoculate a 200-ml culture (LB plus 50 μg/ml ampicillin). The 200-ml culture was grown for 6 h at 37°C. The temperature was then lowered to 22°C and expression was induced with 0.2 mM IPTG. Following overnight induction, the cells were harvested by centrifugation (7000 rpm, 20 min, Beckman JA-10 rotor). The cell pellets were washed with 10 ml Tris buffer (50 mM, pH 7.8) and repelleted. The wet cell pellets were weighed and then stored at −70°C.

To prepare luciferase, the frozen cells were thawed on ice and resuspended in 15 ml lysis buffer (50 mM Tris, pH 7.8) plus 1 mM phenylmethylsulfonyl fluoride (PMSF, Sigma). The cells were lysed by sonication. Sonication was done in three 20-s bursts with the cells on ice to prevent excessive heating of the lysate. The cell lysate was clarified by centrifugation (15,000 rpm, JA-17 rotor, 4°C, 25 min). The clarified lysate was applied to Ni–NTA agarose (Qiagen, Inc.) column that had been preequilibrated with lysis buffer. The Ni–NTA column was washed with three column volumes of lysis buffer and then eluted with an imidazole step gradient (10, 50, 100, 250, and 500 mM imidazole in Tris, pH 7.8). The histidine-tagged BCCP–luciferase was eluted with 100–500 mM imidazole. The BCCP–luciferase was desalted and changed into storage buffer (0.45 M glycylglycine, pH 7.8) using a prepacked Sephadex G-25 column (PD-10 column, Pharmacia). The desalted BCCP–luciferase was concentrated with a Centriprep-10 concentrator (Amicon, Inc.). The purity of the BCCP–luciferase was estimated by SDS–PAGE.

Specific activity and storage stability of BCCP–luciferase. BCCP–luciferase concentrations were estimated with a Bio-Rad protein assay kit (Bio-Rad, Inc.). Bovine serum albumin (BSA) was used as a standard. Bioluminescence was assayed by mixing 20 μl BCCP–luciferase (0.2 mg/ml) with 100 μl assay buffer (0.1 mM luciferin, 10 mM $MgSO_4$, and 25 mM glycylglycine, pH 7.8). To initiate bioluminescence, 250 μl of ATP solution (0.1 mM in 25 mM glycylglycine, pH 7.8) was added to the luciferin–luciferase solution. Bioluminescence was recorded with a spectrofluorometer (I.S.S., Inc.). The storage stability at 4 and −20°C of recombinant luciferase was compared with native luciferase (from Sigma). Glycerol was added (50% v/v final) to freshly prepared BCCP–luciferase (0.2 mg/ml) and to native luciferase in 0.45 M glycylglycine, pH 7.8. For comparison, an equal volume of water was also added to the luciferase solutions. The activity of luciferase was determined after increasing period of storage.

The extent of biotinylation on BCCP–luciferase. SoftLink soft release avidin resin (Promega) is a methacrylate polymeric gel filtration matrix covalently bound with monomeric avidin. The binding capacity is 32.15 nmol biotinylated cytochrome c per milliliter of resin. The avidin resin was packed in column (0.5-ml bed volume) and washed with four column volumes of buffer (0.45 M glycylglycine, pH 7.8). One milliliter of BCCP–luciferase (0.4 mg/ml) was then applied to the column. The first 0.25 ml of luciferase-free eluate was discarded. The rest of the eluate was collected and reapplied to the column three times. To ensure that the binding of BCCP–luciferase to avidin resin was complete, the final eluate was applied to a second avidin resin column and the above binding procedure was repeated.

The amount of BCCP–luciferase before and after binding was determined by UV absorbance at 280 nm. BSA was used in the same procedure to determine the dilution factor. The activity of BCCP–luciferase in solution, before and after binding, was also determined.

Urea and thermal denaturation of native luciferase and BCCP–luciferase. Native luciferase and BCCP–luciferase were dissolved in glycylglycine buffer to make 0.65 mg/ml solution separately. Urea (absolute grade, Research Plus Inc.) in 0.45 M glycylglycine, pH 7.8, was added to native luciferase and BCCP–luciferase to a final concentration ranging from 0 to 6 M. After 5 min, the luciferase intrinsic fluorescence (305 to 385 nm) was determined using a multifrequency fluorometer (I.S.S., Inc.). The enzyme activity after incubated with urea was also assayed.

Thermal denaturation was measured by the change of enzyme activity when temperature was increased from 10 to 44°C. Luciferase was incubated 10 min at each temperature before the enzyme activity was determined. BCCP–luciferase incubated with avidin (in a molar ratio of 1 to 3.6) was studied with the same method.

Immobilization of BCCP–luciferase on avidin-coupled Emphaze beads. The preparation of avidin-coupled Emphaze beads was described elsewhere (14). BCCP–luciferase and native luciferase (0.5 mg/ml in phosphate buffer, pH 8) directly immobilized on Emphaze beads without avidin were also prepared with the same method. Twenty milligrams of avidin-coupled Emphaze beads (0.22 mg avidin on the beads) was mixed with 0.6 ml of supernatant of cell lysate or purified BCCP–luciferase (0.5 mg/ml). A brief rocking was applied to the mixture for the binding of BCCP–luciferase to avidin. The mixture were then loaded into a

Bio-Spin chromatography column (Bio-Rad). The beads settled to the bottom of the column and the solution was collected and reapplied to the column. After two cycles of reloading, the beads were washed with 0.8 ml washing buffer (25 mM glycylglycine buffer with 2 mM dithiothreitol (DTT), pH 7.8) three times. The beads with immobilized BCCP–luciferase were stored in washing buffer at 4°C.

The stock solution containing 0.5 mM luciferin, 10 mM $MgSO_4$, and 2 mM DTT was prepared with 25 mM glycylglycine buffer, pH 7.8. ATP solution (10^{-4} M) was prepared with the same buffer. The column packed with immobilized luciferase beads was installed in the holder of a spectrofluorometer. Two hundred fifty microliters of ATP solution was mixed with 100 μl of stock solution and applied to the column. The bioluminescence emitted from the column was recorded. The beads containing immobilized luciferase were regenerated by washing with three aliquots of 0.8 ml washing buffer. The activity of luciferase on the regenerated beads was tested immediately or tested after storage at 4°C. The activity of immobilized BCCP–luciferase, washed and stored without 2 mM DTT, was also studied.

Immobilization of BCCP–luciferase on avidin-coupled quartz slide. The quartz slides (9.5 mm by 25 mm), cleaned with chromic acid, were silanized by immersion in 5% (v/v) 3-aminopropyldimethylethoxy silane (APS, Pierce) in toluene for 1 h at room temperature. The silanized quartz were rinsed and stored in phosphate buffer, pH 8.0. The amino-silane surface was derivatized with biotin by incubation in NHS–biotin (0.25 mg/ml) in phosphate buffer, pH 8.0, for 2 h at room temperature.

The biotinylated quartz slide was rinsed with PBS and incubated with 0.45 mg/ml avidin for 1 h at room temperature. The slides was washed extensively with PBS to remove unbound physically adsorbed avidin. Control avidin–quartz slides, used to test for nonspecific adsorption of BCCP–luciferase, were prepared by incubating the avidin slides with 2.5 mg/ml biotin (in PBS) at room temperature for 1 h to block the biotin binding sites of the immobilized avidin. The avidin-coupled quartz slides, with or without biotin binding sites blocked, were rinsed thoroughly with 0.45 M glycylglycine buffer and immersed in solution with 0.1 mg/ml BCCP–luciferase or Sigma luciferase at room temperature for 45 min. The clean quartz slides were also immersed in luciferase solution to study the nonspecific adsorption of luciferase. After incubation with luciferase, the quartz slides were rinsed and the luciferase activity was determined by adding 100 μl luciferin stock solution and 300 μl ATP (0.1 mM).

RESULTS

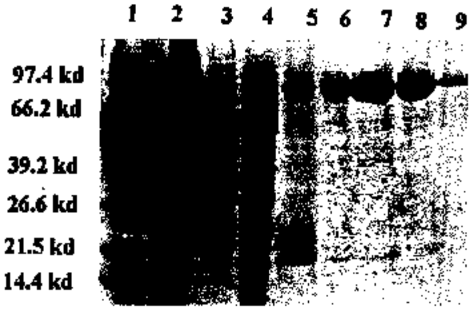

FIG. 1. SDS–polyacrylamide gel electrophoresis of purified BCCP–luciferase. The fraction eluted by imidazole from Ni–NTA column was boiled with 5% SDS, 10% 2-mercaptoethanol, 20% glycerol, and 0.2% bromphenol blue. The protein was stained by Coomassie blue staining method. Lane 1, marker; lane 2, eluted by buffer; lanes 3–5, eluted by 10, 50, and 100 mM imidazole; lanes 6–8, eluted by 250 mM imidazole; lane 9, eluted by 500 mM imidazole.

Purification of BCCP–luciferase. The cell lysate was loaded directly into a Ni–NTA column. After washing with low imidazole, BCCP–luciferase was eluted with 250 and 500 mM imidazole. SDS–PAGE showed high-purity BCCP–luciferase for these fractions (Fig. 1). The yield of protein and the recovery of activity is shown in Table 1. A 200-ml cell culture yielded 9.1 mg luciferase, which is about the amount of luciferase purified from 1800 fireflies by the method of DeLuca and McElroy (15). The high activity recovery and purity of BCCP–luciferase suggest that the Ni–NTA column can purify BCCP–luciferase efficiently with minor protein inactivation.

Molecular weight of BCCP–luciferase. The molecular weight of BCCP–luciferase calculated from the amino acid sequence, which includes the sequence of firefly luciferase (550 amino acid residues), BCCP (87 amino acid residues), and six histidine residues, is 71 kDa. The molecular weight calculated from the SDS–PAGE data (Fig. 1) is 77 kDa, which is slightly greater than the sum of amino acid residues. The small discrepancy may be caused by the unusual amino acid sequence of BCCP domain (13).

Storage stability of BCCP–luciferase. Since the stability of enzyme is important in different storage and preparation conditions, BCCP–luciferase and native luciferase were prepared and stored under several conditions. Both luciferases stored with or without glycerol at 4°C lost about 3% activity after 1-week storage and lost 15 to 20% activity after 4-week storage. No significant difference was observed between native and recombinant luciferase. Addition of glycerol to luciferase solution showed little influence on enzyme stability when stored at 4°C.

Ford *et al.* reported that 13 freezing–thawing cycles resulted in 47% loss of activity for native luciferase and 32% for recombinant luciferase (16). To reduce unnecessary freezing–thawing cycles, glycerol was added to the luciferase solution to keep the sample unfrozen to

TABLE 1

Yield of High-Purity BCCP–Luciferase from 200-ml Cell Culture

	Total protein (mg)	Specific activity (10^{-3} × counts/mg)	Activity recovery (%)
Extract of cell lysate	53.4	379	100
Purified BCCP-luciferase	9.1	1602	72
Sigma luciferase	—	1509	—

Note. The specific activity of BCCP–luciferase was assayed with 100 μl stock solution and 250 μl ATP (0.1 mM) and compared with Sigma luciferase.

−20°C. The sample diluted with DI water was divided into several aliquots before freezing and was thawed only once before test. After storage at −20°C for 4 weeks, both luciferases retain more than 93% activity. The results suggest BCCP–luciferase is as stable as native luciferase under different storage conditions.

Extent of biotinylation on BCCP–luciferase. Biotin was added to BCCP in *E. coli* posttranslationally. To estimate the success of posttranslation labeling, BCCP–luciferase was incubated with an excess amount of avidin resin. The UV absorbance at 280 nm for BCCP–luciferase in solution was 0.28 before loading onto the column and 0.12 after binding; for BSA it was 0.61 before loading and 0.57 after loading. The dilution factor, based on the dilution of BSA, was calculated as 0.94. The percentage of biotinylated BCCP–luciferase was estimated at 55%, after correction for dilution factor. The relative bioluminescence intensity for BCCP–luciferase before and after binding with avidin decreased from 100% to 42%. The decrease of activity suggested 58% of BCCP–luciferase bound to the avidin resin. The nonbinding BCCP–luciferase was reapplied to fresh avidin resin to confirm the completeness of binding. Luciferase activity on the avidin resin was tested and the result showed only trace bioluminescence (about 0.5% of first avidin resin) for this second binding, indicating the binding was complete in the first column. The extent of biotinylation was therefore 55 to 58% of the total purified BCCP–luciferase.

Urea denaturation of luciferase. The stability of native and BCCP–luciferase were compared using intrinsic fluorescence. The intrinsic fluorescence of native luciferase was mainly due to two tryptophan residues at positions 417 and 426. The BCCP domain on the recombinant luciferase does not contain tryptophan. For folded luciferase, the tryptophan fluorescence reached a maximum at 325 nm, suggesting that both residues were buried in a nonpolar environment. After incubation in 6 M urea solution, the intrinsic fluorescence was quenched 67% for native luciferase and 55% for BCCP–luciferase. The ratio of fluorescence intensity ($E_{355\,\mathrm{nm}}/E_{325\,\mathrm{nm}}$) before and after incubation with 6 M urea increased from 0.7 to 1.0 for native luciferase and from 0.7 to 1.1 for BCCP–luciferase. A red shift was observed because of unfolding of luciferase, which exposed the tryptophan residues to aqueous solution.

A two-state folding mechanism was used to calculate the fraction of unfolding (17). The results show that both native luciferase and BCCP–luciferase are 50% unfolded at 2.2 ± 0.1 M urea (Fig. 2), suggesting the presence of the BCCP domain in recombinant luciferase showed little influence on luciferase conformational stability.

The activity of luciferase was decreased by 50% at 1.8 M urea for both BCCP–luciferase and Sigma luciferase (data not shown). The decrease of luciferase activity was roughly proportional to the population of unfolded luciferase.

Thermal stability of BCCP–luciferase. The activity of native luciferase and BCCP–luciferase reached maximum at 25°C (Fig. 3). When the temperature was lower than 20°C, the enzyme activity decreased due to lower enzyme turnover rate. The bioluminescence was yellow–green and the activity of enzyme was recovered when temperature returned to 25°C. When the temperature increased to 40°C, which was close to the thermal transition temperature of both luciferases (43.1°C for native luciferase, 43.7°C for BCCP–luciferase) (14), less than 50% of activity was retained. The bioluminescence turns orange–red and the activity of enzyme was not recoverable when temperature decreased to 25°C. When the temperature increased above the thermal transition temperature, both luciferases lost almost all of the activity. There was no significant change of BCCP–luciferase activity/stability in the presence of avidin. The biotin–avidin interaction neither enhances the stability of BCCP–luciferase nor inactivates the activity of BCCP–luciferase.

Immobilization of BCCP–luciferase on avidin-coupled supports. The biotin molecule on the BCCP–luciferase provides a binding capability to avidin. The biotin–avidin binding served as a bridge for immobilization of BCCP–luciferase on avidin-coupling supports. Luciferases were also directly coupled to Emphaze beads which involved the reaction between azlactone ring on the Emphaze beads and the nucleo-

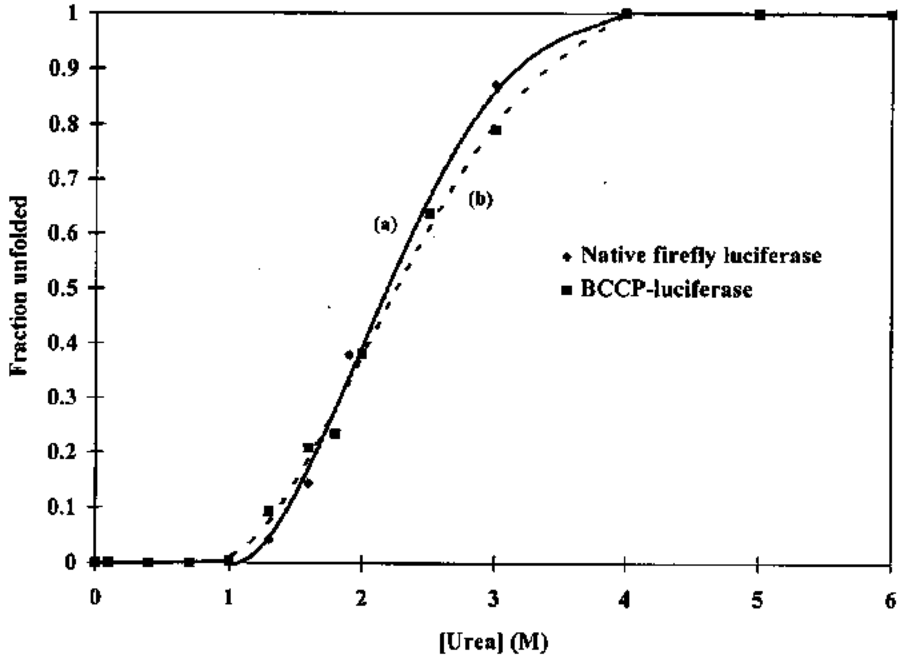

FIG. 2. Urea unfolding of luciferase. (a) Native firefly luciferase unfolded in the presence of urea (solid line). A two-state unfolding mechanism and fluorescence emission at 325 nm were used to calculate the fraction of unfolding. (b) BCCP–luciferase unfolded under the same conditions as in a (dash line).

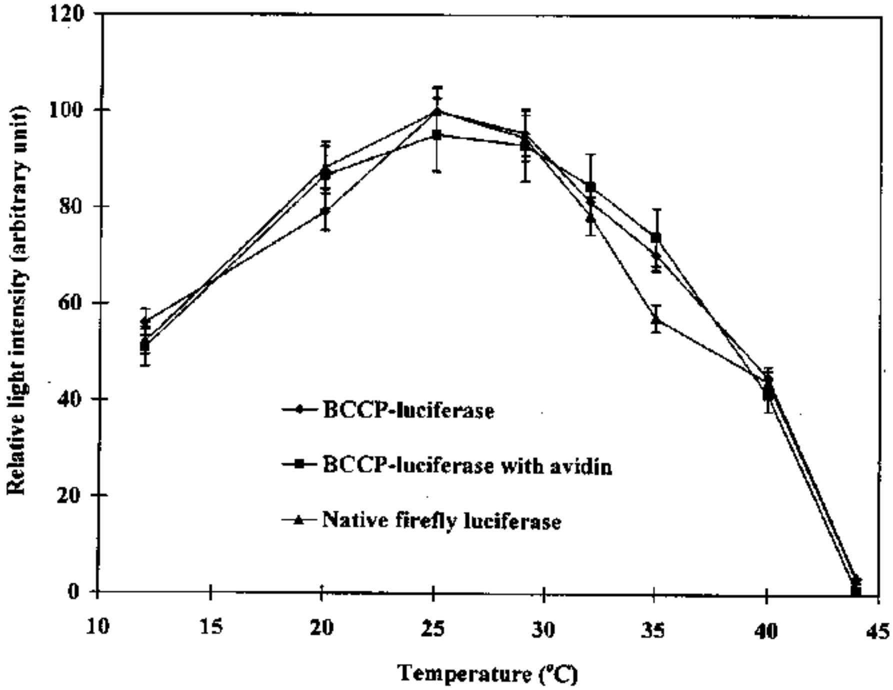

FIG. 3. Thermal stability of BCCP–luciferase and native luciferase. Luciferase activity was assayed after 10-min incubation at each temperature.

TABLE 2

Reusability of Immobilized BCCP-Luciferase

	Activity retained (%)	
	Immobilized BCCP–luciferase stored with 2 mM DTT	Immobilized BCCP–luciferase stored without 2 mM DTT
Freshly prepared	100	100
1-day storage	94	39
3-day storage	90	3
1-week storage	67	0

Note. The storage temperature is 4°C. The activity is determined by maximum bioluminescence emitted at room temperature.

philes on the luciferases, such as amine, sulfhydryl, and hydroxyl groups (18). The activity of immobilized BCCP–luciferase was compared based on the total enzyme added. BCCP–luciferase immobilized on the avidin beads showed 5.8-fold higher bioluminescence intensity than BCCP–luciferase directly coupled to Emphaze beads and 6.6-fold higher bioluminescence than native luciferase directly coupled on Emphaze beads. These results suggested that immobilization of BCCP–luciferase on avidin supports prevents the inactivation of luciferase caused by directly reacting with preactivated Emphaze beads.

One important advantage of immobilized enzymes is reusability. The bioluminescence of immobilized luciferase was repeatedly assayed after washing with 25 mM glycylglycine buffer with 2 mM DTT, pH 7.8. The 10th measurement showed 91% of the bioluminescence of the first measurement. The immobilized luciferase preserved with washing buffer containing 2 mM DTT lost 6% activity after 1-day storage at 4°C and lost 10% activity after 3-day storage (Table 2). The immobilized luciferase washed without 2 mM DTT retained only 52% activity after 10 continuous uses. When stored at 4°C without DTT, the activity of immobilized luciferase decreased dramatically to 39% after 1 day, and retained only 3% activity after 3 days. In comparison, soluble luciferase without DTT retained over 98% activity after 3-day storage. Luciferase is destabilized by immobilization. However, the results showed that DTT provided a short-term stabilization effect on immobilized BCCP–luciferase, which was similar to other studies (7). For long-term stabilization, Brovko *et al.* showed that immobilized luciferase can be lyophilized and stored at −70°C for 1 year without the loss of activity (19).

Biotinylated quartz slides were prepared and incubated with avidin. The avidin-coupled quartz slides were incubated with BCCP–luciferase. The activity of BCCP–luciferase immobilized on avidin-coupled quartz slides was 13-fold higher than that of physically adsorbed BCCP–luciferase (Table 3). An avidin-coupled quartz slide, preincubated with excess biotin to block avidin binding sites, was also incubated with BCCP–luciferase. Very low bioluminescence intensity was present. As a control, native luciferase from Sigma was incubated with avidin-coupled quartz slides with and without preincubation with biotin. Very low total activity was detected with either slide, demonstrating that native luciferase does not bind to an avidin-coated surface (Table 3).

DISCUSSION

The firefly luciferase gene, *luc*, is frequently used as a reporter of genetic function, or for producing recombinant luciferase (20). To simplify the purification process, luciferase was fused with the BCCP domain and six histidine residues on its N-terminus. The BCCP–luciferase bound to Ni–NTA agarose through the strong chelating interaction between the 6× His tag and Ni^{2+} directly from the cell lysate. The specific activity of the expressed BCCP–luciferase was better than native luciferase (from Sigma). A high purity recombinant luciferase with a yield of 72% was achieved. The good recovery and specific activity of BCCP–luciferase suggested the high efficiency of the purification protocol. The extent of biotinylation for BCCP–luciferase was 55 to 58% in this study. The deficiency of biotin in the culture medium caused lower biotinylation extent. The addition of biotin in the culture medium may help to increase the biotinylation extent (21).

The fused BCCP domain on the recombinant luciferase did not affect firefly luciferase stability. BCCP–luciferase shared similar properties with native luciferase in the stability study. The urea unfolding curve showed the midpoint of urea concentration was 2.2 ± 0.1 M for both native luciferase and BCCP–luciferase. Similar results were obtained in the study of thermal stability. The binding of BCCP–luciferase to avidin did not change the activity of luciferase. When stored in 50% glycerol and −20°C, BCCP–luciferase retained up to 93% activity after a 4-week storage. No significant difference was observed when compared with native luciferase under several storage conditions.

The second benefit of the novel BCCP–luciferase is the specific binding capability to avidin or streptavidin. Since immobilization of luciferase is important in biosensor application, much effort has gone into the immobilization of luciferase by chemical modification (7–10) or physical adsorption (11). Direct modification of luciferase in those previous studies resulted in the loss of enzyme activity. Firefly luciferase was also found to adsorb fast on the dimethyldichlorosilane-treated quartz slide and aggregate on the clean quartz slide (22). Both adsorptions led to luciferase conformation

TABLE 3

Relative Activity of Physically Adsorbed and Specifically Immobilized Luciferase on Quartz Slides

Condition	Relative light intensity
BCCP–luciferase on avidin-coupled quartz	100
BCCP–luciferase on clean quartz	7.1
BCCP–luciferase on biotinylated quartz	1.7
BCCP–luciferase on avidin-coupled quartz which preincubated with biotin	9.6
Sigma luciferase on avidin-coupled quartz	1.0
Sigma luciferase on biotin–avidin-coupled quartz which preincubated with biotin	0.1

change and loss of enzymatic activity after prolonged incubation. The instability of luciferase on the physical adsorption surface made the adsorption method less favorable.

A better immobilization protocol was developed using the biotin domain on the BCCP–luciferase. A tough protein, avidin was first bound to preactivated Emphaze beads, or a biotinylated quartz slide. The avidin-coupled support was used as the "receptor" for BCCP–luciferase. The high activity of immobilized BCCP–luciferase was obtained after a short incubation with the avidin-coupled support. This immobilization protocol circumvents the possible inactivation pathways and makes the immobilization of enzyme controllable. An immobilized BCCP–luciferase monolayer with uniform orientation is possible and may be applied to design more sensitive biosensors.

ACKNOWLEDGMENTS

This study is part of C. Y. Wang's Ph.D. dissertation. This work was partially supported by Protein Solutions, Inc. (Salt Lake City, UT) via funding provided by an NSF STTR grant. We thank Dr. J. Cronan, Jr., University of Illinois, for helpful discussions concerning biotinylation of proteins in *E. coli.* We thank Drs. J. Herron and V. Hlady for access to equipment and facilities. We thank the 3M Corp. (Dr. P. Coleman) for a gift of Emphaze beads.

REFERENCES

1. McElroy, W. D., and Seliger, H. H. (1961) *in* Light and Life (McElroy, W. D., Ed.), pp. 219–257.
2. Seliger, H. H., and McElroy, W. D. (1960) *Arch. Biochem. Biophys.* **88,** 136–145.
3. Leach, F. R. (1981) *J. Appl. Biochem.* **3,** 473–517.
4. Leach, F. R., and Webster, J. J. (1986) *in* Methods in Enzymology (DeLuca, M., Ed.), Vol. 133, pp. 51–70, Academic Press, San Diego.
5. Green, K., and Kricka, L. J. (1984) *Talanta* **31,** 173–176.
6. Blum, L. J., Gautier, S. M., and Coulet, P. R. (1989) *J. Biolumin. Chemilumin.* **4,** 543–550.
7. Rajgopal, S., and Vijayalakshmi, M. A. (1984) *Enzyme Microb. Technol.* **6,** 482–490.
8. Lee, Y., Jablonski, I., and DeLuca, M. (1977) *Anal. Biochem.* **80,** 496–501.
9. Ugarova, N. N., Brovko, L. Y., and Kost, N. V. (1982) *Enzyme Microb. Technol.* **4,** 224–228.
10. Blum, L. J., Coulet, P. R., and Gautheron, D. C. (1986) *Biotechnol. Bioeng.* **28,** 1154–1158.
11. Filippova, N. Y., Dukhovich, A. F., and Ugarova, N. N. (1989) *J. Biolumin. Chemilumin.* **4,** 419–422.
12. Janknecht, R., de Martynoff, G., Lou, J., Hipskind, R. A., Nordheim, A., and Stunnenberg, H. G. (1991) *Proc. Natl. Acad. Sci. USA* **88,** 8972–8976.
13. Li, S., and Cronan, J. E., Jr. (1992) *J. Biol. Chem.* **267,** 855–863.
14. Wang, C.-Y. (1996) Ph.D. dissertation. University of Utah.
15. DeLuca, M., and McElroy, W. D. (1978) *in* Methods in Enzymology, Vol. 57, pp. 3–15, Academic Press, New York.
16. Ford, S. R., Hall, M. S., and Leach, F. R. (1992) *J. Biolumin. Chemilumin.* **7,** 185–193.
17. Pace, C. N., Shirley, B. A., and Thomson, J. A. (1989) *in* Protein Structure: A Practical Approach (Creighton, T. E., Ed.), pp. 311–330, IRL Press, Oxford, England.
18. Coleman, P. L., Walker, M. M., Milbrath, D. S., Stauffer, D. M., Rasmussen, J. K., Krepski, L. R., and Heilmann, S. M. (1990) *J. Chromatogr.* **512,** 345–363.
19. Brovko, L. Yu., Romanova, N. A., and Ugarova, N. N. (1994) *Anal. Biochem.* **220,** 410–414.
20. Sherf, B. A., and Wood, K. V., Promega Notes, Vol. 49, pp. 14–21.
21. Tatsumi, H., Fukuda, S., Kikuchi, M., and Koyama, Y. (1996) Poster, 9th International Symposium on Bioluminescence and Chemiluminescence.
22. Hlady, V., Yeh, P. Y., and Andrade, J. D. (1991) *J. Fluorescence* **1,** 47–55.

BIOTINYLATION OF FIREFLY LUCIFERASE IN VIVO: PURIFICATION AND IMMOBILIZATION OF BIFUNCTIONAL RECOMBINANT LUCIFERASE

CY Wang, S Hitz, JD Andrade, and RJ Stewart
Dept. of Bioengineering, University of Utah, SLC, UT 84112, USA

Introduction

Firefly luciferase is an enzyme which catalyzes a bioluminescent reaction in the presence of luciferin, adenosine 5'-triphosphate (ATP), magnesium ion and oxygen (1). The bioluminescent reaction features a high sensitivity for ATP and a high quantum yield, 0.88 (2). The methods used to obtain high purity luciferases from firefly lanterns have been reviewed (3). Long purification times and low yields makes highly purified native luciferase expensive. Distinguishing firefly habitats makes collection of fireflies ecologically inappropriate. The labile nature of firefly luciferase also makes immobilization of luciferase less successful than other enzymes (3).

The success of de Wet et al. who isolated firefly luciferase cDNA (4), broadens the applications of firefly luciferase through genetic engineering. The plasmid containing the luciferase gene (luc) was constructed and inserted as a gene reporter. Novel fusion proteins, such as protein A-luciferase and streptavidin-luciferase are now available (5, 6).

A plasmid encoding a novel fusion luciferase (BCCP-luciferase) was constructed and inserted into E. coli in our laboratory. The BCCP-luciferase contains a biotin carboxyl carrier protein (BCCP), a subunit of acetyl-CoA carboxylase (7). Post-translational modification of the BCCP domain on the fusion protein results in a biotin molecule on a specific lysine residue. The BCCP-luciferase also contains six histidine residues at the N-terminal, which bind strongly to Ni^{2+}-nitrilotriacetic acid (Ni^{2+}-NTA) agarose (8, 9). The highly purified BCCP-luciferase was obtained with a one-step purification protocol and compared with native luciferase purified from firefly lanterns (9). Both luciferases presented similar activity and stability.

Avidin, a glycoprotein with four biotin binding sites, was immobilized on Emphaze beads (see below) and served as the "receptor" for BCCP-luciferase. Via biotin-avidin bridges, the biotinylated firefly luciferase is immobilized on the avidin beads without direct modification of the luciferase domain. This novel bi-functional luciferase is easy to purify and immobilize with high bioluminescence activity.

Materials and Methods

Construction of the pRSET-BCCP-luc plasmid and culture of transformed E. coli were described elsewhere (9). The cells were harvested and disintegrated by sonication (Fisher Scientific 550 sonic dismembrator) on an ice bath with 1 mmol/L phenylmethylsulfonyl fluoride (PMSF, in isopropanol, from Sigma). The supernatant containing the recombinant luciferase was collected and applied directly to 3 mL of Ni^{2+}-NTA agarose (from Qiagen), which was packed in an Econo-column (BioRad) and washed with 20 mL Tris buffer (50 mmol/L, pH 7.8). The unbound proteins were eluted with two aliquots of 2 mL Tris buffer. Three aliquots of 2 mL imidazole solutions at 10, 50, 100, 250, and 500 mmol/L were applied to the Ni^{2+}-NTA column sequentially. The eluate was collected and the buffer changed to glycylglycine buffer (0.45 mol/L, pH 7.8) or phosphate buffer saline (PBS) with a PD-10 column (Pharmacia). Molecular weight and purity of purified BCCP-luciferase was determined by 10% sodium dodecyl sulphate-polyacrylamide gel electrophoresis (SDS-PAGE) and detected with Coomassie Blue.

Luciferase activity was determined by injecting 250 μL ATP solution (0.1 mmol/L) into the mixture of 20 μL luciferase solution and 100 μL stock solution (0.1 mmol/L luciferin and 10 mmol/L $MgSO_4$ in 25 mmol/L glycylglycine buffer, pH 7.8). The bioluminescence was recorded with a spectrofluorometer (I.S.S., Inc.) and the peak height was interpreted as the enzyme activity. The amount of total protein was determined by BioRad protein assay with a Perkin Elmer Lambda 6 UV/VIS spectrophotometer. A standard curve (A_{595} vs. protein amount) was generated for bovine serum albumin (BSA).

SoftLink soft release avidin resin (from Promega), with covalently linked monomeric avidin, was used to determine the extent of biotinylation. 1 mL BCCP-luciferase (0.4 mg/mL) was fully mixed with avidin resin and packed to the column. The eluate was collected and applied to the second column packed with fresh avidin resin. BSA was used in the same procedure to calculate the dilution factor. The amount and activity of proteins before and after binding were determined by UV absorbance at 280 nm and by ATP assay.

Avidin was mixed with dry Emphaze Biosupport Medium AB1 (a gift from 3M) to make avidin-coupled beads. The cell lysate was mixed with avidin-coupled Emphaze beads and packed into the column. Unbound luciferase was removed by washing the beads with 0.8 mL of glycylglycine buffer (25 mmol/L with 2 mmol/L dithiothreitol (DTT)). Luciferase activity was determined by applying 250 μL of the ATP solution (2 mmol/L DTT) and 100 μL of the stock solution to the column. The coupling of luciferase directly to Emphaze beads and quenched beads (no azlactone functionality) were also studied with the same method.

The beads containing immobilized luciferase were regenerated by washing the column with 0.8 mL glyculglycine buffer (with DTT) three times. The activity of luciferase on the regenerated beads were tested immediately or stored at 4 °C for later use. The work was also repeated without DTT in all solutions.

Results and Discussion

An average yield of 1.1 g wet E. coli cells were recovered from 200 mL culture. The cells were disintegrated and the supernatant of cell lysate was loaded directly on to the Ni^{2+}-NTA column. The activity of BCCP-luciferase was first detected when the concentration of imidazole increased to 100 mmol/L. The highest activity was found in the fraction eluted by 250 mmol/L imidazole. The result of SDS-PAGE showed a single band (Figure 1) suggesting that the single-step purification with the Ni^{2+}-NTA column is effective to obtain high purity BCCP-luciferase. A 200 mL cell culture yielded 9.1 mg pure luciferase with 72% total activity recovered, which is about the

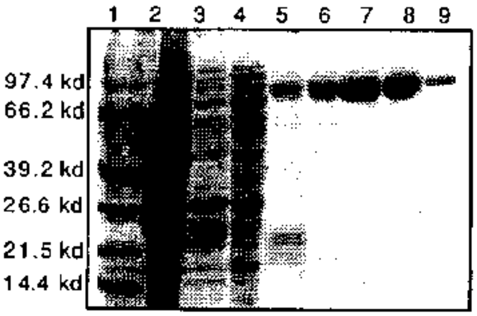

Figure 1. Purity of BCCP-luciferase on SDS-PAGE. 1: marker; 2: eluted by buffer; 3-5: eluted by 10, 50 and 100 mmol/L imidazole; 6-8: eluted by 250 mmol/L imidazole; 9: eluted by 500 mmol/L imidazole.

Table 1. Reusability of immobilized BCCP-luciferase stored at 4 °C (% activity retained).

	Storage with 2 mmol/L DTT	Storage without 2 mmol/L DTT
Fresh	100	100
After 10 uses	91	52
1 day storage	94	39
3 day storage	90	3
1 week storage	67	0

amount of luciferase purified from 1800 fireflies by the method of DeLuca & McElroy (10). The specific activity is about 6% higher than that of Sigma luciferase. The high activity recovery and purity of BCCP-luciferase suggest the Ni^{2+}-NTA column can purify BCCP-luciferase efficiently with minor protein inactivation. The molecular weight calculated from the SDS-PAGE data (Figure 1) is 77 kd, slightly greater than the sum of amino acid residues, 71 kd. The small discrepancy may be caused by the unusual amino acid sequence of BCCP domain (7).

The percentage of biotinylated luciferase was estimated to be 55% of the luciferase recovered. The solution of BCCP-luciferase after binding reaction retained 42% bioluminescence, suggesting up to 58% of BCCP-luciferase binding to avidin resin. Re-applying the non-binding BCCP-luciferase to fresh avidin resin resulted in trace bioluminescence on the avidin resin (about 0.5 % of the first avidin resin), indicating the binding is complete in the first column. The biotinylation extent was thus estimated within 55% to 58% of the total purified BCCP-luciferases.

The supernatant from the E. coli lysate was directly incubated with avidin coupled Emphaze beads. BCCP-luciferase bound to the immobilized avidin via biotin-avidin bridges. Unlike the solution assay, there was no flash of bioluminescence upon the addition of ATP and luciferin stock solution to the immobilized BCCP-luciferase. There was no luciferase activity after incubation with quenched Emphaze beads and very low Sigma luciferase activity after incubation with avidin-beads, suggesting the binding of BCCP-luciferase on avidin-beads was specific. The activity of BCCP-luciferase immobilized via biotin-avidin bridges was more than three fold of luciferases directly immobilized on Emphaze beads. Luciferase directly coupled to Emphaze beads may be inactivated during the chemical modification.

One important advantage of immobilized enzyme is its reusability. BCCP-luciferase in buffer solution retained 98% activity after one week storage at 4 °C (9). The activity of regenerated luciferase was shown in Table 1. The results suggested that the major mechanism of luciferase inactivation was via formation of disulfide bond. Exhaustion of DTT may speed the formation of disulfide bond and the inactivation of immobilized luciferase. The stabilization effect of DTT on immobilized luciferase was consistent with other reports (3).

The one-step purification protocol using the Ni^{2+}-NTA column is efficient to obtain high purity BCCP-luciferase, which was as stable as native luciferase (9). In vivo biotinylation of BCCP-luciferase provides a specific binding capability to avidin or streptavidin. High activity of immobilized BCCP-luciferase can be obtained by directly incubating the cell lysate with avidin coupled Emphaze beads. This immobilization protocol prevents possible inactivation pathways and can be applied in the design of luciferase based biosensors.

Acknowledgement

This work was partially supported by Protein Solutions, Inc., Salt Lake City, Utah via funding provided by an NSF STTR grant. We thank Drs. J. Herron and V. Hlady for access to equipment and facilities. We thank the 3M corp. (Dr. P. Coleman) for a gift of Emphaze beads. We thank Dr. J. Cronan, Jr., University of Illinois, for helpful discussions concerning biotinylation of proteins in E. coli.

References

1. McElroy WD Seliger HH. Mechanisms of Bioluminescent reactions. In: McElroy WD, Glass B, editor. Light and Life. Baltimore: John Hopkins Press, 1961:219-57.
2. Seliger HH, McElroy WD. Spectral emission and quantum yield of firefly bioluminescence. Arch Biochem Biophys 1960;88:136-45.
3. Rajgopal S, Vijayalakshmi MA. Firefly luciferase: purification and immobilization. Enzyme Microb Technol 1984;6:482-90.
4. De Wet JR, Wood KV, Helinski DR. DeLuca M. Cloning of firefly luciferase cDNA and the expression of active luciferase in Escherichia coli. Proc. Natl Acad Sci USA 1985;82:7870-73.
5. Kobatake E, Iwai T, Ikariyama Y, Aizawa M. Bioluminescent immunoassay with a protein A-luciferase fusion protein. Anal Biochem, 1993;208:300-5.
6. Karp M, Lindqvist C, Nissinen R, Wahlbeck S, Akerman K, Oker-Blom C. Identification of biotinylated molecules using a baculovirus-expressed luciferase-streptavidin fusion protein. BioTechniques 1996;20:452-459.
7. Li S, Cronan Jr., JE. The gene encoding the biotin carboxylase subunit of Escherichia coli acetyl-CoA carboxylase. J Biol Chem 1992;267:855-63.
8. Janknecht R, de Martynoff G, Lou J, Hipskind RA, Nordheim A, Stunnenberg HG. Rapid and efficient purification of native histidine-tagged protein expressed by recombinant vaccinia virus. Proc Natl Acad Sci USA 1991;88:8972-6.
9. Wang C-Y, Hitz S, Andrade JD, Stewart R. Biotinylation of firefly luciferase in vivo: a recombinant protein with a specific immobilization site," in preparation 1996; Wang C-Y, Ph. D. Dissertation, University of Utah, Oct. 1996.
10. DeLuca M. McElroy WD. Purification and properties of firefly luciferase. Methods Enzymol 1978;57:3-15.

SURFACTANTS AND COENZYME A AS COOPERATIVE ENHANCERS OF THE ACTIVITY OF FIREFLY LUCIFERASE

CY Wang and JD Andrade
Dept. of Bioengineering, University of Utah, SLC, UT 84112, USA

Introduction

Since protein folding depends on physical interactions with the solution, activators or inhibitors may modify protein structure via changes in the local solution environment, facilitating or inhibiting protein activity. Kricka and DeLuca found that nonionic surfactants, such as Triton X-100 and Tween 20, and some polymers, such as polyethylene glycol (PEG) and polyvinylpyrrolidone (PVP), stimulated luciferase activity (1). However, anionic and cationic surfactants failed to stimulate luciferase activity and behaved as inhibitors. They further titrated the active sites with dehydroluciferin and ATP-Mg^{2+} and showed the stimulation effect was not caused by recruitment of new active sites. Although the actual mechanism of stimulation is still unknown, they suggested that the binding of Triton X-100 or polymers to luciferase mat account for the stimulation effect. Other studies showed similar stimulation effects in some cases but not in others (2, 3). The inconsistent results may result from different preparations of firefly luciferases.

Coenzyme A (CoA) was found to reduce the decay rate of luciferase bioluminescence (4). Schroder found firefly luciferase (Photinus pyralis) was related to a plant enzyme, 4-coumarate CoA ligase, which utilized ATP and CoA (5). Since similarity between enzymes may suggest the conservation of specific functions, the existence of a CoA binding site is possible, although CoA is not a required substrate for firefly bioluminescence.

The enhancement effects of surfactants and polymers were determined with and without CoA. A significantly cooperative enhancement was observed in the presence of both surfactant/polymer and CoA. Triton X-100 was also found to be a protectant against the inhibition effect of 1,2-dioleoyl-sn-glycerol-3-[phospho-L-serine] (DOPS). Luciferase inactivated by DOPS recovered over 60% activity after incubation in Triton X-100.

Materials and Methods

Triton X-100 (avg. MW 650, density 1.059), Tween 20 (polyoxyethylene sorbitan monolaurate, MW 1228), PVP (MW 40,000) and PEG (MW 5,000) were purchased from Sigma. The stock solution for 10% (w/w%) Triton X-100 and Tween 20 and 10% (w/v%) PVP and PEG were prepared with glycylglycine buffer (0.45 mol/L, pH 7.8). The stock solutions were then diluted to 1%, and 0.1% with the same buffer.

Firefly luciferase (from Sigma, chromatographically prepared and lyophilized; showed a single band on SDS-PAGE) was used to prepare the enzyme-surfactant mixtures. 20 µL of luciferase solution (0.5 mg/mL) was mixed with 13.1 µL of glycylglycine buffer and 248.5 µL of surfactant or polymer solution. The final concentration of additives is 0.4800%, 0.0480%, and 0.0048%. In the control experiment, glycylglycine buffer was used to replace surfactant solution. 100 µL of luciferin stock solution (0.1 mmol/L luciferin and 10 mmol/L $MgSO_4$) was added to 20 μL of luciferase mixture and incubated for 3 minutes. 250 μL of ATP solution (10^{-4} mol/L or 10^{-6} mol/L) was then injected to initiate the bioluminescence reaction. The light intensity was recorded with a spectrofluorometer (I.S.S., Inc.).

The optimum concentration (the highest enhancement effect) of each individual additive was then mixed in combinations of two. The additivity of enhancements on luciferase activity was examined by assaying luciferase activity.

CoA (free acid, from Sigma) was added to ATP solution (10^{-4} mol/L and 10^{-6} mol/L) to make a 10^{-4} mol/L CoA solution. The ATP solution containing CoA was then added to the luciferase/surfactant mixtures and the enzyme activity determined as before.

For the protection experiment, 20 μL of luciferase (0.5 mg/mL) was first incubated with 248.5 μL Triton X-100 (10%) for 30 min. Preparation of 1,2-dioleoyl-sn-glycerol-3-phosphocholine (DOPC) and DOPS liposomes was described elsewhere (6). 13.1 μL of DOPS liposomes were added to the mixture and incubated for another 30 min. The final concentration of Triton X-100 was 0.48% and the molar ratio of DOPS to luciferase was 500:1. The activity of luciferase was then assayed. For the reactivation experiment, luciferase was first incubated with DOPS for 30 min. The Triton X-100 was then added and incubated for another 30 min. The activity of luciferase recoved was assayed. DOPC liposomes were used (in a molar ratio of 500 DOPC to 1 luciferase) to replace Triton X-100 and the experiments were repeated.

Results and Discussion

Some nonionic surfactants and polymers were effective in enhancing luciferase activity (1-3). In this study, all four additives were found to increase luciferase activity, which showed 28% to 118% higher initial velocity (maximum light intensity) at the 10^{-4} mol/L ATP concentration. PEG 5000 and Triton X-100 showed the most promiment enhancing effect at the peak intensity of bioluminescence. At the optimum concentration, Triton X-100 showed the slowest decay rate, which was maintained up to 326% of control at the plateau of bioluminescence, while PEG 5000 maintained the lowest bioluminescence (160%) in the same period (Table 1).

The optimum concentration for the four additives was further examined at 10^{-6} mol/L ATP. Higher stimulation effects at low ATP concentration was observed than at high ATP concentration (Table 1).

Table 1. Enhancement of additives at high and low ATP concentration. The bioluminescence intensity of pure luciferase solution is normalized as 100%.

Additives	Final concentration	Peak (%)	Plateau (%)	Peak (%)	Plateau (%)
		10^{-4} mol/L ATP		10^{-6} mol/L ATP	
Triton X-100	0.4800%	218	326	324	333
Tween 20	0.0048%	187	242	212	194
PEG 5000	0.4800%	198	160	267	140
PVP 40000	0.0480%	179	173	288	151

The surfactants and polymers were mixed in pairs to examine the additivity of the enhancement effects. The results showed that Triton X-100 mixed with Tween 20 and PEG 5000 further enhanced the peak intensity 28 to 48%. There was no significantly further enhancement for the other combinations. The presence of other additives in the Triton X-100 solution further enhanced the light intensity at plateau. However, PVP and PEG hinder the enhancing effect of Tween 20 at plateau.

Coenzyme A was effective in preventing the decay of bioluminescence. The total light output increased 6 fold over a 30 sec period when using 10^{-4} mol/L ATP and 0.1 mol/L CoA as the substrates. CoA mixed with any one of the four surfactants/ polymers resulted in a significant cooperative enhancement (Table 2). The combination of Triton X-100 and CoA had the most significant enhancement, increasing the total light output up to 23 fold for the first 30 sec (Figure 1). The mechanisms of stimulation for these two chemicals was different and cooperative. A less prominent enhancement was also observed for 10^{-6} mol/L ATP.

Table 2. Cooperative enhancing effects of CoA (final concentration: 0.068 mmol/L) and surfactants/polymers (at concentration as Table 1). Light count was integrated for first 30 sec. The count of luciferase solution without additives and CoA was used as the reference. The enhancement was calculated by dividing each output result by the reference.

	Enhancement (fold)	
Components	ATP (10^{-4} mol/L)	ATP (10^{-6} mol/L)
Luciferase and CoA	7	1.1
Luciferase, CoA and Triton X-100	23	5.4
Luciferase, CoA and Tween 20	20	4.7
Luciferase, CoA and PEG 5000	12	1.9
Luciferase, CoA and PVP 40000	19	2.3

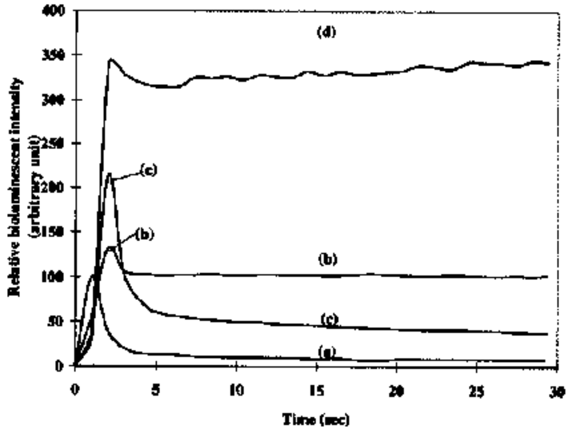

Figure 1. The Cooperative enhancement of Triton X-100 (0.4800%) and CoA on luciferase activity. (a) Luciferase; (b) luciferase with CoA; (c) luciferase with Triton X-100; (d) luciferase with CoA and Triton X-100.

Firefly luciferase was inactivated by negative charged lipids (6, 7). The presence of Triton X-100 (0.4800%) prevented inactivation by DOPS. Luciferase inactivated by DOPS can be partially reactivated by incubation with Triton X-100, the activity recovering from 17% to 64%. Although the mechanism is unknown, the recovered enzyme activity may be due to the replacement of DOPS by Triton X-100 at the same binding site; Triton X-100 may also enhance the activity of the remaining native enzyme. In the same experiment, DOPC was used to replace Triton X-100. There was no protection or reactivation effect for DOPC against DOPS.

The micelle environment was not required condition for the stimulation, since PEG and PVP do not form micelles. A large complex found by Kricka and DeLuca was proposed to be the enzyme-surfactant complex (1). The lack of an additivity effect between the combination of surfactants/polymers indicate a similarity to the enhancing mechanism. The binding of surfactants/polymers helps reactivate luciferase, which may have been inhibited by its substrates. Triton X-100 and Tween 20 may also help to modify the conformation and speed the release of oxyluciferin, enhancing enzyme turnover. Coenzyme A behaves differently with surfactants and polymers and probably binds to luciferase at a specific site. When added with Triton X-100, the bioluminescence intensity was enhanced further and maintained at a maximum level for at least 2 minutes. The high turnover rate was not inhibited by the accumulation of oxyluciferin. Other combinations with CoA produce less but still prominant total light output. The additivity effect enables a constant light output at high intensity. It is useful to develop direct reading biosensors which require those characteristics.

Acknowledgement
This work was partially supported by Protein Solutions, Inc., Salt Lake City, Utah via funding provided by an NSF STTR grant. We thank Drs. J. Herron and V. Hlady for access to equipment and facilities.

References

1. Kricka LJ, DeLuca M. Effect of solvents on the catalytic activity of firefly luciferase. Arch Biochem Biophys 1982;217:674-81.
2. Yeh PY. The properties of firefly luciferase in solution and at interfaces. Master thesis, University of Utah, 1989.
3. Simpson WJ, Hammond JRM. The effect of detergents on firefly luciferase reactions. J Biolumin Chemilumin 1991;6:97-106.
4. Airth RL, Rhodes WC, McElroy WD. The function of coenzyme A in luminescence. Biochim Biophys Acta 1958;27:519-32.
5. Schroder J, Protein sequence homology between plant 4-coumarate: CoA ligase and firefly luciferase. Nucleic Acids Res 1989;17:460-2.
6. Wang C-Y, Firefly Luciferase: Activity, Stability and Sensor Applications. Ph.D. Dissertation, University of Utah, Oct. 1996.
7. Dukhovich AF, Filippova NYu, Efimov AI, Ugarova NN, Berezin IB. Choline-containing phospholipids as specific activators and stabilizers of firefly luciferase. Dokl Akad Nauk SSSR, 1988;298:1257-60.

SURFACTANTS AND COENZYME A AS COOPERATIVE ENHANCERS OF THE ACTIVITY OF FIREFLY LUCIFERASE

CY Wang and JD Andrade
Dept. of Bioengineering, University of Utah, SLC, UT 84112, USA

Introduction

Since protein folding depends on physical interactions with the solution, activators or inhibitors may modify protein structure via changes in the local solution environment, facilitating or inhibiting protein activity. Kricka and DeLuca found that nonionic surfactants, such as Triton X-100 and Tween 20, and some polymers, such as polyethylene glycol (PEG) and polyvinylpyrrolidone (PVP), stimulated luciferase activity (1). However, anionic and cationic surfactants failed to stimulate luciferase activity and behaved as inhibitors. They further titrated the active sites with dehydroluciferin and ATP-Mg^{2+} and showed the stimulation effect was not caused by recruitment of new active sites. Although the actual mechanism of stimulation is still unknown, they suggested that the binding of Triton X-100 or polymers to luciferase mat account for the stimulation effect. Other studies showed similar stimulation effects in some cases but not in others (2, 3). The inconsistent results may result from different preparations of firefly luciferases.

Coenzyme A (CoA) was found to reduce the decay rate of luciferase bioluminescence (4). Schroder found firefly luciferase (Photinus pyralis) was related to a plant enzyme, 4-coumarate CoA ligase, which utilized ATP and CoA (5). Since similarity between enzymes may suggest the conservation of specific functions, the existence of a CoA binding site is possible, although CoA is not a required substrate for firefly bioluminescence.

The enhancement effects of surfactants and polymers were determined with and without CoA. A significantly cooperative enhancement was observed in the presence of both surfactant/polymer and CoA. Triton X-100 was also found to be a protectant against the inhibition effect of 1,2-dioleoyl-sn-glycerol-3-[phospho-L-serine] (DOPS). Luciferase inactivated by DOPS recovered over 60% activity after incubation in Triton X-100.

Materials and Methods

Triton X-100 (avg. MW 650, density 1.059), Tween 20 (polyoxyethylene sorbitan monolaurate, MW 1228), PVP (MW 40,000) and PEG (MW 5,000) were purchased from Sigma. The stock solution for 10% (w/w%) Triton X-100 and Tween 20 and 10% (w/v%) PVP and PEG were prepared with glycylglycine buffer (0.45 mol/L, pH 7.8). The stock solutions were then diluted to 1%, and 0.1% with the same buffer.

Firefly luciferase (from Sigma, chromatographically prepared and lyophilized; showed a single band on SDS-PAGE) was used to prepare the enzyme-surfactant mixtures. 20 μL of luciferase solution (0.5 mg/mL) was mixed with 13.1 μL of glycylglycine buffer and 248.5 μL of surfactant or polymer solution. The final concentration of additives is 0.4800%, 0.0480%, and 0.0048%. In the control experiment, glycylglycine buffer was used to replace surfactant solution. 100 μL of luciferin stock solution (0.1 mmol/L luciferin and 10 mmol/L $MgSO_4$) was added to 20 µL of luciferase mixture and incubated for 3 minutes. 250 µL of ATP solution (10^{-4} mol/L or 10^{-6} mol/L) was then injected to initiate the bioluminescence reaction. The light intensity was recorded with a spectrofluorometer (I.S.S., Inc.).

The optimum concentration (the highest enhancement effect) of each individual additive was then mixed in combinations of two. The additivity of enhancements on luciferase activity was examined by assaying luciferase activity.

CoA (free acid, from Sigma) was added to ATP solution (10^{-4} mol/L and 10^{-6} mol/L) to make a 10^{-4} mol/L CoA solution. The ATP solution containing CoA was then added to the luciferase/surfactant mixtures and the enzyme activity determined as before.

For the protection experiment, 20 µL of luciferase (0.5 mg/mL) was first incubated with 248.5 µL Triton X-100 (10%) for 30 min. Preparation of 1,2-dioleoyl-sn-glycerol-3-phosphocholine (DOPC) and DOPS liposomes was described elsewhere (6). 13.1 µL of DOPS liposomes were added to the mixture and incubated for another 30 min. The final concentration of Triton X-100 was 0.48% and the molar ratio of DOPS to luciferase was 500:1. The activity of luciferase was then assayed. For the reactivation experiment, luciferase was first incubated with DOPS for 30 min. The Triton X-100 was then added and incubated for another 30 min. The activity of luciferase recoved was assayed. DOPC liposomes were used (in a molar ratio of 500 DOPC to 1 luciferase) to replace Triton X-100 and the experiments were repeated.

Results and Discussion

Some nonionic surfactants and polymers were effective in enhancing luciferase activity (1-3). In this study, all four additives were found to increase luciferase activity, which showed 28% to 118% higher initial velocity (maximum light intensity) at the 10^{-4} mol/L ATP concentration. PEG 5000 and Triton X-100 showed the most promiment enhancing effect at the peak intensity of bioluminescence. At the optimum concentration, Triton X-100 showed the slowest decay rate, which was maintained up to 326% of control at the plateau of bioluminescence, while PEG 5000 maintained the lowest bioluminescence (160%) in the same period (Table 1).

The optimum concentration for the four additives was further examined at 10^{-6} mol/L ATP. Higher stimulation effects at low ATP concentration was observed than at high ATP concentration (Table 1).

Table 1. Enhancement of additives at high and low ATP concentration. The bioluminescence intensity of pure luciferase solution is normalized as 100%.

Additives	Final concentration	Peak (%)	Plateau (%)	Peak (%)	Plateau (%)
		10^{-4} mol/L ATP		10^{-6} mol/L ATP	
Triton X-100	0.4800%	218	326	324	333
Tween 20	0.0048%	187	242	212	194
PEG 5000	0.4800%	198	160	267	140
PVP 40000	0.0480%	179	173	288	151

The surfactants and polymers were mixed in pairs to examine the additivity of the enhancement effects. The results showed that Triton X-100 mixed with Tween 20 and PEG 5000 further enhanced the peak intensity 28 to 48%. There was no significantly further enhancement for the other combinations. The presence of other additives in the Triton X-100 solution further enhanced the light intensity at plateau. However, PVP and PEG hinder the enhancing effect of Tween 20 at plateau.

Coenzyme A was effective in preventing the decay of bioluminescence. The total light output increased 6 fold over a 30 sec period when using 10^{-4} mol/L ATP and 0.1 mol/L CoA as the substrates. CoA mixed with any one of the four surfactants/ polymers resulted in a significant cooperative enhancement (Table 2). The combination of Triton X-100 and CoA had the most significant enhancement, increasing the total light output up to 23 fold for the first 30 sec (Figure 1). The mechanisms of stimulation for these two chemicals was different and cooperative. A less prominent enhancement was also observed for 10^{-6} mol/L ATP.

Table 2. Cooperative enhancing effects of CoA (final concentration: 0.068 mmol/L) and surfactants/polymers (at concentration as Table 1). Light count was integrated for first 30 sec. The count of luciferase solution without additives and CoA was used as the reference. The enhancement was calculated by dividing each output result by the reference.

	Enhancement (fold)	
Components	ATP (10^{-4} mol/L)	ATP (10^{-6} mol/L)
Luciferase and CoA	7	1.1
Luciferase, CoA and Triton X-100	23	5.4
Luciferase, CoA and Tween 20	20	4.7
Luciferase, CoA and PEG 5000	12	1.9
Luciferase, CoA and PVP 40000	19	2.3

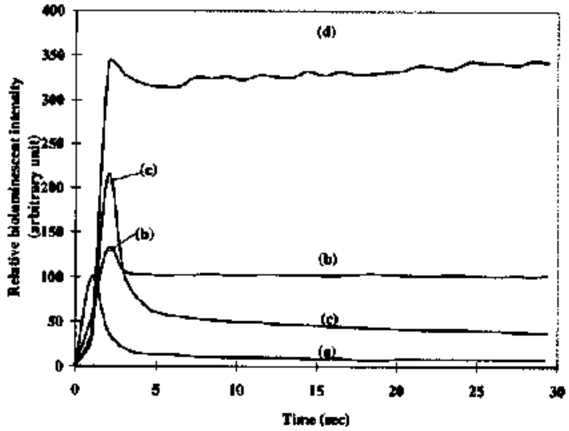

Figure 1. The Cooperative enhancement of Triton X-100 (0.4800%) and CoA on luciferase activity. (a) Luciferase; (b) luciferase with CoA; (c) luciferase with Triton X-100; (d) luciferase with CoA and Triton X-100.

Firefly luciferase was inactivated by negative charged lipids (6, 7). The presence of Triton X-100 (0.4800%) prevented inactivation by DOPS. Luciferase inactivated by DOPS can be partially reactivated by incubation with Triton X-100, the activity recovering from 17% to 64%. Although the mechanism is unknown, the recovered enzyme activity may be due to the replacement of DOPS by Triton X-100 at the same binding site; Triton X-100 may also enhance the activity of the remaining native enzyme. In the same experiment, DOPC was used to replace Triton X-100. There was no protection or reactivation effect for DOPC against DOPS.

The micelle environment was not required condition for the stimulation, since PEG and PVP do not form micelles. A large complex found by Kricka and DeLuca was proposed to be the enzyme-surfactant complex (1). The lack of an additivity effect between the combination of surfactants/polymers indicate a similarity to the enhancing mechanism. The binding of surfactants/polymers helps reactivate luciferase, which may have been inhibited by its substrates. Triton X-100 and Tween 20 may also help to modify the conformation and speed the release of oxyluciferin, enhancing enzyme turnover. Coenzyme A behaves differently with surfactants and polymers and probably binds to luciferase at a specific site. When added with Triton X-100, the bioluminescence intensity was enhanced further and maintained at a maximum level for at least 2 minutes. The high turnover rate was not inhibited by the accumulation of oxyluciferin. Other combinations with CoA produce less but still prominant total light output. The additivity effect enables a constant light output at high intensity. It is useful to develop direct reading biosensors which require those characteristics.

Acknowledgement

This work was partially supported by Protein Solutions, Inc., Salt Lake City, Utah via funding provided by an NSF STTR grant. We thank Drs. J. Herron and V. Hlady for access to equipment and facilities.

References

1. Kricka LJ, DeLuca M. Effect of solvents on the catalytic activity of firefly luciferase. Arch Biochem Biophys 1982;217:674-81.
2. Yeh PY. The properties of firefly luciferase in solution and at interfaces. Master thesis, University of Utah, 1989.
3. Simpson WJ, Hammond JRM. The effect of detergents on firefly luciferase reactions. J Biolumin Chemilumin 1991;6:97-106.
4. Airth RL, Rhodes WC, McElroy WD. The function of coenzyme A in luminescence. Biochim Biophys Acta 1958;27:519-32.
5. Schroder J, Protein sequence homology between plant 4-coumarate: CoA ligase and firefly luciferase. Nucleic Acids Res 1989;17:460-2.
6. Wang C-Y, Firefly Luciferase: Activity, Stability and Sensor Applications. Ph.D. Dissertation, University of Utah, Oct. 1996.
7. Dukhovich AF, Filippova NYu, Efimov AI, Ugarova NN, Berezin IB. Choline-containing phospholipids as specific activators and stabilizers of firefly luciferase. Dokl Akad Nauk SSSR, 1988;298:1257-60.

Effective Refractive Index of Adsorbed Protein Layers

Jinyu Wang, V. Hlady, J. D. Andrade, and Y. Q. Zhang,
Department of Bioengineering, University of Utah, Salt Lake City, Utah 84112, USA

ABSTRACT

We suggest an improved method to measure the effective index, n2, of the adsorbed protein layer by analyzing the relation between the angular distribution of fluorescence emission from adsorbed layer and n_2. The theoretical analysis is suported by experiments and can be used in the development of fiber optic sensors .

INTRODUCTION

The use of evanescent wave phenomena to measure absorption in surface adsorbed layers has been discussed by Harrick [1]. Lukosz, et. al. have derived a two-media model to evaluate the emission angular distribution from magnetic and electric dipoles close to a plane dielectric interface [2,3,4]. In this paper, we consider a three-media model consisting of a waveguide core, a layer of adsorbed protein and a buffer solution (PBS). We expect that the angular distribution of the light emitted from the adsorbed protein layer will depend on the refractive index of this layer i.e. on the surface protein concentration.

THEORETICAL ANALYSIS

Fig. 1 shows the three-media model. The media 1, 2 and 3, i.e. the waveguide core, the adsorbed protein layer and the buffer solution, are considered to be homogeneous isotropic loss-free dielectrics of refractive indices n_1, n_2 and n_3, respectively. We analyse the angular distribution of light emitted from the medium 2 and detected at the end of the waveguide. Two beams of the light are emitted to medium 1 by dipoles located in medium 2 at a distance z from the interface. The beam I which reaches point P directly and the beam II which is reflected by interface D and then reaches point P will meet at P. We can presume that the beam II comes from the image of the dipole (Fig. 1, dashed line). The problem we are concerned with is that the waves come from the two dipoles (one is the dipole itself and the another is its virtual image) interfere at point P and then transmit to medium 1.

The electric field of I at P can be written as

$$E1=E1(\alpha_2)\exp(-ikn_2z'/\cos\alpha_2) \tag{1}$$

and that of II

$$E2=r_{23}E2(\alpha'_2)\exp(-ikn_2(2D-z')/\cos\alpha'_2) \tag{2}$$

We get the sum of the two electric fields as follows

$$E_p=E1+E2 \tag{3}$$

The regions of the incident angles we discuss are near 90, D is smaller than D/cosα, so we have

$$\alpha_2=\alpha'_2 \text{ and } E1(\alpha_2)=E2(\alpha'_2) \tag{4}$$

then

$$E_p=E(\alpha_2)\left[\exp(-i\beta z/D)+r_{23}\exp(-i\beta(2-z/D))\right] \tag{5}$$

where

$$\beta=kn_2D/\cos\alpha_2 \quad \text{and } k=2\pi/\lambda \tag{6}$$

For the dipole can be at any position between 0 and D, we get the average value of E_p

$$\overline{E}_p/E(\alpha_2)=\frac{1}{D}\int_0^D\left[e^{-i\beta z/D}-e^{-i(\delta_{23}-\pi+\beta(2-z/D))}\right]dz \tag{7}$$

The transmittance of the thin layer for Ep can be written as

$$T_{21}^{(s,p)}=\left|\frac{t_{21}^{(s,p)}}{1-r_{12}^{(s,p)}r_{23}^{(s,p)}e^{-i2\delta}}\right|^2 \tag{8}$$

where $\delta=kn_2D\cos\alpha_2=\beta\cos^2\alpha_2.$ (9)

Lukosz et. al. have given the expressions for the normalized (time-averaged) power $P(\alpha)$ radiated within unit solid angle $d\Omega=\sin\alpha d\alpha d\phi$, into direction **u**, where α is the angle between u and the -z axis. In an unbounded medium 2 for magnetic dipole [4]

$$P_{\infty}^{(s)}(\alpha,\phi)=\frac{3}{8\pi}\left[\cos\theta\sin\alpha+\sin\theta\cos\phi\cos\alpha\right]^2 \tag{10}$$

and

$$P_{\infty}^{(p)}(\alpha,\phi)=\frac{3}{8\pi}\sin^2\theta\sin^2\phi \tag{11}$$

while for the electric dipole the polariztions (s) and (p) have to be interchanged in Eqs (10) and (11). In medium 1 ($0<\alpha_1<90$), for $\alpha_1<\alpha_{1c}$ ($\alpha_{1c}=\cos^{-1}(n_2/n_1)$), if $n_2<n_1$, and $\alpha_1<90$ if $n_1<n_2$. The fraction of light intensity angular distrbution of end-collection is

$$P^{(s,p)}(\alpha_1,\phi)=P_{\infty}^{(s,p)}(\alpha_2,\phi)T_{21}^{(s,p)}(\alpha_2)\frac{4}{\beta^2}\left[1-\cos(\pi-\delta_{23}^{(s,p)}-\beta)\right]\left[1-\cos\beta\right] \tag{12}$$

Our objective is to calculate the angular distribution of light collected by the end of the waveguide, or in other words, transmittance pattern of the adsorbed protein layer for three medium system. We have the transmittance pattern as follows

$$T^{(s,p)}(\alpha_1)=\frac{4}{\beta^2}T_{21}^{(s,p)}(\alpha_2)\left[1-\cos(\pi-\delta_{23}^{(s,p)}-\beta)\right]\left[1-\cos\beta\right] \tag{13}$$

Fig. 2 shows the angular distribution of end-collection calculated from equation (13), where n_1, n_3 and D/λ are known. $T(\alpha_1)$ mostly depends on n_2, the refractive index of the adsorbed protein layer. If we measure the angular distribution pattern, we can evaluate n_2. This suggests a method which can be used to measure the refractive index of an adsorbed protein layer, and consequently, the surface concentration of the protein.

EXPERIMENTAL

The experimental optical system used was similar to the one described in ref [5]. Fig. 3 shows only the major differences. The 488 nm laser beam is directly coupled into the planar waveguide through one end using the near cut-off modes. The flow cell and the waveguide, which is made of a quartz slide, were sealed by the blades. The thickness of the 25 mm-by-75 mm slide is 1 mm. The two ends of the slide were polished. The angular distribution of the fluorescence emitted by surface-adsorbed fluorescein-labeled Bovine Serum Albumin (FITC-BSA) layer is collected by the fiber bundle mounted on a rotation arm. The other end of the waveguide is placed right at the rotation center. The fluorescence was separated from the 488 nm laser line with monochromator. The solution of FITC-BSA in PBS is injected in the flow cell. Prior to the actual measurements the nonadsorbed FITC-BSA is flushed out of the cell leaving only irreversible surface-adsorbed protein layer. Different FITC/BSA labelling ratio, i.e. 2 and 5.4, was used in experiments .

RESULTS AND DISCUSSION

Fig. 4 shows the experimental results obtained after FITC-BSA adsorption from solution of different concentrations, C. The curves are well-matched with the function of $T(\theta)$ shown in

Fig. 2. This comparison suggests that a self-calibrated measurement of the refractive index of an adsorbed protein layer, i.e. the surface concentration of protein, is possible. We also find that the experimental angular distribution of emitted fluorescence neither depends on the protein-dye labelling ratio, nor on the intensity of the exciting light, but only on the refractive index n_2 (provided that n_1, and n_3, are constant).

Futher support for the proposed model can be found using already published literature data. For example, Slovacek et. al. had used fiber optic immunosensors for studying antigen-antibody reaction. They found that the fluorescent signal collection is a function of numerical aperture but did not analyse the angular distribution of signal [5]. We re-analysed their data according to the three-media model by exchanging the numerical aperture and the molar FITC concentration, F, (Fig. 4 in ref [5]). The results which are shown in Fig. 5. are fully supportive to the proposed model. In conclusion, by measuring the angular distribution curves for a set of certain waveguide-protein layer-solution combination one can. in principle, obtain a calibration curve which can be used in analytical determination of the refractive index of adsorbed protein layer or the surface concentration of the protein.

ACKNOWLEDGEMENT

The authors would like to thank Drs D. Christensen, J. Ives, and E. Brynda for discussion on these topics. This work was funded in part by NIH Grant HL#37046.

REFERENCES

[1] N. J. Harrick, Internal Reflection Spectroscopy, New York. Harrick Scientific Corporation, 1979.

[2] W. Lukosz and R. E. Kunz, "Light emission by magnetic and electric dipoles close to a plane interface. I. Total radiated power", J. Opt. Soc. Am., Vol. 67,1607-1615 (1977).

[3] W. Lukosz and R. E. Kunz, "Light emission by magnetic and electric dipoles close to a plane interface. II. Radiation patterns of perpendicular oriented dipoles", J. Opt. Soc. Am., Vol. 67,1615-1619 (1977).

[4] W. Lukosz, "Light emission by magnetic and electric dipoles close to a plane interface. III. Radiation patterns of dipoles with arbitrary orientation", J. Opt. Soc. Am., Vol. 69,1495-1503 (1979).

[5] R.Slovacek, B. Bluestein, M. Craig, C. Urcioli, L. Stundtner, M. Lee, and I.Walckzak, Ciba-Corning Diagnostics, 63 North Street, Medfield, MA 02052; W. Love and T. Cook, Corning Glass Works Research and Development, Sullivan Park, Corning, NY 14831, "Fiber Optic Immunosensors".

FIGURE CAPTIONS

Fig. 1. The three media model. The two beams will interfere at point P; the beam I will reach P directly and the beam II will reflect at the interface D and then reach P. We can suppose that the beam II comes from the image of the dipole as indicated by the dashed line.

Fig. 2. The enhancement of $T(\theta)$ as a function of the angle, θ ($\theta = 90 - \alpha_1$), as calculated from Eq. 12.
____ s-polarized light, ... p-polarized light.

Fig. 3. The optical arrangement of angular detection system of fluorescence.

Fig. 4. Normalized fluorescence intensity of adsorbed FITC-BSA shown as a function of detection angle, θ. The degree of FITC labeling of BSA equals 2. The concentrations of FITC-BSA solution from which the actual adsorption took place are indicated in the figure legend.

Fig. 5. Signal dependency on numerical aperture of end-collection. Data taken from ref. [5].

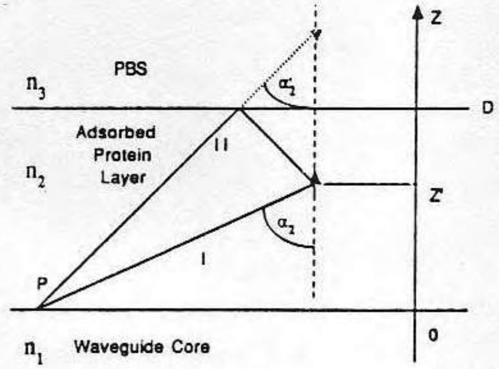
Z
PBS
n_3
α_2
D
Adsorbed
Protein
Layer
II
n_2
Z'
α_2
I
P
0
n_1
Waveguide Core

Fig. 1

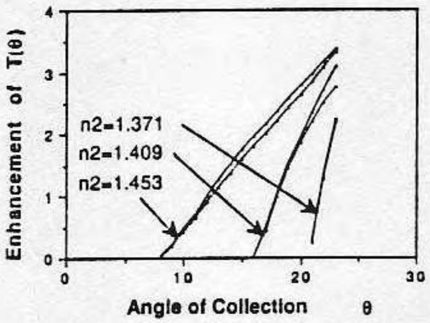

Fig. 2

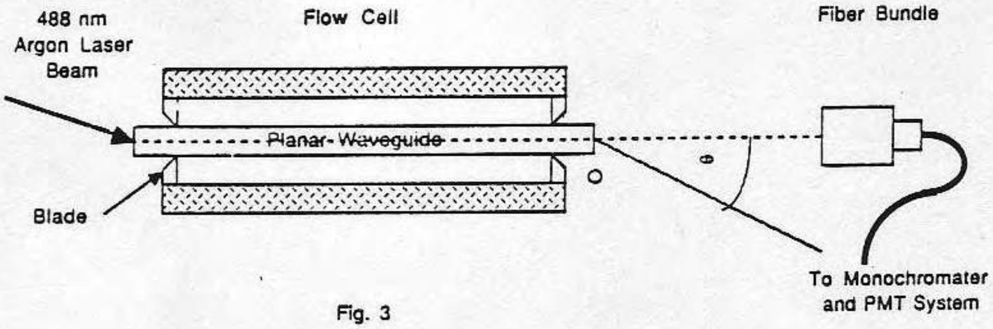
488 nm
Argon Laser
Beam
Flow Cell
Fiber Bundle
Planar-Waveguide
θ
O
Blade
To Monochromater
and PMT System

Fig. 3

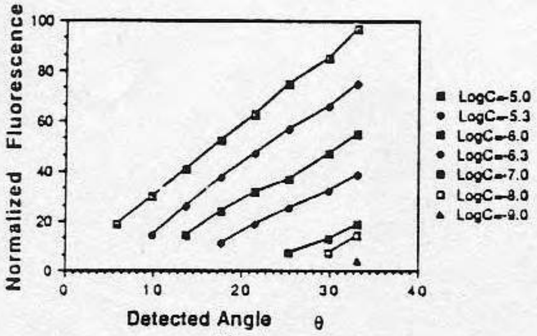

Fig. 4

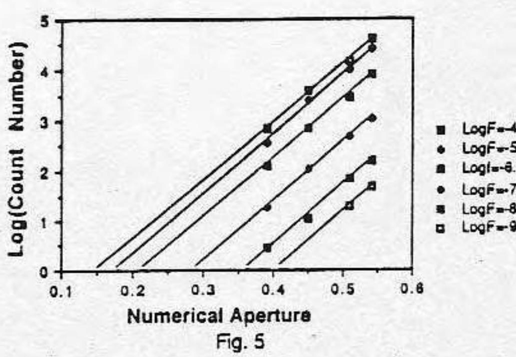

Fig. 5

TS
517.2
O65
1989

OPTICAL COATINGS

Proceedings of International Symposium 23-25 May 1989, Shanghai, China

Sponsored by
Chinese Optical Society
In Cooperation with
Optical Society of America

Edited by
Tang Jinfa
Yan Yixun

'89ISOC

IAP
INTERNATIONAL ACADEMIC PUBLISHERS
(A Pergamon– CNPIEC Joint Venture)

SENSITIVITY ANALYSIS OF EVANESCENT FIBER OPTIC SENSORS

Jinyu Wang, D. Christensen, E. Brynda, J. Andrade, J. Ives and J-N. Lin

Department of Bioengineering, University of Utah, Salt Lake City,Utah 84112

ABSTRACT

Evanescent fiber optic sensors are being developed for remote in situ immunoassay. The single reflection total internal reflection fluorescence (TIRF) geometry can serve as a well-defined model against which evanescent waveguide devices can be compared and evaluated. This paper addresses the problem of optimizing the sensitivity of an evanescent fiber optic sensor (EFOS). Two aspects are discussed: (1) the modes of exciting laser light in the fiber have an effect on the sensor efficiency and signal-to-noise ratio; (2) in a fiber biosensor, there is generally a protein layer attached to the core surface; the thickness of the layer is at least 5nm. If the refractive index of the protein layer can be made equal to the refractive index of the core, we can get a new fiber waveguide in which the core also contains the protein layer. The fluorescent emission sources are thus inside the core region and generate the highest signal collection efficiency. We also discuss the situation when the refractive index of the protein layer is larger or smaller than that of the optical fiber core.

1 INTRODUCTION

Evanescent fiber optic sensors (EFOS) can be used to study protein adsorption and antigen (Ag)-antibody (Ab) interactions and are being developed for remote in situ immunoassay. This kind of sensor can be used for certain industrial chemicals, biochemicals, toxins and microooganisms. A number of authors have discussed EFOS and their applications [1-15].

The sensitivity of immunoassay techniques is determined by the affinity of the Ab for the Ag. The higher the binding constant, the stronger the interaction between the Ab and the Ag, which results in more Ab-Ag complexes at low concentrations [1].

The intrinsic fluorescence background of human serum [16] also affects the sensitivity, since the signal-to-noise ratio may be reduced by the intrinsic fluorescence background of serum. Tetramethylrhodamine, whose absorption and fluorescence emission occur at longer wavelengths (540 nm and 580 nm, respectively) than fluorescein, can be used to improve the signal-to-noise ratio [17].

Several papers [11-15] have investigated EFOS for surface sensitive homogeneous assays. Slovacek, et. al. [12] have detected fluorescein-labelled digoxin (Molecular Weight=833 daltons) and human ferritin (M. W. =450,000 D) with a lower detection limit of $6*10^{-10}$M and 10^{-11}M, respectively. Sutherland, et. al. [13] have studied fluorescein labelled immunoglobulin G (M. W. =150,000 D) with a sensitivity of $3*10^{-8}$M.

The general principle of EFOS is the same as total internal reflection fluorescence (TIRF) but the sensitivity is lower. Using the TIRF geometry, the immunoassay technique has the sensitivity to detect 10^{-12}M. [18] However, with EFOS, 10^{-12}M may not be detected. This is because the optical configuration of EFOS is different from that of TIRF, in both fluorescence excitation and signal collection.

This paper addresses the problem of analyzing and improving the optical arrangement to optimize the sensitivity of EFOS. The evanescent wave spectroscopy of EFOS is the same as that of TIRF; however, the evanescent field is generated by guided modes in EFOS and by single or multi-reflection in TIRF. The modes of exciting laser light in the sensor fiber have an effect on the sensor efficiency and signal-to-noise ratio. Moreover, the fluorescent signal in EFOS is guided in the fiber in the direction of the fiber axis. When the fluorescent species is placed at the end of the fiber core, the sensing surface is normal to the fiber axis. In this case, the fluorescent signal end-couples into the attached fiber, but the area of the surface is small and the electric field which excites the fluorescence is not an evanescent field. When the fluorescent molecules are located on the fiber core surface, the sensing surface is parallel to the fiber axis. The advantage of this case is that the area of the surface may be increased for detecting lower concentrations, but the fluorescent signal collection is very different in the two geometries. We must therefore consider the back coupling efficiency and the refractive indices of the fiber core, the solution and the proteins, including the numerical aperture of the attached fiber. Marcuse has derived a model to evaluate the back coupling efficiency [19], but did not consider the case where the fluorescing layer had a different refractive index than the cladding.

Actually, when we dip the sensor fiber into a protein solution, there is always some adsorption of protein molecules onto the fiber core surface. According to the effective medium theory [20], there is an effective layer with an effective refractive index n2 on the surface, provided that the refractive index of the protein is not equal to that of the solution. We consider a model which contains three zones: fiber core, effective layer and solution. With this model, we analyze the relation between the signal back coupling efficiency and the refractive indices, especially the refractive index of the effective layer.

Experimental measurements with a 600 micrometer diameter optical fiber and FITC-labelled IgG were performed. The refractive index of the adsorbed protein layer was adjusted, and the results agreed with the effective index model.

2 THEORY

The fundamental phenomenon employed in EFOS is that of exciting and detecting fluorescence in the protein layer which is adsorbed or bonded to the surface of the waveguide core. The excitation is accomplished through the evanescent field associated with propagation of guided modes in a sensor fiber. The fluorescent light detected is that portion of the total emission which couples back into the fiber and is guided. The sensor geometry is shown as Fig.1. As mentioned, the binding constant, the intrinsic background, the evanescent absorption, Ae, and the fraction of the emitted fluorescence that is detected, Ec, affect the sensor sensitivity. Based on these, Glass, et. al. [21] wrote a general expression for the signal from an EFOS as

$$S = K A_e E_c \qquad (1)$$

where S is the intensity of the signal and K is a proportionality constant, incorporating such nonwaveguide dependent factors as the fluorophore concentration, fluorescent quantum efficiency and the spectral transmission of the optical components.

There are three optical media: the fiber core, the adsorbed protein layer and the surrounding solution with refractive indices nco,n2 and ns, respectively. The evanescent absorption, Ae, is different in the two cases of a film and a bulk sample. Harrick [22] has shown that the optical absorption can be expressed as an increased effective thickness of the layer, the effective thickness being the thickness that absorbs the same optical power in normal propagation as is absorbed evanescently. In the case of randomly polarized light, the average factor of increase for the thickness of a thin layer is given by [21]

$$D_{av}/D = \frac{2n_{co}n_2\sin\theta_z}{n_{co}^2-n_s^2}\left[1+f(\theta_z)\right] \qquad (2)$$

where

$$f(\theta_z) = \frac{\left|\left(1+(n_s/n_2)^4\right)\cos^2\theta_z-(n_s/n_{co})^2\right|}{\left|\left(1+(n_s/n_{co})^2\right)\cos^2\theta_z-(n_s/n_{co})^2\right|} \qquad (3)$$

and θz is the angle of incidence, Dav and D are the average thickness and the thickness of the layer, respectively. The larger the effective thickness, the more the absorbed optical power, and thus the greater the fluorescent signal.

We can evaluate the optimum incident angle, (θz)op, at which the effective thickness reaches its maximum value from

$$F(\theta_z)=d(D_{av}/D)/d\theta_z \qquad (4)$$

Letting $F(\theta_{zm})=0$, and after mathematical treatment, we have

$$\theta_{zm}=\cos^{-1}\Delta \qquad (5)$$

where

$$\Delta^2=\frac{\left|n_{31}^2(4+n_{31}^2+3n_{32}^4)+\sqrt{(n_{31}^2-n_{32}^4)\left[(4+n_{31}^2)^2+(8-n_{31}^2)n_{32}^4\right]}\right|}{\left[2(1+n_{31}^2)(2+n_{31}^2+n_{32}^4)\right]} \qquad (6)$$

and $n1=nco$, $n3=ns$, provided that $n32^4/n31^2$ is smaller than or equal to unity. We have $F(\theta z)>0$, when $\theta z<\theta zm$. In the case of $n32^4/n31^2$ larger than unity,we always have $F(\theta z)>0$. $F(\theta z)>0$ means A_θ increases with θ. For weakly guiding waveguides we always have the maximum value of A_θ when $(\theta z)op=\theta ca$. However, it is practically impossible to adjust the fiber parameters so exactly that it operates precisely at the cutoff of any given mode. Although a mode near cutoff suffers high losses due to any fiber irregularity, it is still suitable for carrying exciting laser light and has the benefit of improving the signal-to-noise ratio for remote EFOS.

Now we discuss Ec, the fraction of emitted fluorescence reaching the detector, i. e. the collection efficiency (see equation 1).

According to waveguide theory [23], if the waveguide is perfect, infinitely long, a light source is presumed inside the core, and the light source is located at minus infinity, there will be guided modes inside the core, radiation modes outside the core, and leaky waves. The former two are standing waves. Snyder [24] gives the solution from Maxwell's equations for fibers. Using intuitive notions concerning the propagation of rays, he described the ray propagation along a multimode fiber. Ec increases with the number of bound modes, which transmit the excited fluorescence. If θz and $\theta\phi$ are spherical polar angles relative to the axis of a fiber with axisymmetric refractive-index profile $n(r)$, where r is the cylindrical radius, then the number of bound modes, Mbm, is given by

$$M_{bm}=\frac{k^2}{\pi}\int_0^{\rho} n^2(r)\,r\,dr\int_0^{\theta_c} d\theta_z\int_0^{2\pi}\sin\theta_z\cos\theta_z\,d\theta_\phi \qquad (7)$$

where ρ is the radius of the fiber core, θc is the critical angle, $\theta c=\cos^{-1}(ncl/nco)$, and $k=2\pi/\lambda$.

For an EFOS, we assume fluorescent labelled protein molecules adsorbed on the core surface to form a monomolecular layer. The thickness of the layer is in the order of 10 nm. The refractive index of the layer is different from the bulk material. An estimate of the refractive index of such a layer utilizes the effective medium approximation [20]:

$$\sum\frac{f_i(\varepsilon_i-\langle\varepsilon\rangle)}{(\varepsilon_i-2\langle\varepsilon\rangle)}=0 \qquad (8)$$

which in general form gives the pseudodielectric permittivity $\langle\varepsilon\rangle$ of a mixture of *i* materials each with volume fraction fi, permittivity εi, where

$$\varepsilon_i=n_i^2 \qquad (9)$$

Let us assume two phases in the film(adsorbed protein layer): voids (composed of the phosphate buffer solution, PBS, we use for protein solution) with $\varepsilon 1=ns^2$ and volume fraction f1, and adsorbed protein with $\varepsilon 2=np^2$ (e. g. np=1.544 [25]) and volume fraction f2=1-f1. We can calculate $n2=(\langle\varepsilon\rangle)^{0.5}$; $0<f2<1$, and thus $ns<n2<np$.

The effective refractive index may be larger than or equal to that of the fiber core, $n2>nco$, or smaller than nco but still larger than that of the cladding, $nco>n2>ncl$, or not larger than ncl, $ncl>n2$. We discuss the signal collection efficiency, Ec, associated with the fraction of the bound modes in these three cases individually and use ray optics for illustration. The three zone, core-film-PBS system is shown in Fig.1, where θca ($\theta ca=\cos^{-1}(ncl/nco)$) and θcs ($\theta cs=\cos^{-1}(ns/nco)$) are the critical angles for attached fiber and sensor, respectively. Because of ncl>ns, we have

$$\theta_{ca}<\theta_{cs} \qquad (10)$$

The modes which are bound in the attached fiber are all bound in the sensor fiber. We need not consider the film-PBS interface and only discuss the film-core interface. ρ is the core radius, and $\Delta\rho$ is film thickness.

First we deal with the case of nco>n2>ncl. $\theta c1$ ($\theta c1=\cos^{-1}(n2/nco)$) and $\theta c2$ ($\theta c2=\cos^{-1}(ns/n2)$) are the critical angles for the film-core and the film-PBS interfaces, respectively. Fig.2-b yields the fraction of fluorescent emission which, after traversing the film-core interface, are guided by the attached fiber. If we view the rays in the film, all the rays with incident angles $0<\theta<\theta 2$, can enter into the core and be guided. In the core, this range is $\theta_{c1}<\theta<\theta_{ca}$. Using Eq. (7) we get

$$M_{bm}=\frac{k^2}{\pi}\left|\int_0^{\rho} n_{co}^2 r dr\int_{\theta_{c1}}^{\theta_{ca}} \sin\theta_z\cos\theta_z d\theta_z+\int_{\rho}^{\rho+\Delta\rho} n_2^2 r dr\int_0^{\theta_2}\sin\theta_z\cos\theta_z d\theta_z\right|\int_0^{2\pi} d\theta_\phi \qquad (11)$$

$$M_{bm}=k^2(\rho+\Delta\rho)^2(n_2{}^2-n_{cl}{}^2)/2 \qquad (12)$$

From Eq. (12), we understand that the Mbm mostly depends on the effective refractive index of the layer. When n2 is equal to ncl, we have Mbm=0; no fluorescent signal ray can enter the attached fiber. If n2 is equal to nco, we get the maximum value of Mbm. If we determine the angle $\theta c1$, or determine the angular distribution of the signal, we can determine n2; further we can work out the surface concentration. This method is similar to that of Lukosz [26].

Fig.2-a yields the case of n2>nco. This time $\theta c1=\cos^{-1}(nco/n2)$. Changing the upper and lower limits of θz, from Eq.(11) we have

$$M_{bm}=k^2(\rho+\Delta\rho)^2(n_{co}{}^2-n_{cl}{}^2)/2 \qquad (13)$$

The value of Mbm depends on the thickness of the layer and is independent of the effective refractive index of the layer.

The case of n2<ncl is shown in Fig.2-c. There are not any rays which enter the fiber core and become bound modes in the attached fiber. Marcuse [19].[23] has analysed a similar case and derived a model to evaluate the back coupling efficiency which is much lower than our model. He investigated the question of incoherent excitation of step-index optical fiber with light sources that are located in the cladding. In terms of ray optics, light from sources in the fiber cladding can not be trapped as truly guided core modes in a positively guiding fiber. He treated this problem using evanescent field back coupling. Here we do not consider the back coupling efficiencies generated by the evanescent field.

The effective thickness, $\Delta\rho$, is much smaller than ρ, the radius of the fiber core. We can use ρ instead of $\rho+\Delta\rho$, when we calculate the number of bound modes. Fig.3 shows the curve of relative number of bound modes, Mr=Mbm(n2)/Mbm(nco), versus n2. From Fig.3, one can see clearly that, Mr=0 when n2<ncl, Mr remains constant when n2>nco and when ncl<n2<nco, Mr decreases monotonically with n2 . The curve coincides with the experiments done by Yoshida [17] .

From Eq.(1), the signal S is a function of Ae and Ec, and Ec is a function of ncl, nco, ρ/λ, n2. To get higher sensitivity, we should increase the difference between nco and ncl, i. e., increase the numerical aperture of the attached fiber. Of course, a larger value of ρ/λ is better for the sensitivity. We should also improve the adsorption condition, that means we should maximize n2 and $\Delta\rho$.

3 EXPERIMENT

The optical configuration of EFOS, is similar to that of Yoshida [17] and is shown in Fig.4. The 488nm light from an air-cooled argon laser (Model No. 5490 ASL, Ion Laser Technology) is coupled into the fiber by lens L3 (focal length fl=12.5 cm). To maximize the sensitiviy, the laser beam is focused to a spot on the face of the fiber near the core-cladding interface at an angle near cutoff [27].

The back coupled fluorescence collected from the distal end of the fiber is first collimated by L1(fl=7.3 cm), then passes through the 488 nm rejection filter (Pomfret Research Optics) and the glass high pass filter (Newport Corp OG500) and is focused by lens L2 (fl=12.5 cm) into the monochromator (Instrument SA, Inc. HR-640). The output is detected by a photomultiplier tube (Hamamatsu R585) and photon counting instrumentation (EGG Ortec).

The core of a 600 mm optical fiber is used as the sensor, which includes the attached fiber. Approximately 3 cm of the Tefzel coating is removed from the midsection using a scalpel. Next, most of the cladding, which is made of silicone resin, can be easily scraped off by a wooden tool. The cladding residue can be removed by immersing the fiber in 85C chromic acid for 20 minutes [28]. The sensor is placed in a cylindrical flow cell to allow the introduction of solutions.

Next, various concentration of fluorescein-labelled human IgG (H-IgG) (Cappel Laboratories) in PBS were used for the optical studies. We injected H-IgG solution ($2.67*10^{-8}$M/L) into the flow cell. The average labelling ratio is 3.75 labels per protein molecule. The fluorescent signal increases with time as the protein molecules are adsorbed to the sensor surface, shown as Fig.5. We then inject PBS to remove the protein solution (position B in Fig. 5). Next we introduce unlabelled H-IgG ($3.33*10^{-7}$M/L) which is more than 10 times that of the labelled H-IgG. The fluorescent signal increases and reaches a new plateau (C in Fig. 5). It increases about 15%. Similar experiments have been done using a single reflection side-collection TIRF system, but the increase of the fluorescent signal was not found as the higher concentration of unlabelled protein was introduced.

We suggest that the observed increase comes from the increase in the effective refractive index of the adsorbed protein layer. We get an adsorbed protein layer on the sensor surface when we inject the labelled protein solution. As n2>ncl, we get signal collection. The signal decreases after the PBS is injected. Because the adsorption process is semi-reversible, a dynamic equilibrium between adsorption and desorption can be established, such that rates of adsorption and desorption are equal [29]. Some of the protein molecules desorb, and the signal goes down. Notice, two factors make the signal go down: the first is the decrease of fluorescein which makes the fluorescent light decrease, the second is the decrease of the effective refractive index of the layer which leads to decreased signal in the region of n2<nco. When we introduce the higher concentration of unlabelled protein, the increase of n2 generates the increase of signal collection and the signal goes up. The effect is not observed in a TIRF experiment because of the very different collection geometry, as discussed earlier.

The experiments match the theoretical analysis very well. When we inject labelled H-IgG solution of low concentration ($2.67*10^{-13}$ M/L), we get only the background signal collection of 300 counts/sec, but when we introduce unlabelled H-IgG whose concentration is $3.33*10^{-7}$ M/L, we get a signal increase of 50 counts/sec. The unlabelled protein (including the previously introduced labelled protein within it) increases the index of the layer, so a larger value of Mbm is generated, which can be used to transmit the fluorescent signal. The signal collection is thus improved. Using this method we measured a series of concentrations of H-IgG in PBS. The results are shown in Fig.6, curve A, while curve B shows the results without using higher concentration unlabelled H-IgG. See Fig. 6 caption for details. This simple method can improve the sensitivity.

4 CONCLUSION

The commercial fiber with a loss of about 1dB/km is very good waveguide for making a sensor. Using the fiber to fabricate EFOS, the fluorescent signal comes mainly from the surface. We conclude that if the effective index n2 of the effective layer is not larger than the refractive index ncl of the cladding, and the core is the same as sensor fiber core, Marcuse's analysis is valid. When n2>ncl our analysis is valid and shows a higher fluorescent signal back coupling efficiency than that of the Marcuse model.

The sensitivity of EFOS can be improved by higher evanescent absorption and collection efficiency. We predict that the EFOS can demonstrate the same sensitivity as TIRF when we improve the adsorption condition to generate a higher value of n2 or when we adjust the fiber parameters to decrease the value of ncl and increase the numerical aperture of the attached fiber. Determining the angular distributions of the fluorescent signal and then evaluating the surface concentration is another, perhaps better, approach which is now being evaluated.

5 ACKNOWLEDGMENT

The authors thank Dr. Peter A. Suci and Ms. Dawn E. Yoshida for help and useful discussions.

This work was supported in part by the National Institutes of Health Grant HL 37046 and by the Center for Biopolymer at Interfaces, University of Utah.

Jinyu Wang acknowledges a faculty leave from Tsinghua University, Beijing, PRC.

E. Brynda acknowledges the inter institutional collaboration between the Inst. for Macromolecular Chemistry (Prague) and the University of Utah Dept. of Bioengineering.

REFERENCE

[1] J. D. Andrade, J. N. Lin, J. Herron, M. Reichert, and J. Kopecek, "Fiber optic immunodetectors: sensors or dosimeter?", Proc. SPIE, vol. 718, pp. 280, 1986.

[2] R. Narayanaswamy, "Optical fiber sensors in chemical analysis", Anal. Proc. (London), vol. 22, pp. 204-206, 1985.

[3] S. M. Angel, "Optrodes: chemically selective fiber-optic sensors", Spectrosopy, vol. 2, pp. 38-46, 1987.

[4] R. Narayanaswamy, "Optical fiber chemical sensors", Proc. Electrochem Soc., 87-9(Proc. Symp. Chem. Sens.), pp. 428-437, 1987.

[5] T. G. Giallorenzi, J. A. Bucaro, A. Dandridge, G. H. Sigel, J. H. Cole, S. C. Rashleigh, and R. G. Priest,"Optical fiber sensor technology", IEEE J. Quantum Electron, vol. QE-18, pp.626-665.

[6] V. I. Busurin, A. S. Semenov, and N. P. Udalov,"Optical and fiber-optic sensors (review)", Sov. J. Quantum Electron, vol. 15, pp. 595-621, 1985.

[7] O. S. Wolfbeis, "Fiber-optic sensors in biomedical sciences", Pure and appl. Chem., vol. 59, pp. 663-672, 1987.

[8] A. M. Smith, "Biomedical sensing using optical fibers", Anal. Proc. (London), pp. 212, 1985.

[9] B. J. Tromberg, M. J. Sepaniak, T. Vo-Dinh, and G. D. Griffin, "Fiber-optic chemical sensors for competitive binding fluoroimmunoassay", Anal. Chem., vol. 59, pp. 1226-1230, 1987.

[10] J. D. Andrade, R. A. Yan Wagenen, D. E. Gregonis, K. Newby, and J. N. Lin,"Remote fiber-optic biosensor based on evanescent-excited fluoro-immunoassay: concept and progress", IEEE. Trans. Electron, Dev. vol. ED-32, pp. 1175-1179, 1985.

[11] T. Hirschfeld, U. S. Patent No. 4,447,546, May 8, 1984.

[12] R. Slovacek, B. Bluestein, M. Craig, C. Urcioli, L. Stundtner, M. Lee, T. Wickzsk, W. Love, and T. Cook, "Fiber optic immunosensors", Proc. Electrochem. Soc., 87-9(Proc. Smyp. Chem. Sens.), pp. 456-463, 1987.

[13] R. M. Sutherland, C. Dahne, J. R. Place, and A. S. Ringrose, "Optical detection of antbody-antigen reactions at a glass-liquid interface", Clin. Chem., vol. 30, pp. 1533-1538, 1984.

[14] D. E. Yoshida, J. T. Ives, W. M. Reichert, D. A. Christensen, and J. D. Andrade, "Development of a fiber optic fluoroimmunoassay: proximal versus distal end collection geometries of a fiber sensor", Proc. SPIE, vol. 904, pp. 57-60, 1988.

[15] K. Newby, W. M. Reichert, J. D. Andrade, and R. E. Benner, "Remote spectroscopic sensing of chemical adsorption using single multimode optical fiber", Applied Optics, vol. 23, pp. 1812-1815, 1984.

[16] E. Koller, O. Quehenberger, G. Jurgens, O. S. Wolfbeis, and H. Esterbaur, "Investigation of human plasma low density lipoprotein by three-dimensional fluorescence spectroscopy" Federation European Biochem, Soc., vol. 198, pp. 229-234, 1986.

[17] D. E. Yoshida, "Characterization of an evanescent fiber optic immunosensor using tetramethylrhodamine", MSC. Thesis, University of Utah, June, 1988.

[18] J. N. Lin, Hlady, V., and J. D. Andrade, "Flat-Plate Total Internal Reflection Fluorescence (TIRF) Immunoassay" in Preparation.

[19] D. Marcuse, "Launching light into fiber cores from sources located in the cladding", IEEE J. Lightwave Technology, vol. 6, pp. 1273-1279, 1988.

[20] D. E. Aspnes, "Optical Property of Thin Films", Thin Solid Films, 89, 249, 1982.

[21] T. R. Glass, S. Lackie, and T. Hirschfeld, "Effect of numerical aperture on signal level in cylindrical waveguide evanescent fluorosensors", Appllied Optics, vol. 26, pp. 2181-2187, 1987.

[22] N. J. Harrick, Internal Reflection Spectrscopy, New York: Harrick Scientific Corporation, 1979.

[23] D. Marcuse, Theory of Dielectric Optical Waveguide, pp. 19-20, Academic press, New York and London, 1974.

[24] A. W. Snyder and J. D. Love, Optical Waveguide Theory, pp. 692-705, Chapman and Hall, London and New York, 1983.

[25] H. Arwin, "Optical Properties of Thin Layers of Bovine Serum Albumin, gama-Globulin, and Hemoglobin", Applied Spectroscopy, vol. 40, No. 3, pp. 313-317, 1986.

[26] Ph. M. Nellen, K. Tiefenthaler and W. Lukosz"Integrated Optical Input Grating Couplers as Biochemical Sensors", Eurosensors, '87, First European Conference on Sensors and their Applications, Cambridge, U. K., September 22-24, 1987.

[27] Chin-Lin Chen, "Excitation of higher order modes in optical fiber with parabolic index profile", Applied Optics, vol. 27, pp. 2353-2356, 1988.

[28] K. E. Newby, "A Remote Interfacial Chemical Sensor Using a Single Multimode Optical Fiber", Master's Thesis, University of Utah, 1984.

[29] Yu-Ling Cheng, Brent K. Lok and Channing R. Robertson, "Interactions of Macromolecules with Surfaces in Shear Fields Using Visible Wavelength Total Internal Reflection", in J. D. Andrade ed, Surface and Interfacial Aspects of Biomedical Polymers, vol. 2 Protein Adsorption, pp. 121-135, Plenum Press, New York, 1985.

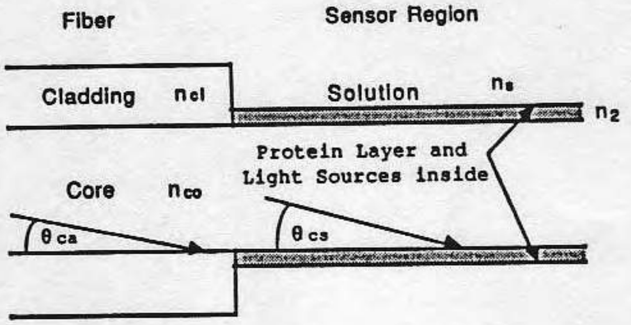
Fiber
Sensor Region
Cladding
n_{cl}
Solution
n_s
n_2
Protein Layer and
Light Sources inside
Core
n_{co}
θ ca
θ cs

Fig.1 Evanescent Fiber Optic Sensor geometry. The fluors are located in the adsorbed protein layer and excited by the evanescent field.

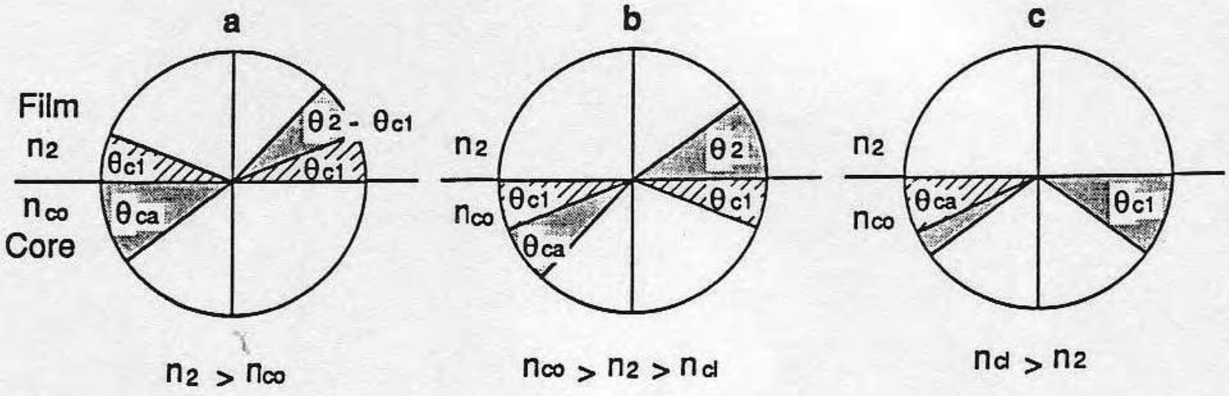
a
b
c
Film
n_2
n_{co}
Core
$\theta_2 - \theta_{c1}$
θ_{c1}
θ_{ca}
θ_2
$n_2 > n_{co}$
$n_{co} > n_2 > n_{cl}$
$n_{cl} > n_2$

Fig. 2 The film-core interface

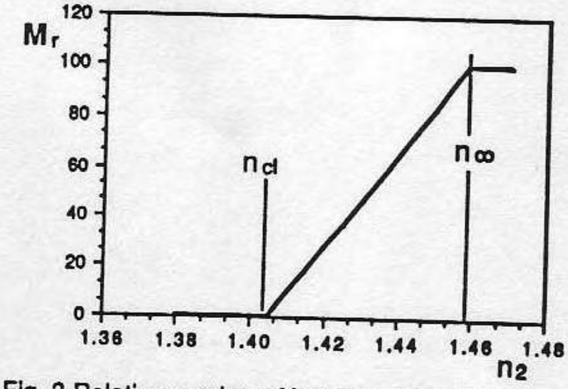

Fig. 3 Relative number of bound modes, Mr, as a function of protein film refractive index, n_2; calculated by Equation 11.

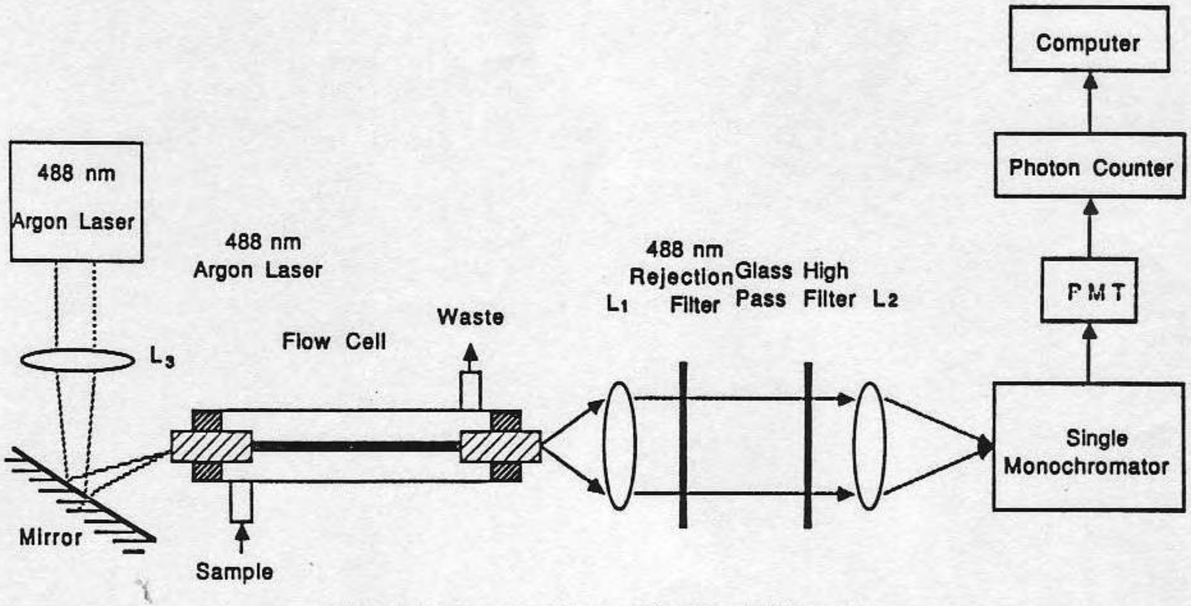
488 nm
Argon Laser
L3
Mirror
488 nm
Argon Laser
Flow Cell
Waste
Sample
L1
488 nm
Rejection
Filter
Glass High
Pass Filter
L2
Single
Monochromator
PMT
Photon Counter
Computer

Fig.4 Experimental configuration for optical system

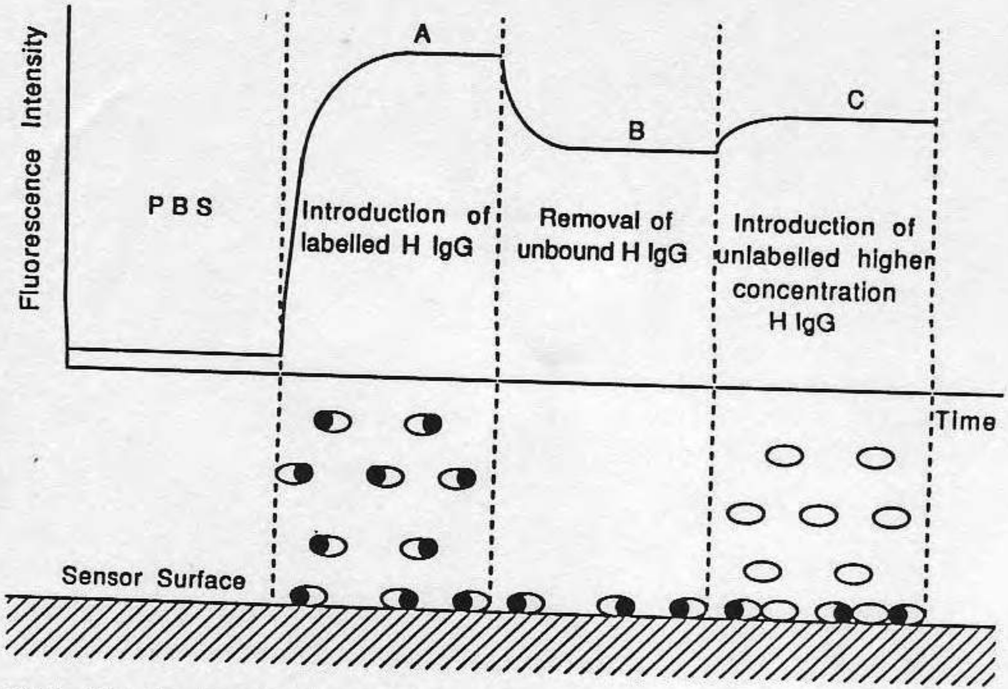
Fluorescence Intensity
A
B
C
P B S
Introduction of labelled H IgG
Removal of unbound H IgG
Introduction of unlabelled higher concentration H IgG
Time
Sensor Surface

Fig.5 The denser adsorbed layer is helpful for the signal collection.
◐ represents fluoresent labelled protein
○ represents unlabelled protein
A: low concentration of protein, surface protein concentration is low, and n2 is low.
B: wash step, surface protein concentration, and n2 is low.
C: higher concentration of protein, surface protein concentration is high, and n2 is increased.

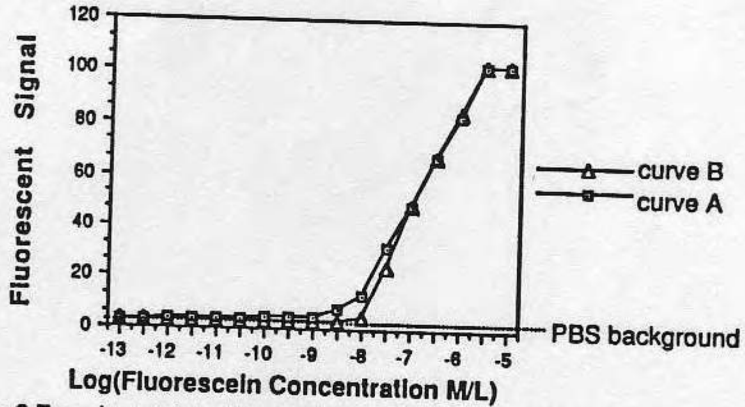

Fig.6 Experimental curves of relative signal versus fluorescein concentration. Curve B represents a sequence of measurements comparable to Figure 5 A and B. Curve A represents a similar set of measurements, but with 3.33 X 10^{-7}M/L of unlabelled protein added after each concentration step (comparable to C in Figure 5). Curve B represents the expected adsorption isotherm. The surface is about half saturated at about 10^{-7}M and fully saturated at about 10^{-6}M. Note that in the range of 10^{-9}M to 10^{-7}M, the addition of 3.33 X 10^{-7}M of unlabelled IgG enhances the signal significantly, due to the adsorption of the unlabelled IgG, and the resultant increase in n_2.

Pha

Chemi
Uni

Li
ships a
distrib
ase wer
lipid p
substra

N
and phy
ingly s
It woul
terist
natura
nally
associ
whethe
mechan
has sh
lipid
concer
ation (
system
lectin
bindin
basis
rather
proces
membra

C
(BLMs)
phosph
of a s
water
of mon
gaseo
phase
phase

PROCEEDINGS
SPIE—The International Society for Optical Engineering

Optical Fibers in Medicine IV

Abraham Katzir
Chair/Editor

18–20 January 1989
Los Angeles, California

Sponsored by
SPIE—The International Society for Optical Engineering

Cooperating Organizations
American Academy of Dermatology
American Academy of Otolaryngology—Head and Neck Surgery, Inc.
American Association of Physicists in Medicine
American College of Surgeons
The American Heart Association
American Society for Dermatologic Surgery, Inc.
American Society for Laser Medicine and Surgery, Inc.
Association for the Advancement of Medical Instrumentation
Indonesian Society for Laser Medicine
Society for Analytic Cytology
Under the auspices of the European Laser Association

Published by
SPIE—The International Society for Optical Engineering
P.O. Box 10, Bellingham, Washington 98227-0010 USA
Telephone 206/676-3290 (Pacific Time) • Telex 46-7053

SPIE PROCEEDINGS SERIES

Volume 1067

SPIE (The Society of Photo-Optical Instrumentation Engineers) is a nonprofit society dedicated to advancing engineering and scientific applications of optical, electro-optical, and optoelectronic instrumentation, systems, and technology.

The papers appearing in this book comprise the proceedings of the meeting mentioned on the cover and title page. They reflect the authors' opinions and are published as presented and without change, in the interests of timely dissemination. Their inclusion in this publication does not necessarily constitute endorsement by the editors or by SPIE.

Please use the following format to cite material from this book:
Author(s), "Title of Paper," *Optical Fibers in Medicine IV,* Abraham Katzir, Editor, Proc. SPIE 1067, page numbers (1989).

Library of Congress Catalog Card No. 89-60029
ISBN 0-8194-0102-1

Copyright © 1989, The Society of Photo-Optical Instrumentation Engineers.

Copying of material in this book for sale or for internal or personal use beyond the fair use provisions granted by the U.S. Copyright Law is subject to payment of copying fees. The Transactional Reporting Service base fee for this volume is $2.00 per article and should be paid directly to Copyright Clearance Center, 27 Congress Street, Salem, MA 01970. For those organizations that have been granted a photocopy license by CCC, a separate system of payment has been arranged. The fee code for users of the Transactional Reporting Service is 0-8194-0102-1/89/$2.00.

Individual readers of this book and nonprofit libraries acting for them are permitted to make fair use of the material in it, such as to copy an article for teaching or research, without payment of a fee. Republication or systematic or multiple reproduction of any material in this book (including abstracts) is prohibited except with the permission of SPIE and one of the authors.

Permission is granted to quote excerpts from articles in this book in other scientific or technical works with acknowledgment of the source, including the author's name, the title of the book, SPIE volume number, page number(s), and year. Reproduction of figures and tables is likewise permitted in other articles and books provided that the same acknowledgment of the source is printed with them, permission of one of the original authors is obtained, and notification is given to SPIE.

In the case of authors who are employees of the United States government, its contractors or grantees, SPIE recognizes the right of the United States government to retain a nonexclusive, royalty-free license to use the author's copyrighted article for United States government purposes.

Address inquiries and notices to Director of Publications, SPIE, P.O. Box 10, Bellingham, WA 98227-0010 USA.

SPIE San Diego
July, 1990

paper # 1324-08

IMPROVED SENSITIVITY IN ELLIPSOMETRY OF THIN BIOCHEMICAL FILMS BY EMPLOYING SUBLAYERS

JINYU WANG, J. D. ANDRADE, JINNAN LIN AND D. A. CHRISTENSEN

DEPARTMENT OF BIOENGINEERING
UNIVERSITY OF UTAH, SALT LAKE CITY, UT 84112, USA

Abstract

Ellipsometry is widely used for investigating the optical properties of thin films on planar substrates, including films of adsorbed proteins or polymers. The average thickness and effective refractive index of the adsorbed layer are calculated by measuring the Δ and Ψ ellipsometry parameters. Unfortunately the thickness of the adsorbed protein layers is often too thin to significantly affect the Δ and Ψ parameters. However, using a substructure consisting of an additional sublayer placed between the substrate and the adsorbed layer, we can improve the sensitivities of both Δ and Ψ to changes in the adsorbed layer, provided that the thickness of the sublayer is optimized. We show that for a SiO2 layer on a Si wafer, the optimum SiO2 thickness is about 1350 Å when the incident angle is 70 degrees and the wavelength is 6328 Å. The materials of the sublayer can be metal, semiconductor and/or dielectric.

1 Introduction

Ellipsometry is currently employed to investigate the optical properties of solids and thin films at interfaces. In biochemical applications, ellipsometry has been used for studying physical and chemical adsorption.

De Feijter, et al. [1] and Kawaguchi, et al. [2] [3] mentioned the applicability of ellipsometry for investigating the adsorption behavior of macromolecules at the air-water interface. The properties of adsorbed macromolecular films depend not only on the amount adsorbed, but also on the conformation of the adsorbed molecules. The advantage of ellipsometry is that it provides information on both aspects. Cuypers, et al. [4] used ellipsometry as a tool to study protein films at liquid-solid interfaces. They suggested that an automatic ellipsometer for biochemical work should have a sensitivity of about 0.005 degree, corresponding to a layer thickness sensitivity of 5 Å. With this sensitivity, the resolution of the instrument permits monomolecular layers of biomolecules to be observed. Arwin, et al. [5] and Nygren et al [6] studied protein adsorption and antibody and antigen reactions. They measured the optical properties of protein films at air-solid interfaces with ellipsometry.

We know the sensitivity of ellipsometry increases with increasing difference between the refractive indices of the substrate and the adsorbed layer. This is the reason why most publications on the subject deal with macromolecules adsorbed on to semiconductor or metal surfaces.

Arwin [5] pointed out that if the substrate is absorbing and its polarizability is relatively low, then both the refractive index and the thickness of the adsorbed layer can be separately obtained. The problem therefore reduces to one of selecting a suitable substrate. But unfortunately, the substrates applied in biochemical studies may not have the proper refractive index values. From optical thin film theory [7], we know that a substrate and a sublayer can form a substructure which has an effective refractive index. Changing the thickness or/and the refractive index of the sublayer means changing the effective refractive index of the substructure. In this way, we can deduce a substructure which fits our requirements. In this paper we give the analysis, calculation, and experiment for selecting a suitable substructure.

. SPIE Proc. 1519 (1991) in press.

Study of PEO on LTI Carbon Surfaces by Ellipsometry and Tribometry

Jinyu Wang, Eric Stroup, Xingfa Wang and J. D. Andrade
Bioengineering Department, University of Utah, SLC, UT 84112, U.S.A.

Key words: Ellipsometry, Tribometry, Polyethylene Oxide, Low Temperature Isotropic Carbon.

Abstract

Proteins adsorb to almost all surfaces during the first few minutes of exposure [1]. Surfaces which show minimal protein adsorption are important in many biomedical applications. Moreover, patient discomfort due to poor lubricating action between tissue and various medical devices, especially contact lenses, is a serious medical problem. An effective polymer for protein-resistant surfaces and improved lubrication properties appears to be polyethylene oxide (PEO) [2] [3]. Here we report a study of PEO films on low temperature isotropic (LTI) carbon surfaces, including preparation using a photochemical reaction, characterization of the thickness of the PEO layer by ellipsometry and measurement of coefficient of friction with a custom built tribometer.

Introduction

Ellipsometry is used to measure the optical properties of thin films on planar substrates, including films of adsorbed proteins or polymers [4]. The average thickness and effective refractive index of the adsorbed layer is calculated by measuring the Δ and ψ ellipsometry parameters. The in situ optical properties of the adsorbed layer provides information related to physical, chemical, and structure properties.

Protein adsorb to almost all surfaces during the first few minutes exposure [2]. Surfaces which show minimal protein adsorption are important in many applications, including blood-contacting devices, membranes for separation processes, sensors, chromatographic supports, contact lenses, immunoassays, blood and protein storage applications, etc. An effective polymer for protein-resistant surfaces appears to be poly ethylene oxide [3].

Low friction of surfaces is required for medical devices, such as contact lenses, catheters or guide wires, which are contact with mucous membranes of different parts of the human body. The poor lubricating action between membranes and various medical devices is not only accompanied by pain, but may also damage the mucous membranes. Tribometry is used for investigating friction and lubrication phenomena on PEO films.

Low temperature isotropic (LTI) carbon is widely used as the disk component of artificial heart valves [5]. The LTI carbon surface is a suitable surface for UV induced-grafting of PEO and a good substrate for ellipsometry measurement [6].

Principles and Analysis of Ellipsometry

The ellipsometer is described in Fig. 1. A light beam incident on a sample surface will undergo reflection and refraction [7] [8] [9]. The effect of reflection on purely polarized monochromatic incident light may be described by considering the reflection of two mutually perpendicular electric field components, whose resultant forms the electric field of the incident ray. Usually these components, E_p and E_s, are chosen to be parallel and perpendicular, respectively, to the plane of incidence. The complex reflection coefficients are defined by

$$r_p=E_{rp}/E_{ip} \tag{1a}$$

$$r_s=E_{rs}/E_{is} \tag{1b}$$

and the ratio of these two coefficients gives the fundamental equation of ellipsometry:

$$\rho=r_p/r_s=\tan(\psi)\exp(j\Delta) \tag{2}$$

The two measurable parameters Δ and ψ relate, respectively, to the relative phase and amplitude change upon reflection. Δ and ψ are functions of the optical constants of the surface, N_2; the wavelength of the light used, λ; the angle of incidence, ϕ; the optical constants of the ambient medium, n_0; and, for a film-covered surface, the thickness, d_1, and optical constants of the film, n_1.

We can write formally

$$\rho_{meas}=\rho\ (n_0, n_1, N_2, d_1, \lambda, \phi) \qquad (3)$$

In biochemical applications only the thickness, d_1, and the refractive index,n_1, of the adsorbed layer are unknown. In principle, they can be estimated by Δ and ψ. Often the adsorbed layer is too thin to affect ψ, meaning that only Δ changes with adsorption. Fortunately, the refractive index of LTI carbon is a complex number, $N_2=n_2-jk_2=1.70-j0.80$, and n_2 and k_2 are of the same order, therefor, both Δ and ψ change with adsorption. This can be seen directly from the first-order approximation for ρ for very thin films which can be written as [10]

$$\frac{\delta\rho}{\rho}=\frac{\delta\tan\psi}{\tan\psi}+j\delta\Delta=\frac{j4\pi n_0 d_1\cos\phi}{\lambda}\,\frac{n_2^2\left(n_1^2-n_0^2\right)\left(n_2^2-n_1^2\right)}{n_1^2\left(n_2^2-n_0^2\right)\left(n_2^2\cot^2\phi-n_0^2\right)} \qquad (4)$$

where $\delta\rho$, $\delta\tan\psi$ and $\delta\Delta$ represent the first-order changes in the respective ellipsometric parameters. From equation (4) we have

$$\delta\tan\psi/\tan\psi=-0.957\times2\pi d_1/\lambda \qquad (5a)$$

$$\delta\Delta=1.635\times2\pi d_1/\lambda \qquad (5b)$$

when $\phi=60.0$, $n_0=1.0$ and $n_1=1.50$.

We can calculate Δ and ψ as a function of the refractive index, n_1, and thickness, d_1, of the adsorbed layer. The theoretical calculations were carried out for adsorbed films covering LTI carbon substrates in the thickness range of 0-50 Å. Since the refractive index, n_1, of the adsorbed layer varies with adsorption procedure, calculations were made with 6 values of n_1 for the wavelength of 6328 Å. The result is shown in Fig. 2. From the results, we understand that, for a small change in thickness of 1 Å, Δ and ψ change 0.05 and 0.02 degree, respectively, and for a refractive index change of 0.01, Δ has a change of more than 0.03 degree, when the thickness of the adsorbed layer is about 20 Å. Often the thickness of the adsorbed layer is about or more than 20 Å. Using a RUDOLPH RESEARCH RR2000 Automatic Ellipsometer and the software developed in our group for data analysis, we can measure and evaluate the refractive index and the thickness of the adsorbed layer to an accuracy of 0.01 and 1 Å, respectively.

Sample Preparation and Characterization by Ellipsometry

Low temperature isotropic (LTI) carbon has been widely used as the disk component of artificial heart valves and in other medical devices due to its good biocompatibility and mechanical properties. A monomolecular film of PEO on carbon surfaces should improve compatibility and lubrication properties. The ellipsometry results indicated that it is possible to detect thin PEG films on polished pyrolytic carbon.

LTI carbon surfaces are polished by ceric oxide powder and cleaned with ethanol. The samples are then submerged in hot chromic acid solution for 5 minutes and rinsed using distilled water. The surface of the sample is precleaned in methanol, before treatment in a PEG/H_2O solution (BBE-PEG(3350)-OH in H_2O, 5 mg/ml) for 10 minutes [11]. The sample is then rinsed in deionized (DI) water by dipping (once) and is then dried vertically in air. Half of the sample surface is exposed to UV light of 4.7 mW/cm^2 for 5 minutes, 48 cm distance from source. The samples are then stored in DI water.

After air drying, ellipsometry measurements were made to determine the optical parameters of the PEO layer (Fig. 3). The results of the ellipsometric measurements suggest that the BBE-PEG layer adsorbed to the carbon surface (no UV exposure) is about 20 Å thick and is easy to rinse away. The samples exposed to UV light have a PEO layer about 25 Å thick, which is difficult to remove, even under polishing by ceric oxide powder in water. These observations suggest that a photochemical reaction probably resulted in the covalent binding of the PEO molecules to the carbon surface.

The ellipsometry studies of PEG on pyrolytic carbon surfaces are shown in Fig. 3. The circles represent LTI carbon disks. The small integers represent the positions and time sequence of the analysis of disks. The larger number is the PEG film thickness measured by ellipsometry. The upper two circles show the control experiment, where PEG adsorbed to the carbon disk surface. The thickness of the PEO layer decreases with time. From point 1 to point 8, the time interval for each point is 30 minutes. The samples are stored in deionized water between the measurements. There is no significant difference between the masked area and the area which was exposed to UV light. The lower two circles show the photo PEG attached to the carbon surface. Two samples were measured at different times. The left one measured right after preparation and the right one was measured one day later. The data for these two samples are nearly the same. The photo active PEG layer on the surface is clearly stable and is on the order of 20 Å thick.

Friction Measurement

When, under the action of a normal force perpendicular to the common boundary, one body is made to move relative to the surface of the other [12]. The tangential resisting force is defined as friction. The frictional force F is proportional to the normal force N

$$F=\mu N \qquad (6)$$

the proportionality constant μ is called the coefficient of friction.

There are several techniques for measuring static and dynamic frictional coefficients. Our preliminary dry friction measurements on PEG-treated LTI carbon were made on a crude friction apparatus. The instrument uses a rotating silica fiber of 0.5 mm radius; fiber velocity is 4 mm/s, with a normal force, N, the fiber rotates against the LTI carbon curved disk. Using a Wilhelmy Balance, we measured both the normal force and frictional force. Then we calculated the coefficient of friction with Eq. (6). The design of the instrument is shown as Fig. 4. F_1 is the weight of the heart valve disk, F_2 and F_3 are the optical fiber static and dynamic balance records, respectively. The frictional coefficient

$$\mu=\frac{F}{N}=\frac{F_2-F_3}{F_1\sin\alpha} \qquad (7)$$

where

$$\alpha=\cos^{-1}(F_2/F_1) \qquad (8)$$

and the forces F_1, F_2 and F_3 can be measured by the Wilhelmy balance, separately. In this way, we can measure the dynamic frictional coefficient between a rotating optical fiber and the PEO attached on a LTI carbon heart valve disk. An example of original record data is shown as Fig. 5. The instrument is suitable for the measurements of low frictional coefficients.

Using the technique and instrument developed in our lab, we measured the dynamic coefficient of friction of optical fiber and LTI carbon in the dry state for two conditions: the bare LTI carbon surface and the surface attached with PEO. The dry dynamic coefficient of friction of LTI carbon and optical fiber is $\mu=0.35\pm0.01$, shown in Fig. 6. The dynamic coefficient of friction of LTI carbon attached with PEO and optical fiber is $\mu=0.18\pm0.01$ under normal force of 2.8 mN, shown as Fig. 7. PEO attached to carbon surface appears to improve lubrication.

The relationship between normal force and frictional coefficient are shown in Fig. 6 and Fig. 7. Fig. 6 shows the surface friction character; the frictional coefficient μ is independent of the normal force. The frictional coefficient decreases with normal force in Fig. 7, this shows a molecular friction feature and Eq. (6) is inapplicable to this situation. For typical molecular friction, the shear stress was independent of the driving velocity and applied load [13]. This means that the friction force should be constant. There may still be some surface friction component in the measurement, as the 20 Å PEO layer, compared with the surface roughness, is not thick enough to prevent surface friction.

Medical devices usually work in fluid environments. The frictional coefficient should be measured in wet conditions. Nagaoka et. al. [14] used a method for measuring static coefficient of friction of a hydrophilic polymer surface in water or physiological fluid. They coated poly (vinyl pyrrolidone) (PVP) and poly (hydroxyethyl methacrylate), p(HEMA), on the surface of polyurethane tubes. Then the catheter was wetted with physiological saline solution and a weight of 100 g cross-linked collagen film, with thickness of about 100 μm, was placed on the end of the catheter. The cross-linked film is a kind of biological tissue model and was attached on the bottom of the weight. The film was wetted with the same fluid. One end of the glass plate was gradually inclined to obtain the initial inclination angle required for the weight to begin slipping. The static coefficient of friction, μ, was calculated according to the formula

$$\mu=\tan\theta \qquad (9)$$

They mentioned that the static coefficients of friction decreased with increase in molecular weight of the hydrophilic polymer up to 400,000. The static coefficient of friction of an uncoated polyurethane catheter was 0.32±0.02. The polyurethane catheter coated with hydrophilic p(HEMA) showed a frictional coefficient of 0.18±0.02.

Attia et. al. [15] studied adsorption of polymers on contact lens surfaces in relation to biolubrication. They measured the dynamic coefficients of friction, between PMMA (Polymethylmethacrylate) plate and PMMA ball of 0.25 inch in radius (stylus velocity of 400 mm/s with a vertical load of 5 g). The values were in the range of 0.112-0.243 with various ophthalmic solutions. Our data are comparable with the data listed above.

In vivo experiments by Nagaoka et. al. showed that the insertion and manipulation of the polyurethane catheter with a hydrophilic low frictional surface was much easier than the non-coated catheter. Almost no friction was felt between the catheter and blood vessel in the case of the coated catheter. All of the hydrophilic slippery surface showed no thrombus formation or adhesion of blood components. The hydrophilic low frictional surface improved the biocompatibility and decreased the damage of mucous membranes.

Discussion and Future

The roughness of the polished LTI carbon surfaces is under 10 Å and the thickness of the PEO layer is about 20 Å. The PEO covered LTI carbon surface and the optical fiber surface are molecular smooth surfaces. The friction coefficient between the optical fiber and the PEO covered LTI carbon surfaces is a molecular tribological property. Both the the normal and the tangential stresses during sliding are concerned with molecular interactions and conformation changes in the molecules.

Photoactive PEO has been used for glass eyes [16]. BioCoat Ocular Prosthesis Treatment (OPT) has been developed as a component for newly fabricated and existing PMMA ocular prostheses to enhance patient comfort. The photo-activated PEO bonding to the prosthesis surface is accomplished in only three minutes and the entire OPT applications takes 15 minutes in an ocularist's laboratory. The PEO layer can last up to six months.

Work on hydrophilic low friction surfaces is developing. An understanding of the phenomena is helpful for improving surface modifications for low friction applications.

Jeon et. al. [17] [18] studied protein-surface interactions in the presence of polyethylene oxide. They calculated the steric repulsion and Van der Waals attraction. A proper model is required for connecting the microscopic understanding with the macroscopic quantities in tribology. We suggest that there is a sol-gel layer on the hydrophilic slippery surface. The sol-gel layer may be PEO, PVP or p(HEMA) in water. According to the concept of gelation, the backbone may be the substrate, for example, the PEO chains bonding on the substrate entangled in each other. The surface of PEO in water is the same as the sol-gel surface. With the sol-gel model, tribological concepts and formulae [19] [20] can be used for explaining lubrication phenomena and calculating tribologic parameters. The larger the molecular weight, the thicker the the sol-gel layer. Thicker sol-gel layers will supply a larger deformation without the plow phenomenon which produces higher friction and damage of the surfaces. This may be an explanation as to why larger molecules are helpful for lubrication [14].

Acknowledgement

The Photoactive PEG reagents were a gift from Biometric System, Inc., St. Paul, MN.

Reference

[1] J. D. Andrade and V. Hlady, 'Protein Adsorption and Materials Biocompatibility: A Tutorial Review and Suggested Hypotheses', Adv. Polymer Science, 79(1986) 1.

[2] J. H. Lee, J. Kopecek and J. D. Andrade, 'Protein-resistant surfaces prepared by PEO-containing block copolymer surfactants', J. Biomed. Materials Research, 23, 355-358(1989).

[3] P. M. McGuigga, J. N. Israelachvili, M. L. Gee and A. M. Homola, 'Measurements of Static and Dynamic Interactions of Molecularly Thin Liquid Films between Solid Surfaces', Mat. Res. Soc. Symp. Proc., 140,79-88(1989).

[4] B. Ivarsson and I. Lundstrom, 'Physical Characterization of Protein Adsorption on Metal and Metaloxide Surfaces', CRC Crit. Rev. Biocompat. 2, 1 (1986)

[5] J. C. Bokros, 'Carbon Biomedical Devices', Carbon, 15, 355-371 (1977).

[6] A. W. Moore, 'Highly Oriented Pyrolytic Graphite', Chem. and Phys. of Carbon, 11, 130-132 (1973).

[7] M. Born and E. Wolf, PRINCIPLES OF OPTICS-Electromagnetic Theory of Propagation, Interface and Diffraction of Light, (5th ed.), Pergamon Press, 1975.

[8] D. E. Aspnes in B. O. Seraphin (ed), Optical properties of solid : New development, North Holland Amsterdam 1976.

[9] R. M. A. Azzam and N. M. Bashara (ed), Ellipsometry and Polaraized Light, North-holland Publishing Company, 1977.

[10] H. Arwin, 'Determination of Optical Properties of Thin Organic Films by Spectroellipsometry', Thin Solid Film 138, Ellectronics and Optics, 195-207 (1986).

[11] S. C. Dunkirk and P. E. Guire, 'Surface-Modification of Polymers for Increased Wettability', The 15th Annual Meeting of the Society for Biomaterials, April 28- May 2, 1989, Lake Buena, Vista, Florida, USA.

[12] M. B. Peterson and W. O. Winter ed., Wear Control Handbook, ASME, New York,1143-1303 (1980).

[13] P. M. McGuiggan, J. N. Israelachvili, M. L. Gee and A. M. Homola, 'Measurements of Static and Dynamic Iteractions of Molecularly Thin Liquid Films Between Solid Surfaces', Mat. Res. Soc. Symp. Proc. 140 79-88 (1989).

[14] S. Nagaoka and R. Akashi, 'Low-friction hydrophilic surface for medical devices', Biomaterials, 11, 419-424 (1990).

[15] Y. A. Attia, B. M. Moudgil and S. Chander (ed), 117-130, Iterfacial Phenomena in Biotechnology and Materials Processing, Elsevier Science Publishers B. V., Amsterdam, 1988.

[16] 'BioCoat Ocular Prosthesis Treatment', Literature from Bio-Metric Systems, Inc., 9924 W 74th street, Eden Prairie, MN 55344, USA.

[17] S. I. Jeon, J. H. Lee, J. D. Andrade and P. G. de Gennes, 'Protein-Surface Interactions in the Presence of Polyethylene Oxide I. Simplified Theory', J. Colloid Interface Science, in Press.

[18] S. I. Jeon and J. D. Andrade, 'Protein-Surface Interactions in the Presence of Polyethylene Oxide II. Effect of Protein Size', J. Colloid Interface Science, in Press.

[19] F. P. Bowden and L. Leben, 'The nature of sliding and the analysis of friction', Proc. Roy. Soc. A, 169, 371 (1938-39).

[20] F. P. Bowden and D. Tabor, 'The area of contact between stationary and between moving surfaces', Proc. Roy. Soc. A, 169, 391 (1938-39).

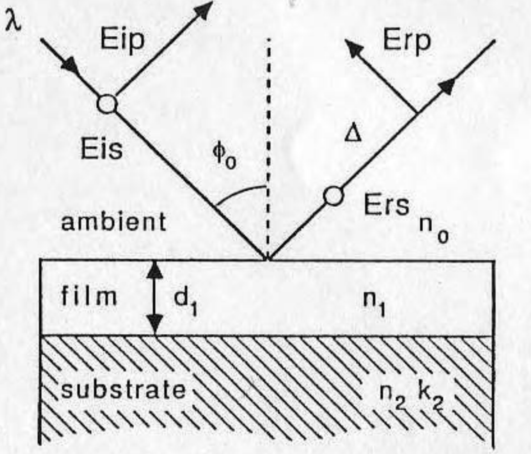
λ
Eip
Erp
Eis
ϕ_0
Δ
Ers
n_0
ambient
film
d_1
n_1
substrate
n_2 k_2

Fig. 1 The incident and reflected light and the film covered substrate.

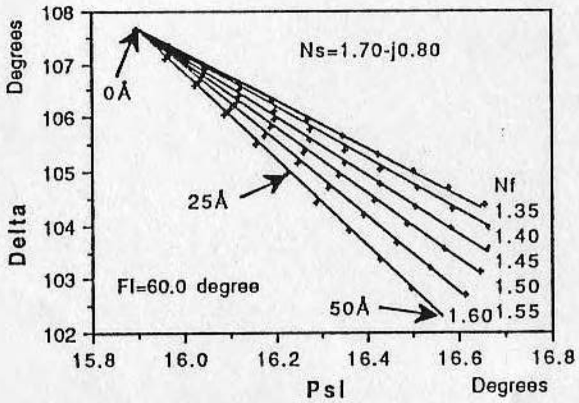

Fig. 2 Delta and Psi plot for thin films with different thickness and refractive indices on LTI-carbon.

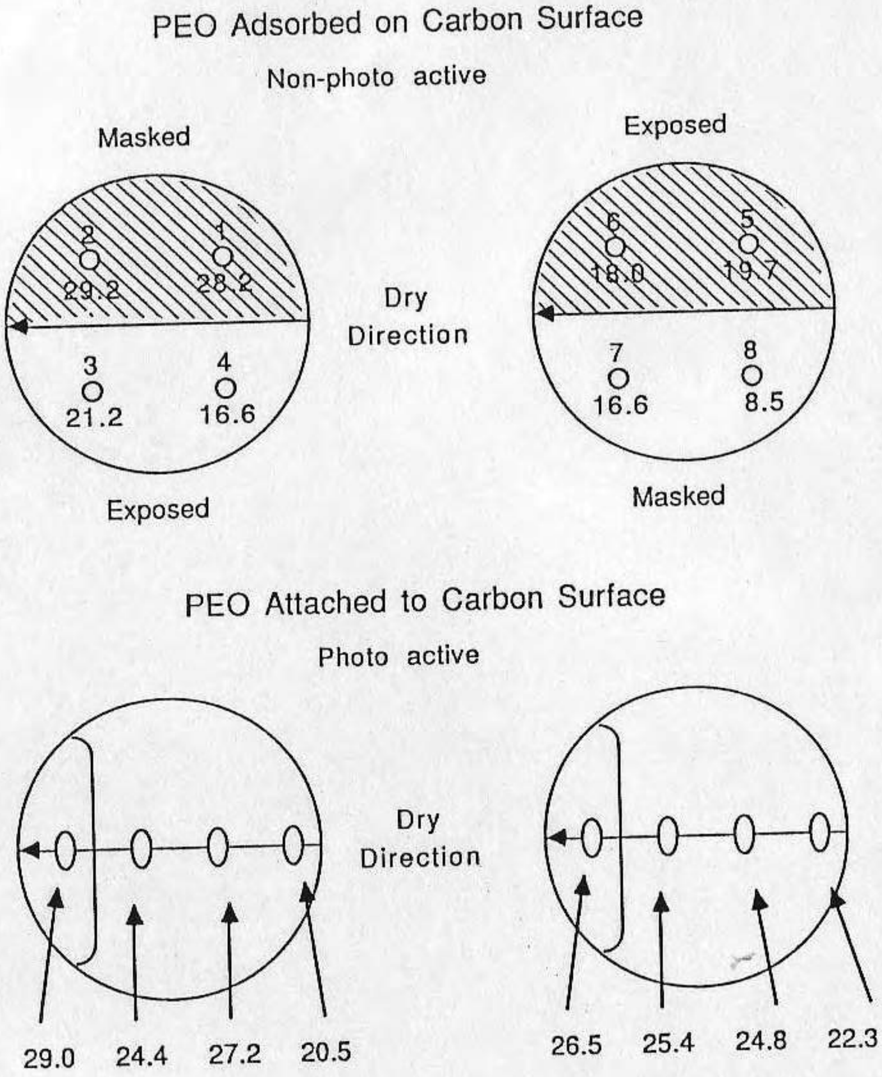
PEO Adsorbed on Carbon Surface
Non-photo active
Masked
Exposed
2
29.2
1
28.2
3
21.2
4
16.6
Exposed
Dry
Direction
6
18.0
5
19.7
7
16.6
8
8.5
Masked
PEO Attached to Carbon Surface
Photo active
Dry
Direction
29.0
24.4
27.2
20.5
26.5
25.4
24.8
22.3

Fig. 3 Summary of Ellipsometry Studies of PEG on Pyrolytic Carbon.

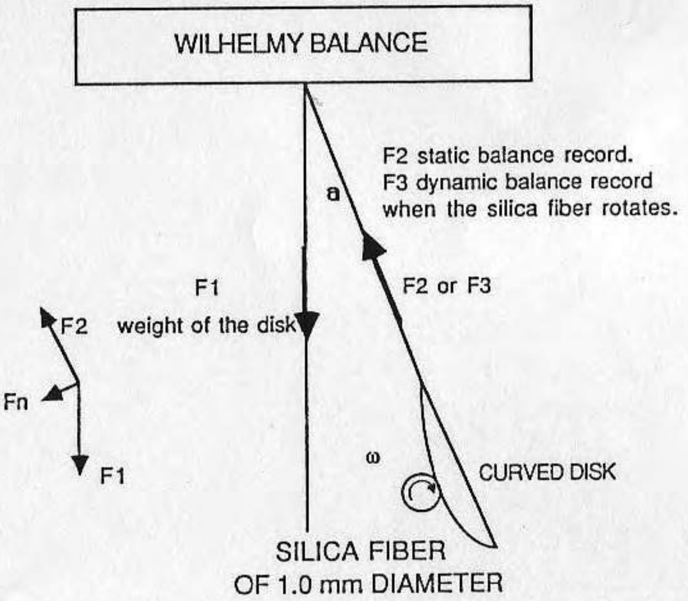
WILHELMY BALANCE
F2 static balance record.
F3 dynamic balance record
when the silica fiber rotates.
a
F1
weight of the disk
F2 or F3
F2
Fn
F1
ω
CURVED DISK
SILICA FIBER
OF 1.0 mm DIAMETER

Fig. 4 The diagram of the friction apparatus consisting of a rotating silica fiber against a solid substrate. F1 is the weight of the curved disk. F2 and F3 are the static and dynamic records, respectively. Fn is the normal force. The difference between F3 and F2 is the force of friction.

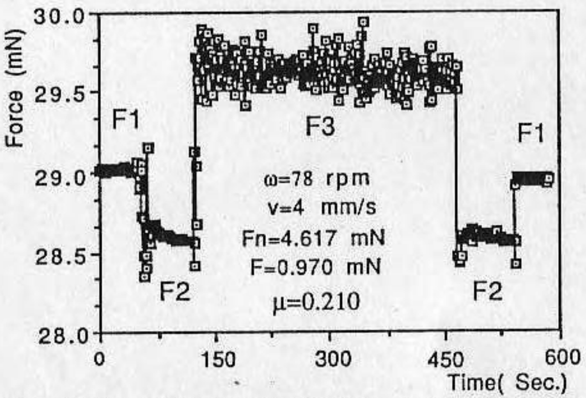

Fig. 5 An example of friction measurements (with PEO layer). Record rate 1point/sec.

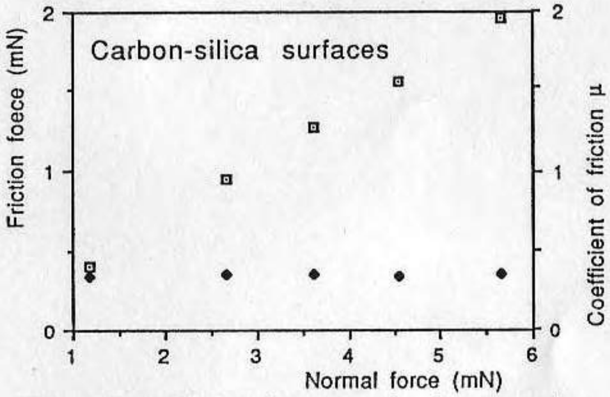

Fig. 6 The relation between the force or the coefficient of friction and the normal force.

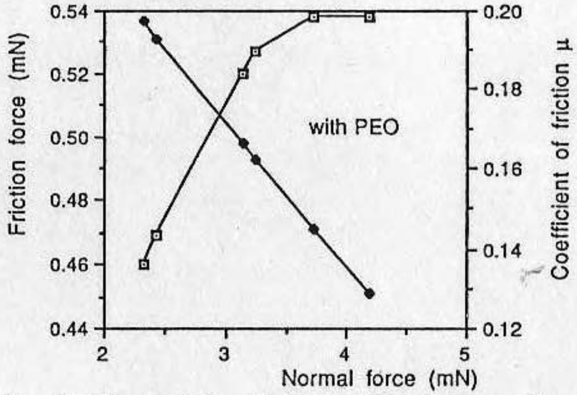

Fig. 7 The relation between the force or the coefficient of friction and the normal force.

2 Theoretical Analysis

A light beam incident on a nominally specular surface will undergo reflection and refraction [8] [9] [10]. The electric fields of the incident and reflected light beams are described by the complex amplitudes Ei and Er. Each of these can be resolved into two components parallel (p) and perpendicular (s) to the plane of incidence, where the plane of incidence is defined by the incident beam and the normal of the surface. The complex reflection coefficients are defined by

$$r_p=\frac{E_{rp}}{E_{ip}} \qquad (1)$$

$$r_s=\frac{E_{rs}}{E_{is}} \qquad (2)$$

and the ratio of these two coefficients gives the fundamental equation of ellipsometry.

$$\rho=\frac{r_p}{r_s}=\tan\psi\, e^{j\Delta} \qquad (3)$$

The two parameters Δ and ψ relate to the relative phase and amplitude change upon reflection, respectively.

A film covered substrate, three media system, is shown as Fig. 1. N_0, N_1 and N_2 are the refractive indices of the ambient, the film and the substrate, respectively; d is the thickness of the film; and ϕ is the angle of incidence. Assuming that the layer is planar, homogeneous and infinite in extent, we know

$$r_p=\frac{r_{01p}+r_{12p}X}{1+r_{01p}r_{12p}X} \qquad (4)$$

$$r_s=\frac{r_{01s}+r_{12s}X}{1+r_{01s}r_{12s}X} \qquad (5)$$

where

$$x=\exp(-j4\pi d_1(N_1^2-N_0^2\sin^2\phi)^{0.5}/\lambda) \qquad (6)$$

and r_{ij} is Fresnel reflection coefficient of the ij interface and written as

$$r_{ij}=\frac{\eta_i-\eta_{i+1}}{\eta_i+\eta_{i+1}} \qquad (7)$$

where η_i is the optical admittance, $\eta=\cos\phi/n$ for p-wave, $\eta=n\cos\phi$ for s-wave.

The fundamental equation of ellipsometry can be represented as a function of the refractive indices N_0, N_1 and N_2 of the ambient, the film and the substrate, respectively; the thickness, d_1, of the film; the angle of incidence, ϕ; and the wavelength, λ, of the light. We can write formally

$$\rho_{exp}=\rho\,(N_0, N_1, N_2, d_1, \lambda, \phi) \qquad (8)$$

where ρ_{exp} is the quantity determined experimentally. We assume that ρ_{exp}, N_0, N_2, λ and ϕ are known, and then solve equation (8) implicitly for the optical parameters of the film, which are concerned with material properties such as the microstrcture, the composition and void fraction.

The adsorbed organic layer usually is transparent, k_1 is zero, and there are only two unknown optical parameters, d_1 and n_1 of the film. We can get two real equations from equation (8), which is complex. In principle, d_1 and n_1 can be determined by

$$\rho_{exp}=\tan\psi\,\exp(i\Delta) \qquad (9)$$

For adsorbed layers which are too thin to significantly affect ψ, only Δ changes with adsorption. This can be seen directly from the first-order approximation for ρ for very thin films, which can be written as [9]

$$\frac{\delta\rho}{\rho}=\frac{\delta\tan\psi}{\tan\psi}+j\,\delta\Delta=\frac{j\,4\,\pi\,n_0 d_1\cos\phi}{\lambda}\,\frac{n_2^2\left(n_1^2-n_0^2\right)\left(n_2^2-n_1^2\right)}{n_1^2\left(n_2^2-n_0^2\right)\left(n_2^2\cot^2\phi-n_0^2\right)} \qquad (10)$$

where $\delta\rho$, $\delta\tan\psi$ and $\delta\Delta$ represent the first-order changes in the respective ellipsometric parameters. From equation (10), we understand that $\delta\Delta=0$, when $n_2=n_1$ or $n_1=n_0$, that is, if the refractive index of the adsorbed layer is equal to the ambient or to the substrate, the right-hand side of equation (10) is zero; this means the sensitivity of ellipsometry is very low. On the other hand, when $n_2\cot\phi=n_0$ or $n_2=n_0$ for a symmetric system, $\delta\Delta$=infinity, and we get the highest sensitivity. The refractive index of the dielectric substrate is real in the visible range, then the right-hand side of equation (10) is purely imaginary and consequently

$$\delta\psi=0 \qquad (11)$$

and only one datum $\delta\Delta$ can be measured.

One way for solving this difficulty is to choose a substrate with complex refractive index at the wavelength employed. In this case, the right-hand side of equation (10) is complex and both Δ and ψ change in different ways with n_1 and d_1. This is why so many authors prefer semiconductor or metal substrates to dielectric ones. In the case of the semiconductor substrate, $k_2<<n_2$, (for silicon substrate, $N_2=3.85$ - j 0.02 at wavelength of 633 nm), so the right-hand side of equation (10) is nearly imaginary. Thus the measurement yields a negligible change in ψ for small d_1. In contrast, $\delta\Delta$ can be very large. In an individual situation, we can have $\delta\Delta/\delta d=0.5$ degree per nm. As one can easily measure $\delta\Delta$ with a precision of 0.01 degree or better, it is clear that the detection limit is well below atomic dimensions. However, even though the detection sensitivity for non-absorbing films on silicon substrates is high, one of the two unknowns, n_1 or d_1, must be guessed or determined independently.

Now we consider the metal substrate, where the imaginary part of refractive index is much larger than the real part, $|N_2|>>n_1$. Another difficulty arises, and equation (10) can be approximated as [5]

$$\frac{\delta\rho}{\rho}=\frac{j\,4\,\pi\,n_0 d_1\sin\phi\,\tan\phi}{\lambda}\,\frac{n_1^2-n_0^2}{n_1^2} \qquad (12)$$

Once again we find that the right-hand side of equation (10) or (12) is purely imaginary, so we are still left with a situation of having one datum and two unknowns, although the scaling factor for the thickness d_1 is now different. For some metals, the real and imaginary parts of its refractive index are of the same order in magnitude, and is suitable for obtaining two ellipsometric quantities.

Using a substructure which consists of an additional sublayer placed between the substrate and the adsorbed layer may be another way for overcoming this difficulty. It is suitable for dielectric, semiconductor and metal materials. Of course, the thickness and the refractive index of the sublayer should be optimized.

Now we consider a four media system, shown as Fig. 2. N_0, N_1, N_2, and N_3 of the ambient, the adsorbed layer, the sublayer and the substrate respectively; d_1 and d_2 are the thicknesses of the adsorbed layer and the sublayer. From optical thin film theory the characteristic matrix of one single layer can be written as

$$M_i=\begin{bmatrix}\cos\delta_i & j/\eta_i\sin\delta_i\\ j\eta_i\sin\delta_i & \cos\delta_i\end{bmatrix} \qquad (13)$$

where $\delta_i=2\,\pi\,n_i d_i\cos\phi_i/\lambda$.

The characteristic matrix of the substructure can be written as

$$\begin{bmatrix}B\\ C\end{bmatrix}=\begin{bmatrix}\cos\delta_2 & j/\eta_2\sin\delta_2\\ j\eta_2\sin\delta_2 & \cos\delta_2\end{bmatrix}\begin{bmatrix}1\\ \eta_3\end{bmatrix} \qquad (14)$$

The effective optical admittance of the substructure is

$$Y = \frac{C}{B} \tag{15}$$

Usually Y is complex and a function of ϕ, λ and the optical parameters of the substrate and the sublayer.

We analysis the problem using the concept of effective refractive index and effective admittance of the substructure. Substituting equation (14) into equation (15) we have

$$Y_s = \frac{\eta_{3s}\cos\delta_2 + j\,\eta_{2s}\sin\delta_2}{\cos\delta_2 + j\,\eta_{3s}/\eta_{2s}\sin\delta_2} \tag{16}$$

for s-wave and

$$Y_p = \frac{\eta_{3p}\cos\delta_2 + j\,\eta_{2p}\sin\delta_2}{\cos\delta_2 + j\,\eta_{3p}/\eta_{2p}\sin\delta_2} \tag{17}$$

for p-wave.

Assuming the substructure has an effective refractive index G, we can write the effective admittance as

$$Y_s = G\cos\Phi \tag{18}$$

$$Y_p = \cos\Phi/G \tag{19}$$

G and $\cos\Phi$ are functions of N_3, n_2, d_2, ϕ and λ.

From equations (16), (17), (18) and (19) we have

$$G\cos\Phi = \frac{\eta_{3s}\cos\delta_2 + j\,\eta_{2s}\sin\delta_2}{\cos\delta_2 + j\,\eta_{3s}/\eta_{2s}\sin\delta_2} \tag{20}$$

and

$$\cos\Phi/G = \frac{\eta_{3p}\cos\delta_2 + j\,\eta_{2p}\sin\delta_2}{\cos\delta_2 + j\,\eta_{3p}/\eta_{2p}\sin\delta_2} \tag{21}$$

From two complex equations, (20) and (21), we can evaluate two complex unknowns. If we know N_3, ϕ and λ, changing n_2 and d_2 we can get different G. This means that we may have any refractive index value of the substructure. Substituting G for n_2 in equation (10) we have

$$\frac{\delta\rho}{\rho} = \frac{\delta\tan\psi}{\tan\psi} + j\,\delta\Delta = \frac{j\,4\,\pi\,n_0 d_1\cos\phi}{\lambda}\,\frac{G^2\left(n_1^2-n_0^2\right)\left(G^2-n_1^2\right)}{n_1^2\left(G^2-n_0^2\right)\left(G^2\cot^2\phi-n_0^2\right)} \tag{22}$$

We can optimize the thickness and the refractive index of the sublayer with equation (22). The optimum values of n_2 and d_2 make both $\delta\tan\psi/\tan\psi$ and $\delta\Delta$ large enough for much higher sensitivity of ellipsometry.

3 Numerical Calculation and Experimental Result

It is usually more convenient to deal with the corresponding changes $\delta\psi$ and $\delta\Delta$ of the ellipsometric angles ψ and Δ. From equation (3) we have

$$\delta\psi = \frac{1}{2}\sin2\psi\,\mathrm{Re}\left(\delta\rho/\rho\right) \qquad \delta\Delta = \mathrm{Im}\left(\delta\rho/\rho\right) \tag{23}$$

For simplification, we assume that $\delta\rho/\rho$ is caused by a fractional change of film thickness $\delta d/d$ and rewrite equation (23) as

$$\delta\psi = \frac{1}{2}\sin2\psi\,\mathrm{Re}(K)\,\delta d/d \qquad \delta\Delta = \mathrm{Im}(K)\,\delta d/d \tag{24}$$

where

$$K=\frac{4\pi n_2 d_2 \cos\phi_2}{j\lambda} X \left(\frac{r_{23p}}{r_{12p}+r_{23p}X} - \frac{r_{12p}r_{23p}}{1+r_{12p}r_{23p}X} - \frac{r_{23s}}{r_{12s}+r_{23s}X} + \frac{r_{12s}r_{23s}}{1+r_{12s}r_{23s}X} \right) \quad (25)$$

and

$$X=\exp(-j4\pi n_2 d_2 \cos\phi_2/\lambda)$$

In a difference way, $\delta\psi$ and $\delta\Delta$ can be written as

$$\psi = \psi_0 + S_\psi \delta d_2 \qquad \Delta = \Delta_0 + S_\Delta \delta d_2 \quad (26)$$

where

$$S_\psi(d_2) = \delta\psi/\delta d_2 = 180/\pi \frac{1}{2}\sin 2\psi \, \mathrm{Re}(K)/d_2 \quad (27a)$$

$$S_\Delta(d_2) = \delta\Delta/\delta d_2 = 180/\pi \, \mathrm{Im}(K)/d_2 \quad (27b)$$

respectively, in units of degree per angstrom.

S_ψ and S_Δ are ψ and Δ sensitivity factors that determine the extent to which small changes of thickness of the film phase influence the ellipse of polarization of the reflected light beam. Using equations (27), we can calculate S_ψ and S_Δ as functions of d_2. The calculation results are shown as Fig. 3(a), for a Si substrate and SiO_2 sublayer. From the results it is clear that S_Δ is large when d_2 is very small, but S_ψ is approximately equal to zero. If the substrate is a Si wafer with natural oxidized SiO_2 sublayer, only one datum, Δ, can be obtained for protein absorption. If the thickness of the sublayer is about 1350 Å, both S_ψ and S_Δ are much larger, when the incident angle is 70 degrees and the wavelength of the light employed is 6328 Å. Fig. 3(b) shows Δ and ψ plot for different refractive indices and thickness of adsorbed layer on the substructure consisting of 1300Å SiO2 sublayer on Si wafer.

A series of experiments with different sublayer thickness values were done. The SiO_2 films of high quality on Si wafers were supplied by the HEDCO Microelectronics Lab, University of Utah. A chemical vapor deposition process was used for coating SiO_2 sublayers. Different concentrations of human IgG were used in the experiments. The experimental results, shown in Fig. 4, are fully supportive of the concept that a substrcture, consisting of an additional sublayer placed between the substrate and the adsorbed layer, can be used for improving the sensitivities of both Δ and ψ to changes in the adsorbed layer.

The material of the sublayer can be metal, semiconductor, and /or dielectric. The optimized thickness can be evaluated provided that the materials of sublayer, substrate and environment are chosen.

4 Acknowledgements

The authors would like to thank Mr. Y. N. Chang for protein adsorption samples and Ms. Danka Petelenz for coating SiO2 on Si wafer. This work was funded by the Center for Biopolymers at Interfaces, University of Utah.

References

[1] J. A. De Feijter, J. Benjamins, and F. A. Veer, 'Ellipsometry as a Tool to Study the Adsorption Behavior of Synthetic and isopolymers at the Air-Water Interface', Biopolymers, 17, 1759-1772 (1978).

[2] Masami Kawaguchi, Masahiro Tohyama, and Akiro Takahashi, 'Ellipsometric Study of Polymer Monolayers Spread at the Air-Water Interface. 1. Thickness of Monolayers', Langmuir (1988) 4, 407-410.

[3] Masami Kawaguchi, Masahiro Tohyama, Yuhji Mutoh, and Akiro Takahashi, 'Ellipsometric Study of Polymer Monolayers Spread at the Air-Water Interface. 2. Adsorbed Amount of Polymers', Langmuir (1988) 4, 411-413.

[4] P. A. Cuypers, W. Th. Hermens, and H. C. Hemker, 'Ellipsometry as a Tool to Study Protein Films at Liquid-Solid Interface', Analytical Biochemistry 84 , 56-67 (1978).
[5] H. Arwin, 'Determination of Optical Properties of Thin Organic Films by Spectroellipsometry', Thin Solid Film 138, 195-207 (1986).
[6] Haken Nygren, Matti Kartinen and Manne Stenberg, 'Determination by Ellipsometry of the affinity of Monoclonal Antibodies', J. Immunological Methods. 92, 219-225 (1986).
[7] H. A. Macleod, 'Thin-Film Optical Filter', American Elsevier Publishing Company, pp 8-31 (1969).
[8] M. Born and E. Wolf, PRICIPLES OF OPTICS (5th ed.), Pergamon Press, 1975.
[9] D. E. Aspnes in B. O. Seraphin (ed), Optical properties of solid : New development North Holland Amsterdam 1976.
[10] R. M. A. Azzam and N. M. Bashara, Ellipsometry and Polarized Light, North-Holland Publishing Company, 1977.

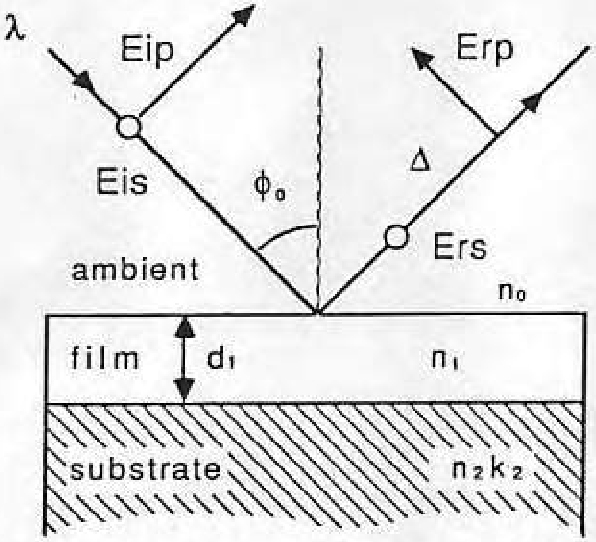
λ
Eip
Erp
Δ
Eis
φ₀
Ers
ambient
n₀
film
d₁
n₁
substrate
n₂k₂

Fig. 1 The incident and reflected light and film covered substrate.

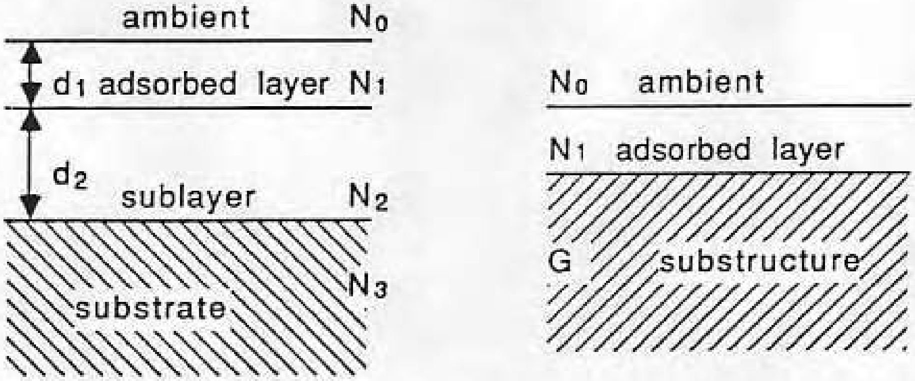
ambient
N₀
d₁ adsorbed layer
N₁
d₂
sublayer
N₂
substrate
N₃
N₀ ambient
N₁ adsorbed layer
G
substructure

Fig. 2 Four medium system and diagram of substructure consisting of a sublayer placed between substrate and adsorbed layer.

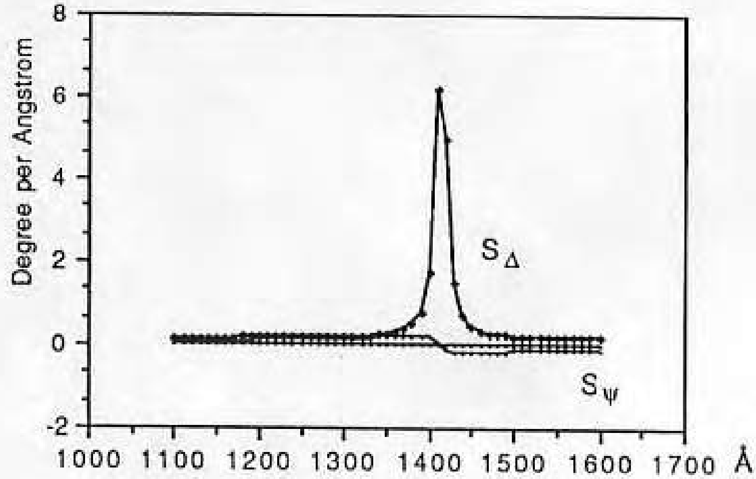

Fig. 3(a) Sensitivity Factor of Ellipsometry

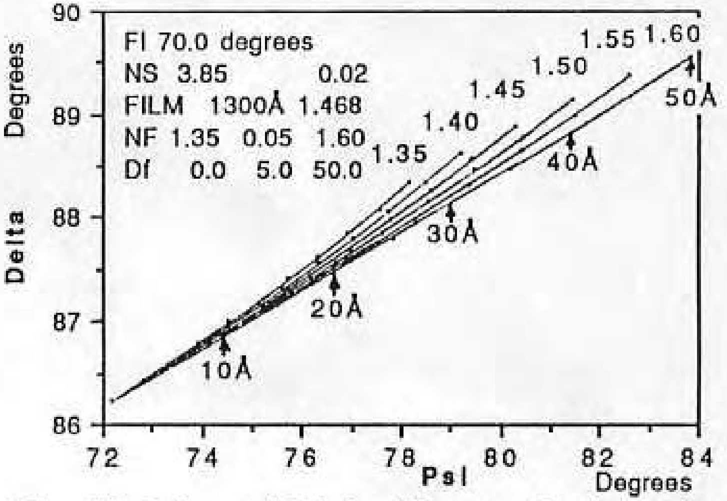

Fig. 3(b) Delta and Psi for different refractive indices and thickness of adsorbed layer on the substructure consisting of SiO2 sublayer on Si wafer.

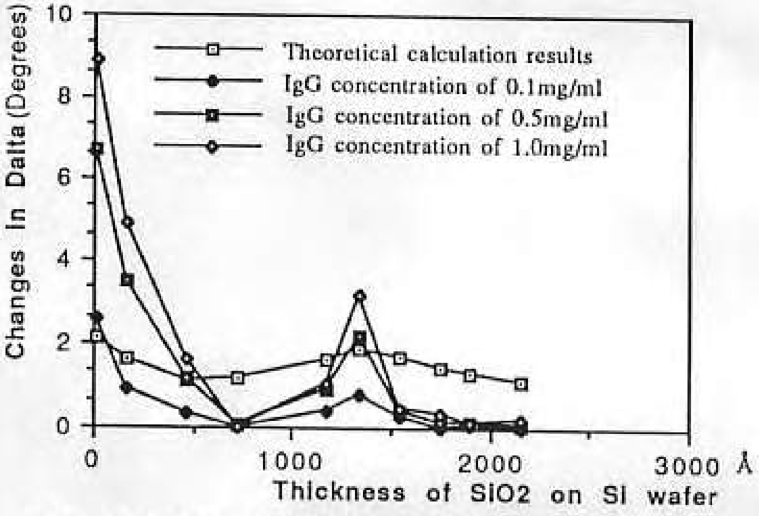

Fig. 4 (a) Sensitivity of Delta changes with the thickness of SiO2 layer on Si wafer.

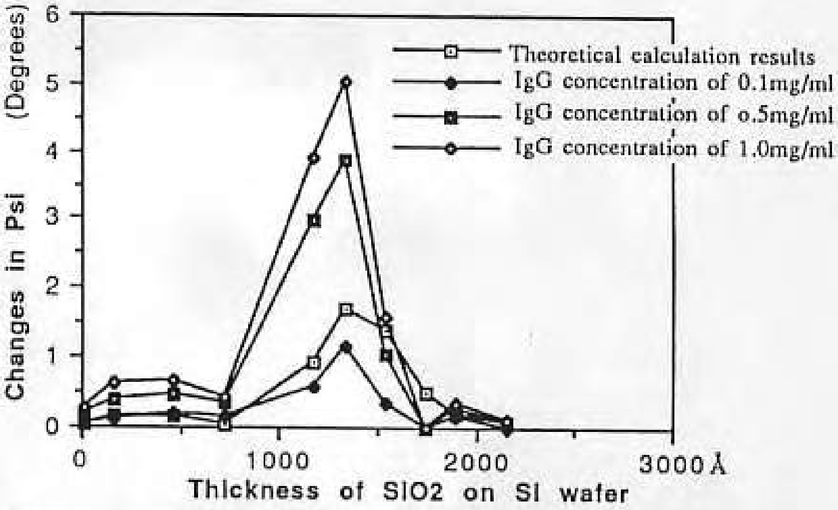

Fig. 4 (b) Sensitivity of Psi changes with the thickness of SiO2 layer on Si wafer.

Multi-parameter Representation of Proteins and Their Interfacial Behavior: The 'Tatra' Plot

Ai-Ping Wei, James N. Herron and Joseph D. Andrade*

ABSTRACT

Correlation of the behavior of proteins at the air-water interface with their intrinsic properties is represented as a pattern in a 12-parameter coordinate system which we call the Tatra Plot. Parameters related to intrinsic conformational stability, effective surface hydrophobicity, and surface tension kinetics were chosen to construct the 12 axes. Data for myoglobin, superoxide dismutase and lysozyme are used to illustrate application of the plot. The characteristics of a protein can be readily visualized by examination of its Tatra Plot. Since the patterns are distinctive for proteins with distinctive surface and denaturation properties, they can be used to better interpret protein adsorption data and to aid in the design of new hypotheses and experiments.

A Report Article
Submitted to ***SCIENCE***
August, 1990

Departments of Bioengineering and Pharmaceutics
University of Utah, MEB 2480
Salt Lake City, Utah 84112

---

*To whom correspondence should be addressed. Tel: (801)581-4379; Fax: (801)581-8926

The interfacial properties of proteins are important in studies of biomaterials, biosensors, chromatography, food formulation, drug delivery, and other biomedical or biotechnological processes[1]. It is a challenging question to understand and predict the structural changes that may occur during and after protein adsorption at various surfaces. [While attempting to correlate the behavior of proteins at the air-water interface with their intrinsic conformational stability, effective surface hydrophobicity, type of secondary structures, number of disulfide bonds, and atomic solvent accessible areas[2], we found it was desirable to present these correlations in a simple multi-parameter pattern which we call the "Tatra Plot".] A Tatra Plot is defined as a graphical representation of proteins and their interfacial behavior in a multi-axis coordinate system with each axis being a surface or solution parameter. The axes were arranged in such a way that correlated parameters were put next to each other and the most striking feature of a protein (or a group of proteins) is exhibited. In this paper, we emphasize the effective hydrophobicity, steady-state surface properties, and intrinsic stability, because we believe they are the primary parameters that needs to be first characterized in order to better understand the behavior of proteins at interfaces. We feel the protein adsorption data generally available in the literature can be more informative by consideration of such protein characteristics as stability, hydrophobicity, secondary structures, number of domains, etc.

break
into
2 or more
sentances

What does
TATRA
mean?

We use myoglobin (MYG), superoxide dismutase (SOD) and lyzozyme (LYZ) to illustrate the method. They were chosen as model proteins because they are small, single-domain proteins with well-known three-dimensional structures. They are similar in size but different in secondary structures. MYG has only α-helices and SOD only β-sheets, while LYZ contains both α-helices and β-sheets. The nearly equal molecular sizes can minimize mass transport differences from bulk to surface and allow us to compare experimental results solely on a structural basis. The air-water interface is of interest because it serves as the simplest hydrophobic model surface for studying adsorption[3]. The use of such a model system will allow investigation of the correlation between protein structure and surface properties and other fundamental issues of proteins at interfaces.

We measured the surface tension kinetics for each of these three proteins by the Wilhelmy Plate method. The rate constants were obtained by assuming a first-order kinetic model[4]. Conformational stability was determined by both thermal and guanidinium hydrochloride denaturation methods[5]. Values of effective surface hydrophobicity were obtained from titration curves using the hydrophobic fluorescent probe, cis-parinaric acid[6] and from hydrophobic interaction chromatography[7]. Atomic solvent accessible areas were calculated according to Richmond and Richards[8]. Moments of α-helices and β-sheets were calculated according to Eisenberg[9]. There are twelve axes in the Tatra Plot. Explanations to each of the axis are provided in Table 1.

With these twelve axes in place, each of the three model proteins was plotted. We examined the Tatra plots of five proteins, including SOD, MYG, LYZ, ribonuclease-A (RNASE) and Cytochrome-c (CYTC). Since RNASE has similar solution and surface properties as LYZ, and CYTC as MYG[2], their Tatra Plots were found, not surprisingly, to be similar. Therefore, only SOD, MYG and LYZ are reported here.

SOD is a protein with eight strands of β–sheets which constitute 36 % of its amino acid sequence[10]. It is highly stable both thermally ($T_m = 92^oC$) and in GdnHCl solution ($[GdnHCl]_{1/2} = 5.9$ M)[11]. This character was primarily attributed to its β-barrel structure which forms a very hydrophobic interior core[10]. Because there are many charged and polar residues on its molecular surface, as revealed by computer molecular graphics, SOD has very low degree of surface hydrophobicity in its native state. These intrinsic properties of SOD were reflected in its interfacial behavior, especially its surface tension kinetics. SOD exhibits a very low rate constant for the lowering surface tension at the air-water interface and gives very low steady-state surface pressure values. The Tatra Plot pattern for SOD illustrates these features by showing high values in the stability axes and low values in the hydrophobicity axes (Fig. 1)

MYG has eight segments of α-helix which constitute 79 % of its amino acid sequence[10]. Examination of the three-dimensional structures of MYG by computer graphics concludes that, since it doesn't contain any disulfide bonds, the tertiary structure formed by packing of these eight amphiphilic α-helices are easily disrupted[10]. This makes MYG relatively unstable ($T_m = 60\ ^oC$, $[GdnHCl]_{1/2} = 2.3$ M)[11]. The most striking feature of MYG is that it gave the highest steady-state surface pressure values at all bulk concentrations studied (0.01-1 mg/ml). There are two possible explanations for this observation. According to Krebs and Phillips[12], the interaction of α-helical proteins with air-water interface was mediated by the amphipathic α-helices within the protein. They found very good correlation between the steady-state surface pressure values and the product of the mean helical hydrophobic moment (μ_α) and fraction of α-helices in the protein (F) for some 12 proteins. Since MYG has the highest value of $\mu_\alpha \bullet F$, it is expected to exert the highest surface pressure at steady-state according to this theory. In the meantime, it is noted that MYG has 46% of nonpolar residue content, calculated on a molar basis, in contrast to 35% for SOD and 37% for LYZ[11]. This leads to the other explanation. Instead of being α-helices, the steady states of helical proteins at the air-water interface may be partially unfolded semi-random coils, which would permit the nonpolar residues to contact the surface without constraints from the secondary structure. Although these two mechanisms are different, we feel that they both may be present, depending upon the bulk concentration used, because there is evidence in the literature that proteins at air-water interface tend to unfold to a greater extent at low bulk solution concentrations than at high bulk concentrations[13]. We also found that a better correlation exists between nonpolar residue content and steady-state surface pressure values at bulk concentrations of 0.01 and 0.05

mg/ml than at 0.5 and 1 mg/ml for SOD, MYG, LYZ, RNASE and CYTC[2]. From the Tatra Plot of MYG in Fig. 2, we can predict that if a protein molecule has high α-helices and nonpolar residue contents, moderate effective surface hydrophobicity, and low stability, it will probably be very surface active at steady state. Tatra plots of this type can provide us with guidelines to select surface active proteins for practical applications.

LYZ contains both α-helices and β-sheets and is a relatively stable molecule (T_m=70°C, $[\text{GdnHCl}]_{1/2}$=4.3 M)[11]. It is the most surface hydrophobic of the five proteins studied. LYZ was shown by several investigators to have the longest retention time among RNASE, MYG and CYTC on hydrophobic interaction chromatography under non-denaturing conditions[6]. The Tatra Plot of LYZ in Fig. 3 suggests three important parameters. First, the rate constant ($K_{1(\text{high})}$) of the surface tension kinetics at 1 mg/ml is highest for LYZ, indicating it reduces surface tension through fast adsorption and molecular reorientation. Second, LYZ shows a high degree of enhancement in the fluorescence of a hydrophobic probe, cis-parinaric acid (cis-PnA). According to the studies of Nakai, the slope of the cis-PnA titration curve is a good measure of the effective surface hydrophobicity (ESH) of proteins[5]. Third, it was interesting to note that the percent of solvent accessible areas of charged oxygen atoms (O^- %) in the overall accessible areas was the smallest for LYZ. This value tends to increase as LYZ (2.2%), RNASE (2.7%), MYG (4.0%), CYTC (4.4%) and SOD (5.5%), whereas the ESH values decrease in the same order. Our explanation to this observation is that for small proteins of similar size, the hydrophobicity of nonpolar residues in the molecular surface may be masked because they are dispersed among polar residues. The ability of the surface apolar groups to manifest their hydrophobicity is controlled by the number of accessible neighboring polar or charged groups because they have a high degree of solvation. The reason that O^- % values correlates with the ESH is probably due to its more negative solvation energy than $-NH_3^+$ groups[14]. With the above in mind, it is not difficult to see why LYZ adsorbs preferably on hydrophobic surfaces[15]. In addition, because the Tatra Plot of LYZ is extended along the axes representing stability and hydrophobicity, we expect only small conformational changes of this molecule at the air-water interface. Indeed, adsorbed lysozyme has been found by serveral investigators to exhibit slow rate of unfolding and contain mostly native structures at the air-water interface[16].

In summary, we have demonstrated the construction of Tatra Plots of proteins and their application in studies of proteins at interfaces. In light of the current interests in protein adsorption, we feel that plotting experimental data of intrinsic stability, effective hydrophobicity and surface properties of a protein molecule in a Tatra Plot form will help investigators to 'see' the multi-variate nature of protein interfacial activity. This will in turn help to develop new hypotheses and to design new experiments. In addition, since we are interested in the surface properties of multi-domain proteins, e.g. albumin, fibrinogen, it will be very useful to look at the characteristics of each of the individual domains of a complex protein by the Tatra plot. With the information that we now know about single-domain model proteins, patterns of individual domains will give us a preliminary idea as to the behavior of a complex protein at the air-water surface. Althogh our work to date has focused on the air-water interface, we are now formulating appropriate axes for various solid-water interfaces.

References:

1. J. D. Andrade, J. N. Herron, V. Hlady and D. G. Horsley, Croatica Chemica Acta, **60,** 49, (1987).
   T. A. Horbett, Protein Engineering, **2**, 172, (1988).
   S. Nakai and E. Li-Chan, eds. Hydrophobic Interactions in Food Systems, CRC Press, 1988.
   F. E. Regnier, Science, **238**, 319, (1987).
2. A. -P. Wei, J. N. Herron and J. D. Andrade, i~~n 'From Clone to Clinic~~', ~~D. J. A. Crommelin,~~ Biotherapy ~~ed~~. in press (1990).
   A. -P. Wei, M.S. Thesis, University of Utah, October, 1990.
3. J. R. Hunter, P. K. Kilpatrick and R. G. Carbonell, J. Colloid and Interface Sci., **237**, 462, (1990).
4 K. B. Song and S. Damodaran, J. Agric. Food Chem., **35**, 236, (1987).
5 C. N. Pace, B. A. Shirley and J. A. Thomson, in 'Protein Structure: A Practical Approach' edited by T.E. Creighton, IRL Press, (1989).
6 A. Kato and S. Nakai, Biochim. Biophys. Act. **624**, 13, (1980).
7 S. C. Goheen and A. Stevens, Bio Techniques, **Jan/Feb**, 48, (1985).
   D. L. Gooding, M. N. Schmuck and K. M. Gooding, J. Chromatography, **196**, 107, (1984).
   Y. Kato, T. Kitamura and T. Hashimoto, J. Chromatography, **266**, 49, (1984).
   J. T. Fausnaugh, L. A. Kennedy and F. E. Regnier, J. Chromatography, **317**, 141 (1984).
   R. H. Ingraham, S. Y. M. Lau, A. K. Tanejan and R. S. Hodges, J. Chromatography., **327**, 77, (1985).
8 T. J. Richmond and F. M. Richards, J. Mol. Biol., **119**, 537, (1978).
9 D. Eisenberg, R.M. Weiss and T. C. Terwilliger, Proc. Natl. Acad. Sci. USA, **88**, 140, (1984)
10 MYG, SOD, LYZ, CYTC and RNASE discussed in this report are from sperm whale, bovine liver, hen egg, tuna heart and bovine pancreas, respectively. Amino acid compositions were calculated from their sequences. X-ray crystallographic coordinates were obtained from Protein Data Bank, Brookhaven National Laboratory, Upton, NY 11973. Computer molecular graphics were studied using the INSIGHT software on a Silicon Graphics workstation.
11 The thermal denaturation temperatures (T_d) were measured in PBS buffer (pH=7.3, $[KH_2PO_4]$=13 mM, $[Na_2HPO_4]$=54 mM, [NaCl]=0.1 M) on a calorimeter by Hart Scientific (Pleasant Grove, Utah). The GdnHCl concentration required to denature 50% of native protein molecules ($[GdnHCl]_{1/2}$) was determined according to the procedures described in reference 5 using the same buffer as above.
12 K. E. Krebs and M. C. Phillips, FEBS, **175**, 163, (1984).
13 R. K. Sandwick and K. J. Schray, J. Colloid and Interface Sci., **121**, 1, (1988).
14 T. E. Creighton, in 'Proeins: Structures and Molecular Properties' W. H. Freeman and Company, 150, (1984)
15 D. Horsley, J. N. Herron, V. Hlady and J. D. Andrade, in Proteins at Interfaces, edited by J. L. Brash and T. A. Horbett, ACS, (1987).
16 T. Yamashita and H. B. Bull, J. Colloid and Interface Sci., 24, 310, (1967); and **27**, 19, (1968).

D. J. Adams, M. T. Evans, J. R. Mitchell, M. C. Phillips and P. M. Rees, J. Polymer Sci.: Part C, **34**, 167, (1971).
M. C. Phillips, M. T. A. Evans, D. E. Graham and D. Oldani, Colloid and Polymer Sci., **253**, 424, (1975).
17 A. A. Rashin, Biopolymers, **23**, 1605, (1984).
18 The Tatra Plot approach to proteins at interfaces evolved during hikes in the high Tatra Mountains of Czechoslovakia in the summer of 1988. J. D. Andrade thanks J. and P. Kopecek for the productive Tatra excursions. We thank T. Alber and P. Dryden for their kind assistance in some of the calculations and experiments. Also gratefully acknowledged is the Center for Biopolymers at Interfaces of University Utah, a State-University-Industry consortium, for their financial support.to this project.

Table 1. Explanation to the Twelve Axes in Figure 1

No.	Label	Parameters	Value Range	Physical Significance	
1	T_d (^{o}C)	Temperature of thermal denaturation	40 → 100 * (^{o}C)	Intrinsic stability[11]	Intrinsic Stability
2	$[GdnHCl]_{1/2}$ (M)	GdnHCl concentration of 50% denaturation	1 → 6 (M)	Intrinsic stability[11]	
3	K_1(low) (hour^{-1})	Rate constant of surface tension kinetics at low bulk concentration (0.01 mg/ml)	0 ← 1 (hr^{-1})	K_1's were found to be limited by the process of surface-induced denaturation[2].	
4	$Fx\mu_\beta$	Average β-moment multiplied by fraction of β-sheets in molecule	0 → 0.1	A measure of both the quantity and amphilicity of β-sheets in structure[12].	
5	S-S	Number of disulfide bonds	0 → 5	More S-S bonds would make a protein more stable, although the contrary may not be true[17].	
6	log MW	The logarithm of molecular weight	3 → 5	Size of protein	
7	O- %	Percent accessible area of negatively charged oxygen atoms[8]	1 ← 6 (%)	Inversely correlated with the effective hydrophobicity of proteins[2].	Effective Surface Hydrophobicity
8	ESH	Effective surface hydrophobicity measured by cis-PnA binding and hydrophobic interaction chromatography (HIC)[6,7]	0 → 1 [18]	A measure of hydrophobicity of proteins in their native states[6].	
9	K_1(high) (hour^{-1})	Rate constant of surface tension kinetics at high bulk concentration (1 mg/ml)	1 → 4 (hr^{-1})	K_1's were found to be dependent on the hydrophobicity of proteins in their native states[2].	
10	$Fx\mu_\alpha$	Average α-moment multiplied by fraction of α-helices in molecule	0 → 0.25	A measure of both the quantity and amphilicity of α-helices in structure[12].	Steady-state surface activity
11	Π_{SS} (dynes/cm)	Steady-state surface pressure values at bulk concentration of 0.05 mg/ml	0 → 15 (dynes/cm)	Air/water surface activity of proteins at equilibrium.	
12	nonpolar %	Percent of nonpolar residues in sequence, calculated on a molar basis	30 → 50 (%)	Correlated to the steady-state surface pressure values at low bulk concentrations(0.01-0.05 mg/ml)[2].	

* The direction of arrow represents outward direction in the plot.

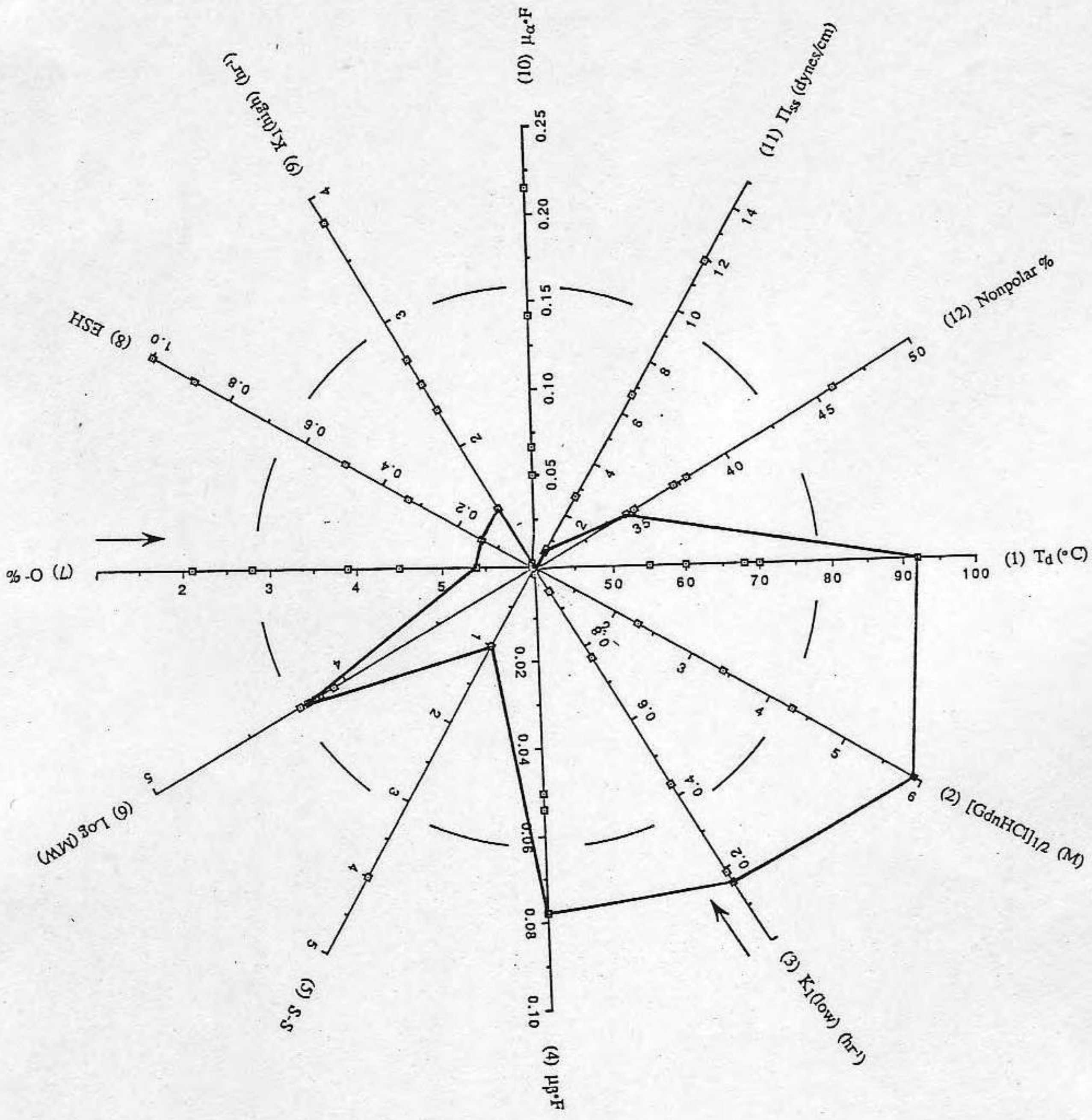

Figure 1. Tatrâ Plot of Superoxide Dismutase (SOD). Axes 1 to 5 are stability or stability-related parameters. Axes 7 to 9 are parameters of effective surface hydrophobicity or related to it. Axes 10-12 are steady-state surface activity. The directions of increase for axes other than 3 and 7 are outward.SOD is a very stable, highly hydrophilic, and non-surface active protein.

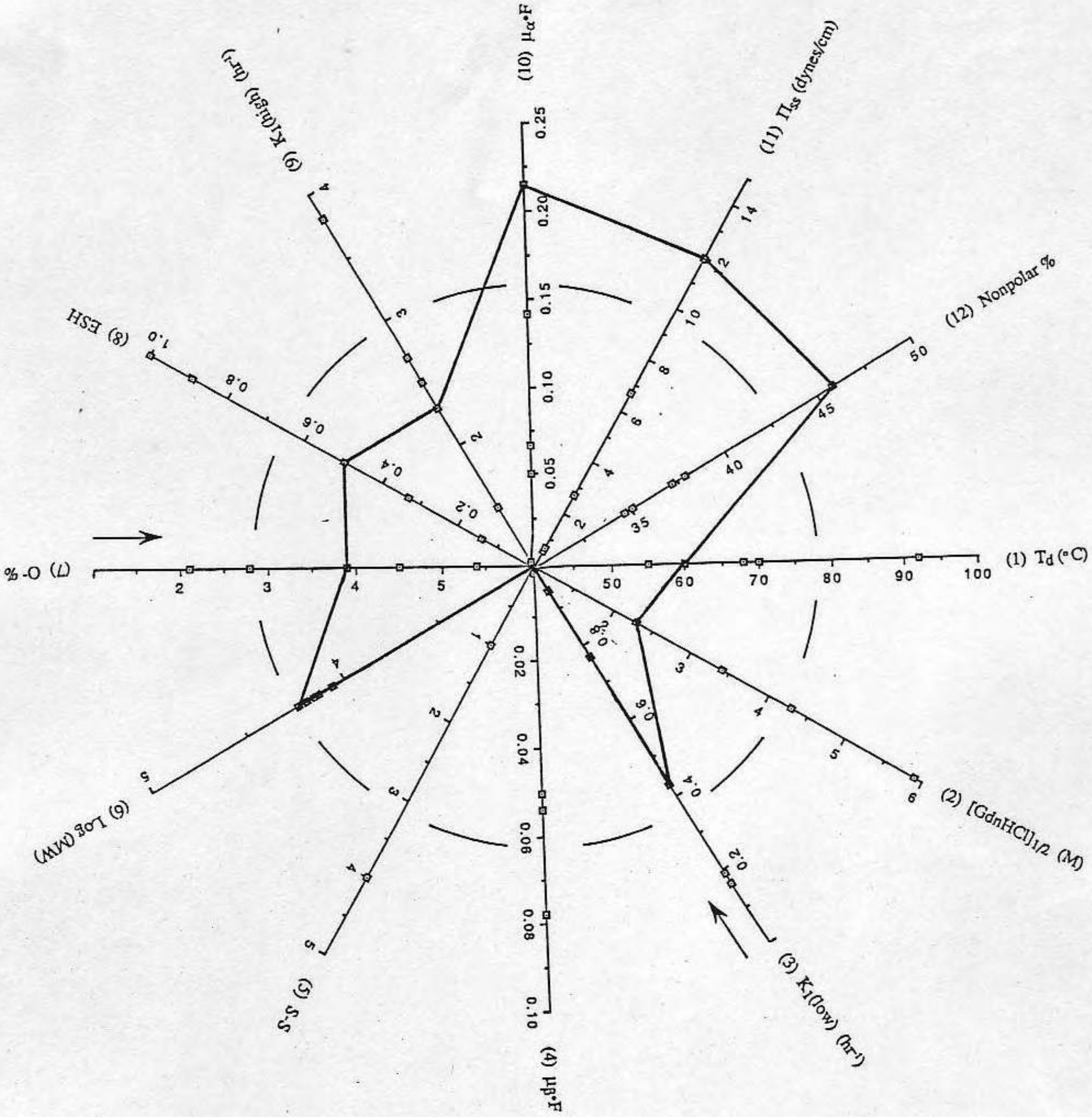

Figure 2. Tatra Plot of Myoglobin (MYG). MYG is relatively unstable, moderately hydrophobic, and very surface active at steay-state.

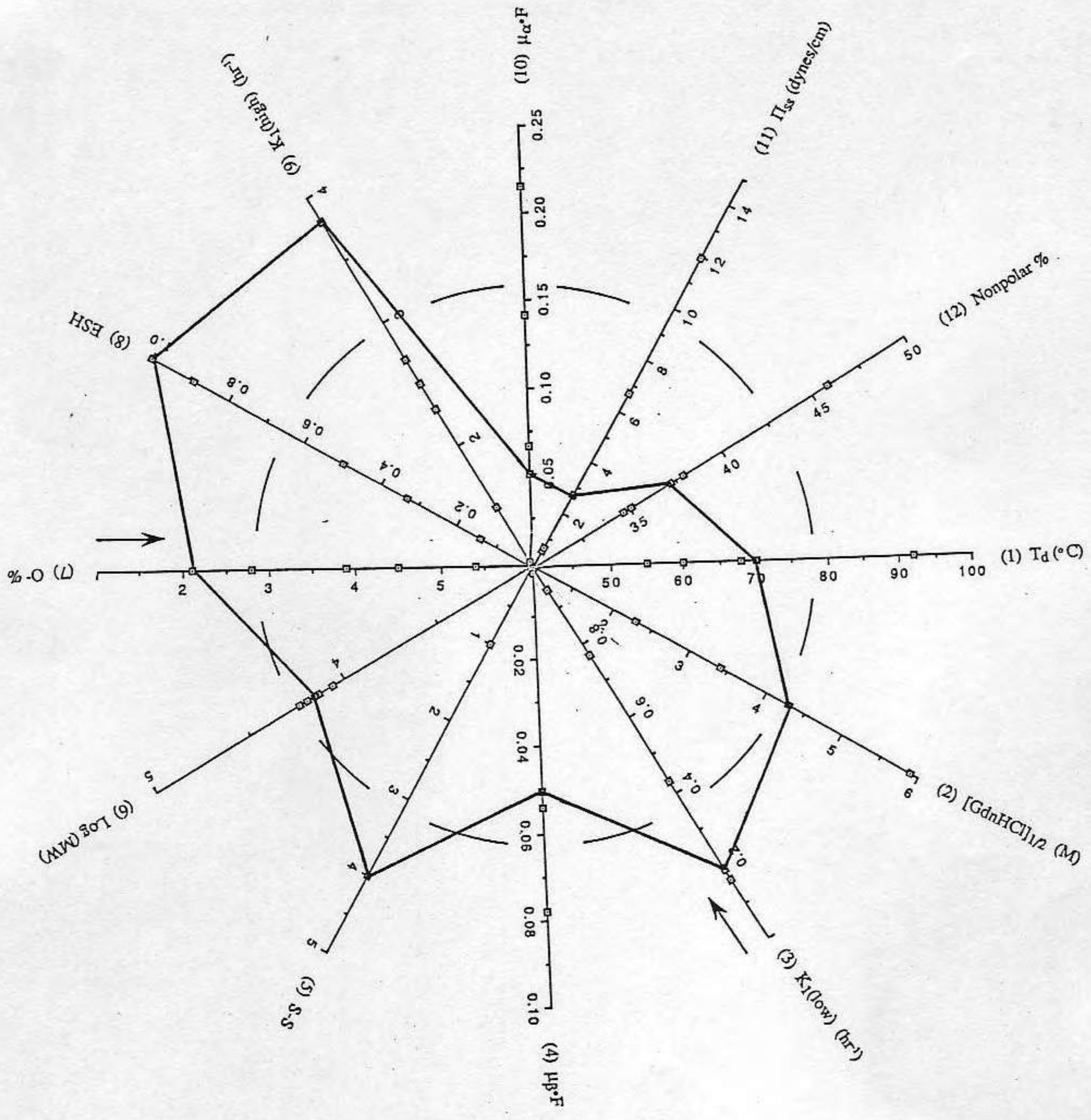

Figure 3. Tatra Plot of Lysozyme (LYZ). LYZ is very hydrophobic, relatively stable, and not very surface active at low bulk solution concentrations (0.05 mg/ml).

THE ROLE OF PROTEIN STRUCTURE IN SURFACE TENSION KINETICS

A. -P. WEI, J. N. HERRON AND J. D. ANDRADE

ABSTRACT. Surface tension kinetics were measured for five model proteins (superoxide dismutase, cytochrome-c, myoglobin, lysozyme and ribonuclease-A) using the Wilhelmy Plate method. These data were correlated to both the stability and hydrophobicity of each protein. At low bulk concentrations, surface tension kinetics reflected the conformational stability of the protein; while at higher concentrations, surface tension kinetics were more strongly correlated with the effective hydrophobicity of the protein. The solvent accessible areas of nonpolar groups in relation with the experimental results were also discussed.

1. Introduction

The interfacial behavior of proteins is important in many biological and technological processes, such as biomaterials, food processing, chromatography, pharmaceutics and biomembranes[1-3]. There have been many studies in the literature concerning protein adsorption, as well as conformational changes which occur upon adsorption. However, the role of protein structure in these processes is not completely understood[5,6]. We believe that a protein's interfacial behavior is strongly influenced by its structural properties, and that such factors need to be considered when interpereting adsorption data. Our approach to this problem has been to study the interfacial behavior of well-characterized model proteins, which have known 3-dimensional structures[7]. In previous studies, we investigated the adsorption behavior of both hen and human lysozyme on solid surfaces using total internal reflection fluorescence (TIRF) spectroscopy and molecular graphics[10]. Recently, we have extended these studies to include five model proteins (lysozyme, ribonuclease-A, myoglobin, cytochrome-c and superoxide dismutase), and have studied their behavior at the air-water interface using dynamic surface tension measurements. All five are small, single domain globular proteins with known three-dimensional structures. Some of their properties are summarized in Table 1. They are similar in size and dimension, but different in amino acid composition and secondary structural units. This will help to minimize the effect of molecular size during the transport of proteins from bulk to surface, and will allow us to compare experimental results solely on a structural basis. In this paper, the dynamic surface tension of these model proteins in aqueous solution was measured as a function of time and bulk concentration. The role of conformational stability, effective surface hydrophobicity and solvent accessible areas was studied.

2. Materials and Method

2.1. PROTEINS AND CHEMICALS

Myoglobin (sperm whale), cytochrome-c (tuna heart) and ribonuclease-A (bovine pancreas) were products of Sigma Chemical, Co. (St Louis, MO). Lysozyme (hen egg white) was purchased from Calbiochem (La Jolla, CA), and superoxide dismutase (bovine liver) was purchased from DDI, Inc. (Mountain View, CA). All proteins were obtained in lyophilized powder form (≥ 90% purity) and used without further purification. Absolute grade guanidinium hydrochloride (GdnHCl) was purchased from Research Plus, Inc. (Bayonne, NJ), cis-parinaric acid from Molecular Probes, Inc. (Eugene, OR).

D. J. A. Crommelin and H. Schellekens (eds.), From Clone to Clinic, 305–313.
© 1990 Kluwer Academic Publishers. Printed in the Netherlands.

TABLE 1. Characteristics of Model Proteins

PROTEINS (ABBR.)	Strands of β-Sheets[1]	No. of α helices[1]	No. of a. a.[1]	Molecular Weight [2]	Dimensions	[1] S-S	pI	Nonpolar Residues[2]
Cytochrome-c (CYTC)	0 (0%)	5 (51.5%)	103	11353	25x25x37 Å	0	10	37.9 %
Myoglobin (MYG)	0 (0%)	8 (79.1%)	153	17183	44x44x25 Å	0	7.8	45.8 %
Superoxide Dismutase (SOD)	8 (36.4%)	0 (0%)	151	15534	36x40x38 Å	1	4.6	35.1%
Lysozyme (LYZ)	5 (15.5%)	4 (27.1%)	129	14296	45x30x30 Å	4	10.7	37.2 %
Ribonuclease-A (RNASE)	3 (37.1%)	3 (26.6%)	124	13673	38x28x22 Å	4	9.6	34.7 %

NOTES:
[1]. According to X-ray crystallographic coordinates obtained from the Protein Data Bank;
[2]. Calculated from amino acid sequences.

2.2. SPECTROSCOPIC MEASUREMENTS

Fluorescence measurements were made on a Greg-200 multi-frequency fluorometer (ISS, Champaign, IL) in the photon counting mode with excitation wavelength at 295 nm and 325 nm for tryptophan and cis-parinaric acid fluorescence, respectively. The excitation and emission monochromator slit-width was 0.5 and 2 mm, respectively. UV absorbance was measured on a Beckman model 135 spectrophotometer.

2.3. DENATURATION/STABILITY STUDIES

Guanidinium hydrochloride (GdnHCl) solutions (0-8 M) were prepared in PBS with pH values of 7.25±0.1. Proteins in GdnHCl were equilibrated overnight at room temperature (23°C) before spectroscopic measurements. Denaturation curves were constructed from shifts in maximum emission wavelength in the UV fluorescence spectra of LYZ, MYG, CYTC. For RNASE, UV differential absorbance at 278 nm (ΔA_{278}) and 287 nm (ΔA_{287}) were measured. ΔA_{278}-ΔA_{287} was used to construct the denaturation curve[11]. For SOD, UV absorbance spectra were measured and A_{270}-A_{280} was chosen to construct the denaturation curve.

2.4. BINDING OF PROTEIN WITH CIS-PNA

Stock cis-PnA solutions were prepared in ethanol. The concentration was determined by absorbance at 303 and 318 nm using the extinction coefficient of 80,000 and 74,000 $cm^{-1}M^{-1}$, where γ_{ss}, γ, γ_o are surface tension values at equilibrium, any time t and time t=0, respectively, and K is the technical first order rate constant. Values for induction period and technical rate constant are listed in Table 2.

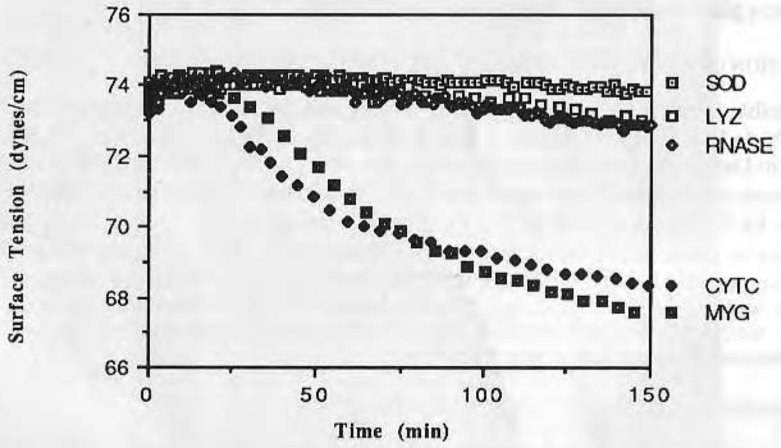

Figure 1. Surface tension kinetics of five protein at low concentration. The differences in the length of induction period and the rate of change for different proteins correlate with their respective stabilities.

TABLE 2. Correlation of Stability with Surface Tension Reduction at Bulk Concentration of 0.01 mg/ml

Proteins	$[GdnHCl]_{1/2}$ (M)	Induction Period (min)	Rate Constant (hr^{-1})
SOD	5.9±0.22	100	0.16
LYZ	4.3±0.15	75	0.19
RNASE	3.4±0.27	40	0.77
CYTC	2.3±0.01	20	0.95
MYG	2.3±0.24	25	0.43

3.1.3. *The Role of Conformational Stability*. The correlation between the stability of a protein and its surface properties was early studied by Hamaguchi in 1955[17]. In his study, a thin film of lysozyme was spread at the air-water interface and pressure-area (π-ΔA) curves were measured. Hamaguchi concluded that proteins with rigid structure were not completely unfolded at the interface unless they were denatured beforehand. Nagel, *et al.* (1976) studied the surface pressure and mechanical precipitability of human hemoglobin variants and found that surface active mutants exhibited low stabilities[18]. The effects of pH, ionic strength and temperature were also studied, but only small differences observed. Therefore, they concluded that conformational stability of proteins is the most influential factor in their surface activities. A more clear demonstration of the stability effect is the recent work by Kato and Yutani using protein engineering techniques[19]. They prepared six mutants of the α-subunit of tryptophan synthase, which was substituted at position 49. The free energy of unfolding in water (ΔG values) of these mutants varies from 4 to 16 kcal/mol. Good correlations were observed between the ΔG values, the surface tension after five minutes, and foaming and emulsifying properties.

where γ_{ss}, γ, γ_o are surface tension values at equilibrium, any time t and time t=0, respectively, and K is the technical first order rate constant. Values for induction period and technical rate constant are listed in Table 2.

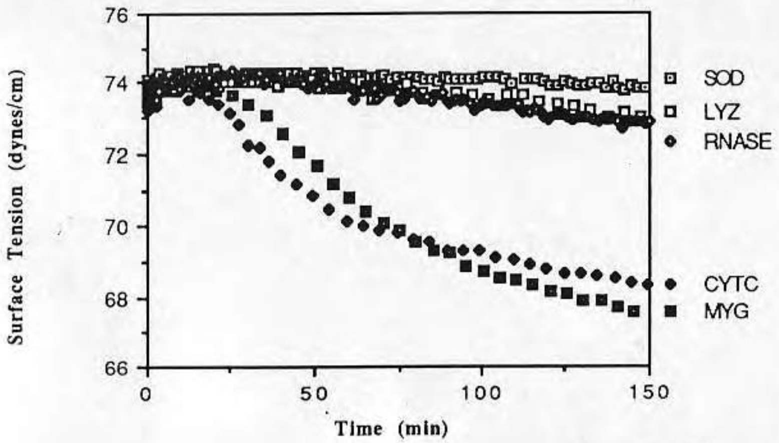

Figure 1. Surface tension kinetics of five protein at low concentration. The differences in the length of induction period and the rate of change for different proteins correlate with their respective stabilities.

TABLE 2. Correlation of Stability with Surface Tension Reduction at Bulk Concentration of 0.01 mg/ml

Proteins	$[GdnHCl]_{1/2}$ (M)	Induction Period (min)	Rate Constant (hr^{-1})
SOD	5.9±0.22	100	0.16
LYZ	4.3±0.15	75	0.19
RNASE	3.4±0.27	40	0.77
CYTC	2.3±0.01	20	0.95
MYG	2.3±0.24	25	0.43

3.1.3. *The Role of Conformational Stability*. The correlation between the stability of a protein and its surface properties was early studied by Hamaguchi in 1955[17]. In his study, a thin film of lysozyme was spread at the air-water interface and pressure-area (π-ΔA) curves were measured. Hamaguchi concluded that proteins with rigid structure were not completely unfolded at the interface unless they were denatured beforehand. Nagel, *et al.* (1976) studied the surface pressure and mechanical precipitability of human hemoglobin variants and found that surface active mutants exhibited low stabilities[18]. The effects of pH, ionic strength and temperature were also studied, but only small differences observed. Therefore, they concluded that conformational stability of proteins is the most influential factor in their surface activities. A more clear demonstration of the stability effect is the recent work by Kato and Yutani using protein engineering techniques[19]. They prepared six mutants of the α-subunit of tryptophan synthase, which was substituted at position 49. The free energy of unfolding in water (ΔG values) of these mutants varies from 4 to 16 kcal/mol. Good correlations were observed between the ΔG values, the surface tension after five minutes, and foaming and emulsifying properties.

The explanation of the induction period has been quite controversial. Due to space limitations, only our own view is presented here (interested readers are refered to refs. 15 & 16). The decrease in surface tension is related to the adsorption of protein molecules at the air/water interface. Whether a protein adsorbs or not depends on the protein concentration in the subsurface phase and on the affinity of the protein for the interface. If the affinity is high, proteins will adsorb even at low concentrations. On the other hand, if the affinity is low, a high concentration of protein will be required for adsorption. The time required for our model proteins to form a monolayer by diffusion from bulk solution to the subsurface is in the range of 200 seconds for the concentration used. As the induction periods are much longer than the diffusion time, a mechanism other than concentration dependent adsorption is suggested, probably surface induced unfolding. This suggestion is consistent with the fact that proteins are susceptible to surface denaturation at low surface pressures[20]. Depending upon the conformational stability of individual proteins, the time needed for denaturation varies. Stable proteins take longer time, unstable proteins take shorter time.

The results presented in Table 2 are consistent with this model. The induction period at 0.01 mg/ml bulk concentration is correlated with protein stability (see Table 2). More stable proteins such as SOD and LYZ have longer induction periods, while less stable proteins (CYTC and MYG) have shorter induction periods. Furthermore, the rate at which the surface tension decreases should also be correlated with stability. This is because decreases in surface tension (at low protein concentrations) are primarily due to adsroption of denatured protein. In Table 2, we see that stable proteins such as SOD and LYZ have lower rate constants than less stable proteins such as CYTC and MYG.

3.2. EFFECTIVE SURFACE HYDROPHOBICITY DETERMINES THE RATE OF SURFACE TENSION REDUCTION AT HIGH BULK CONCENTRATIONS

3.2.1. *Effective Surface Hydrophobicity.* Globular proteins are folded in such a way as to minimize the exposure of apolar amino acid residues to solvent. However, because folding is not a perfect process, a few apolar residues are often found near the surface of the protein. These residues impart a certain hydrophobic character to the exterior of the protein which is called the "effective surface hydrophobicity" (ESH). Several techniques can be used to measure the ESH of a protein, including hydrophobic interaction chromatography (HIC) and binding studies with hydrophobic, fluorescent dyes such as cis-parinaric acid (cis-PnA). The effective surface hydrophobicities of LYS, SOD and RNASE were determined using the method of Nakai[21]. In brief, each protein was titrated with a soluble solution of cis-PnA and the initial slope of the titration curve was used to determine the ESH parameter. These data are shown in Figure 2.

Because the maximum absorbance of the heme group (410 nm) coincides with the emission maximum of cis-PnA, titration data for MYG and CYTC were not obtained. Fortunately, LYZ, RNASE, MYG and CYTC have been widely studied in the literature of hydrophobic interaction chromatography. Hydrophobic parameters based on retention time have been documented by different investigators under non-denaturing conditions (native states). These data are summarized in Table 3. Although these values were determined at a different time and place and by different investigators, the relative order of hydrophobicity of these proteins is constant.

3.2.2. *Surface Tension Kinetics at High Protein Concentration.* Surface tension kinetics were also determined for the five model proteins at a concentration of 1.0 mg/ml. At this concentration, diffusion is relatively rapid (< 1 min. according the Tordai-Word equation[2]) and even proteins with a weak affinity for the surface should adsorb. Under these conditions, an induction period is not expected, and surface tension kinetics are thought to reflect the surface hydrophobicity of the protein, rather than its intrinsic stability[16]. Kinetic data for two of the proteins (LYZ and SOD) are shown in Figure 3. Similar data were obtained for the other three model proteins, but were omitted because of space limitations. As expected, induction periods were not observed.

Kinetics plots at concentrations of 1.0 mg/ml (and higher) exhibited two components - an initial rapid decrease in surface tension, followed by a much slower decrease. By assuming a biphasic process we were able to determine two technical kinetic constants (K_1 and K_2) for each protein. The first kinetic constant (K_1) reflects the surface hydrophobicity of the protein, while the second (K_2) is related to the protein chain length[16]. Values for K_1 are listed in Table 3.

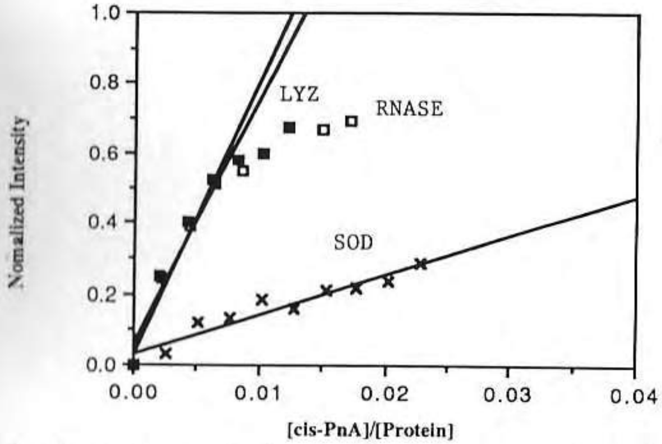

Figure 2. Binding of cis-Parinaric Acid to LYZ, RNASE and SOD. The initial slope of each curve is used as a measure of the effective surface hydrophobicity of the protein[21].

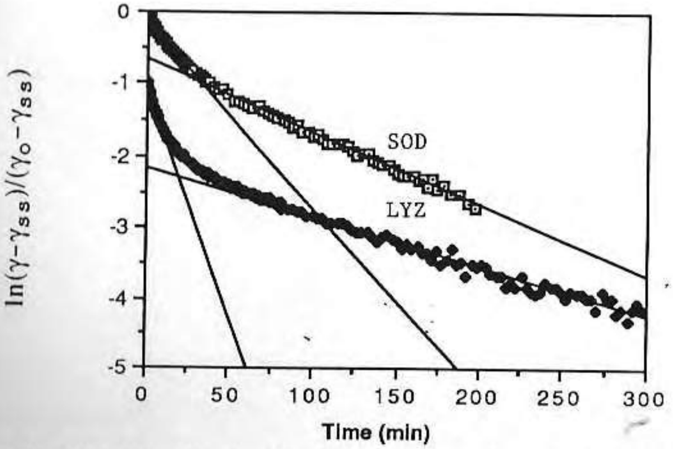

Figure 3. First order kinetic plots [$\ln(\gamma-\gamma_{ss})/(\gamma_o-\gamma_{ss})$ vs. time] for SOD and LYZ, at 1 mg/ml concentration. For the sake of clarity, the curve for LYZ has been offset by one unit in the y axis. Curves were analyzed using a biexponential fit, which gave two rate constants: K_1 and K_2. The first of these (K_1) is thought to reflect the effective surface hydrophobicity of the protein, while the second (K_2) is related to the molecular weight of the protein. Values for K_1 are listed for all five proteins in Table 3.

3.2.3. *The Role of Effective Surface Hydrophobicity.* The role of hydrophobicity in the interfacial behavior of proteins has long been recognized. For example, studies by Norde, Lyklema, Neumann and others have shown that there's a direct correlation between the degree of protein adsorption and the hydrophobicities of both the protein and the surface[2,22]. Vroman, Horbett, Brash and Lundstrom have shown that proteins with high concentration and small size (high collision rate) adsorb initially, but are soon replaced by moelcules which are more surface active. This phenomenon is called the "Vroman Effect." In early studies, the surface activity of a protein was often determined from static surface tension measurements[22]. In some cases, there was a correlation between surface activity and the total apolar amino acid composition of the protein[1,2], but this correlation may held for dilute solutions of proteins which were easily denatured. For more concentrated solutions of proteins, the surface activity is probably more directly related to the effective surface hydrophobicity of the protein. This concept has received increasing attention in the literature[3,21].

TABLE 3. Comparison of Various Hydrophobicity Parameters of Model Proteins with their Rate Constants of Surface Tension Reduction

PROTEINS	[1]HIC[23]	HIC[24]	HIC[25]	HIC[26]	HIC[27]	[2]Binding	[3]K_1(hr^{-1})
LYZ	0.65	26.0	10.8	8.5	14.7	77.7	3.8
RNASE	0.35	16.3	7.0	1.6	N/A	69.6	2.7
MYG	0.23	N/A	5.4	0.8	9.3	N/A	2.3
CYTC	0.00	8.6	3.6	0.6	2.8	N/A	2.5
SOD.	N/A	N/A	N/A	N/A	N/A	11.2	1.5

Notes:

1. HIC: Protein hydrophobicity derived from retention time on hydrophobic interaction chromatography. References are given in the bracket;
2. Binding with cis-PnA. Values are the initial slope of the titration curve;
3. Technical rate constant K_1 at bulk concentration 1 mg/ml.

The role of effective surface hydrophobicity in surface tension kinetics can be considered in terms of the effective collision rate between protein molecules and the air-water interface. For proteins of similar size and at the same bulk concentration, surface tension kinetics should be related to the effective surface hydrophobicity (ESH). The higher the ESH value, the greater the number of effective collisions, the faster the rate of adsorption, and a greater reduction in surface tension at short time. Nakai,*et al.* studied the surface properties of some ten proteins in both native and heat-denatured states[21]. A good correlation was found between the slope of cis-PnA titration curve and surface tension measured after five minutes of adsorption.

At high bulk concentrations (≥ 1 mg/ml), K_1 values are no longer related to protein stability, but tend to correlate with the effective surface hydrophobicity, instead. For example, lysozyme and ribonuclease exhibited the highest K_1 values and were also found to be the most hydrophobic by criteria of hydrophobic interaction chromatography and cis-PnA binding (see Table 3). In contrast, superoxide dismutase exhibited the lowest K_1 value and was very hydrophilic according to both the cis-PnA binding and the surface tension data. Another interesting observation was that the initial induction period of the surface tension vs. time curve tends to disappear with increasing protein concentration (data not shown). This suggests that the high sub-surface concentration drives native protein molecules to bind to the surface without unfolding. Of the five proteins, lysozyme and ribonuclease have the highest ESH values. Proteins with higher ESH values can not only have a greater number of effective collisions with the surface and a greater chance to adsorb but reorient themselves more readily once adsorbed. This will result in faster decrease in surface tension and hence higher K_1 values. The opposite is true for hydrophilic molecules such as SOD, MYG and CYTC.

3.3. SOLVENT ACCESSIBLE AREAS OF NONPOLAR ATOMS SHOW LITTLE CORRELATION WITH THE EXPERIMENTAL HYDROPHOBICITY PARAMETER

To account for the surface tension reduction on a molecular basis, the solvent accessible areas of polar, nonpolar and charged atoms of model proteins were calculated according to Richards[4].

These results are summarized in Table 4. The accessible surface area of nonpolar atoms were found to be proportional to the molecular weight of the protein (Table 1), rather than to its effective surface hydrophobicity. However, it is interesting to note that the accessible areas of charged oxygen (O^-) tend to decrease from SOD to LYZ. For small proteins of similar size, the hydrophobicity of surface hydrophobic residues may be masked because they are dispersed among polar residues. The ability of the surface apolar groups to manifest their hydrophobicity is controlled by the number of accessible neighboring polar groups. Charged groups exert the most influence because they have very negative solvation energies and therefore have the highest degree of solvation[8]. The fact that SOD, CYTC and MYG have higher degrees of accessible negative charges and total charges may explain why they are less hydrophobic than RNASE and LYZ. Katti, *et al.* [9] studied the relationship of molecular areas accessible to a 4 Å diameter probe (2.8 Å is the value for water) with a "hydrophobic interaction parameter(HIP)" derived from hydrophobic interaction chromatography for five proteins. They concluded that the higher the total accessible area, the larger the HIP value. The results were the same for surface areas expressed as total van der Waals areas, nonpolar VDW areas or nonpolar accessible areas. Because the total accessible areas, as well as its nonpolar constituent, are proportional to protein molecular weight, Katti's work actually indicates that the bigger the size of the protein, the stronger will it interact with hydrophobic surfaces.

TABLE 4. Accessible Area of Model Proteins in Folded States (Å^2)

PROTEINS	BACKBONE	SIDE CHAINS					SUM			
	C/CA	N/O	N/O	C/S	N^+	O^-	C/S	N/O	N^+/O^-	TOTAL
SOD	709.9	972.5	1206.8	3582.7	524.3	403.4	4292.6	2179.3	927.7	7399.6
CYTC	479.5	725.5	773.1	2954.9	673.7	259.1	3434.4	1498.6	932.8	5865.8
MYG	613.4	798.6	1277.2	4280.5	922.6	325.3	4893.9	2075.8	1247.9	8217.6
RNASE	415.6	922.9	1406.8	3338.8	562.5	184.7	3754.4	2329.7	747.2	6831.3
LYZ	653.5	994.1	1451.0	2610.2	695.8	143.2	3263.7	2445.1	839.0	6547.8

4. Acknowledgements

The authors thank the University of Utah Center for Biopolymers at Interfaces for their financial support to this project. The Macintosh interface for Wilhelmy Plate apparatus was developed in our laboratory by Mr. Paul Dryden.

5. References

1. W. Norde, "Adsorption of Proteins from Solution at the Solid-Liquid Interface", Adv. Colloid and Interface Sci., 25(1986), 267-340.
2. J. D. Andrade, ed. "Surface and Interfacial Aspects of Biomedical Polymers: Vol.2. Protein Adsorption", Plenum Press, 1985.
3. S. Nakai and E. Li-Chan, eds. Hydrophobic Interactions in Food Systems, CRC Press, 1988.
4. T. J. Richmond and F. M. Richards, "Packing of α-Helices: Geometrical Constraints and Contact Areas", J. Mol. Biol., 119(1978) 537-553.
5. T. A. Horbett, "Molecular Origin of the Surface Activity of Proteins", Protein Engineering, 2(1988), 3, 172-174.
6. S. Damodaran and K. B. Song, "Kinetics of Adsorption of Proteins at Interfaces: Role of Protein Conformation in Diffusional Adsorption", Biochim. Biophys. Acta, 954(1988), 253-264.

7. J. D. Andrade, J. N. Herron, V. Hlady and D. G. Horsley, "Simulation of Protein Adsorption: The Denaturation Correlation", Croatica Chemica Acta, 60(1987), 3, 495-503.
8. D. Eisenberg and A. D. MacLachlan, "Solvation Energy in Protein Folding", Nature, 319(1986), 199-203.
9. A. Katti, Y. F. Maa and Cs. Horvath, "Protein Surface Area and Retention in Hydrophobic Interaction Chromatograpgy", Chromatograpia, 24(1987), 646-650.
10. D. Horsley, J. N. Herron, V. Hlady and J. D. Andrade, "Human and Hen Lysozyme Adsorption" in Proteins at Interfaces, edited by J. L. Brash and T. A. Horbett, ACS, 1987.
11. J. T. Kellis, K. Nyberg, D. Sali and A. R. Fersht, "Contribution of Hydrophobic Interactions to Protein Stability", Nature, 333(1988), 23, 784-786.
12 The Catalog of Molecular Probes, Inc., Eugene, OR 97402.
13. Protein Data Bank Newsletter, No. 46, 1988. Brookhaven National Laboratory, Upton, NY 11973.
14. C. N. Pace, B. A. Shirley and J. A. Thomson, "Measuring the Conformational Stability of a Protein" in Protein Structure: A Practical Approach edited by T.E. Creighton, IRL Press, 1989.
15. J. A. De Feijter and J. Benjamins, "Adsorption Kinetics of Proteins at the Air-Water Interface" in Food Emulsions and Foams edited by E. Dickinson, Royal Society of Chemistry, London, 1986, 72-85.
16. A. -P. Wei, "The Structure of Model Proteins and Their Behavior at the Air-Water Interface", M.S. Thesis, University of Utah, March, 1990.
17. K. Hamaguchi, "Studies on Protein Denaturation by Surface Chemical Method", J. Biochem., 42, 449-459(1955).
18. E. F. Roth, D. Elbaum, R. M. Bookchin and R. L. Nagel, "The Conformational Requirements for the Mechanical Precipitation of Hemoglobins and Other Mutants", Blood, 48(1976), 2, 265-271.
19. A. Kato and K. Yutani, "Correlation of the Surface Properties with Conformational Stabilities of Wild-type and Six Mutant Tryptophan Synthase α-subunits Substituted at the Same Position", Protein Engineering, 2(1988), 2, 153-156.
20. T. L. Donaldson, E. F. Boonstra and J. M. Hammond, "Kinetics of Protein Denaturation at Gas-Liquid Interfaces", J. Colloid and Interface Sci., 74(1980), 2, 441-450.
21. A. Kato and S. Nakai, "Hydrophobicity Determined by a Fluorescence Probe Method and Its Correlation with Surface Properties of Proteins", Biochim. Biophys. Act. 624(1980), 13-20.
22. D. R. Absolom, W. Zingg and A. W. Neumann, "Protein Adsorption to Polymer Particles: Role of Surface Properties", J. Biomed. Mater. Res., 21(1987), 161-171.
23. S. C. Goheen and A. Stevens, "New Techniques for Separating Proteins in Hydrophobic Interaction HPLC", Bio Techniques, Jan/Feb, 1985, 48-50.
24. D. L. Gooding, M. N. Schmuck and K. M. Gooding, "Analysis of Proteins with New, Mildly Hydrophobic High Performance Liquid Chromatograpgy Packing Materials", J. Chromatography, 196(1984), 107-114.
25. Y. Kato, T. Kitamura and T. Hashimoto, "High-Performance Hydrophobic Interaction Chromatography of Proteins", J. Chromatography, 266(1983), 49-54.
26. J. T. Fausnaugh, L. A. Kennedy and F. E. Regnier, "Comparison of Hydrophobic Interaction and Reversed-Phase Chromatography of Proteins", J. Chromatography, 317(1984), 141-155.
27. R. H. Ingraham, S. Y. M. Lau, A. K. Tanejan and R. S. Hodges, "Denaturation and the Effects of Temperature on Hydrophobic-Interaction of and Reversed-Phase High-Performance Liquid Chromatography of Proteins", J. Chromatography., 327(1985), 77-92.

JOURNAL OF BIOMEDICAL MATERIALS RESEARCH
SOCIETY FOR BIOMATERIALS

A. NORMAN CRANIN, Editor-in-Chief
The Dr. Samuel Cranin Center for Dental and Oral Surgery
The Brookdale Hospital Medical Center
Linden Boulevard at Brookdale Plaza
Brooklyn, New York 11212
(212) 240-6281

Assistant Editors
James M. Anderson Jonathan Black Jack C. Bokros Franz Burny
Robert A. James Frederic W. Rhinelander Allan M. Weinstein

11/21/85

Dear Dr. Andrade:

Re: MS # C-973

I am returning your manuscript along with comments of the referees.

It has been suggested that your paper be revised in accordance with the recommendations enclosed.

I welcome the re-submission of this work if you will consider accepting the suggestions accompanying it.

Sincerely yours,

Norman Cranin
A. Norman Cranin

ANC/jn
Encs.

RECEIVED
University of Utah
NOV 25 1985
Dean's Office
Engineering

If you have elected to request the author (s) to revise this manuscript, please explain.

The purpose of this paper is to investigate the possibility of preventing or minimizing protein adsorption to produce a more thromboresistant surface(s). The authors describe well controlled chemical preparation of various modified forms of poly(ethylene oxide) polymers. Although they reference their "preliminary" work on unmodified PEO grafted surfaces, they give little attention to actual _in vitro_ or _in vivo_ protein adsorption onto these polymers. The important aspect of the "Conclusion" is that a stable polymer rich surface of long chain PEO has been coupled onto quartz surfaces via amino silane coupling agents. Projected and proposed work with speculation as to the outcome constitutes the remainder of the "Conclusion". Without actual protein adsorption studies, this paper seems incomplete. The value of the information to the biomaterials community, in its current form, is limited. This paper is a fine piece of chemistry but should be resubmitted when the purposes for which the synthesis was performed are investigated.

Instructions:

1. Please do not sign this page
2. Please type since this will be sent to the author without identification of the reviewer.

[illegible]

If you have elected to request the author (s) to revise this manuscript, please explain.

General

This is an interesting piece of work, generally well done. but the manuscript is weakly written in places. In my opinion, separation of of the Results from the Discussion, and elimination of the "Conclusions", would help a lot. Some information on statistical significance of the data is required.

Specific comments

1. The Abstract is missing

2. p.2, l.4: The sentence "We are currently investigating of PEO..." seems grammatically incorrect, as if the last 2 parts of the sentence were inverted.

3. p.2, l.9: What evidence is there that the geometry of the device influences adsorption?

4. p.5, l.17: The sentence "A similar study..." and the prior discussion do not appear to agree with the data. The decrease of the nitrogen signal in Figures 5 and 6 look very similar to me. I think giving the actual data in a table might be more convincing than the Figures alone.

5. Figure 10 & others: I really couldn't figure out which curve was which from the letters on the Figures, since the curves cross and the letters (esp. B & D) are near each other. The symbols need to be identified in all the Figure legends.

Instructions:

1. **Please do not sign this page**
2. **Please type since this will be sent to the author without identification of the reviewer.**

6. P.7: The discussion of the relative stability of the urethane and urea linkages formed by the chloroformate and isocyanate derivatives, respectively, needs strengthening. It is a central conclusion of the paper. The stability of these linkages has probably been studied before. A good review of the relevant literature seems in order here to help substantiate this conclusion. Further discussion of the chemistry of the stability of the linkages would help a lot.

7. * The angular ESCA analysis is far too sketchily presented. Furthermore, the existence of a patchy overlayer is presented as a result, (e.g., see title of the Figures) when its actually a conclusion. I believe this section needs expansion and clarification to detail now the conclusion of patchiness is reached from the results.

8. I don't understand sentence #2 of the conclusions. I thought that's what they did in this paper!

9. * Statistics are missing throughout. Are the data averages? How many runs? What was the standard deviations? What confidence in the apparent differences can we place?

PROTEIN RESISTANT SURFACES:
1. PREPARATION, CHARACTERIZATION, AND AQUEOUS STABILITY OF POLY(ETHYLENE OXIDE)-AMINOPROPYL SILANE-SILICA SURFACES

S. WINTERS,* D.E. GREGONIS, and J.D. ANDRADE+

Department of Bioengineering
*Department of Pharmaceutics
University of Utah
Salt Lake City, Utah 84112

+ To whom correspondence should be adressed

submitted to Journal of Biomedical Materials Research

INTRODUCTION

The interactions between surfaces and blood proteins has spawned increasing interest in the development of surfaces which exhibit minimal protein adsorption. Poly(ethylene oxide) (PEO) has some unique properties which have led to its consideration for application in implants, oxygenators, dialysis membranes, contact lenses, chromatography supports, and immunoassays. We are currently investigating the protein adsorption properties of PEO surfaces. Current evidence shows that PEO, either by itself or as a component in copolymers, is relatively inert in terms of protein adsorption and platelet adhesion (1-10).

The adsorption of specific proteins at solid surfaces is influenced by the polymer composition, geometry of the device, implant site and the nature of the protein solution or tissue with which the device is in contact. Protein adsorption is generally accepted as being the primary factor which "dictates" subsequent events, including thrombogenesis, complement activation, and cell adhesion (11). Our hypothesis asks if it is possible to prevent or to minimize protein adsorption, will the surface be more thromboresistant ?

PEO has unusual solubility characteristics. It is soluble in water and in a number of common organic solvents including acetonitrile, chloroform, benzene, and dimethyl formamide. At room temperature it is completely miscible with water in all proportions. Aqueous solutions of high molecular weight PEO show a "stringy" character at less than one percent concentration. In water, PEO exhibits an inverse solubility-temperature relationship (12). As the temperature of aqueous solutions are increased to near the boiling point of water, the polymer precipitates. This has been explained by a hydrophobic (ethylene units)- hydrophilic (ether oxygens) balance in the polymer system and the presence of bound water molecules (13,14).

X-ray analysis of crystalized PEO shows that the molecule arranges in a helical conformation with a succession of *trans-gauche-trans* conformers along the chain (15,16). However, in aqueous solutions, Liu

(17) and Maxfield (18) have independently determined that the helical form is largely lost and the structure tends towards a random coil. A hydrogen-bonded complex is formed in the aqueous solution in which three water molecules are involved with each PEO repeat unit.

Merrill *et al* have used the unique solubility and the solution properties of PEO to explain the apparent inertness of PEO surfaces towards blood proteins and platelets(19). Due to the imbibition of water by a PEO surface, these surfaces exhibit a "liquid-like" state with considerable chain flexibility. These interact little if at all with proteins important to the coagulation of blood, or with platelets.

This observed phenomenon, which has been used extensively in protein precipitation processes and exclusion chromatography, can also be explained by an excluded volume theory which adds an active repulsion arguement to the already hydrophilic and amorphous surface. Knoll and Hermans, using PEO ranging in molecular weights from 1,000 to 100,000 and bovine serum albumin, modeled the thermodynamic driving forces for repulsion of globular and rod-shaped proteins from such a surface. (20,21). Flexible, randomly coiled water soluble polymer chains interact unfavorably with long chain protein molecules which tends to favor the formation of phases in which the species are separate. The calculations of these investigators correctly predicted the observed experimental results including the relative ineffectiveness of low molecular weight polymers as precipitating agents.

Because of the reports of reduced protein adsorption by PEO surfaces, and initial studies in our lab confirming these results (22), we have chosen PEO as a good candidate for the development of a protein-resistant surface.

PEO surfaces may be prepared in several ways. It may be physically adsorbed to a substrate material which results in the formation of loops, trains, and tails. However, this may be desorbed from the surface in aqueous solutions. PEO may be incorporated into a copolymer resulting in domains which vary in rigidity and other properties thereby influencing its surface characteristics. PEO chains may be attached to a matrix backbone which is more difficult to control and to characterize (23). Or PEO may be covalently grafted at one end, allowing the molecules to extend out into solution in a bristle-brush manner and present a flexible, fluid-like surface to the environment. We have chosen this last method. Here we describe the synthesis, characterization, and aqueous stability of PEO covalently bound to quartz slides via a γ-aminopropyl triethoxy silane coupling agent.

EXPERIMENTAL

Four different derivatives of PEO at two molecular weights were synthesized (Figure 1); PEO bis-isocyanate, PEO bis-isothiocyanate, PEO bis-chloroformate, and PEO bis-thiochloroformate. Each of these derivatives was synthesized starting with molecular weights of 6,000 and 18,000 from polyethylene glycol (Polysciences, Warrington Pa.). For the isocyanate and isothiocyanate derivatives, an amine capped PEO was prepared using the scheme shown in Figure 2a.

The PEO was dried under vacuum and then dissolved in THF under nitrogen. A 20% excess of 2.2 M n-butyl lithium in hexane was added and stirred for one hour. A 20% excess of tosylchloride was added to the solution and the reaction mixture stirred for 3 days.

The lithium salt of cysteamine was prepared (II in Figure 2a) by adding equivalent amounts of n-butyl lithium to cysteamine in THF dropwise to the solution and stirring overnight. The PEO tosylate solution was added to the cysteamine salt and the mixture stirred for 3 days. THF was removed under reduced pressure and toluene was added to dissolve the residue. The toluene was then washed with 40% KOH four times. The toluene was removed under reduced pressure and the amine capped PEO was reprecipitated three times in diethyl ether (cold) from a minimum amount of methylene chloride. To determine the degree of conversion of PEO to diamino PEO, the amine capped PEO's were titrated using .01 M perchloric acid and acetic acid anhydride. Potassium acid phthalate was used as a standard in the titration. The conversion was determined to be 85%. The amine capped PEO's were then reacted with a 100% excess of phosgene in toluene and stirred for 2 hours (Figure 2b). The excess phosgene was removed by distillation and the toluene removed by rotoevaporation. In the case of the thiocyanate, a 100% excess of thiophosgene in toluene was used instead of phosgene.

The chloroformates were prepared by dissoving PEO in toluene (Figure 2c) to which was added a four times excess of phosgene or thiophosgene. The reaction was accomplished by stirring ovenight and heating to reflux then removing the solvent until no longer acidic. All of the derivatives were stored under nitrogen after being characterized by infrared spectroscopy.

To prepare our surfaces for the immobilization of the PEO derivatives, clean quartz slides were vapor-phase silanized by refluxing for 12 hours in 10 ml APS in 250 ml p-xylene (dried). They were then refluxed for an additional 12 hours in a toluene rinse. Glass beads (50 m) were similarly silanized but in solution phase by stirring vigourously whilie bubbling nitrogen through the silane solution. All glassware was oven dried. XPS analysis was done to determine extent of silane coverage.

The immobilization of the PEO derivatives was performed under nitrogen in a glove bag to prevent hydrolysis of the end groups. The APS derivatized slides were immersed in 3% solutions of the PEO derivatives in methylene chloride, left overnight, rinsed in methylene chloride, ethanol and distilled water. Again, glass beads were derivatized similarly for the purpose of producing high surface area surfaces for subsequent testing.

The aqueous stability of the PEO/silane slides was determined by placing them into a phosphate buffered saline (PBS) solution (pH 7.4) with sodium azide (.01%) added as a bacteriocide . Controls consisted of clean quartz slides and quartz slides with only the APS coupled to them. An APS control slide was adsorbed with underivatized PEO and rinsed with methylene chloride, ethanol, and distilled water to determine non-specific binding.

The surface elemental composition was analyzed by X-ray photoelectron spectroscopy (XPS), using a Hewlett Packard 5950B spectrometer equipped with a monchromatic Alk $_{\alpha}$ 1,2 source at 1487 ev, anode power of 800 watts. An electron flood gun operating at 0.6 mA supplied a source of low energy electrons to compensate for charging of the sample. Scans for carbon 1s, oxygen 1s, nitrogen 1s, and silicon 2s were taken and normalized for their Scofield cross sections (24).

RESULTS

Figure 3a shows a carbon 1s XPS spectrum of pure PEO (MW 6,000). The peak at 285.6 ev (charge referenced to carbon 1s at 284.0 ev) corresponds to a carbon bonded to an ether oxygen and hence is monomodal since all the carbons in PEO are equivalent. The carbon 1s spectrum of Figure 3b shows the aliphatic carbon peak of an APS silanized quartz slide with the peak at 284.0 ev. Figure 3c is again the carbon 1s spectrum, this time it is a spectrum of a quartz slide to which PEO has been bound via the APS coupling agent. The aliphatic carbon of the APS is evident as a distinct shoulder on the lower binding energy side of the etheral carbon peak of the PEO at 285.6 ev. It is the ether carbon component of the total carbon 1s spectrum that we have used to quantitate the amount of PEO on the surface.

The hydrolytic stability of the APS layer was detemined after soaking the quartz APS derivatized slides in PBS buffer for three days and monitoring the relativie intensity of the nitrogen 1s peak. Averages of triplicate samples of each series of 4 runs were used for determination of the signal intensity. In Figure 4, the nitrogen 1s peak appears as a split doublet at 394.8 and 393.1 ev. This splitting of the nitrogen signal only occurs after the slides have been exposed to water and suggests the presence of two nitrogen forms, probably NH_2 and NH_3^+. The relative intensity of the nitrogen signal is plotted (Figure 5) as a function of hydration time in the PBS and indicates that there is little if any loss of the APS layer from the quartz surface after 3 days. The nitrogen signal, after an initial loss in the first 3 to 4 hours of hydration, remains stable. The stability of this layer is also supported by the lack of an increase of the silicon signal from the substrate which would also be indicative of APS detatching from the surface.

Figures 7 and 8 show the carbon/silicon ratio and the percent ether carbon found in the controls consisting of a clean quartz slide soaked in PBS buffer and a silanized quartz slide to which underivatized PEO was adsorbed. Again, these values are the averages of triplicate samples of four separate experiments. Our cleaning procedures typically result in a 5-10% residual total carbon signal on the quartz surface. The ether carbon content of this total carbon signal is what is plotted. This ether carbon is a good indicator of the amount of PEO remaining on the surface of the slide.

In the case of the clean slide, no PEO was adsorbed and therefore the percent ether carbon is very low (13%). It can be seen from Figure 7, curve A, that over the period of three days, the ether carbon signal remained unchanged. This is also reflected in Figure 6, curve A, by the C/Si ratio. Actually, this ratio increased from 0.59 to 1.07 over the three days but we feel this is due to possible contaminants in the PBS buffer and is therefore not significant to the stability issue.

The percent ether carbon and the C/Si ratio of the slides which were silanized but reacted with underivatized PEO to measure physical adsorption of PEO are seen in curve B of Figures 7 and 8. Obviously, some of the underivatized PEO remained physically adsorbed to the APS surface after the rinse but prior to the hydration in PBS, as seen in the slightly higher initial C/Si ratio of 3.0 and the ether carbon content of 32%. This partially desorbed during the three day PBS soak as reflected by the slight decrease of these curves with time. Final parameters for the APS control were C/Si of 2.0 and ether carbon of 22%.

The ether carbon content of the four PEO derivatives, MW 6,000, are seen in Figure 9. The C/Si ratios of these same four derivativatized surfaces are plotted in Figure 10. The PEO chloroformate and thiochloroformate derivatives initially have an average ether carbon content of 70 and 78% respectively, indicating a surface very rich in PEO. However, the resulting PEO layer of the chloroformate and thiochloroformate appears to be somewhat less stable than the cyanate and thiocyanate as reflected by the decrease to a final value of approximately 32% ether carbon and a C/Si ratio of 3.4 for the thiochloroformate and 3.0 for the chloroformate. Possible explanations for this are considered in the discussion section.

The two cyanate derivatives, MW 6,000, have a lower degree of PEO coupling than the chloroformates judging from an initial average ether carbon content of 65% for the isocyanate and 58% for the isothiocyanate. These appear to be more stable over the three day hydration period. Again this is reflected in the C/Si ratios for the cyanate derivatives seen in Figure 10. The final values after three days hydration were 40% and 45% for the ether carbon and 3.8 and 4.0 for C/Si ratio for the isocyanate and the isothiocyanate derivatives, respectively. These values are well above those found for the control slides and a significant improvement over the final values seen in the chloroformate derivatives.

The same trends evident in the lower molecular weight derivatives are also seen in the 18,000 derivatives (Figures 11 and 12). Again, the chloroformates appear to couple more readily but are slightly less stable, once on the surface, than the cyanate derivatives. For the isocyanate and isothiocyanate derivatives (18,000) ether carbon content remains at 35% for both, while C/Si ratios are 4.5 and 4.0 respectively.

The quartz beads were similarly XPS characterized; hovever, less extensive testing was performed, to demonstrate the stability of the PEO coatings. Table I summarizes the results of a single study using triplicate samples of the PEO derivatized beads for eah case. These beads were pressed into indium foil for analysis in the spectrometer. Although indium was detected in the scans, any hydrocarbon contamination on the foil did not enter into the elemental percentages for the PEO. This was conveniently avoided due to lack of conductivity of the glass beads leading the peaks to be charged shifted to lower binding energies. Distinct peaks of elements coming from the indium were discernable as can be seen in the carbon 1s spectrum seen in Figure 13. The small peak at 284.2 ev is presumably hydrocarbon contamination on the indium foil.

Variable angle XPS analysis, modeling the thickness and homogeneity of the APS and PEO layers was performed using isocyanate derivatives of 6,000 and 18,000 molecular weights. This technique allows calculation of the thickness or the percent coverage of an ovelayer on a substrate. Data were calculated according to the equations given in (24) . Values used for λ were 30.8 Å for the carbon 1s peak of PEO and 35.1Å for the silicon 2s peak of the quartz substrate. In modeling the PEO layer, the PEO and APS layers were assumed to be a homogeneous overlayer. The results of these calculations for uniform and patchy overlayers of various thicknesses were plotted and the experimental data was least squares fit to the graphs of the theoretical model. The data are shown in Figures 14 and 15.

The fractional surface coverage of APS is given by the different curves in Figure 14. The astericks represent the actual experimental data found by varying the photoelectron take-off angle from 4^{0} to 85^{0}. Using a least squares best fit, the data of the APS layer on the quartz substrate correspond most closely to an overlayer of 50 Å of APS and 50 percent coverage. This is contrary to popular belief that vapor phase silanization creates a homogeneous monolayer; however, each asterick on the graph represents three samples, each silanized in separate reactions. The error in these experiments was no greater than plus or minus 10 percent of the area of the atomic signals.

The results of the variable angle XPS experiments of the PEO layer are seen in Figure 15. Only the ether carbon component of the total carbon signal was used in these calculations. Again, a least squares analysis of the data indicates that the PEO overlayer fits most closely with the equation of a patchy 70 Å thick overlayer with 80 percent surface coverage. There was little detectable difference in the 6,000 and 18,000 molecular weights. This is presumably due to the collapsed nature of the polymer layer in the vacuum of the XPS spectrometer and will be discussed further in the following section.

DISCUSSION

Poly(ethylene oxide) and its derivatives are widely used in various branches of industry. Replacement of the hydroxyl groups by primary amine groups has been reported by a variety of methods., some of which have minimal chain scission or branching problems. (25,26,27) The method reported here used very mild conditions without the use of pyridine which is has been reported to cause chain scission in the preparation of diamino PEO. (28) An 85 percent conversion of PEO to PEO-diamine was found by titration with perchloric acid and acetic acid anhydride. This produced a highly soluble, amine terminated polymer for reaction with phosgene. More direct routes have been reported for the isocyanate derivatizaion of PEO; however, this method was found to produce little chain branching, scission and a highly water soluble polymer. However, infrared spectroscopy showed the end product to be quite labile unless stored under nitrogen. This is one advantage of the method reported here.

The coupling reaction to the primary amine of the APS coupling agent occurred readily for all the derivatives tested. The chloroformates appear to couple more readily but are less stable once immobilized than the cyanate derivatives. Because all slides were rinsed after the PEO coupling reaction identically, it cannot be concluded that this is due to more PEO physically adsorbed in the chloroformate case than in the cyanate terminated PEO.The difference in stability between the isocyanate and chloroformate derivatives could possibly be due to the relative stability of the resulting urethane linkage when bonded to APS with respect to the urea linkages formed by the isocyanate and isothiocyanate derivatives. As previously mentioned, the chloroformate derivatives show greater degree of coupling, but also greater variability with time. The urea linkage is presumably stabilized by resonance of the cation:

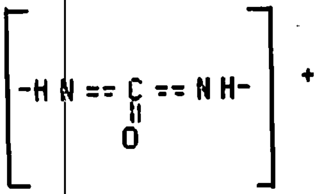

$$\left[-HN == \underset{\underset{O}{\|}}{C} == NH-\right]^{+}$$

When considering the stability of a polymer grafted to a surface and immersed into an aqueous salt medium, a large number of factors must be considered. It is well known that aliphatic ethers react with oxidizing agents such as oxygen to form hydroperoxides which can degrade, generally by chain scission. (29) This reaction may be catalyzed by certain metals such as ferrous, copper and silver ions. Bailey, Callard, and Lundberg, in an unpublished study found that aqueous solutions of PEO undergo a rapid decrease in viscosity at pH 4 if the solutions are contacted with an iron rod. (30) Solutions of PEO are also sensitve to light exposure. (31) Significant decreases in viscosity due to ultraviolet light can be attributed to a free radical degradation mechanism. (32) In our studies, although the initial coupling reaction was carried out under nitrogen, no rigorous precautions were taken to exclude air and room light during the PBS hydration. The slides were also handled using steel forceps which could have been a source of iron ions leading to chain degradation. Even so, the XPS data indicates a surface rich in PEO, particularly for the 6,000 isocyanate and isothiocyanate derivatives. The greater stability of these derivatives would be expected over the higher molecular weight derivatives since the higher polymers are more susceptible to degradation (33,34).

In our preliminary studies of protein adsorption onto PEO grafted surfaces, it was reported that the amount of protein adsorbed from pure solutions and from serum is inversely proportional to the PEO chain length. (22) This is consistent with the results of other investigators using PEO by itself or as the soft segment in a block copolymer system. (19, 35) The excluded volume argument comprises not only geometric exclusion by rigid molecules such as rods and spheres(20), but also includes unfavorable thermodynamic parameters such as free energy, summed over many segments. For random coil polymers such as is the case here, the entropy resulting from the ability of each molecule to claim extra "room" by flexing its segments must also be considered.

This argument also suggests that there should be an optimum concentration of PEO molecules on the surface to prevent the adsorption of proteins and the adhesion of cells and that this concentration can be exceeded (36). This was the reason for attempting to model the patchiness and thickness of PEO on the surface using variable angle XPS. It will be remembered that XPS scans only the top 50 to 70 Å of the surface. Given that, our data would suggest that the PEO grafted layers are less than this distance since the silicon from the underlying substrate may be detected. However, in the XPS spectrometer, the samples are under a high vacuum (10^{-9} torr), and are therefore severly condensed and collapsed against the substrate bearing little resemblance to the flexible chains tethered to the surface extending out in a cilliary manner in a good solvent. Even so, the presence of the silicon signal may suggest an uneven or non-uniform layer of PEO on the surface. The PEO data suggests eighty percent surface coverage with a layer 70 Å thick (Figure 14). Realizing that only 50% of the quartz surface contains free amines for the coupling of the PEO, this may at first appear contradictory. However, in the collapsed state, these PEO chains are likely to "fold" over the areas of exposed quartz. XPS is not capable of detecting such inhomogeneities but does indicate a non-uniform surface. According to the reasoning of Maroudas (36), this low density of PEO chains on the surface may actually increase its protein resistance by allowing greater flexibility of the long chains.

CONCLUSIONS

By derivatizing various molecular weight poly(ethylene oxide) chains, highyly reactive functional end groups may be formed which allow for straight forward coupling to free amines of an APS vapor-phase silanized surface. The reactions result in efficient transformation of the terminal hydroxyl groups to chloroformate, thiochloroformate, isocyanate or isothiocyanate groups depending upon the reagents used. The PEO-bis chloroformate and PEO-bis thiochloroformate, not unexpectedly, were more highly reactive, resulting in more efficient coupling to the surface.

It would be expected that any surface containing free amines would be capable of reacting with the functional end groups of the derivatized PEOs.

The PEOs were characterized with respect to the stability in an aqueous salt medium and found to be stable over the period tested. The PEO-bis chloroformate and PEO-bis thischloroformate were less stable over time presumably due to the relative instability of the urethane linkage over the urea linkage, which possesses additional stability due to the resonance of the adjacent double bonds. The thickness or degree of surface coverage was observed using variable angle XPS. However, due to the collapsed and highly condensed nature of the PEO chains under extreme vacuum, no difference was detected.

The method used here for the synthesis and coupling of long chain PEO onto quartz slides via an amino silane coupling agent produces a stable, polymer rich surface. This chemistry is suitable for PEO immobilization onto the surface of urethanes which could be used for numerous applications requiring mechanical strength not inherent to the PEO. The stability of these surfaces in physiological solutions remains to be tested. The possibility of Fe 2^+ catalyzed oxidation of the PEO chains should also be evaluated. This type of flexible, hydrophilic surface provides for a variety of potential applications. In the second part of this paper, we discuss the protein resisitance of this surface using whole blood and radio-labled proteins and the ability of this PEO-rich surface to minimize platelet adhesion and activation. We have extended this work in an attempt to use the PEO chain as a tether for the attachment of heparin for the purpose of creating a thromboresistant surface. The PEO spacer should allow hydrophilic bioactive molecules to extend from an interface and permit a native and active conformation for the immobilized pharmacologic agent. With further investigation, these surfaces may ultimately provide an optimal non-thrombogenic surface.

Acknowledgements

The authors would like to thank Mr. J-N Lin for the data of the APS stbility in the carbonate buffer system, and Mr. M. Helle and Mr. J. Warenski for their assistance and advice.

This work has been partially supported by the Office of Naval Research, and by NIH Training Grant number HL- 07520-02.

REFERENCES

1. T. Mori, S. Nagaoka, H. Takiuchi, T. Kikuchi, N. Noguchi, H. Tansawa, and Y. Noishiki, "A new antithrombogenic material with long poly(ethylene oxide) chains.", Trans. Am. Soc. Artif. Intern. Organs 28 459-463, (1982).
2. S. Nagaoka, Y. Mori, H. Takiuchi, K. Yokota, H. Tanzawa, S. Nishiuimi, "Interaction between blood components and hydrogels with poly(oxyethylene) chains.", Polymer Preprints 24 (1) 67-68, (1983).
3. T. Matsuda and T. Akutsu, "In vitro and in vivo assesment of blood/material interactions of hydrophobic and hydrophilic segmented polyurethanes.", Seattle ACS Meeting abstracts, March (1983).
4. C. W. Hiatt, A. Shelvkov, E.J. Rosenthal, and J.N. Galimore, "Treatment of Controlled Pore Glass with Poly(ethylene Oxide) to Prevent Adsorption of Rabies Virus", J. Chromatog. 58 (362) (1971).
5. J.N. George, Blood 40 863, (1972).
6. W. Wasiewski, M.J. Fasco, B.B. Martin, J.C. Detwiler, and J.W. Fenton, "Thrombin adsorption to surfaces and prevention with polyethylene glycol 6,000", Thromb. Res. Brief Commun. 8 881, (1976).
7. D.J. Lyman and B.H. Loo, J. Biomed. Mater. Res. 1 (17) (1967).
8. S.J. Whicher and J. L. Brash, J. Biomed. Mater. Res 12 (181) (1978).
9. J.L. Brash and S.J. Uniyal, "Platelet Foreign Surface Interactions: Release of Granule Constituents from Adherent Platelets", Polymer Sci. Polymer Symp. 66 377, (1979).
10. Y. Sa de Costa, D. Brier-Russel, G. Trudell III, and E. W. Merrill, "Degradation of Poly(ethylene Oxide)", J. Colloid Interf. Sci. 80 445, (1981).
11. R. I. Leininger, "Polymers as Surgical Implants", CRC Critical Rev. In Bioeng. 1 (3) 333-381, (1972).
12. S. Bluestone, J. E. March, and P.J. Flory, Macromole. 7 325 (1974).
13. M. Rosch, "*Zur Hydratbildung Von Polyglykolatherlosungern Amonder Zahigkeit*", *Kolloid Z.* 147 (78) (1956).
14. M. Rosch, *Felte. Sielen. Anstrichmittel*, 65 223, (1963).
15. H. Tadokoro, Y. Chatani, T. Yoshihara, S. Tahara, and S. Muirahashi, *Makromol. Chem.* 73 109, (1964).
16. W.H.T. Davison, J. Chem Soc. 3272, (1955).

17. K-J Liu, " Nuclear Magnetic Resonance Studies of Polymer Solutions. IV: Polyethylene Glycols", Macromol. 1(3) 213-217, (1968).

18. J. Maxfield, and I. W. Shepard, "Conformation of Poly(ethylene Oxide) in the Solid State, Melt and Solution Measured by Raman Scattering", Polymer 16(7) 505-509, (1975).

19. E.W. Merrill and E. W. Salzman, "Polyethylene oxide as a biomaterial.", ASAIO J. 6 60-64, (1983).

20. J. Hermans, "Excluded-volume theory of polymer-protein interactions based on polymer chain statistics." J. Chem.Phys. 77(4) 2193-2203, (1982).

21. D. Knoll, and J. Hermans, "Polymer-protein interactions: comparison of experiment and excluded volume theory.", J. Biol Chem. 258(9) 5710-5715, (1983).

22. D.E.Gregonis, D.E. Buerger, R.A.Van Wagenen, S.K.Hunter, and J.D.Andrade, "Poly(ethylene glycol) surfaces to minimize protein adsorption", Second World Congress on Biomaterials, abstracts, 266 (1984).

23. A. Silberberg, Hydrogels for Medical and Related Applications, ACS Symp. Series (J.D. Andrade ed.) 31 198-205, (1976).

24. J.D. Andrade, chapter 5 in Surface and Interfacial Aspects of Biomedical Polymers, vol I, Plenum Press, New York (1985).

25. K. Geckeler, "Functionalization of Soluble Polymers. 1. Replacement of the Hydroxyl Groups of Poly(oxyethylene) by Amino Groups", Polymers Bulletin, 1 427-431 (1979).

26. M. Mutter, "Soluble Polymers in Organic Cynthesis: 1. Preparation of Polymer Reagents Using Polysethylene Glycol with Terminal Amino Groups as Polymeric Components," Tetrahedron Lett., 2839-2842 (1978).

27. G. Broze, P.M Lefebure, R. Jerome, and P. Teyssie, "Some Easy Routes for the Specific Functionalization of Polymers by Pendant or End Amino Groups," Makromol. Chem. 178 3171-3174 (1977).

28. J.M. Harris, "Laboratory Synthesis of Polyethylene Glycol Derivatives," JMS Rev. Macromol. Chem Phys., c25 3 325-373) 1985).

29. F.E.Bailey, Jr. and J. V. Koleske, Non-ionic Surfactants, (M.J. Sckick, ed.) Dekker, (1966).

30. F.E. Bailey, Jr. and J.V.Koleske, Poly(ethylene oxide), Academic Press, (1976).

31. C.W. McGary, Jr., " Degradation of Poly(ethylene Oxide)", J. Polymer Sci. 46 51-57, (1960).

32. C. Walling, Free Radicals in Solution, Wiley, New York, (1957).

33. Y. Minoura, T. Kasuya, S. Kawamura, and A. Nakans, "Degradation of Poly(ethylene Oxide) by High Speed Stirring", J. Polymer Sci. A-2, 5 125, (1967).

34. A. Nakano and Y. Minoura, "Degradation of Polymers by High Speed Stirring", J. Appl. Polymer

Sci. 15, 927, (1971).

35. S. Nagaoka, Y. Mori, H. Takiuchi, K. Yokota. H. Tanzawa, and S. Nishiumi, ACS Symp. Series, in press.

36. N.G. Maroudas, "Polymer exclusion, cell adhesion and membrane fusion", Nature, 254 695-696, (1975).

FIGURE CAPTIONS

FIGURE 1: The four reactive derivatives of PEO.

FIGURE 2: The chemical reactions used to synthesize the four derivatives of PEO. I) The preparation scheme for PEO-di tosylate; II) Reaction of cysteamine with n-butyl lithium to form the lithium salt;the diamino PEO with phosgene and thiophosgene to form PEO bis-isocyanate and bis-isothiocyanate; III) Reaction of the PEO-di tosylate to form diamino PEO; IV) Reaction of PEO-diamine with phosgene to form PEO bis-isocyante; V) Reaction of hydroxyl PEO to form isocyante and isothiocyante using phosgene and thiophosgene.

FIGURE 3: The carbon 1s spectrum of a) pure poly(ethylene oxide); b) a quartz slide vapor-phase silanized with amino propyl triethoxy silane; and c) a silanized quartz slide to which PEO has been immobilized.

FIGURE 4: Nitrogen 1S spectrum of an APS-silica surface equilibrated in pH 7.4, (water rinse, ethanol rinse, air dry). The two peaks correspond approximately to $-NH_2$ and $-NH_3^+$ forms (32).

FIGURE 5: XPS elemental analysis of APS-silica after exposure to PBS (pH 7.4) for various times.

FIGURE 6: XPS elemental analysis of APS-silicon after exposure to a carbonate buffer (pH 9.0) for various times. (Data of J-N Lin Univ. of Utah 1985.)

FIGURE 7: The carbon / silicon ratio for the controls after soaking in PBS buffer for various times. Clean quartz soaked in PBS buffer; APS /quartz with underivatized PEO adsorbed, △) MW 18,000 and ◇MW 6,000.

FIGURE 8: The percent of the total carbon signal due to carbon bonded to an ether oxygen. ◆) Clean quartz soaked in PBS buffer; APS /quartz with underivatized PEO adsorbed, △ MW 18,000 and ◇MW 6,000.

FIGURE 9: The percent of the total carbon signal due to carbon bonded to an ether oxygen of the PEO MW 6,000 derivatives soaked in PBS buffer for various times. ◇) PEO-bischloroformate; ◆) PEO-bis thiochloroformate; □) PEO-bis isocyanate; □) PEO-bis isothiocyanate;.

FIGURE10: The carbon / silicon ratio for the PEO MW 6,000 derivatives after soaking in PBS buffer for various times. □) PEO-bischloroformate; □) PEO-bis thiochloroformate; ◇) PEO-bis isocyanate; ◆) PEO-bis isothiocyanate.

FIGURE 11: The percent of the total carbon signal due to carbon bonded to an ether oxygen of the PEO MW 18,000 derivatives soaked in PBS buffer for various times. ◇) PEO-bischloroformate; □) PEO-bis thiochloroformate; □) PEO-bis isocyanate; ◆) PEO-bis isothiocyanate.

FIGURE 12: The carbon / silicon ratio for the PEO MW 18,000 derivatives after soaking in PBS buffer for various times. ◆) PEO-bischloroformate; ◇) PEO-bis thiochloroformate; □) PEO-bis isocyanate; □) PEO-bis isothiocyanate.

FIGURE 13: The carbon 1s spectrum of PEO derivatized glass beads. The small peak at 284.2 ev is the hydrocarbon contamination of the indium foil on which the sample beads were run.

FIGURE 14: Log plot of the ratio of a 50 Å patchy overlayer of APS (I_B) to substrate intensity (I_A) as a function of angle according to the equation given (24). The mean free path of the substrate signal (λ_A) Si 2s is 35.1 Å; mean free path of the overlayer APS signal (λ_B) N 1s is 43.7 Å. The percent

areas covered (x 100) shown are 1.0, 0.75, 0.50, and 0.25. The variable angle data obtained from an actual silanized slide is shown by the *.

FIGURE 15: Log plot of the ratio of a 70 Å patchy overlayer of PEO (I_B) to substrate intensity (I_A) as a function of angle according to the equation shown in Figure 13, (24). The mean free path of the substrate signal (λ_A) Si 2s is 35.1 Å; mean free path of the overlayer PEO signal (λ_B) C 1s is 30.8 Å. The percent areas covered (x 100) shown are 1.0, 0.75, 0.50, and 0.25. The variable angle data obtained from an actual silanized slide coated with PEO is shown by the *.

Four Derivatives of Poly(ethylene Oxide)

1. PEO - BIS ISOCYANATE

   O=C=N - PEO - N=C=O

2. PEO - BIS ISOTHIOCYANATE

   S=C=N - PEO - N=C=S

3. PEO - BIS CHLOROFORMATE

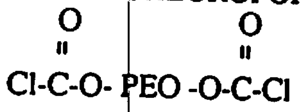

$\mathrm{Cl{-}\overset{\overset{O}{\|}}{C}{-}O{-}PEO{-}O{-}\overset{\overset{O}{\|}}{C}{-}Cl}$

4. PEO - BIS THIOCHLOROFORMATE

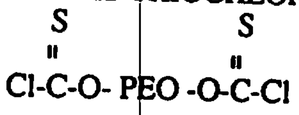

$\mathrm{Cl{-}\overset{\overset{S}{\|}}{C}{-}O{-}PEO{-}O{-}\overset{\overset{S}{\|}}{C}{-}Cl}$

fig 1

fig 2

I.

$H\text{-}(OCH_2CH_2)_n\text{-}OH + 2\ \text{n-butyl lithium} \text{ -------> } Li^+\ {}^-(OCH_2CH_2)_n\text{-}O^-\ Li^+ + CH_3CH_2CH_2CH_3 \uparrow$

$Li^+\ {}^-(OCH_2CH_2)_n\text{-}O^-\ Li^+ + CH_3C_6H_4SO_2Cl \text{ -------> }$

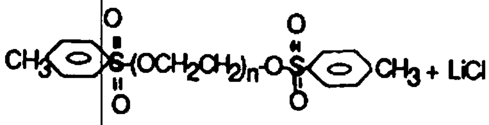

PEO di-tosylate

II.

$HSCH_2CH_2NH_2 + \text{n-butyl lithium} \text{ ---------> } Li^+\ {}^-SCH_2CH_2NH_2 + CH_3CH_2CH_2CH_3 \uparrow$

III.

$\text{PEO di-tosylate} + 2\ Li^+S^-CH_2CH_2NH_2 \text{ -----> } H_2NCH_2CH_2S\text{-}(OCH_2CH_2)_n\text{-}SCH_2CH_2NH_2 + 2\ TsOH$

PEOdi-amine

IV.

$\text{PEOdi-amine} + COCl_2 \text{ ----> } O{=}C{=}N\text{-}CH_2CH_2\text{-}S\text{-}(OCH_2CH_2)_n\text{-}S\ CH_2CH_2N{=}C{=}O + HCl$

PEO-bis isocyanate

$H_2NCH_2CH_2S\text{-}(OCH_2CH_2)_n\text{-}SCH_2CH_2NH_2 + CSCl_2 \text{ ------> }$

$S{=}C{=}N\text{-}CH_2CH_2\text{-}S\text{-}(OCH_2CH_2)_n\text{-}S\ CH_2CH_2N{=}C{=}S + HCl$

PEO-bis isothiocyanate

V.

$H\text{-}(OCH_2CH_2)_n\text{-}OH + COCl_2 \text{ ----> }$

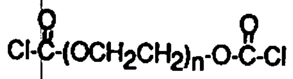

$Cl\text{-}\overset{O}{\overset{\|}{C}}\text{-}(OCH_2CH_2)_n\text{-}O\text{-}\overset{O}{\overset{\|}{C}}\text{-}Cl$

$H\text{-}(OCH_2CH_2)_n\text{-}OH + CSCl_2 \text{ ----> }$

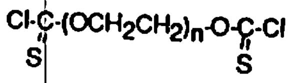

$Cl\text{-}\underset{S}{\underset{\|}{C}}\text{-}(OCH_2CH_2)_n\text{-}O\text{-}\underset{S}{\underset{\|}{C}}\text{-}Cl$

1.53

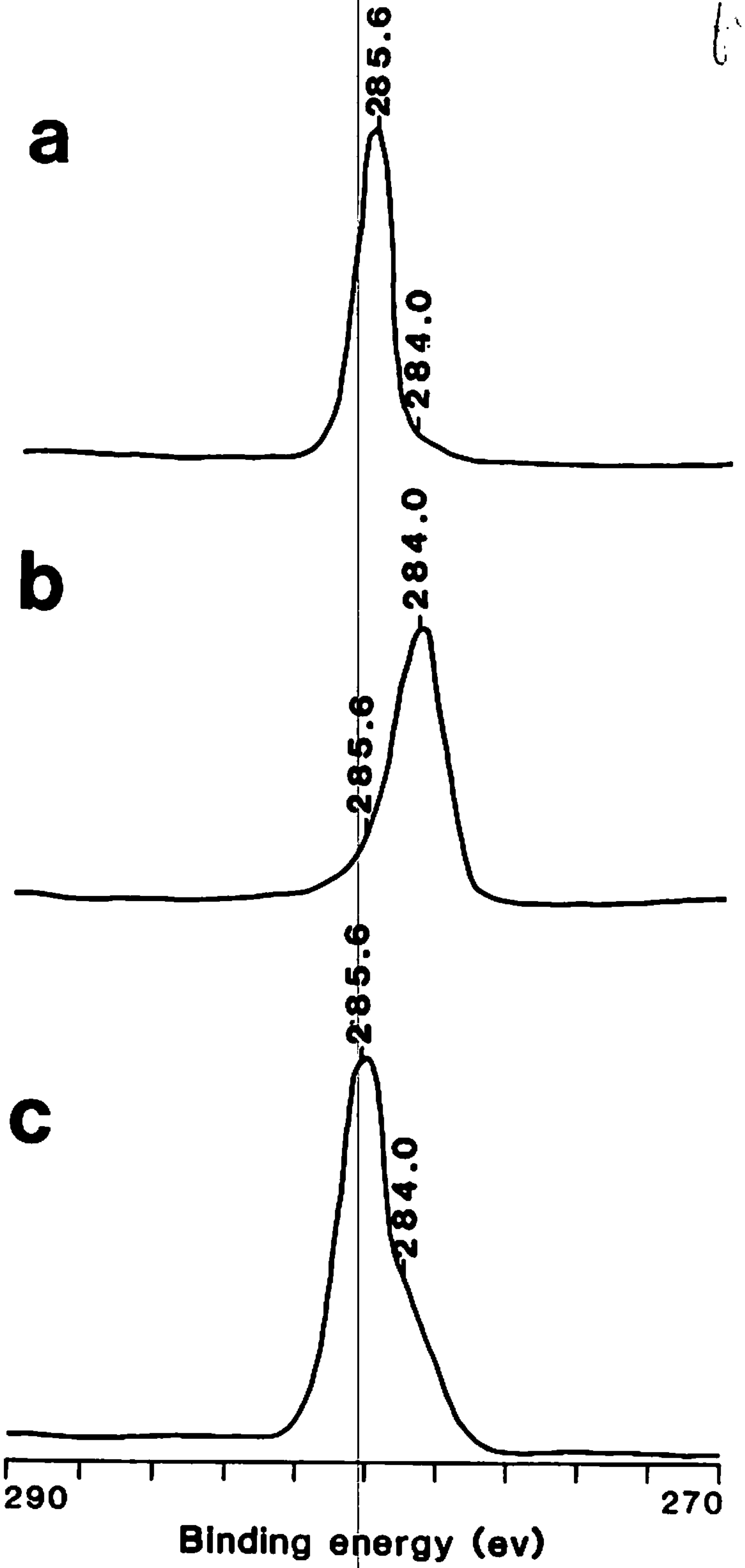

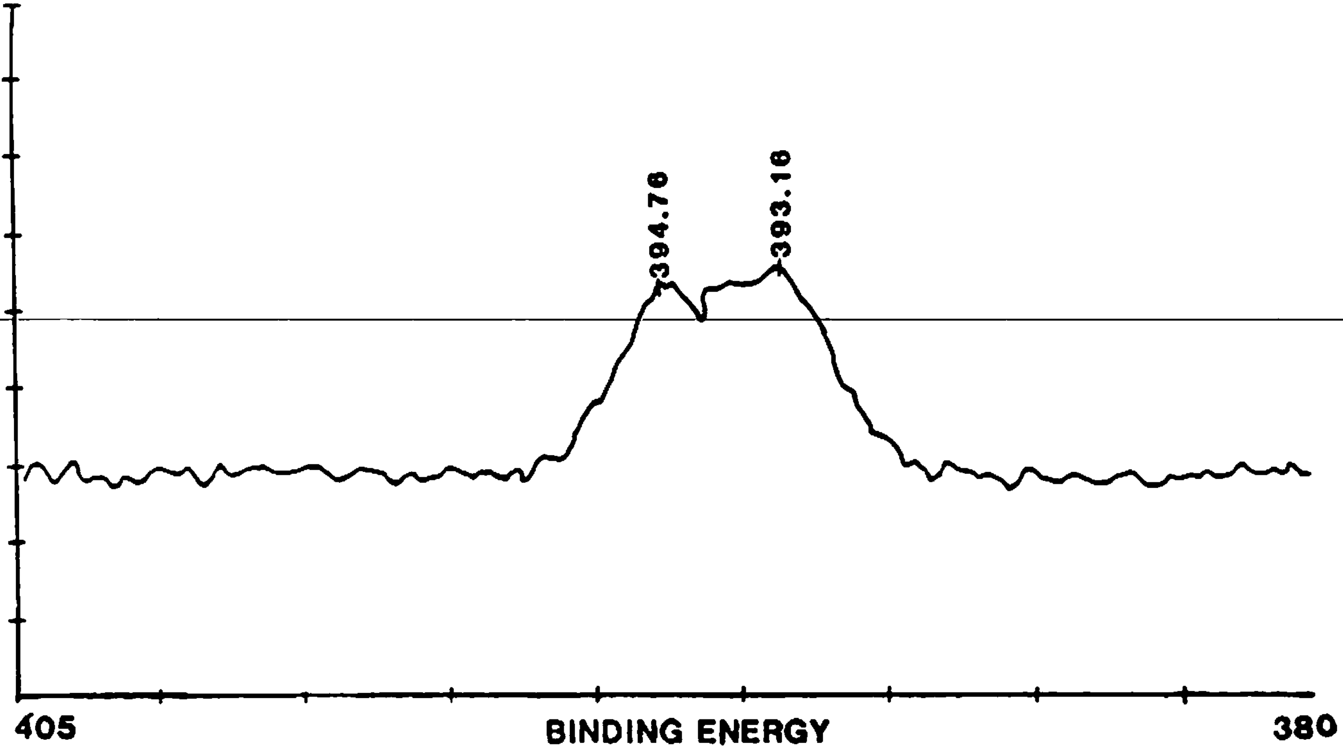

Fig 4

fig 5

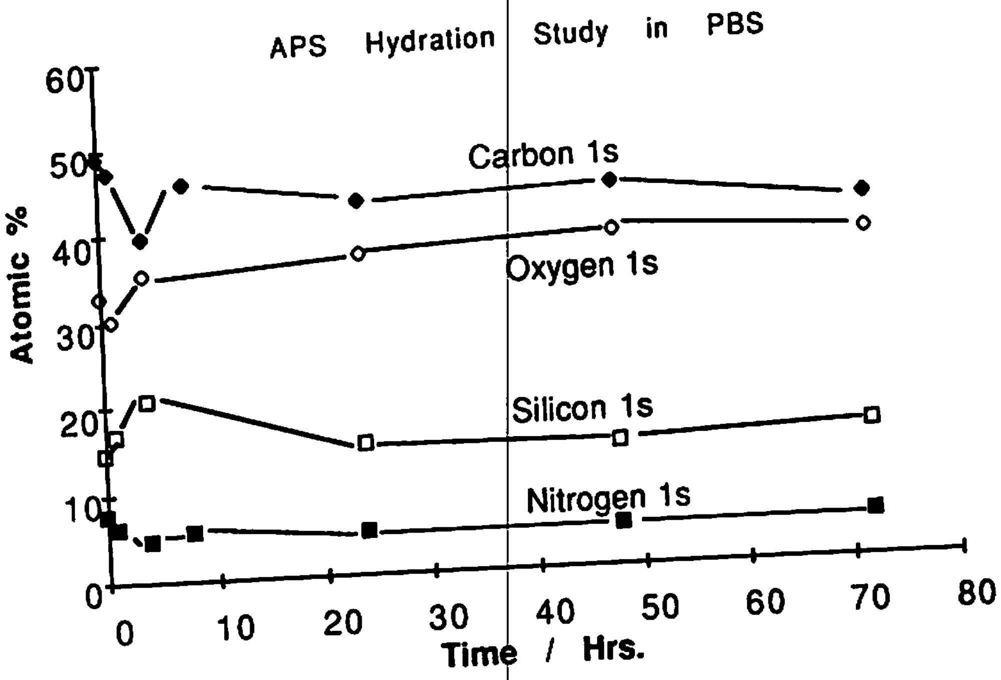
APS Hydration Study in PBS
Atomic %
60
50
40
30
20
10
0
Carbon 1s
Oxygen 1s
Silicon 1s
Nitrogen 1s
0
10
20
30
40
50
60
70
80
Time / Hrs.

fig 6

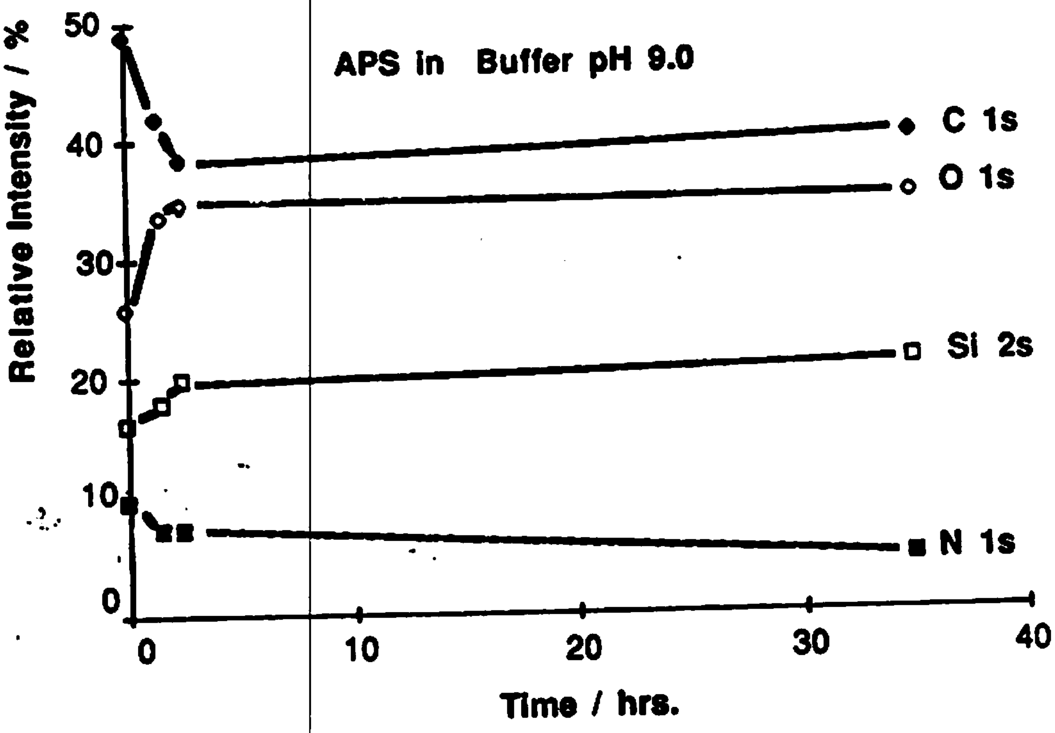
APS in Buffer pH 9.0
Relative Intensity / %
50
40
30
20
10
0
0
10
20
30
40
Time / hrs.
C 1s
O 1s
Si 2s
N 1s

Fig 57

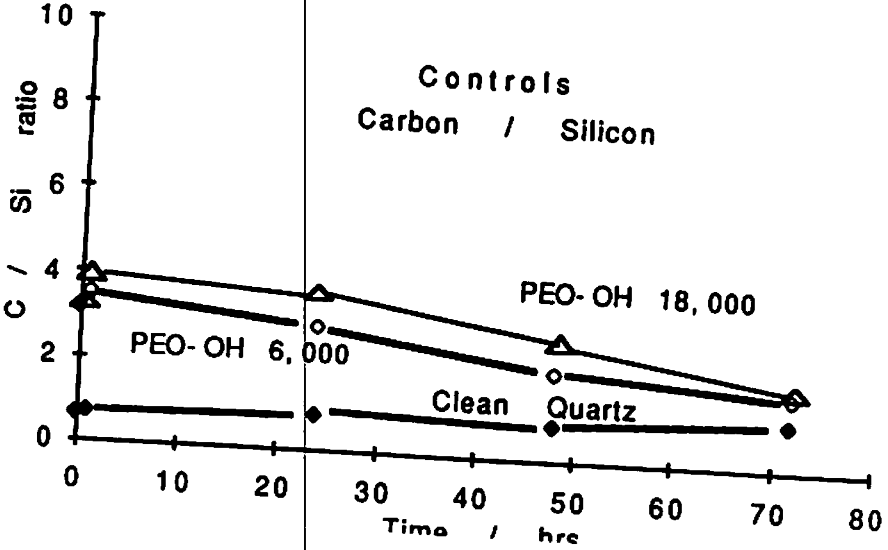
Controls
Carbon / Silicon
C / Si ratio
0
2
4
6
8
10
0
10
20
30
40
50
60
70
80
Time / hrs
PEO- OH 18, 000
PEO- OH 6, 000
Clean Quartz

6.38

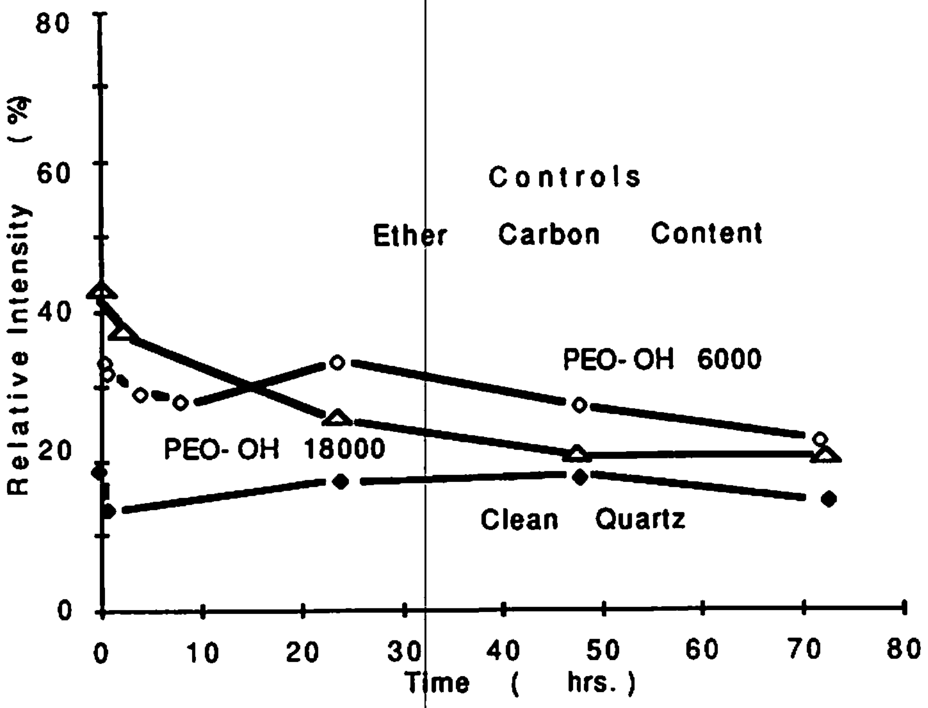
Controls
Ether Carbon Content
Relative Intensity (%)
80
60
40
20
0
0
10
20
30
40
50
60
70
80
Time (hrs.)
PEO-OH 6000
PEO-OH 18000
Clean Quartz

f. 7.4

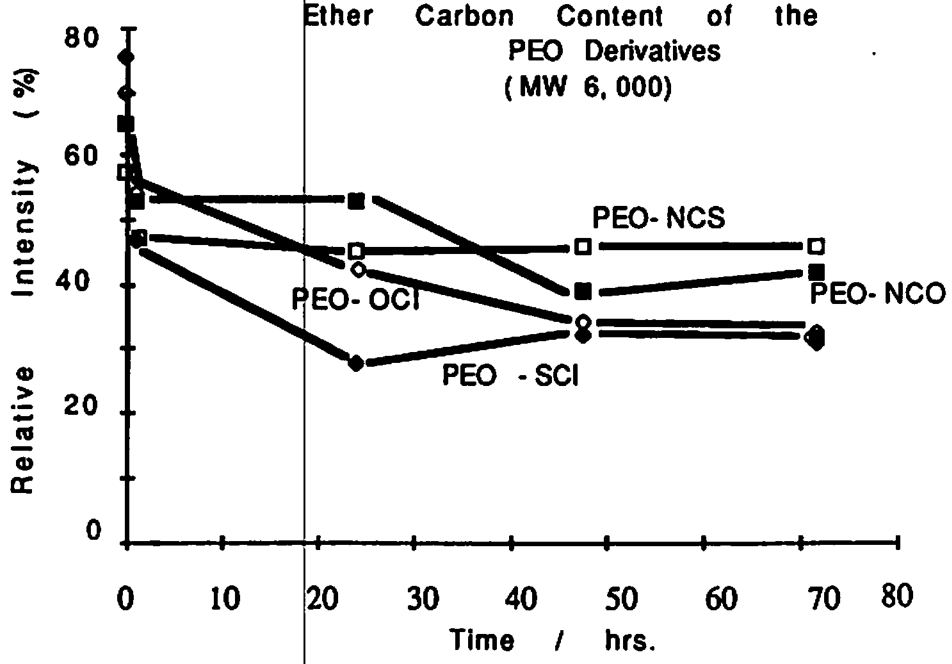
Ether Carbon Content of the PEO Derivatives (MW 6, 000)

Fig 10

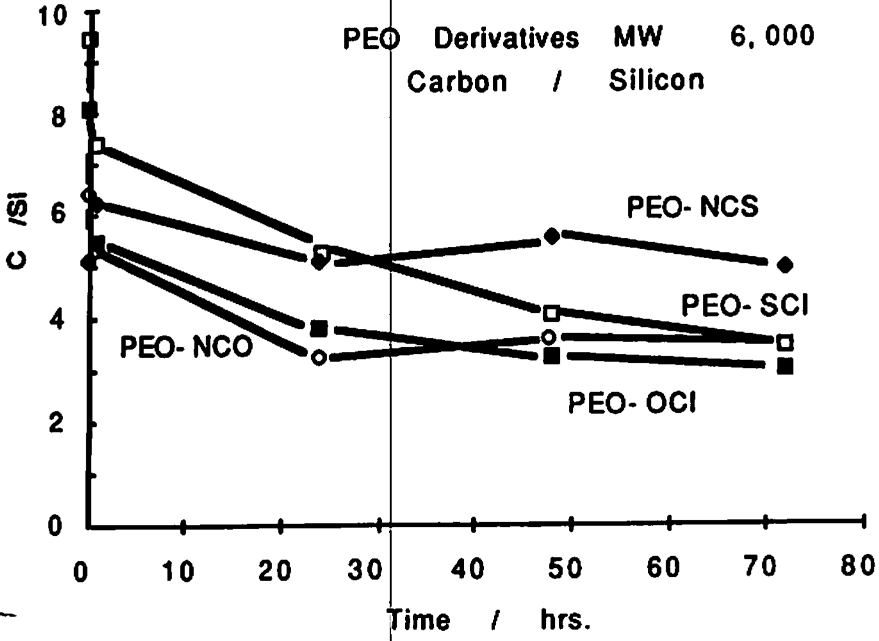
PEO Derivatives MW 6, 000
Carbon / Silicon
C /Si
Time / hrs.
PEO- NCS
PEO- SCl
PEO- NCO
PEO- OCl
0
2
4
6
8
10
0
10
20
30
40
50
60
70
80

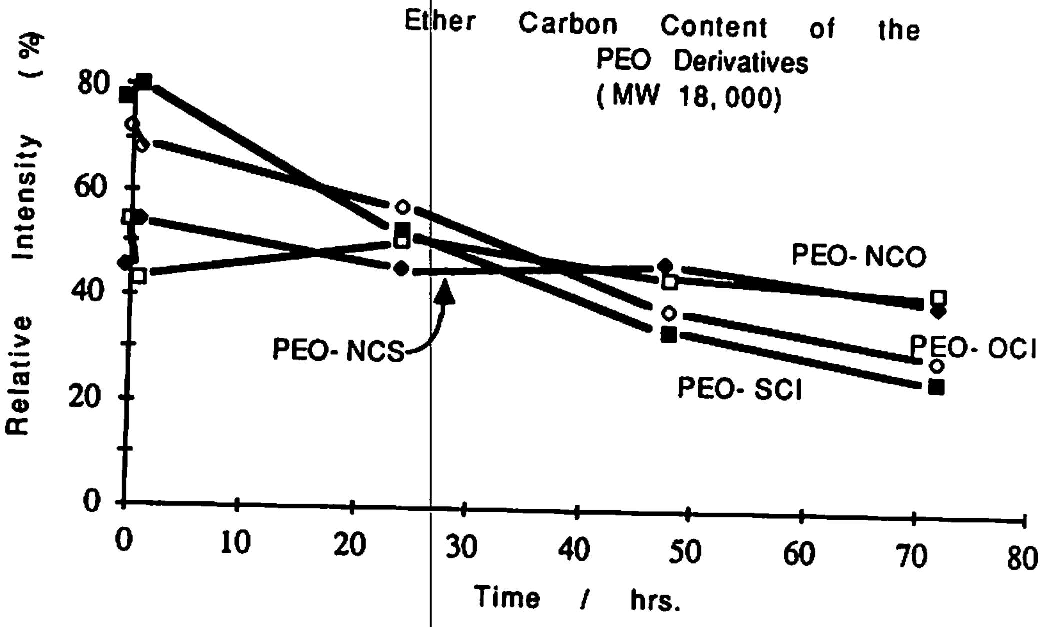
Ether Carbon Content of the
PEO Derivatives
(MW 18, 000)
Relative Intensity (%)
0
20
40
60
80
0
10
20
30
40
50
60
70
80
Time / hrs.
PEO- NCO
PEO- NCS
PEO- OCl
PEO- SCl

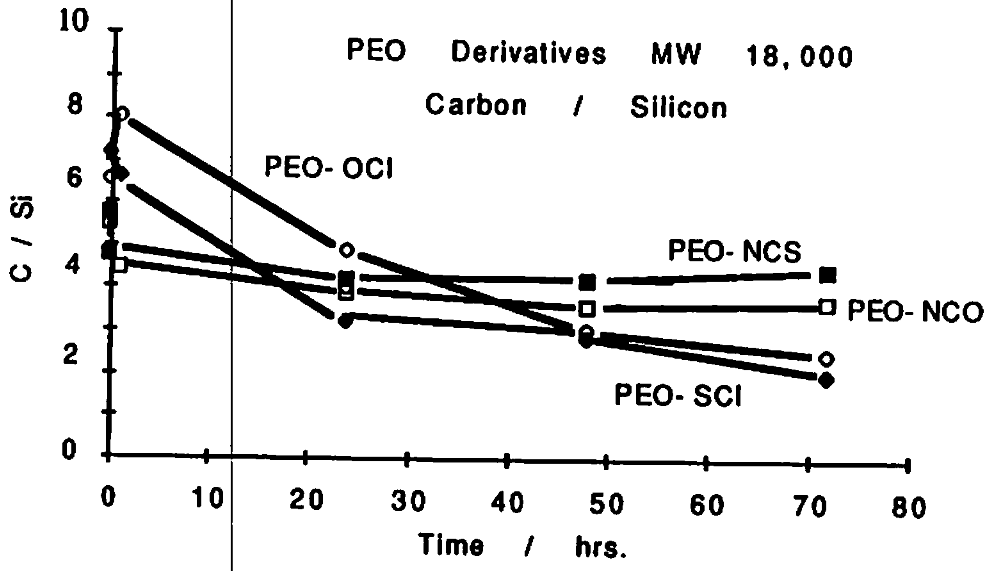
PEO Derivatives MW 18,000
Carbon / Silicon
PEO- OCl
PEO- NCS
PEO- NCO
PEO- SCl
C / Si
0
2
4
6
8
10
0
10
20
30
40
50
60
70
80
Time / hrs.

Table 1

Table

Elemental Analysis of PEO Stability on Glass Beads

Time	C	O	N	Si
1	51	36	2	11
8	47	37	2	14
24	43	37	2	15
48	42	36	2	14
72	42	38	2	15

Fig 5B

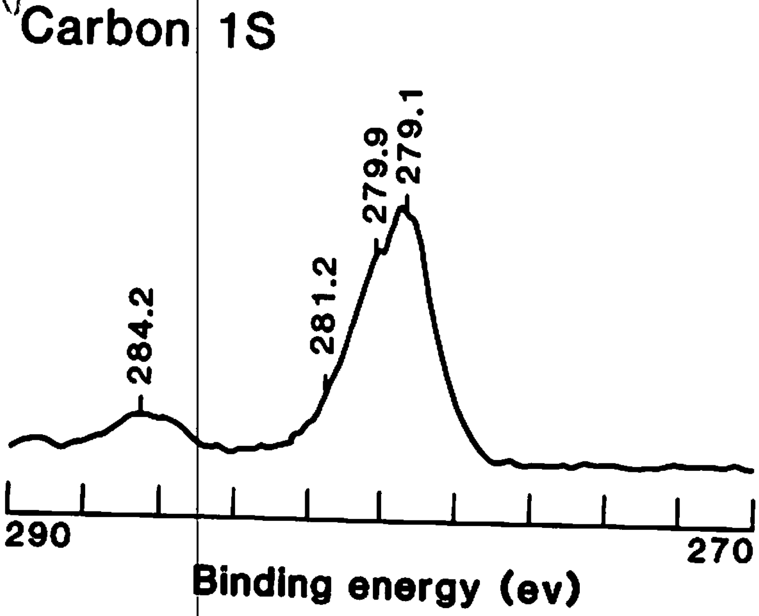

derivatized glass beads. The small
foil on which the

6.5.1

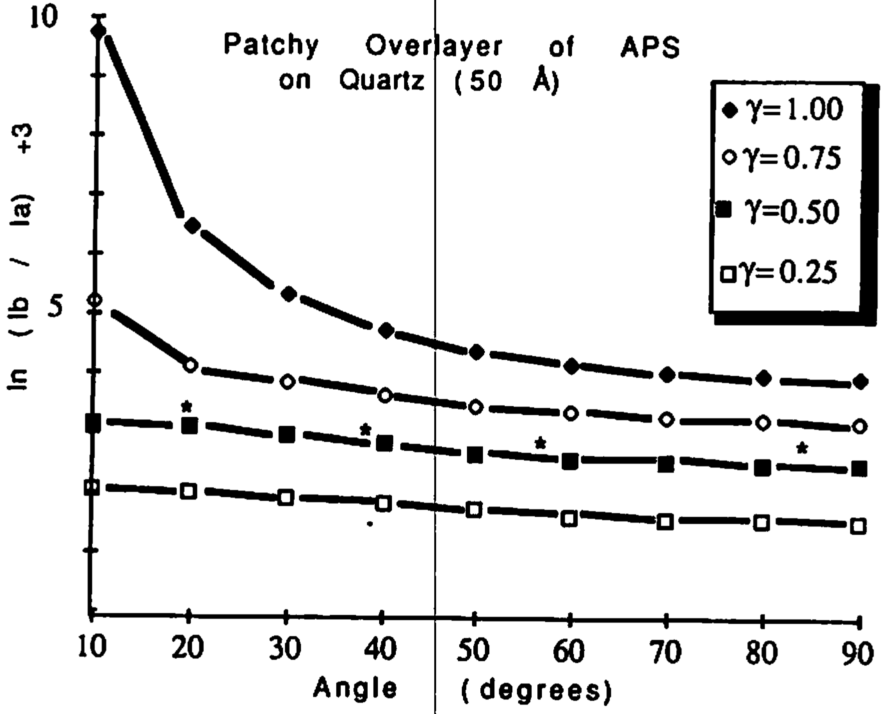
Patchy Overlayer of APS
on Quartz (50 Å)
◆ γ=1.00
○ γ=0.75
■ γ=0.50
□ γ=0.25
ln (Ib / Ia) +3
10
5
10
20
30
40
50
60
70
80
90
Angle (degrees)
*
*
*
*

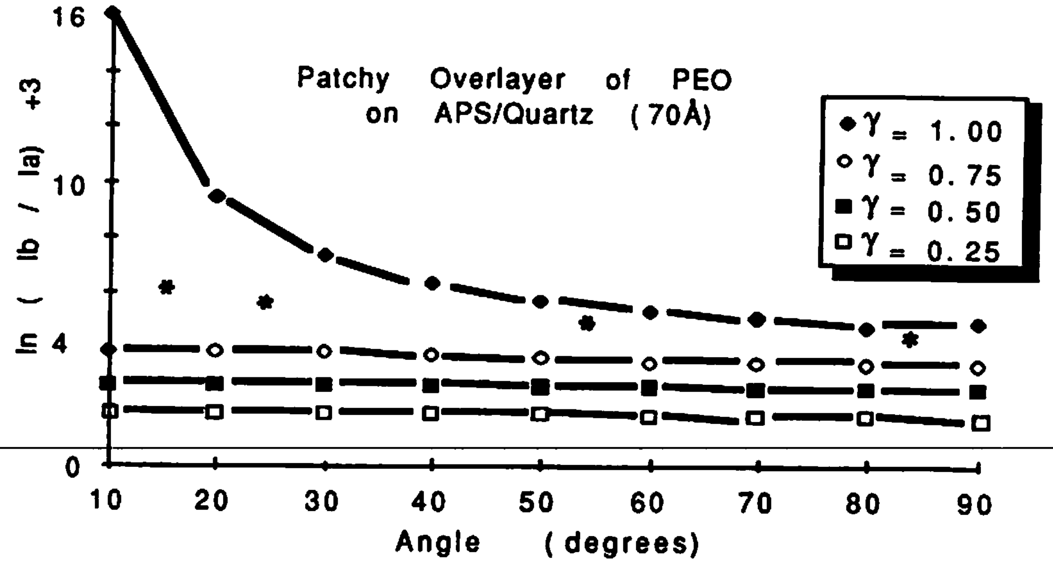
Patchy Overlayer of PEO
on APS/Quartz (70Å)
● γ = 1.00
○ γ = 0.75
■ γ = 0.50
□ γ = 0.25
ln (Ib / Ia) +3
16
10
4
0
10
20
30
40
50
60
70
80
90
Angle (degrees)

fig 15

Heparin Interaction with Protein-Adsorbed Surfaces[1]

LYNN C. WINTERTON,*[,2] JOSEPH D. ANDRADE,* JAN FEIJEN,‡
AND SUNG WAN KIM†[,3]

*Department of Materials Science and Engineering, †Department of Pharmaceutics, University of Utah,
Salt Lake City, Utah 84112; and ‡Department of Chemical Technology, Twente
University of Technology, 7500AE Enschede, The Netherlands

Received October 9, 1985; accepted February 6, 1986

Albumin and fibrinogen show no binding affinity to varied molecular weights of heparin at physiological pH. Human plasma fibronectin was shown to bind heparins in both the solution and adsorbed states. Fibronectin was shown to have six active binding sites for heparins which may be sterically blocked in some adsorbed states. ^{125}I-Fibronectin monolayer concentrations were shown to be significantly different on polyvinyl chloride surfaces when compared to hydrophilic/hydrophobic silica, Biomer, Silastic, and polystyrene surfaces. Preadsorbing fibronectin to various substrates and then allowing heparins to interact with the protein monolayer made it possible to bind up to 0.2 μg/cm^2 heparin in a plasma environment. This fibronectin–heparin complex was at least 85% stable in plasma and buffer solutions for up to 8 h time. The complex was observed to prolong blood clotting times two to three times over that of controls as assayed by Activated Partial Thromboplastin Times. All of the bound heparin was observed to be active by its ability to bind Factor X_a in plasma. Monolayers of blood proteins adsorbed from human serum were not observed to be active in binding heparins. The fibronectin–heparin conjugate showed low activation of blood components compared to protein monolayers preadsorbed from human sera as assayed by Activated Partial Thromboplastin Time. © 1986 Academic Press, Inc.

INTRODUCTION

Great advances have been made during the past decade toward the concept of rendering biomaterials nonthrombogenic (1, 2). It has been proposed that relationships exist between the blood compatibility of foreign substrates and substrate characteristics, such as surface charge, hydrophilicity, surface-free energy, and surface protein interactions (3). Probably the most important unresolved problem with blood-contacting devices is that these devices are not as biologically compatible (inactive) with blood as blood is with the endothelial lining of the vessels. When blood contacts medical devices or foreign surfaces, surface activation of the blood components occurs. Uninterrupted, thrombosis will follow.

Several areas of intense research exist as to how to most effectively render a blood-containing surface nonthrombogenic. These include blood compatibility via: (a) mutually compatible moduli of the implant (medical device) and the surrounding tissue so as not to traumatize the blood (4); (b) controlling the concentration and species of the adsorbed proteinaceous monolayer; (c) stopping platelet adhesion, retention, and/or degranulation following adhesion; and (d) stopping fibrin formation or destroying the crosslinked fibrin clot superstructure. Researchers using the approaches of (b) or (c) have shown that albuminated surfaces or surfaces with an abundance of albumin preferentially adsorbed to them tend to be less thrombogenic than those with a relative abundance of absorbed fibrinogen or gamma-globulin (γ-globulin) (3, 5–7). In these studies, platelet adherence to adsorbed albumin and other adsorbed nonglycoproteins did not occur, due possibly to a lack of carbohydrate moieties, which are plentiful in fibrinogen and γ-globulins (8). Platelet adhesion and the resultant morphological changes seem to be determined both by the composition and the conformation of the initially adsorbed protein monolayer (9). The preferential adsorption of albumin, or maintenance of a preadsorbed albumin monolayer requires that implanted surfaces be passive to most proteins yet "recognize" albumin and bind to it (10). This usually requires surface modification since most surfaces do not preferentially adsorb albumin (11–15).

Methodology (a) above is unique in that it ignores most of the surface effects associated with blood-containing devices and instead focuses upon the bulk properties of the substrate to inhibit surface-induced thrombosis. The hypothesis is that moduli differences are what the body responds to in the activation of the intrinsic coagulation pathway. This methodology, like (b), requires new or modified materials to obtain the required bulk and surface characteristics.

The methodologies listed in (c) and (d) are accomplished by inhibiting platelet adhesion and aggregation and fibrin formation via pharmaceutical approaches. Using platelet and coagulation inhibitors, in conjunction with the medical devices, it is possible to improve blood compatibility by blocking the inherent mechanisms that are the driving force for these normal physiological functions. However, systemic usage of these inhibitors at physiologically necessary concentrations could prove fatal; i.e., vascular hemorrhage would remain unchecked by both coagulation or platelet adhesion. Recognition of this problem has resulted in several unique and innovative approaches for local delivery of small doses of either platelet inhibitors, coagulation inhibitors, or both, in concentrations too low to have bulk effect (16). The most prevalent drug being currently delivered in this fashion is heparin. However, prostaglandins and urokinase (17) have also been utilized successfully for their antiplatelet and fibrinolytic activities, respectively.

A novel approach by Henninck *et al.* (18) to evaluate both antiplatelet activity and anticoagulation has been made utilizing the natural driving force of protein adsorption to decrease surface-free energy. Heparin is delivered onto a medical device using the protein which itself reduces platelet adhesion (7, 19–21). In this methodology, heparin is covalently bound to albumin and preadsorbed to implantable polymers. The albumin coverage inhibits platelet adhesion and retention on the substrate surface while the immobilized heparin inactivates the coagulation cascade on a localized level.

Using this last approach as a type model, it may be possible to improve upon it by preadsorbing blood proteins, that have a natural affinity to heparin, onto medical grade materials. Heparin is then bound to the adsorbed protein monolayer in sufficient quantity to cause a localized inhibition of the coagulation cascade and a resultant depressed platelet response. The advantages of this technique are several fold: (i) there is no compromising of the heparin or protein structure by covalently altering either one; (ii) there is no compromising of the substrate surface or extended chemistries to covalently link the heparin or protein to the surface of interest; (iii) the adoption of a "naturally" occurring physiological phenomenon; (iv) no toxicological side effects from extraneous chemical reactions; (v) no chemical modification of the surface of interest—this allows for choices of materials with desirable mechanical properties without worrying about needed preferential adsorption of specific proteins; and (vi) ease of preparation. In case (iii) the naturally occurring adsorption of serum proteins is used to reduce the surface energy of a blood-contacting medical device followed by affinity binding of heparin to the protein. This process (iii) and resultant protein–heparin ligand may not be physiologically viewed as

---

[1] Presented at the 5th International Conference on Surface and Colloid Science, Clarkson University, Potsdam, N.Y., June 24–26, 1985, as part of a symposium entitled Protein and Polyelectrolyte Adsorption.

[2] Current address: Ciba-Geigy Corporation, 2910 Amwiler Court, Atlanta, Georgia 30360.

[3] To whom all correspondence should be addressed.

0021-9797/86 $3.00
Copyright © 1986 by Academic Press, Inc.
All rights of reproduction in any form reserved.

an antigen thereby having antibodies produced against it.

MATERIALS AND METHODS

Biomer (Ethicon Inc., Somerville, N.J.) was received as a 30% by weight (w/v) solution in *N,N*-dimethylacetamide (DMAC). The solution was diluted to a 15% (w/v) solution in DMAC (Baker Chemical, Phillipsburg, N.J.) and precipitated in distilled water. The polymer precipitate was thoroughly washed, dried, and vacuum-dessicated for 12 h at room temperature. The dried polymer precipitate was stored in the dark, at room temperature, in a dry glass container. This polymer precipitate was the stock of Biomer for the entire study.

Polyvinyl chloride (Bentley Laboratory Inc., Irvine, Calif.) was supplied in the form of "Implant-Tested" cardiovascular bypass tubing. Upon receipt, the tubing was stripped of all inked impressions by cutting those sections out and discarding them. The remainder was cut into small pieces and stored in the dark in a dry glass container at room temperature.

Polystyrene (Corning Glass, Corning, N.Y.) was supplied as sterile culture dishes or as 1.00-mm spherical beads (Sinclair-Koppers Co.). Polystyrene (PS) was chosen as a reference material due to its chemical similarity to pure PVC and since it is available in relatively large pure quantities. The PS beads were used as received, whereas the culture dishes were granularized and stored in the dark in dry glass containers at room temperature.

Polydimethylsiloxane (PDMSO) was supplied as nonreinforced medical grade subdermal implant Silastic sheeting or as Medical Adhesive 891 (both from Dow Corning Corp., Midland, Mich.). PDMSO was chosen because of its current usage in the biomedical field as a common subdermal implant material. PDMSO, of which Silastic is a type, is also a reference material of the National Heart, Lung and Blood Institute (22).

Fused amorphous silica microscope slides and glass beads, 1.00 to 1.05 mm diameter (B. Braun Melsunger, Apperatebau), were utilized as reference hydrophilic substrates. The chemical composition of these glass beads has been determined elsewhere (23). The chemical composition of the fused amorphous silica was considered to be 100% SiO_2 and was verified via X-ray photoelectron spectroscopy.

Serum albumin (human, Fraction V) was obtained from Sigma Chemicals, St. Louis, Mo. (A-2376). The albumin was stored dessicated at 0°C. No further purification or chemical alteration was made to the albumin.

Fibrinogen (bovine, 95% clottable) was obtained from Miles Laboratories, Elkhart, Indiana (Pentex R, Lot 28) and stored dessicated at −20°C. No further purification or chemical alteration was attempted.

Human plasma fibronectin was supplied frozen (−80°C) in Tris buffer (pH 7.4) in 1-ml aliquots as a generous gift from Dr. Deane F. Mosher (Department of Hematology, University of Wisconsin). The fibronectin was stored at −80°C until used.

Sodium heparin derived from porcine intestinal mucosa was obtained from Diosynth Inc., Chicago, Ill. The heparin was stored dessicated and refrigerated. The company assay listed the heparin to have an activity of 165 units per milligram (USP) or 171.3 units per milligram as received.

Solutions [10% (w/v)] of Biomer and polyvinyl chloride were prepared by stirring resins in *N,N*-dimethylacetamide (spectral grade) for 12 to 24 h. The polymer solutions were filtered (0.22 μm) to remove particulates. The filtered solutions were cast against cleaned glass plates. These cast solutions were then heated to 50°C in a vacuum oven, at atmospheric pressure, for 24 h to drive off the solvent. The films were then stripped from the plates and replaced in the heated vacuum oven (50°C, 20 μm Hg Torr) for 24 h to remove all residual solvents.

A 10% (w/v) solution of polystyrene (PS) was made by stirring PS granules in dichloromethane (spectral grade) for 1 to 2 h. The PS solution was then filtered (0.22 μm) and cast against clean glass plates. The cast solution was placed in a laminar flow hood for 24 h at room temperature to allow the solvent to evaporate. The resultant rigid films were then removed from the plate support and placed under heated vacuum (50°C, 20 μm Hg Torr) for 24 h to remove any residual solvent.

The substrate surfaces were cleaned following a protocol described elsewhere (24, 61, 62). The procedure was utilized to remove surface contaminants in the micron range and larger prior to experimental use. All materials were handled with gloved hands or with metal forceps and cleaning was done in a clean room free from micron-sized particles.

Polystyrene beads, 1.00 mm diameter, were cleaned by the methodology of Coleman *et al.* (23). Polystyrene beads were placed in an extraction thimble (fat-extracted cellulose, Whatman) and refluxed in a Soxhlet extractor with petroleum ether (reagent) for 24 h followed by drying under heated vacuum (50°C, 20 μm Hg Torr) for at least 24 h.

Cleaned fused amorphous silica slides were treated for 5 min in oxygen plasma produced by a Plasmod (Tegal Corp., Richmond, Calif.) according to the methodology of King *et al.* (24, 61). Slides prepared in this fashion were immediately used and were never stored for longer than eight hours in glass containers that had been cleaned in a similar fashion.

In order to produce a more hydrophobic surface, previously cleaned and radiofrequency glow-discharged silica slides were vapor-silanized according to the methodology of Haller (25) using *N*-propyltriethoxysilane. This silanization procedure covalently links the silane groups to the surface of the silica slides, masking the hydrophilic silica surface. The resultant silica has *N*-propyltriethoxysilane covalently attached to the surface (NPS-silica).

Disposable polypropylene columns (0.8 × 20.5 cm, Kontex, Vineland, N.J.) were cut to 2-cm lengths and packed with either cleaned glass beads (1.00 to 1.05 mm diameter) or cleaned polystyrene beads (1.00 mm diameter). The glass bead columns were then subjected to polymer solution treatments to coat the beads with the desired polymer after a modification of the methodology of Brier-Russell *et al.* (26), described below.

Solutions [1% (w/v)] of Biomer in spectral grade *N,N*-dimethylacetamide, polyvinyl chloride in *N,N*-dimethylacetamide (spectral grade), polystyrene in dichloromethane (spectral grade), and Silastic adhesive (uncured) in toluene (spectral grade) were prepared and stored in sealed glass containers in a dark environment. These stock solutions were filtered (0.22 μm) just prior to use. Using cleaned glass syringes, the solutions were injected slowly upward into the packed columns. The columns were continuously tapped to prevent or dislodge trapped air pockets. When the reservoir had approximately 5 ml of polymer solution, the solution was allowed to flow back down through the column, under gravity. The last remaining drops were then "wicked" from the bottom, via capillary action, with a clean dry cloth. Columns were stored covered at room temperature for 24 h to allow the solvent to evaporate. The columns were then placed under heated vacuum (50°C, 20 μm Hg Torr) for 24 h to remove all residual solvents. This solution injection/draining procedure was repeated five times to insure complete polymeric coverage of the glass beads.

Random columns were selected for observation and characterization by scanning electron microscopy and X-ray photoelectron spectroscopy. The columns were assumed to have a packing efficiency of 0.74 (a close-packed system) and thus a void volume of approximately 0.8 ml. The volume of the columns was 1.0 cm^3 and, assuming only point contact between spheres, yielded an effective surface area of 50 cm^2 (27).

All substrate materials were characterized according to a modified version of the suggested Level II characterization of surfaces by the National Heart, Lung and Blood Institute (22). The materials were subjected to light microscopy, scanning electron microscopy, surface energetics characterization (Wilhelmy plate contact angle), and X-ray photoelectron spectroscopy (28, 29).

The commercially available sodium salt of heparin was fractionated by gel permeation chromatography.

Samples of low-molecular-weight (LMW), high-molecular-weight (HMW), and commercial sodium heparin were then characterized by an independent laboratory. The molecular weight was determined by high-performance (pressure) liquid chromatography (HPLC) using dextrans of various molecular weight as standards, according to the methodology of Hurst *et al.* (30).

The free amine groups on heparin were reductively methylated using a modification of an earlier protocol (31) patterned after Jentoff and Dearborn (32). The radiolabeled heparin was then lyophilized and stored at $-10°C$ until used. Unless otherwise stated, all labeling procedures had an effective degree of labeling of approximately 0.8 labels per molecule.

Proteins of interest were iodinated using immobilized lactoperoxidase-glucose oxidase with labeled sodium iodide. From 0.25 to 1.00 g of protein was dissolved in 0.375 ml PBS, pH 7.4. A suspension of immobilized lactoperoxidase and immobilized glucose oxidase (Enzymobeads, Bio-Rad, Richmond, Calif.) in 0.25 ml distilled water (rehydrated 24 h prior to use) was added to the protein solution. Then, 1.0 mCi $Na^{125}I$ (New England Nuclear, Boston, Mass.) was added (specific activity 17.4 Ci/mg and concentration 100 mCi/ml) to this reaction mixture. Finally, 0.125 ml, of a freshly prepared solution of 1% (w/v) β-D(+) glucose (Sigma) in water was added to the reaction solution. The solution was capped and allowed to stand unagitated for 30–35 min. The reaction was stopped by passing the reacants through two previously characterized Sephadex G-25 columns. The labeled protein eluted entirely in the void volume while the Enzymobeads did not elute at all. The remaining reactants and unwanted by-products eluted in the last portion of the total volume. The protein concentration was determined by UV spectroscopy (Perkin–Elmer Lamda 7 UV-Vis spectrophotometer). All radiolabeled proteins were freshly prepared and were discarded after 24 h. All iodinations had a degree of labeling of approximately 0.5 labels per molecule.

In order to insure that the iodination procedure did not denature the proteins, all radioiodinated proteins were characterized by ultraviolet spectroscopy, fluorescence spectroscopy and polyacrylamide gel electrophoresis. The stability of the iodinated species, with respect to the substituted iodine, was determined and any quenching effects of the iodine label on the fluorescence emission and UV absorbance was noted.

Two systems of equilibrium dialysis were utilized to detect heparin binding to proteins in solution. The first was a system wherein dialysis tubing (Spectrapor 6, Spectrum Medical Industries, molecular weight cutoff 25,000) was used to house both the protein and heparin, and the second was a system where the same dialysis tubing was cut into sheet form and clamped between two identical chambers. The advantage of the second method, when compared to the first, is that it was easier to insure that leakage into the buffer reservoir did not occur. The first system utilized a 2-ml reservoir and a 6-ml buffer surround. The second system consisted of two identical chambers of 5 ml volume each separated by dialysis sheeting.

The systems were characterized (33) in separate control experiments by placing tritium-labeled heparins (LMW, HMW, and commercial sodium heparin) with phosphate-buffered saline (PBS), pH 7.4 (2 mM KH_2PO_4, 8 mM Na_2HPO_4, and 145 mM NaCl), in the reservoirs and allowing them to diffuse until equilibrium was reached.

Protein binding to heparin was determined for all three heparins by adding the proteins and ^{3}H-heparin in the same reservoir (33) so that the final concentration of protein was 1.5×10^{-6} M. The final ^{3}H-heparin concentration was 50, 25, and 10 μg/ml, in separate experiments. The buffer was mildly stirred (system 1) or the entire system was rotated gently (system 2) on a laboratory rotator for 24 h, at which time the samples were taken. The extent of binding and binding kinetics were determined by comparing the amount of ^{3}H-heparin on the reservoir side versus the unbound ^{3}H-heparin concentration diffused to the buffer side. The amount of bound ^{3}H-heparin to protein (C_B^{Hep}) is determined by

$$C_B^{Hep} = C_{Res}^{Hep} - C_{Buffer}^{Hep} \qquad [1]$$

where

C_{Res}^{Hep} = Concentration of ^{3}H-heparin remaining in the reservoir
= Concentration bound ^{3}H-heparin + Concentration free ^{3}H-heparin in solution
C_{Buffer}^{Hep} = Concentration of unbound ^{3}H-heparin diffused to the buffer side
= Free heparin concentration

TABLE I

Contact Angle Results Using Wilhelmy Plate (Mean ± SD)

Material	$\theta_{Advancing}$	$\theta_{Receding}$
Amorphous silica[a] (n = 12)	0°	0°
Amorphous silica[a] (Hydrated[b]; n = 4)	0°	0°
Cleaned glass (n = 6)	3 ± 5°	0°
Cleaned glass (Hydrated; n = 6)	0°	0°
Polydimethyl siloxane (n = 4)	100 ± 1°	49 ± 2°
Polydimethyl siloxane (Hydrated; n = 4)	104 ± 4°	63 ± 1°
Polystyrene (n = 3)	101 ± 10°	35 ± 6°
Polystyrene (Hydrated; n = 4)	100 ± 1°	32 ± 2°
Biomer (n = 4)	104 ± 1°	32 ± 2°
Biomer (Hydrated; n = 4)	84 ± 11°	20 ± 1°
Polyvinyl Chloride (n = 4)	90 ± 3°	40 ± 3°
Polyvinyl chloride (Hydrated, n = 4)	96 ± 0°	34 ± 3°
N-Pentyl silanized silica[c] (n = 6)	76 ± 1°	58 ± 1°

[a] Radiofrequency glow discharge.

[b] Hydrated refers to soaking for 24 h in phosphate-buffered saline.

[c] Not studied hydrated due to hydrolysis of silane groups.

^{3}H-Heparin concentrations were determined by liquid scintillation counting. The binding constants of ^{3}H-heparin to protein were determined by Scatchard plots (35) which also yielded the number of binding sites (n) according to

$$\frac{\bar{\nu}}{[A]} = nK - K\bar{\nu} \qquad [2]$$

where

$\bar{\nu}$ = moles bound ligand (heparin)/moles total protein
K = binding (association) constant
[A] = ligand (heparin) concentration
n = number of identical, noninteracting sites.

Therefore, plotting $\bar{\nu}$/[A] versus $\bar{\nu}$ yields a slope of $-K$ and an intercept of nk on the $\bar{\nu}$/[A] axis or n on the $\bar{\nu}$ axis.

Protein adsorption onto cleaned Biomer, polyvinyl chloride, polydimethylsiloxane (Silastic), amorphous silica, and polystyrene substrate disks was done in an adsorption cell. The cells themselves were 1-ml disposable cuvettes capped with clean 00 corks. Tygon tubing was introduced into bored holes in the corks and stoppered on the outer ends with three-way stopcocks.

Substrates were introduced into the cells with clean forceps and the cells then corked. The closed cells were then primed with degassed PBS (pH 7.4) until all air was removed. The cells were allowed to sit at room temperature for at least 1 h prior to the introduction of labeled protein solution. Radiolabeled protein solutions were then introduced by injec-

TABLE II

Molecular Weight Determination of Heparins (Mean ± SD)

Low molecular weight	7,600
Medium molecular weight (n = 4)	14,800 ± 3,700
High molecular weight (n = 4)	27,700 ± 8,600
Commercial heparin (n = 4)	20,800 ± 10,200

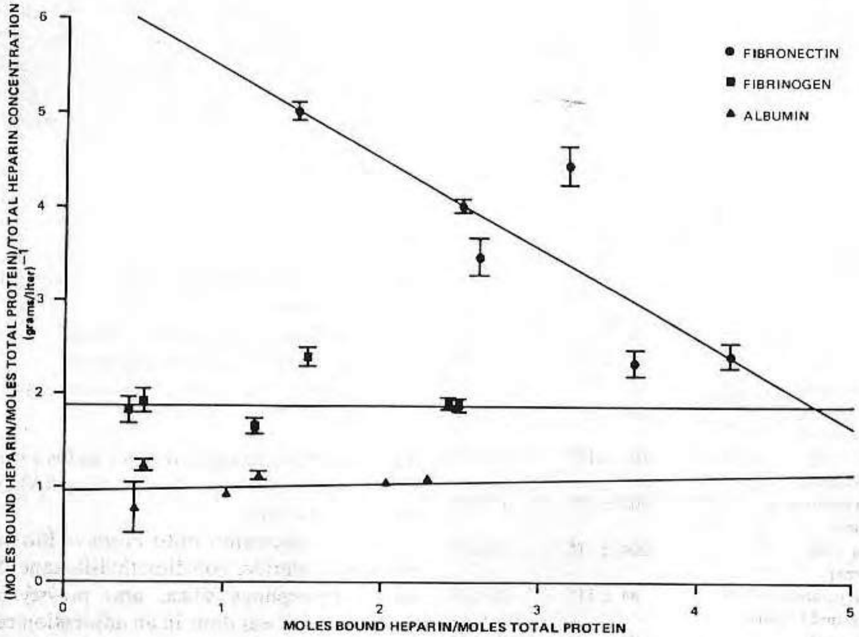

FIG. 1. Scatchard analysis of the solution binding of labeled heparins to proteins in solution. The values given are for commercial heparins but those for low-molecular-weight and high-molecular-weight heparins were not significantly different. Values are mean ± SD ($n = 6$), fibronectin, slope = −1.02, intercept = 6.63, $r = 0.82$; albumin: slope = 0.59, $r = 0.90$; fibrinogen: slope = 0.036, $r = 0.92$.

tion from clean disposable syringes. Ten milliliters of protein solution was injected into the cell at the rate of 40 ml/min to remove all priming buffer and to introduce the protein solution in desired concentrations. Care was taken so as not to introduce any air into the system. The cells were then allowed to remain stationary, at room temperature, for up to 24 h. To terminate protein adsorption each cell was flushed with 30 ml PBS buffer at 60 ml/min, to insure that the substrates were not removed through a protein-solution/air interface. Previous studies with priming solution of Blue Dextran 2000 (Pharmacia Fine Chemicals), using light spectroscopy (639 nm), indicated that the dextran was removed after a 5- to 6-ml flush, at 40 ml/min. Substrates were then removed and placed in dry scintillation vials. Adsorbed protein concentrations were determined by gamma counting on a gamma radiation detector.

Desorption of the protein from the substrates was determined by allowing preadsorbed protein films to desorb in fresh PBS buffer, for up to 24 h, in new vials. The cells were then flushed to remove all desorbed protein. Remaining protein concentrations were determined by γ radiation counting. Verification of the concentration of initially adsorbed protein layer required that the desorbed protein solution, flushed at the termination of the experiment, be counted in similar fashion.

Desorption of adsorbed radioiodinated proteins was also done in freshly prepared bovine platelet-poor plasma (PPP). Fresh whole slaughterhouse blood was collected and mixed in a 9:1 (v/v) ratio with a 3.8% (w/v) solution of sodium citrate (reagent grade) in water. PPP was prepared by centrifugation of the whole blood for 20 min at 1300g force. PPP was then pipetted off and used immediately. The desorption experiments with PPP was the same as above, except that PPP was used as the desorption medium. Flushing was still done with PBS buffer. Maximum desorption time was 8 h with PPP.

Native proteins were adsorbed onto clean Biomer, PVC, PS, PDMSO, and glass substrate disks (planchettes) from 0.3 mg/ml protein solution left for 24 h. After buffer flushing, 10 ml of 0.1 mg/ml solution of either LMW, HMW, or commercial ^{14}C-heparin, in PBS, was injected into the cell. The ^{14}C-heparin was allowed to interact with the adsorbed protein layer for 1 h whereupon the cells were flushed with 30 ml PBS buffer at 60 ml/min to remove all desorbed protein and unbound heparin. The substrates were then air-dried at room temperature and the amount of bound ^{14}C-heparin determined by counting on a "planchet type" gas ionization radiation detector (Internal Proportional Counter, Eberline 2200) for 5 min (high voltage at 96.75 V, window at 96 V, and threshold at 40 V).

Quantitation was done by subtraction of CPM of ^{14}C-heparins on controls (no adsorbed protein) from CPM of ^{14}C-heparins bound to adsorbed protein substrates. This modified CPM was further corrected by dividing by the efficiency, found from a calibrated γ-source, yielding effective degradations per minute (DPM). This DPM value was then divided by the specific activity to yield the amount of ^{14}C-heparin bound.

Previously prepared columns of polystyrene beads, glass beads, and polymer-coated glass beads of Biomer, polyvinyl chloride, and polydimethylsiloxane were primed, from the bottom, with PBS for 1 h. Excess buffer was then pipetted off and 10 ml of native protein solution (0.3 mg/ml) was introduced the same way as was the buffer. Proteins were allowed to adsorb for 24 h. After having excess protein solution pipetted from the column reservoir, the columns were then flushed with 30 ml PBS buffer. Solutions (0.1 mg/ml) of ^{14}C-labeled heparin of commercial molecular weight, were then introduced, as above, in 10-ml aliquots and allowed to interact for up to 8 h.

Kinetics of ^{14}C-heparin binding were monitored by solution depletion techniques. The stock ^{14}C-heparin solution activity was compared to the activity of 100-μl samples drawn from the bottom of the column. Activity and quantitation were accomplished by liquid scintillation counting.

Release (desorption) of ^{14}C-heparin was done in both PBS buffer and bovine platelet poor plasma (PPP). At binding equilibrium, the ^{14}C-heparin solution was pipetted from the reservoir and the column flushed with 30 ml PBS buffer. Again, excess buffer was removed from the reservoir. At this time PBS buffer release of ^{14}C-heparin was initiated. Samples were taken by injecting 1 ml PBS buffer from below and removing the same volume of buffer from the reservoir. Desorption was allowed for up to 24 h.

TABLE III

Values for ^{3}H-Heparin Binding to Proteins[a]

Protein	K_{assoc}[b] (g/liter)$^{-1}$	Binding sites[b] (n)
Albumin		
Low-molecular-weight heparin	≈0.00	—
High-molecular-weight heparin	−0.15	—
Commercial heparin	−0.59	—
Fibrinogen		
Low-molecular-weight heparin	≈0.00	—
High-molecular-weight heparin	≈0.00	—
Commercial heparin	≈0.00	—
Fibronectin		
Low-molecular-weight heparin	0.43	5.96
High-molecular-weight heparin	1.10	6.32
Commercial heparin	1.02	6.48

[a] $n = 3$.

[b] For confidence levels, see Fig. 1.

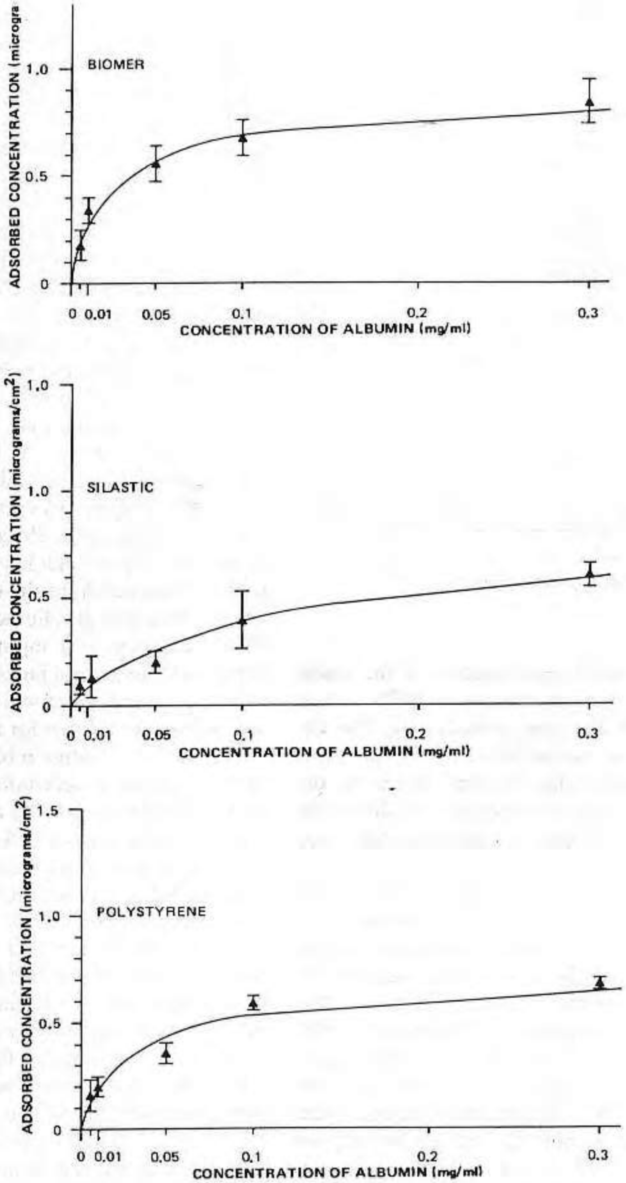

FIG. 2. ^{125}I-Albumin static adsorption isotherms on disks taken at room temperature. Values given are mean ± SD ($n = 3$) for all points except 0.3 mg/ml, where $n = 9$. (a) Biomer, (b) Silastic, (c) polystyrene, (d) polyvinyl chloride.

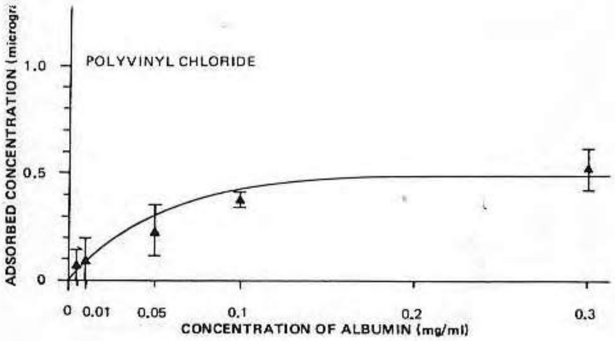

FIG. 2—*Continued.*

Release of ^{14}C-heparin in bovine PPP was done as above except that PPP was introduced by a second flush of 20 ml plasma to remove excess PBS buffer. Samples were taken in a similar manner. Plasma release studies were done for up to 8 h.

All plasma and buffer samples were counted by liquid scintillation counting.

The total amount of ^{14}C-heparin released could be due to: (a) released ^{14}C-heparin from nondesorbing protein, C_R; and (b) "released" heparin still bound to desorbed protein, C_B. If C_B is equal to the amount of desorbed protein (C_p) (previously determined) then the true amount of ^{14}C-heparin actually released from protein, C, is given by

$$C = C_H - C_p \qquad [3]$$

where

$C_H = C_R + C_B$

= Amount determined by liquid scintillation counting.

Fresh human whole blood was obtained from healthy donors and immediately mixed in a 9:1 (v/v) ratio with a 3.8% (w/v) solution of sodium citrate (Reagent grade). Platelet poor plasma (PPP) was obtained by centrifugation of the whole blood for 10 min at 2200g force. The PPP was decanted off and used immediately or stored frozen for up to 2 weeks. Human PPP was introduced into buffer primed Biomer columns according to the methodology previously discussed. PPP was allowed to remain in the columns for 1 h to allow for plasma protein adsorption, then the columns were flushed with 30 ml PBS (pH 7.4) at approximately 60 ml/min. Solutions of commercial ^{14}C-heparin (0.1 mg/ml) were introduced and the kinetics of binding monitored for up to 24 h via solution depletion. Release of ^{14}C-heparin was done as previously described in both PBS buffer and human PPP.

Activated partial thromboplastin time (APTT) and anti-X$_a$ assays (34) were performed to determine the activity/presence of the bound and/or released heparins from substrates coated with plasma fibronectin and pooled human PPP.

RESULTS AND DISCUSSION

The substrate surfaces characterized were clean. There were no observed particulates or chemical impurities in the matrix. Most of the surfaces were macroscopically smooth. However, some roughness was observed on Biomer, Silastic, polystyrene beads, and glass bead surfaces at high magnification (36). All surfaces were wettable to different extents (see Table I)

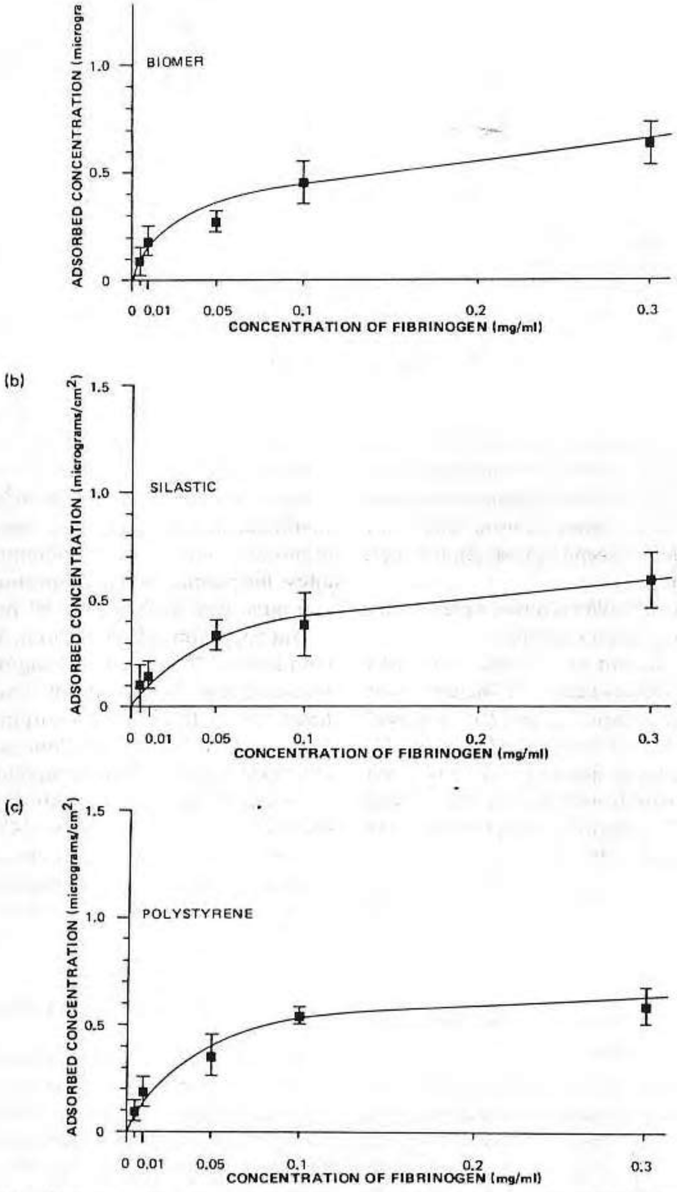

FIG. 3. ^{125}I-Fibrinogen static adsorption isotherms on disks taken at room temperature. Values are mean ± SD ($n = 3$) for all points except for 0.3 mg/ml ($n = 9$). (a) Biomer, (b) Silastic, (c) PS, (d) PVC.

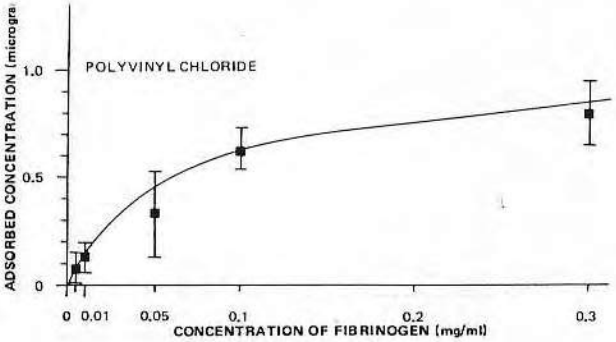

FIG. 3—*Continued.*

as indicated by the receding angle observed via Wilhelmy plate energetics. The substrate surfaces were clean and chemically accounted for by XPS examination. The solution technique of coating the glass bead supports was shown to be complete by scanning electron microscopy and XPS analyses (36).

Utilizing high-pressure liquid chromatography, the fractionated heparins were characterized by reference to known dextran molecular weights. This methodology yields the molecular weight relative to dextrans; therefore, the absolute molecular weights are still unknown. Another disadvantage to this methodology is that the molecular weight distribution (i.e., weight average molecular weight, number average molecular weight) remains unresolved. However, the relative values were consistent and thus considered reliable. Since heparins are chain-like structures and not globular in nature, like dextrans, it was necessary to multiply the values obtained by an empirically derived factor (30) to compensate and yield more "accurate" relative molecular weights. The results are listed in Table II for LMW fractions, medium-molecular-weight fractions (not utilized), and HMW fractions. The average molecular weight for commercial heparin was determined from the values listed.

The optical properties of the labeled proteins, studied here, which are indicative of conformation, seem to be identical to the native proteins (36). Also, the electrophoretic mobility was unchanged, which indicates similar conformation and that no fragmentation occurred during iodination (64). Even so, it still cannot be concluded that the iodinated protein is equivalent to the native structure. Indeed, iodide has a relatively large atomic radius and is extremely large when compared to the hydrogen atomic size that it has been substituted for. In this study the iodination performed was done under conditions much milder than the manufacturers' recommendations for iodination and the resultant specific labeling was much lower than those reported by the manufacturers. Since there was only up to one label per protein considered (usually only 0.5), it is highly unlikely that the same tyrosine is labeled every time in the respective proteins considered. This being the case, perhaps the localized iodine effects are either masked by the large surrounding host or so small that accommodation by the relatively immense protein is accomplished without any macroscopically observable effects. In either case, one may be certain that the electronegativity and size of the iodide substitution has a massive localized effect. It is assumed

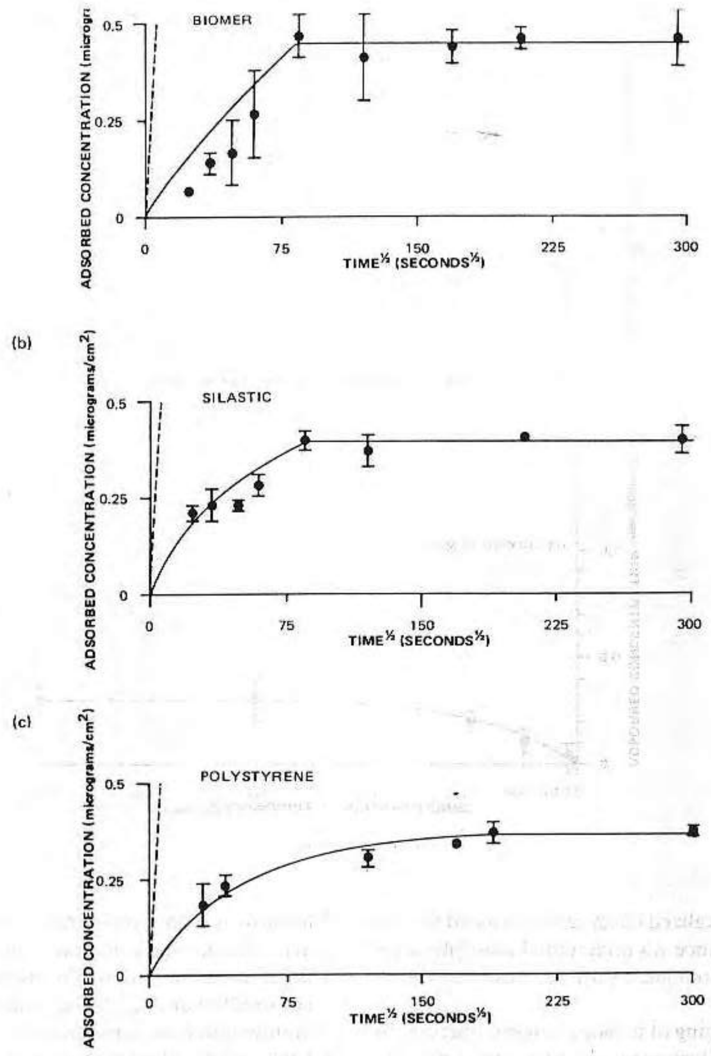

FIG. 5. Kinetics of ^{125}I-fibronectin static adsorption on disks. Concentration = 0.05 mg/ml. Dashed line is the theoretically calculated diffusion control process. Values are mean ± SD ($n = 3$) (last point $n = 6$). (a) Biomer, (b) Silastic, (c) PS, (d) PVC, (e) hydrophilic silica.

dependent sites. Fibronectin has been shown (37–41) to have three binding sites for heparin on each of its two segments. Thus, the binding of six heparins per fibronectin molecule, in solution, indicates that in the "native" solution state that all six sites are active in binding.

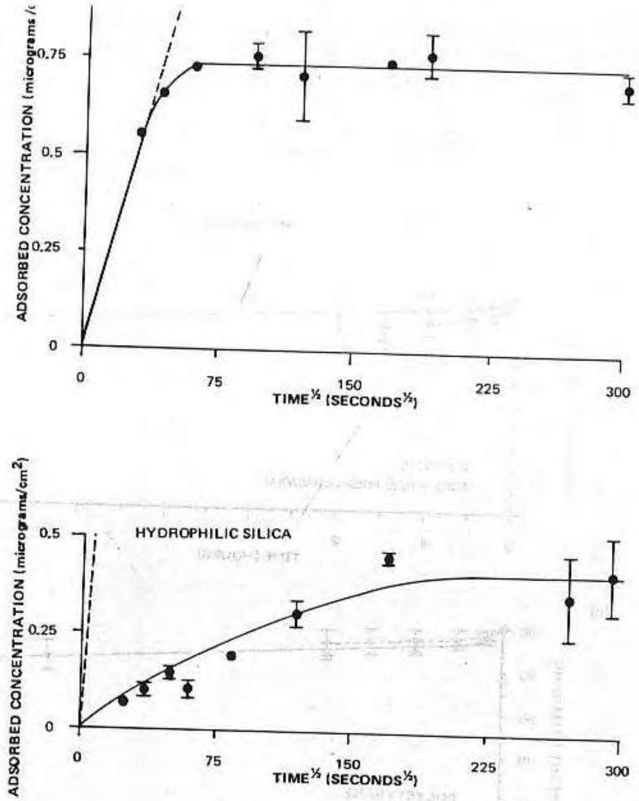

FIG. 5—*Continued.*

While it is customary to report K_{assoc} in erms of moles per liter (M), due to the polylispersity of heparin and the heparin fractions sed herein, it was felt that reporting K_{assoc} in rms of grams per liter is much more descripive (see Table III).

In this study, each adsorption was run at ast three times using ratios of labeled to unbeled protein of approximately 1:4, 1:2, and :1 to determine the effect of protein labeling n adsorption. Each of the labeled protein actions had approximately equal degrees of beling (approximately 0.5). No increase in sorption was observed with increased labeled-protein concentration. All adsorption values were within the error limits of gamma counting efficiency. The preferential and nonpreferential adsorption of the same labeled species has been shown to be substrate (system) dependent (7, 42). For example, in this study, iodinated (iodine-125) albumin was shown to nonpreferentially adsorb to polystyrene while others have shown preferential adsorption onto polystyrene latices (43). Those latices were well oriented with respect to charge and backbone, while the polystyrene utilized herein was random in nature. Conjugated albumin has also shown no preferential adsorp-

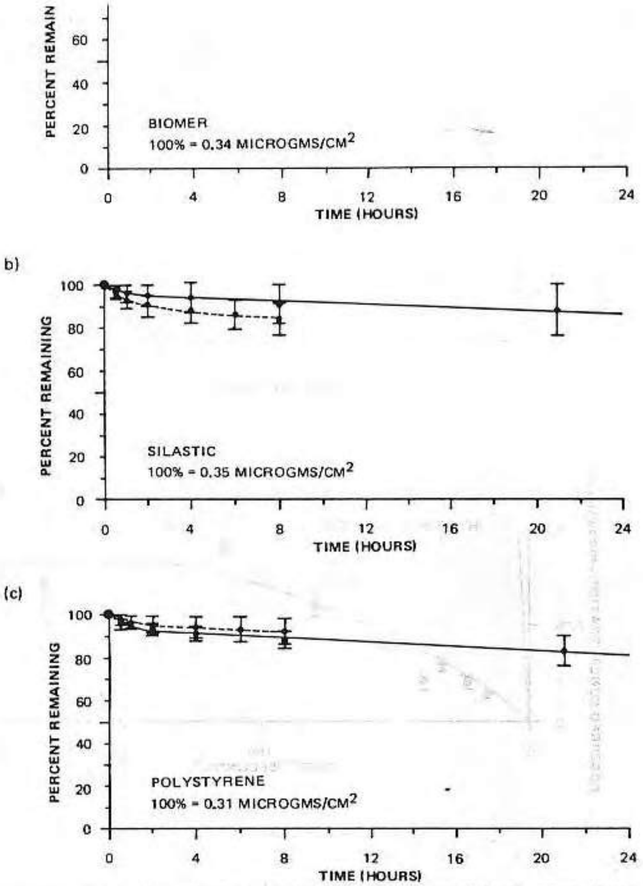

FIG. 6. Static desorption of ^{125}I-fibronectin on disks. Dashed line is in plasma medium and solid line is in PBS buffer. Values given are mean ± SD ($n = 3$). (a) Biomer, (b) Silastic, (c) PS, (d) PVC, (e) hydrophilic silica.

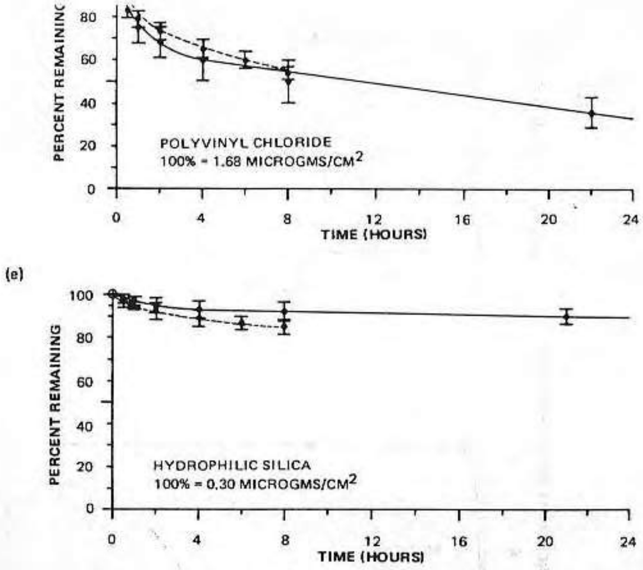

FIG. 6—*Continued.*

tion onto amorphous silica, Biomer, Silastic, and cellulose acetate (7). Similarly, concerning labeled fibrinogen, this study showed no preferential adsorption while others (7) have shown preferential adsorption elsewhere. It should be noted, however, that these substrate surfaces here are different than those previously reported.

Figure 2 shows the adsorption isotherms of ^{125}I-labeled albumin on the polymeric substrates utilized. The adsorbed amount, for a 0.3 mg/ml solution of iodinated albumin, falls very near to the reported values of others (44–50) and nearly equal to the approximate 0.7 μg/cm^2 monolayer concentration reported on polystyrene and polyurethane substrates (45, 46). Assuming that the iodinated albumin undergoes no multilayering, significant structural changes upon adsorption, and that surface irregularities can be neglected (36) on the polyvinyl chloride (PVC) or Silastic surfaces, then this study's albumin coverage on the substrates can be taken as follows: (a) polystyrene, 97% coverage; (b) PVC, 77% coverage; (c) Silastic, 86% coverage; and (d) Biomer, 100% coverage. Adsorption of albumin to a lesser extent on polyurethanes or polystyrenes under similar conditions has also been shown elsewhere (45).

The isotherms of iodine-labeled fibrinogen (Fg) are shown in Fig. 3. The adsorption values are similar to those reported in the literature (45, 51) and the similar lack of a saturated monolayer on the surface at these concentrations is well depicted. Monolayer coverage is reported to be in the range of 0.8 to 1.2 μg/cm^2 for Fg. If a 1.0 μg/cm^2 coverage is taken as 100% monolayer coverage, then the percentage coverage of Fg on these substrates can be given as: (a) polystyrene, 59%; (b) PVC, 79%; (c) Silastic, 59%; and (d) Biomer, 59%.

Iodine-labeled fibronectin (Fn) adsorption isotherms are given in Fig. 4 for the polymeric substrates and hydrophilic silica. The values listed are comparable to those given in the literature (52–60) using similar concentrations. Except for the complete isotherms given by Bornzin and Miller (50), much of the adsorption work has ignored the possibilities of preferential adsorption of labeled Fn and/or the air–solution interface. These problems, in addition to incompletely characterized substrates, results in a large uncertainty as to actual monolayer coverage values. Therefore, the values of Fig. 4 will be assumed to be 100% monolayer coverage, since no preferential adsorption was seen to occur in this study. The large difference in plateau values of the sub-

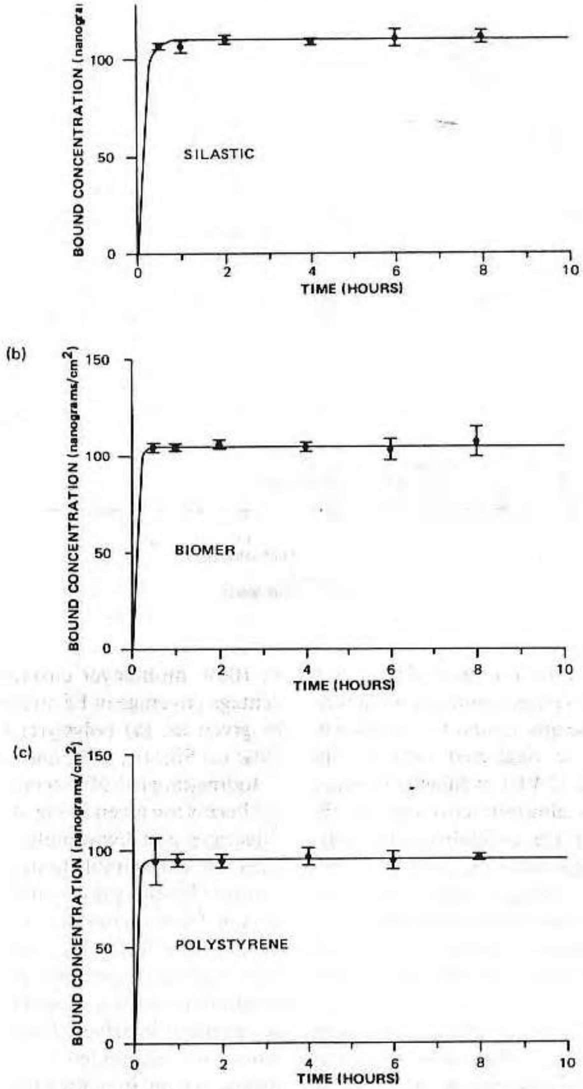

FIG. 7. ^{14}C-Labeled heparin binding to adsorbed fibronectin disks. Values given are mean ± SD ($n = 3$). (a) Biomer, (b) Silastic, (c) PS, (d) PVC, (e) hydrophilic glass.

strates, as compared to PVC, could be explained by the occurrence of a conformational change in Fn upon adsorption onto PVC (discussed below). This accommodation of Fn increases the total amount of Fn present on the PVC surface. Such a change was reported ear-

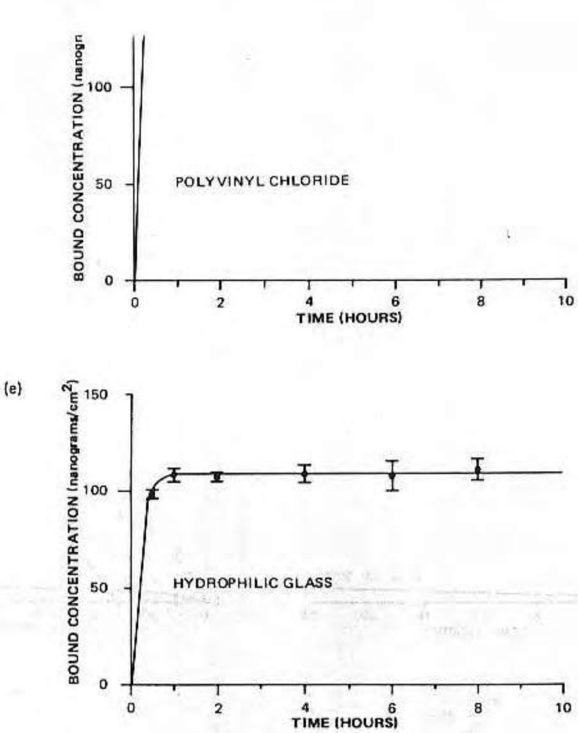

FIG. 7—*Continued.*

lier for Fn adsorption onto hydrophobic silica surface (53, 61).

Figure 5 shows kinetics of adsorption for ^{125}I-Fn. In all cases steady-state values were reached within 2 h, except for hydrophilic silica and within 1 h for adsorption onto PVC. ^{125}I-Fn adsorption onto PVC can be fit to an ideally controlled process by diffusion, for the first 30 min. Thereafter, for the next 5 to 7 min a change in the type of adsorption was seen and then the onset of steady state followed. This pattern was quite similar to the pattern observed in the total internal reflection fluorescence (TIRF) mode for hydrophobic NPS-silica except for the concentration of Fn adsorbed under those conditions was calculated to be much less (61). In the TIRF mode, the Fn adsorbed onto the hydrophobic silica was observed to be in a different environment (conformation) than that on the hydrophilic silica. It was thus hypothesized that this conformational change accounted for the increased accommodation of Fn on the hydrophobic silica surface. It is probable then that the differences in the adsorption rate and concentration of Fn on PVC, as compared to the other substrates was due to it also being in a different conformation on that substrate. It is interesting to note that the adsorption kinetics of ^{125}I-labeled Fn onto hydrophilic silica appears very similar to the second time phase of the TIRF monitoring of Fn adsorption on the same surface (61). The static adsorption seemed to take longer; however, this was not

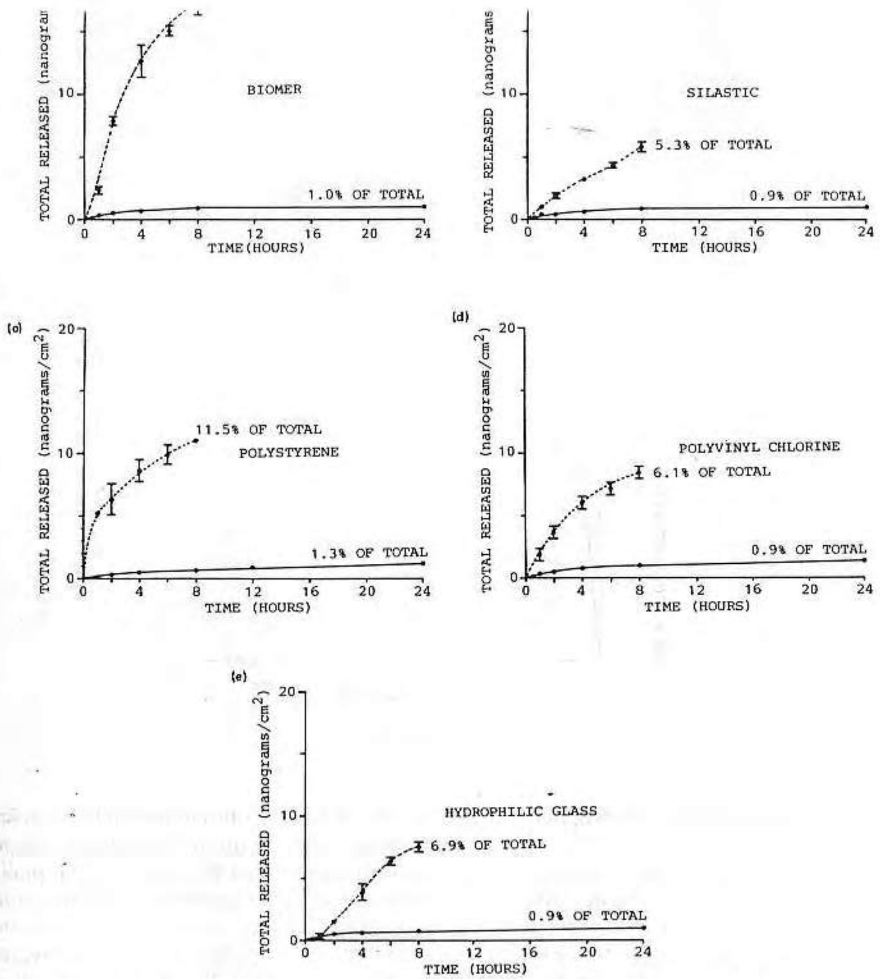

FIG. 8. Release of ^{14}C-labeled heparin from fibronectin-coated disks. Dashed line is release in plasma and solid line is release in PBS buffer. Values given are mean ± SD ($n = 3$). (a) Biomer, (b) Silastic, (c) PS, (d) PVC, (e) hydrophilic glass.

unexpected since no flow or turbulent convection were occurring in the static cell which would aid in mass transport to the surface or through the diffusional boundary layer. These static adsorption kinetics were very similar to those reported in the literature for monitoring Fn adsorption by TIRF under static conditions (62).

It is tempting to say that most of the static adsorption processes depicted here deviate from an ideal diffusion-controlled process. This cannot be said for certain, however, since the first samples were taken (experiments terminated) after 15 min of adsorption time. It is probable that diffusion does have a part in the very early stages of the adsorption process (63) only it was not observed here due to the sampling protocols.

Desorption of adsorbed ^{125}I-Fn monolayer films is shown in Fig. 6 in buffer and plasma solutions. The monolayers were adsorbed from 0.3 mg/ml solutions of radiolabeled protein. Fibronectin shows significant losses on PVC surfaces with both PBS and plasma. However, the other surfaces show only a 10 to 15% loss in PBS and plasma.

The adsorbed Fn generally appears quite stable. The PVC, however, shows FN monolayer losses of 40% in plasma and 60% in PBS buffer. This is due perhaps to the nature of the adsorption process. Adsorbing quite rapidly (diffusion controlled), the protein may be in a conformation that is a steady-state equilibrium with the Fn "sink," yet not in a preferred orientation. Under desorption conditions, this steady-state condition is no longer the equilibrium state and thus the surface concentration is reduced considerably possibly to accommodate reorientation.

The kinetics of binding and release of ^{14}C-labeled heparin with Fn-coated substrates are shown in Figs. 7 and 8, respectively. ^{14}C-heparin solutions were not observed to be significantly depleted when passed over columns preadsorbed with monocomponent fibrinogen and albumin solutions, over the same period of time (36).

The kinetics of binding for adsorbed fibronectin (see Fig. 7) show that steady state occurred in all cases within 1 h. The concentra-

Protein and substrate	Concentration of bound heparin (μg/cm²): Solution depletion technique	Concentration of bound heparin (μg/cm²): Ionization technique	Concentration of adsorbed protein (μg/cm²)	Molar ratio: heparin to protein: Solution depletion technique	Molar ratio: heparin to protein: Ionization technique	Release in PBS (24 h), %: Protein	Release in PBS (24 h), %: Heparin	Release in plasma (8 h), %: Protein	Release in plasma (8 h), %: Heparin
Fn									
Silastic	0.11	0.11	0.35	5.8:1.0	5.8:1.0	12	0.9%		5.3%
PS	0.10	0.09	0.31	6.0:1.0	5.5:1.0	18	1.3%	16	11.5%
PVC	0.14	0.15	1.68	1.5:1.0	1.6:1.0	65	0.9%	8	6.1%
Biomer	0.11	0.11	0.34	5.5:1.0	6.0:1.0	10	1.0%	47	17.0%
Hydrophilic								10	
Silica	0.11	—	0.30	6.6:1.0	—	10	0.9%	15	6.9%
Fg									
Silastic	0	—	0.59	0:1	—	14	—	61	—
PS	0	—	0.59	0:1	—	7	—	6	—
PVC	0	—	0.79	0:1	—	22	—	12	—
Biomer	0	—	0.64	0:1	—	15	—	21	—
Albumin									
Silastic	0	0	0.60	0:1	0:1	18	—	63	—
PS	0	0	0.68	0:1	0:1	22	—	38	—
PVC	0	0	0.52	0:1	0:1	12	—	20	—
Biomer	0	0	0.84	0:1	0:1	15	—	22	—

[a] Data derived from Figs. 1–8.

Substrate	Heparin	Rel. units activity of heparin	Time (s)	Equivalent concentration of heparin[b] (μg/cm²)
Silastic	None ($n = 3$)	[a]	11.4 ± 0.7	[a]
	LMW ($n = 3$)	0.03	24.5 ± 3.9	0.18
	HMW ($n = 3$)	0.02	23.6 ± 1.7	0.12
	Regular ($n = 3$)	0.02	23.5 ± 2.9	0.12
Biomer	None ($n = 3$)	[a]	32.0 ± 6.9	[a]
	LMW ($n = 3$)	0.03	45.3 ± 11.4	0.18
	HMW ($n = 3$)	0.02	44.4 ± 13.1	0.12
	Regular ($n = 3$)	0.03	44.7 ± 8.1	0.18
PS	None ($n = 3$)	[a]	16.2 ± 2.5	[a]
	LMW ($n = 3$)	0.03	29.5 ± 4.7	0.18
	HMW ($n = 3$)	0.02	27.8 ± 4.7	0.12
	Regular ($n = 3$)	0.03	28.7 ± 3.6	0.18
PVC	None ($n = 3$)	[a]	14.1 ± 0.3	[a]
	LMW ($n = 3$)	0.05	27.9 ± 5.5	0.30
	HMW ($n = 3$)	0.04	26.0 ± 2.2	0.24
	Regular ($n = 3$)	0.05	27.4 ± 1.9	0.30
Human plasma-coated biomer	Regular ($n = 3$)	0.00	35.8 ± 7.3	0.00

[a] Taken as zero.

[b] Assuming 165 units/mg heparin.

tions of ^{14}C-heparin bound to the adsorbed fibronectin were approximately 90 to 150 ng per square centimeter area. It is interesting to note that the "steady-state" results in a fairly straight line with a positive slope, when fit by linear regression. The slopes vary from 0.14 to 0.35. Glass, Biomer, and polystyrene all had constant steady-state slopes of approximately 0.25 while Silastic and PVC had slopes of 0.14 and 0.35, respectively. It seems that since Fn desorbs from all of these substrates that more scatter would be seen using a technique that measures the solution protein depletion, due to protein adsorption, and the concurrent protein desorption from the same substrate. However, this was not observed. It remains to be elucidated whether the binding of heparin to fibronectin changes the sticking coefficient of fibronectin by allosteric binding of the ligand.

Figure 8 shows the release of bound ^{14}C-heparin in PBS buffer and plasma. In all systems, the total amount of released heparin did not equal that predicted by Eq. [3], which accounts only for released protein (see Fig. 6). This may be explained by several possible mechanisms of which two are discussed: (a) heparin binding to adsorbed fibronectin alters the adsorbed protein sticking coefficient thus making it adhere more tenaciously to the various substrates. Perhaps by allosterically binding heparin to the adsorbed protein, the resulting conformational change in the protein gives it a better "foot hold" on the substrate surface. This allosteric change in Fn induced by the binding of heparin has been suggested (64, 65) for the mechanism by which fibronectin increases its ability to bind to immobilized collagen and complex solution phase collagen; (b) solution-bound heparin may be released more readily and reorientation of the protein monolayer may accommodate the rebinding of the free heparin. This mechanism seems feasible for the PVC surface where Fn is apparently sterically hindered due to the high concentration of surface adsorbed Fn in

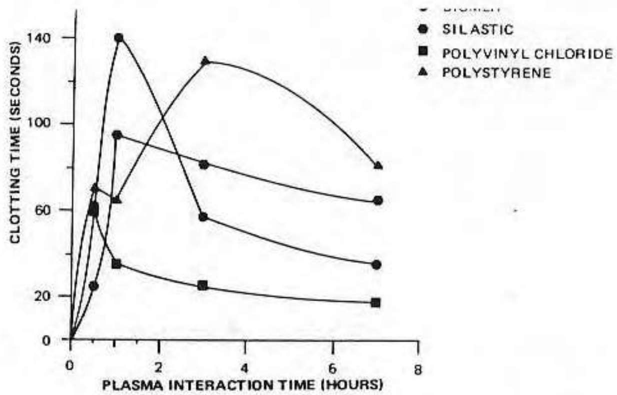

FIG. 9. Activated partial thromboplastin times on column controls. The columns were preadsorbed with native fibronectin only. The values given are means. The standard deviations were approximately ±50 to 100 s.

comparison with other substrates; however, it is less likely for the other surfaces where the absorbed Fn is apparently more "spread out."

In all cases, no more than 2% of the total ^{14}C-heparin was released in PBS buffer and no more than 17% of the total ^{14}C-heparin was released in the plasma environment. The great increase in the plasma release of ^{14}C-heparin was probably due to the binding of heparin to blood factors rendering them inactive, and to the bacteriological and enzymatic attack of the protein monolayer or bound heparin. Exchange of the adsorbed protein in plasma could also increase the amount of released heparin in a bound state to the original protein.

The results of ^{14}C-heparin binding protein monolayers as determined by gas ionization counting of the ^{14}C-label are given in Table IV. For ease of comparison, the tabulated results from Figs. 2 through 8 are also given. All six binding sites for heparin on fibronectin, as determined by Scatchard analysis, were active and available in the adsorbed state for all substrates except PVC. The increased concentration of Fn adsorbed onto the PVC surfaces or its resultant different adsorbed conformation (64, 65) probably sterically blocked the majority of the binding sites in that system. It appears that two heparin binding sites are hindered on both sides of the protein dimer and that a third may be hindered somewhat on one of the sides. Most likely, energy supplied by thermal fluctuations or convective turbulence probably renders this one semihindered site somewhat available for heparin binding. This explains the molar ratio of one fibronectin to approximately 1.5 heparin molecules.

^{14}C-Heparin binding to the proteinaceous monolayer left after human serum interaction was not observed (36). In columns with surface areas up to 100 cm², the introduced ^{14}C-heparin solution did not decrease in activity over a 24-h period. Assuming that the protein monolayer is at least as stable as a composite of the aforementioned monocomponent systems (Table IV) of albumin, fibrinogen, and fibronectin in PBS (pH 7.4), the possibility of total protein desorption and thus undetected solution binding can be eliminated. After buffer flush, desorption/release was carried out in a buffer environment for 24 h or in a canine plasma environment for 8 h. All samples were

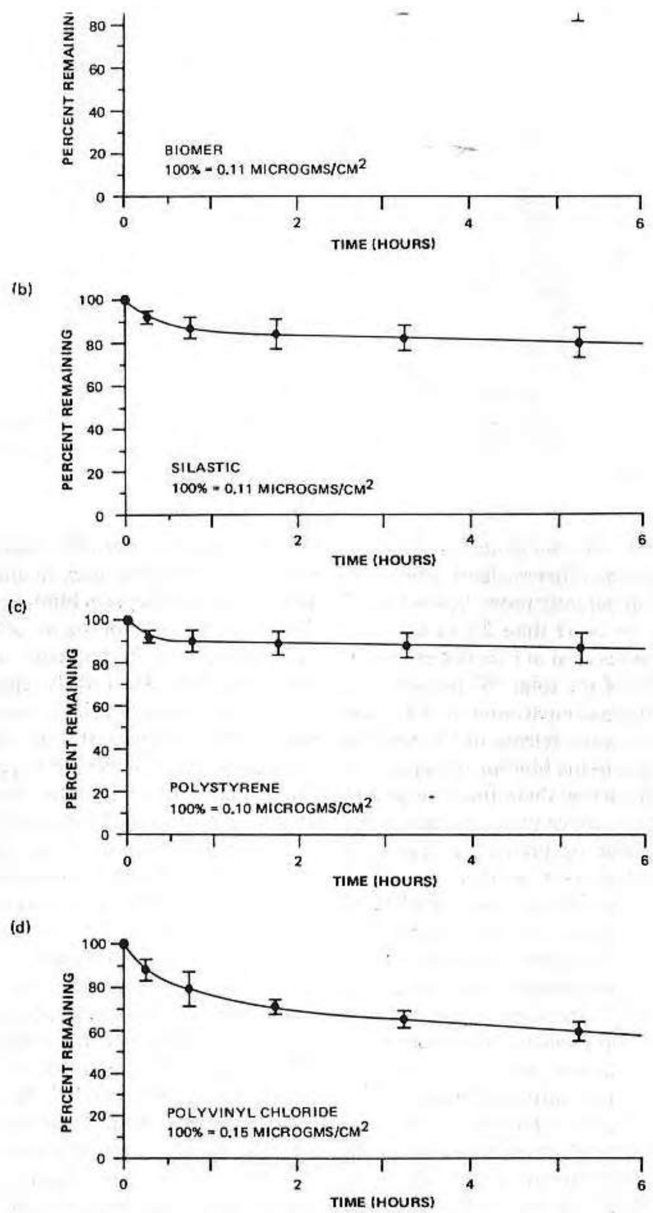

FIG. 10. Factor X_a assay for heparin released in plasma for column type adsorption. Values given are mean ± SD ($n = 3$). (a) Biomer, (b) Silastic, (c) PS, (d) PVC, (e) hydrophilic glass.

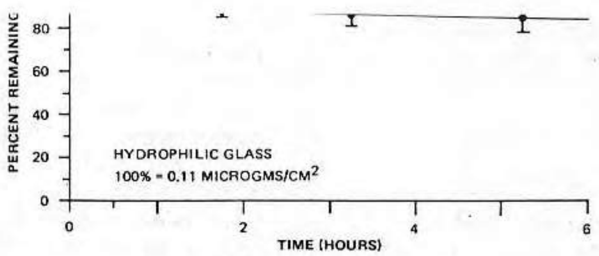

FIG. 10—*Continued.*

equivalent to background counts or within the error of the standard deviation. Thus, it may be concluded that the proteinaceous monolayer cannot bind heparin and, therefore, must contain very little fibronectin or inhibited fibronectin which is unable to bind heparins.

Activated partial thromboplastin time (APTT) assays for heparin are generally considered valuable; however, they are nonspecific in nature (66, 67) in that: (a) bound heparin and solution heparin may be treated equivalently and (b) any adsorption, and thus loss, of coagulation factors will prolong the resultant assay time. The results of APTT coagulation times done on plasma that had been in contact with polymer substrate discs, pretreated with adsorbed Fn and bound heparin fractions, are given in Table V. The assay showed generally that all the prebound heparin was available for prolongation of coagulation times. The excessive prolongation of some observed clotting times is probably due to the depletion of coagulation factors (68). The depletion of these factors could occur by adsorption to container or substrate surfaces or inactivation by binding to either adsorbed or desorbed Fn molecules. If loss of coagulation factors were causing excessively prolongated coagulation times not accounted for by the heparin present, it would be magnified in systems with much larger surface areas. Figure 9 shows prolongation of clotting times with increasing plasma contact time on column control substrates preadsorbed only with fibronectin. The erratic behavior can be explained by the binding or adsorption and subsequent release or desorption with time, of coagulation factors. This behavior caused the scatter (SD) of times to be so great that the coagulation times could not be distinguished from those of the column substrate controls. Therefore, to determine the increase in coagulation times attributable to the bound and released heparin from the column experiments, heparin colorimetric assays run concurrently or at the end of the plasma incubation of the substrate columns had to be done.

Activated Factor X assay is very sensitive and specific for heparin in plasma environments (34). The method involves the use of a chromogenic substrate (S2222) that is susceptible to the presence of X_a. Unknown concentrations of heparin are introduced which bind to known quantities of X_a. The X_a–heparin complex is inactive toward the S2222 substrate. The remaining X_a activity is quantitated by amidolysis of the S2222 substrate. The amidolysis is stopped by the addition of acetic acid after a specified time. This methodology can detect 0.02 units of heparin per milliliter of plasma tested.

Concurrent with APTT testing of plasma subjected to column substrates, each sample was tested, in duplicate, for released heparin activity via activated Factor X assay. The results are given in Fig. 10 (also reference Table plasma. Small differences in the amounts of heparin released may be due to the different plasmas utilized in the two studies (bovine versus canine).

CONCLUSIONS

This *in vitro* study has shown several important aspects relating to localized heparin delivery at a foreign surface–blood interface. First, albumin, albeit a carrier of metabolic by-products and some anticoagulants, does not bind heparin at physiological pH in solution or in the adsorbed state. The same can be stated for fibrinogen. Plasma fibronectin, on the other hand, binds heparin in either state. Fibronectin was shown to have six binding sites for heparin which may be sterically blocked if fibronectin adsorbs in such a fashion as to increase the surface concentration of the adsorbed protein. Next, it has been shown that by using adsorbed fibronectin as an intermediate, it is possible to deliver heparin, prebound to the adsorbed protein, in concentrations up to approximately 0.2 $\mu g/cm^2$ in a plasma environment. Also, active surface-bound heparin was maintained at approximately 83 to 99% of original-bound heparin concentrations for up to 6 to 8 h time. The stability of the Fn monolayer was increased by the binding of heparin, probably due to an allosteric change upon binding the drug moiety, increasing the sticking coefficient of Fn (64, 65).

It is also interesting to note that human serum, allowed to adsorb onto Biomer surfaces, does not bind heparin even though fibronectin occurs in most healthy adults in the range of 300 to 500 $\mu g/ml$ plasma. Therefore, Fn appears not to be preferentially adsorbed from multicomponent systems. Or, if it is, it adsorbs from such systems in conformations unable to bind heparin. Comparing APTT results of the fibronectin-precoated substrates bound to heparin, to controls precoated with increase the intrinsic activation of the coagulation cascade but rather increases the relative normal coagulation times two to three times over those observed with monocomponent human plasma or fibronectin. When the APTT results of this fibronectin–heparin complex are compared to the albumin–heparin covalent conjugate (7, 18–21), it can be seen that the times are similar, indicating that both are effective in prolonging clotting times. However, the comparison of direct times is not the important factor; rather that both tend to double or triple their clotting times relative to controls is significant.

The trends observed throughout this section seem to indicate that the bound heparin is active in prolonging clotting times (APTT and X_a assays) and that the fibronectin adsorbed monolayer may indeed aid in reducing the intrinsic activation of Factor XII. Furthermore, the amount of heparin remaining bound to the monolayer is greater than predicted by protein desorption alone.

ACKNOWLEDGMENTS

The generous gift of human plasma fibronectin from Dr. Deane F. Mosher was greatly appreciated. The study was funded by NIH Grant HL-17623-10.

REFERENCES

1. Salzman, E. W., *Blood* **38**, 509 (1971).
2. Forbes, C. D., and Prentice, C. R., *Brit. Med. Bull.* **34**, 201 (1978).
3. Lyman, D. J., Brash, J. L., Chaikin, S. W., Klein, K. G., and Carini, M., *Trans. Amer. Soc. Artif. Intern. Organs* **14**, 250 (1968).
4. Lyman, D. J., *in* "Structural Order in Polymers" (F. Cierdelli and P. Gusti, Eds.), pp. 205–220. Pergamon, Oxford, 1981.
5. Young, B. R., Lambrecht, L. K., Cooper, S. L., and Mosher, D. F., "Biomaterials: Interfacial Phenomena and Applications," Vol. 199, pp. 317–350. Advances in Chemistry Series, Amer. Chem. Soc., Washington, D.C., 1982.
6. Lee, E. S., and Kim, S. W., *Trans. Amer. Soc. Artif. Intern. Organs* **25**, 124 (1979).
7. Hennink, W. E., Dost, L., Feijen, J., and Kim, S. W.,

8, 393 (1983).
9. Horbett, T. A., *Adv. Chem. Ser.* **199**, 233 (1983).
10. Munro, M. S., Quattrone, A. J., Ellsworth, S. R., Kulkarni, P., and Eberhart, R. C., *Trans. Amer. Soc. Artif. Intern. Organs* **27**, 499 (1981).
11. Kim, S. W., and Lee, R. G., "Adsorption of Blood Proteins onto Polymer Surfaces," Vol. 145, pp. 218–229. Advances in Chemistry Series, Amer. Chem. Soc., Washington, D.C., 1975.
12. Stoner, G. E., Srinivasan, S., and Gileadi, E., *J. Phys. Chem.* **75**, 2107 (1971).
13. Ihlenfeld, J. V., and Cooper, S. L., *J. Biomed. Mater. Res.* **13**, 577 (1979).
14. Lee, R. G., Adamson, C., and Kim, S. W., *Thromb. Res.* **4**, 485 (1974).
15. Brash, J. L., and Davidson, V. J., *Thromb. Res.* **9**, 249 (1976).
16. Kim, S. W., Ebert, C. D., Lin, J. Y., and McRea, J. C., *Amer. Soc. Artif. Intern. Organs* **6**, 76 (1983).
17. Kim, H. P., Byon, S. M., Yeom, Y. I., and Kim, S. W., *J. Pharm. Sci.* **72**, 225 (1983).
18. Hennink, W. E., Feijen, J., Ebert, C. D., and Kim, S. W., *Thromb. Res.* **29**, 1 (1983).
19. Hennink, W. E., Ebert, C. D., Kim, S. W., Breemhar, W., Bantjes, A., and Feijen, J., *Biomaterials* **5**, 264 (1984).
20. Hennink, W. E., Kim, S. W., and Feijen, J., *J. Biomed. Mater. Res.* **18**, 911 (1984).
21. Hennink, W. E., Dost, L., Van Hken, W. G., Kim, S. W., and Feijen, J., "Biomaterials and Artificial Organs," Symposium at Strathclyde, U.K., in press.
22. "Guidelines for Physicochemical Characterization of Biomaterials," U.S. Department of Health and Human Services, NIH Publication No. 80-2186, September 1980.
23. Coleman, D. L., Atwood, A. I., and Andrade, J. D., *J. Bioeng.* **1**, 33 (1976).
24. King, R. N., Andrade, J. D., Ma, S. M., Gregonis, D. E., and Brostrom, L. R., *in* "Fundamentals of Interfacial Phenomena: Research Needs and Priorities" (J. Bers, Ed.). Proceedings of the National Science Foundation Workshop, Seattle, Washington, 1979.
25. Haller, I., *J. Amer. Chem. Soc.* **100**, 8050 (1978).
26. Brier-Russell, D., Salzman, E. W., Lindon, J., Hendin, R., Merrill, E. W., Dincer, A. K., and Wu, J. S., *J. Colloid Interface Sci.* **81**, 311 (1981).
27. Ogston, D., and Bennett, B., "Haemostasis: Biochemistry, Physiology and Pathology." Wiley, New York, 1977.
28. Gregonis, D. E., Hsu, R., Buerger, D. E., Smith, L. K., and Andrade, J. D., *in* "Macromolecular

"Physiochemical Aspects of Polymer Surfaces." Plenum, New York, 1982.
30. Hurst, R. E., Van Dedem, G., and Settine, J. M., *Thromb. Res.* **22**, 633 (1981).
31. Rice, R. H., and Mean, G. E., *J. Biol. Chem.* **246**, 831 (1979).
32. Jentoff, N., and Dearborn, D. G., *J. Biol. Chem.* **254**, 4359 (1979).
33. McNamara, P. J., and Bogardus, J. B., *J. Pharm. Sci.* **71**, 1066 (1982).
34. Teien, A. N., Lie, M., and Abildgaard, U., *Thromb. Res.* **8**, 413 (1976).
35. Scatchard, G., *Ann. N.Y. Acad. Sci.* **51**, 660 (1949).
36. Winterton, L. C., "Control of Initial Events in Surface Thrombosis by Protein-Heparin Complexes," Ph.D. dissertation. University of Utah, Salt Lake City, Utah, 1985.
37. Mosher, D. F., *Ann. Rev. Med.* **35**, 561 (1984).
38. Ruoslahti, E., Hayman, E. G., Perishcbacher, M., and Engvall, E., "Methods in Enzymology" (L. W. Cunningham and D. W. Frederiksen, Eds.), Vol. 82, pp. 803–831. Academic Press, New York, 1982.
39. Yamada, K. M., *in* "The Glycoconjugates" (M. I. Horowitz and W. Pigman, Eds.), Vol. 3. Academic Press, New York, 1982.
40. Peterson, T. E., Thorgersen, H. C., Skorstengaard, K., Vibe-Peterson, K., Sottrup-Jensen, L., and Magnusson, S., *Proc. Natl. Acad. Sci. (USA)* **80**, 137 (1983).
41. Skorstengaard, K., Thorgersen, H. C., and Peterson, T. E., *Eur. J. Biochem.* **140**, 235 (1984).
42. Grant, W. H., Smith, L. E., and Stromberg, R. T., *J. Biomed. Mater. Res. Symp.* **8**, 33 (1977).
43. Van der Scheer, A., Feijen, J., Elhorst, J. K., Krugers Dagneaus, P. G. L. C., and Smolders, C. A., *J. Colloid Interface Sci.* **66**, 136 (1978).
44. Horbett, T. A., *J. Biomed. Mater. Res.* **15**, 673 (1981).
45. Brash, J. L., and Uniyal, S., *J. Polym. Sci., Polym. Symp.* **66**, 377 (1979).
46. Feijen, J., data to be published.
47. Morrissey, B. W., *Ann. N.Y. Acad. Sci.* **283**, 50 (1982).
48. Soderquist, M. E., and Walton, A. G., *J. Colloid Interface Sci.* **75**, 386 (1980).
49. MacRitchie, F., *in* "Advances in Protein Chemistry" (C. B. Anfinsen, M. L. Anson, J. T. Edsall, and F. M. Richards, Eds.), Vol. 32, pp. 283–326. Academic Press, New York, 1978.
50. Bornzin, G. A., and Miller, I. F., *J. Colloid Interface Sci.* **86**, 539 (1982).
51. Elhorst, J. K., Olthuis, F. M. F. G., Bargeman, D., Smolder, C. A., and Feijen, J., *Int. J. Artif. Organs* **1**, 288 (1978).

52. Grinnell, F., and Feld, M. K., *J. Biol. Chem.* **257,** 4888 (1982).
53. Grinnell, F., and Feld, M. K., *J. Biomed. Mater. Res.* **15,** 363 (1981).
54. Jonsson, U., Ivarsson, B., and Berghem, L., *J. Colloid Interface Sci.* **90,** 148 (1982).
55. Adams, G. A., and Feuerstein, I. A., *Trans. Amer. Soc. Artif. Intern. Organs* **27,** 219 (1981).
56. Koltisko, B. M., Jr., "Chromotographic Analysis of Protein Adsorption," M.S. thesis. Case Western Reserve University (1981).
57. Hughes, R. C., Pena, S. D. J., Clark, J., and Dourmashkin, R. R., *Exp. Cell Res.* **121,** 307 (1979).
58. Klebe, R. J., Bentley, K. L., and Schoen, R. C., *J. Cell. Physiol.* **109,** 481 (1981).
59. Haas, R., and Culp, L. A., *J. Cell. Physiol.* **113,** 289 (1982).
60. Young, B. R., Lambrecht, L. K., Cooper, S. L., and Mosher, D. F., *in* "Biomaterials: Interfacial Phenomena and Applications" (S. L. Cooper and N. A. Peppas, Eds.), Vol. 199. Advances in Chemistry Series, Amer. Chem. Soc., Washington, D.C., 1982.
61. Iwamoto, G. K., Winterton, L. C., Stoker, R. S., Van Wagonen, R. A., Andrade, J. D., and Mosher, D. F., *J. Colloid Interface Sci.* **106,** 459 (1985).
62. Iwamoto, G. K., Van Wagonen, R. A., and Andrade, J. D., *J. Colloid Interface Sci.* **86,** 581 (1982).
63. Van Dulm, P., and Norde, W., *J. Colloid Interface Sci.* **91,** 248 (1983).
64. Johansson, S., and Hook, M., *Biochemistry J.* **187,** 521 (1980).
65. Jilek, F., and Hormann, H., *Hoppe-Seylers' Z. Physiol. Chem.* **360,** 597 (1979).
66. Stathakis, N. E., and Mosesson, M. W., *J. Clin. Invest.* **60,** 855 (1977).
67. Teien, A. N., and Abildgaard, U., *Thromb. Haemostasis* **35,** 592 (1976).
68. Merrill, E. W., Salzman, E. W., Wory, P. S. L., Ashford, T. P., Brown, A. H., and Austen, W. G., *J. Appl. Physiol.* **29,** 723 (1970).

Hydrogels for Medical and Related Applications, J. D. Andrade, ed., ACS Symp., 1976

6

Diffusion through Hydrogel Membranes

I. Permeation of Water Through Poly(2-hydroxyethyl methacrylate) and Related Polymers

S. J. WISNIEWSKI, D. E. GREGONIS, S. W. KIM, and J. D. ANDRADE

Departments of Applied Pharmaceutical Sciences and Materials Science and Engineering, University of Utah, Salt Lake City, Utah 84112

Hydrogels are known for their unique physical properties and potential biomedical applications. The transport phenomena of some poly(2-hydroxyethyl methacrylate) (poly HEMA) membranes have been previously investigated (1-4). Ratner and Miller (5) have shown that poly HEMA membranes have a high permeability to urea due to interaction between the solute and membrane, and, in addition, consider the existence of pores in the poly HEMA gel structure, with the water regions of the gel acting as "pores" for solute transport.

Recently Chen found (6) that the absorption of water by dehydrated poly HEMA was a function of crosslinker content. In his study diffusion coefficients were calculated from absorption kinetic data using Fick's law. Several factors influence the structure of hydrogels and subsequently their diffusion characteristics. These factors include initiator, crosslinking agents, crosslinker content, equilibrium water content and impurities.

Yasuda et al. (1,11) have utilized a theory, based on a free-volume concept of diffusive transport, for hydrated homogeneous membranes. They concluded that this concept excellently explains the diffusive transport parameters as a function of water content over a wide hydration range.

In this study, we have been concerned with varying crosslinker concentrations and water content. It is hoped that this data will provide additional information on the basic transport mechanisms for water in different gel systems and on the role of water in the transport of other solutes.

Experimental

Hydroxyethyl methacrylate was obtained as a gift from Hydron Laboratories (New Brunswick, New Jersey) and was used without additional purification. Methoxyethyl methacrylate and methoxyethoxyethyl methacrylate were prepared in our laboratories by base catalyzed transesterification of methyl methacrylate with

the corresponding alcohol. Ethylene glycol dimethacrylate (Monomer Polymer Laboratories, Philadelphia, Pennsylvania) and tetraethylene glycol dimethacrylate (Polysciences, Warrington, Pennsylvania) were purified by base extraction to remove inhibitor followed by distillation. Azobismethylisobutyrate, prepared by the method of Mortimer (7), was used to initiate polymerization at a concentration of 7.84 m moles/liter monomer. Crosslinker concentration was calculated on a mole-to-mole basis with HEMA. The desired monomer solution was mixed with 45% v/v distilled water and polymerized between glass plates at 60°C for 24 hours.

A glass diffusion cell, which contains two compartments of equal volume (175 ml), was designed. Each chamber was stirred at a constant rate to reduce boundary layer effects. At the beginning of each experiment, one compartment was filled with tritiated water, the other was filled with distilled water. The increase in tritiated water was monitored by removing 50μℓ aliquots at various times. These aliquots were placed in 10 ml of liquid scintillation "cocktail" (Aquasol, New England Nuclear Company) and counted in a Packard Scintillation counter. The thickness of the wet membrane was measured using a light micrometer (Van Kauren Company). Membrane densities were measured by weighing sections of wet membrane of known volume. Water content was obtained from the difference in weight of wet and dry membrane (dried to constant weight under vacuum at about 60°C). All experiments were run at 23°C ± 1°C.

Results and Discussion

The equation used to treat our data was derived elsewhere (8) and is given as follows:

$$\ln (1 - 2\, C_t/C_0) = -\left(\frac{1}{V_1} + \frac{1}{V_2}\right) AUt,$$

where C_t = ^3H_2O count at time t; C_0 = ^3H_2O count at time 0; V_1 = V_2 = compartment volume = 175 ml; A = membrane contact area = 14.9 cm^2; U = permeability (cm/sec); and t = time (seconds).

A plot of $\ln (1 - 2\, C_t/C_0)$ vs. time will yield a straight line with slope = $-(1/V_1 + 1/V_2)AU$. Substituting our values of A, V_1 and V_2 gives U = -5.87 x slope (cm/sec). The diffusion coefficients are given by $D = Ud/K_D$, where d = wet membrane thickness and K_D is the partition coefficient. By definition K_D = water concentration in membrane/water concentration in bulk, which for our case reduces to $K_D = (P_M/P_W)W_f$. P_M and P_W are the wet membrane density and the density of water at 23°C, respectively. W_f is the weight fraction of water in the wet membrane and is equal to W_W/W_M, where W_W is the weight of water and W_M is the weight of the wet membrane.

Table 1 lists the obtained parameters for the various gels used. The data for the ∿ 0.2 mole-% diester crosslinker poly HEMA gels and unreported data on gels approximately 3-4 times thicker indicate that the permeability U is roughly proportional to 1/d, while D is essentially independent of thickness. Variations in D for the same gels appear to be mainly due to errors in the thickness measurement and a small degree of non-uniformity in thickness.

W_f and K_D decrease as crosslinking content increases, as expected. However, K_D seems to increase again at approximately 6 mole-% crosslinker. The increasing K_D of the higher crosslinked gels may be the result of greater interaction between water and a highly crosslinked polymer network. This water, a relatively small fraction of the total gel water, is not available for transport or is involved in a much slower diffusion process. (13,14).

A plot of diffusion coefficients vs. percent EGDMA and TEGDMA crosslinkers is shown in Figure 1. The diffusion coefficients decrease as the crosslinker content increases, approaching a limiting value at about 6 mole-% crosslinker. This behavior may indicate a "partition" type membrane. Diffusion coefficients rapidly increase with decreasing crosslinker content below about 2.5 mole-% crosslinker, suggesting the development of "loose pores."

Two basic mechanisms have been considered in explaining solute transport through a polymer membrane: 1) a microporous type, which can act as a sieve with the solute molecules being transported thourgh the minute pores of the membrane, and 2) a "partition" type membrane, which further acts to slow the diffusion process due to the interaction between diffusing solute and membrane matrix or membrane water. Craig's work (9) showed that, in general, a linear relationship exists between molecular weight and half time rates of transfer for porous membranes. However, the effect of molecular weight on the half time rates through certain "partition" membranes indicated no such trend (10). Recently, Chen (6) has described three different diffusion mechanisms from his water absorption studies: 1) a dissolution mechanism for higher crosslinking content, 2) a pore flow mechanism for low crosslinking content, and 3) an intermediate mechanism at intermediate crosslinker concentrations. We have found similar results from our study. Water diffuses through the crosslinked poly HEMA membranes via a predominantly pore mechanism from 0% crosslinker to approximately 2.5 mole-% crosslinker. Above 4 mole-% crosslinker, water transport is mainly controlled by the interaction of water with the gel matrix. The intermediate region lies between 2.5 to 4 mole-%.

A description of the homogeneous membrane model and the theoretical assumptions involved in the derivation of the relation between diffusion coefficients and water content is found

TABLE I.

Diffusion Coefficients, Permeabilities and Hydrogel Composition

45% H_2O-HEMA EGDMA-mole-%	d(cm)	P(g/cc)	W_f	K_D	$D \times 10^6$ (cm^2/sec)	$U \times 10^5$ (cm/sec)
7.5	0.0777	1.26	0.381	0.481	2.3	1.4
5.3	0.0713	1.22	0.348	0.426	2.3	1.4
3.8	0.0717	1.20	0.355	0.427	2.4	1.4
2.3	0.0696	1.20	0.376	0.452	2.6	1.7
0.75	0.0739	1.25	0.403	0.505	3.0	2.1
0.38	0.0679	1.27	0.417	0.531	3.3	2.6
≃0.02	0.0717	1.20	0.415	0.499	3.6	2.5
	0.0583	1.25	0.419	0.525	3.4	3.1
	0.0638	1.30	0.420	0.547	3.4	2.9
	0.0682	1.22	0.418	0.511	3.3	2.5
45% H_2O-HEMA TEGDMA-mole-%						
7.5	0.0776	1.20	0.405	0.488	2.5	1.6
4.6	0.0736	1.22	0.368	0.450	2.6	1.6
2.5	0.0702	1.23	0.377	0.465	2.7	1.8
1.4	0.0697	1.23	0.402	0.496	3.1	2.2
0.46	0.0793	1.33	0.418	0.557	3.4	2.4
Copolymers: Volume-%						
MEMA	0.0660	1.22	0.0348	0.0426	0.23	0.015
33% HEMA-67% MEMA	0.0694	1.25	0.173	0.217	0.58	0.18
67% HEMA-33% MEMA	0.0686	1.29	0.308	0.397	1.6	0.94
MEEMA	0.0901	1.11	0.631	0.702	7.6	5.9
33% HEMA-67% MEEMA	0.0733	1.20	0.504	0.605	5.1	4.2
67% HEMA-33% MEEMA	0.0747	1.20	0.444	0.534	3.9	2.8

MEMA - methoxyethyl methacrylate

MEEMA - methoxyethoxyethyl methacrylate

HEMA - hydroxyethyl methacrylate

elsewhere (11), and that relation is given as follows:

$$\ln D/D_0 = \beta x(1-\alpha)/(1+x\alpha),$$

where $x = (1-K_D)/K_D$, $\alpha = V_p/V_w$, $\beta = V^*/V_w$, D = experimental diffusion coefficient with partition coefficient K_D, D_0 = diffusion coefficient of water in pure water, V_w = free volume in unit volume of pure water, V_p = free volume in unit volume of polymer phase, and V^* = a characteristic volume parameter describing the diffusion of a permeant molecule in the medium.

It is possible to rearrange this equation in order to obtain a linear plot. That is,

$$(\ln D/D_0)^{-1} = -\frac{1}{\beta(1-\alpha)}\,x^{-1} - \frac{\alpha}{\beta(1-\alpha)}\,.$$

A plot of $(\ln D/D_0)^{-1}$ vs. x^{-1} should yield a straight line with slope = $-1/\beta(1-\alpha)$ and intercept = $-\alpha/\beta(1-\alpha)$. Table II gives values of $(\ln D/D_0)^{-1}$ and x^{-1} for the gels studied, using $D_0 = 2.4 \times 10^{-5}$ cm²/sec from (12). The values for poly HEMA, uncrosslinked (~ 0.02 mole-%), are an average of four different gels. Figure 2 is a plot of $(\ln D/D_0)^{-1}$ vs. x^{-1} for all but the crosslinked gels. Least squares fit yields values of $\alpha = 0.69$ and $\beta = 11$ with a correlation coefficient of -0.998. The intercept yields a value of 1.6×10^{-7} cm²/sec for the hypothetical zero water content polymer. Inclusion of crosslinked poly HEMA gels yields values of $\alpha = 0.72$ and $\beta = 13$ with a correlation coefficient of -0.988. Even though a fair correlation is obtained with the inclusion of the crosslinked gels, these gels seem to exhibit a trend of their own. These results and previous results (11) indicate that structural differences of the monomers used may play some role in the diffusion process other than just determining water content. Changing of the water content of swollen gels for pure systems by varying polymerization water concentration may shed some light on structural effects in the diffusion process. This study is being continued.

Acknowledgements

This work was supported by NHLI Grant No. HL 16921-01. The donations of generous quantities of hydroxyethyl methacrylate from Hydro Med Sciences, Inc., is gratefully acknowledged.

Abstract

Water transport through fully swollen poly (2-hydroxyethyl methacrylate) (poly HEMA) hydrogels, containing varying concentrations of ethylene glycol dimethacrylate (EGDMA) and tetraethylene

TABLE II.

Values of $(\ln D/D_0)^{-1}$ and x^{-1} for Hydrogels Studied

(Using $D_0 = 2.4 \times 10^{-5}$ cm²/sec)[12]

Hydrogel (Copolymers in volume-%)	$\ln(D/D_0)^{-1}$	$x^{-1} = K_D/1-K_D$
MEMA	-0.22	0.0445
33% HEMA-67% MEMA	-0.27	0.277
67% HEMA-33% MEMA	-0.37	0.658
MEEMA	-0.87	2.36
33% HEMA-67% MEEMA	-0.55	1.15
67% HEMA-33% MEEMA	-0.65	1.53
HEMA	-0.51	1.09
Mole-% EDGMA		
7.5	-0.43	0.927
5.3	-0.43	0.742
3.8	-0.43	0.745
2.3	-0.45	0.825
0.75	-0.48	1.02
0.38	-0.50	1.13
Mole-% TEGDMA		
7.5	-0.44	0.953
4.6	-0.45	0.818
2.5	-0.46	0.869
1.4	-0.49	0.984
0.46	-0.51	1.26

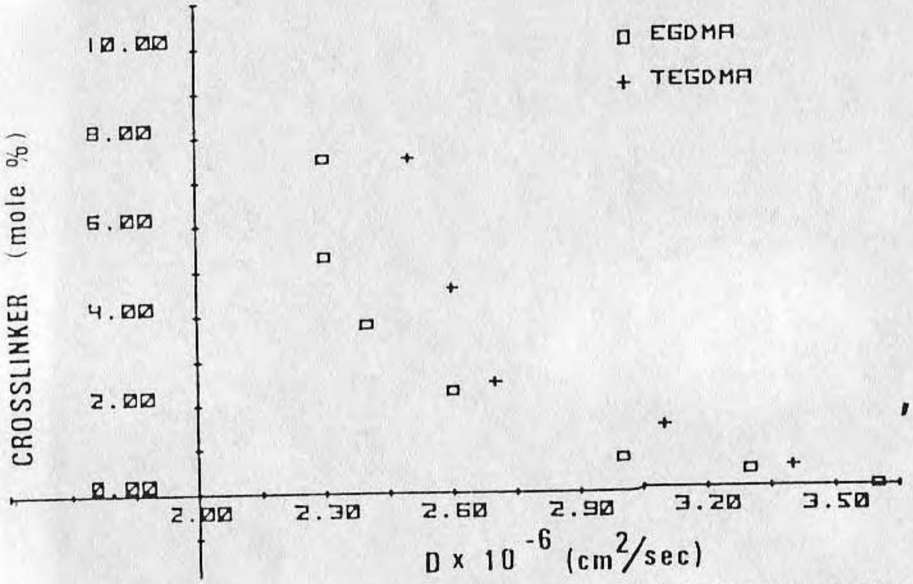

Figure 1. Plot of diffusion coefficients vs. mole % EGDMA and TEGDMA in PHEMA hydrogel

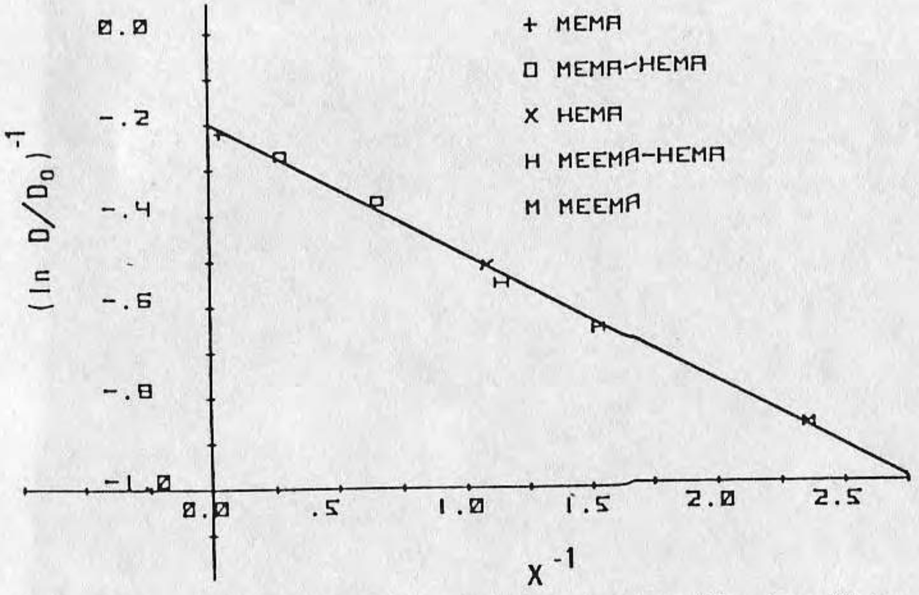

Figure 2. Plot of $(\ln D/D_o)^{-1}$ vs. X^{-1} for hydrogels swollen to different equilibrium water concentrations

glycol dimethacrylate (TEGDMA) crosslinkers, was investigated using tritiated water and a designed diffusion cell. Diffusion coefficients obtained in these experiments decrease as the concentration of crosslinker increases. This decrease is very sharp at crosslinker concentrations of 0-2.5 mole-%. At higher crosslinker concentrations (2.5-7.5 mole-%), the diffusion coefficients appear to reach a limiting value. This study indicates that a crosslinked poly HEMA membrane may provide both "partition" and "pore" mechanisms of solute transport based on crosslinker concentration.

Hydrogels of varying water content were prepared to investigate the relationship between water content and diffusion coefficient. Poly(methoxyethyl methacrylate) (poly MEMA), poly(methoxyethoxyethyl methacrylate) (poly MEEMA) and copolymers of MEMA and MEEMA with HEMA were formulated to give hydrogels with water content ranging from approximately 3% to 63%. The results of the diffusion experiments were examined in light of a free-volume model of diffusive transport. Excellent theoretical-experimental correlation was obtained for the hydrogels used in this study.

Literature Cited

1. Yasuda, H., Lamaze, C., and Ikenberry, L., Makromol. Chem. (1968) 118, 19.
2. Spacek, P., and Kubin, M., J. Poly. Sci., Part C, (1967) 16, 705.
3. Ikenberry, L., Yasuda, H., and Clark, H., Chem. Eng. Prog. Sym. Ser. (1968) 64 (84) 69.
4. Refojo, M. F., J. Appl. Poly. Sci. (1964) 9, 3417.
5. Ratner, B. D., and Miller, I. F., J. Biomed. Matl. Res. (1973) 7, 353.
6. Chen, R. Y. S., Polymer Preprints (1974) 15, No. 2, 387.
7. Mortimer, G. A., J. Org. Chem. (1964) 30, 1632.
8. Mah, M. Y., Master's Thesis, University of Utah, 1972.
9. Craig, L. C., and Konigsberg, W., J. Phys. Chem. (1961) 65 116.
10. Lyman, D. J., Trans. Am. Soc. Art. Int. Org. (1964) 10, 17
11. Yasuda, H., Lamaze, C. E., and Peterlin, A., J. Poly. Sci. A-2 (1971) 9, 1117.
12. Wang, J. H., Robinson, C. V., and Edelman, I. S., J. Amer. Chem. Soc. (1953) 75, 466.
13. Chang, Y. J., Chen, C. T., and Tobolsky, J. Poly. Sci., Po Phys. Ed., (1974), 12, 1.
14. Hoffman, A. S., Modell, M., and Pan, P., J. Appl. Poly. Sci., 14, 285 (1970).